BICYCLIC GUANIDINIUM OLIGOMERS FOR RECOGNITION, CELL DELIVERY, AND MOLECULAR MATERIALS

Julián Valero Moreno

Dipòsit Legal: T. 276-2012

UNIVERSITAT ROVIRA I VIRGILI
BICYCLIC GUANIDINIUM OLIGOMERS FOR RECOGNITION, CELL DELIVERY, AND MOLECULAR MATERIALS
Julián Valero Moreno
DL:T. 276-2012

UNIVERSITAT ROVIRA I VIRGILI
BICYCLIC GUANIDINIUM OLIGOMERS FOR RECOGNITION, CELL DELIVERY, AND MOLECULAR MATERIALS
Julián Valero Moreno
DL:T. 276-2012

Julián Valero Moreno

Bicyclic Guanidinium Oligomers for Recognition, Cell Delivery, and Molecular Materials

TESI DOCTORAL

Dirigida pel Prof. Javier de Mendoza Sans

Institut Català d'Investigació Química

UNIVERSITAT ROVIRA I VIRGILI

Tarragona

2011

UNIVERSITAT ROVIRA I VIRGILI
BICYCLIC GUANIDINIUM OLIGOMERS FOR RECOGNITION, CELL DELIVERY, AND MOLECULAR MATERIALS
Julián Valero Moreno
DL:T. 276-2012

Av. Països Catalans 16
43007 Tarragona
Tel: +34 977 920 200
E-mail: jmendoza@iciq.es

FAIG CONSTAR que aquest treball, titulat "Bicyclic Guanidinium Oligomers for Recognition, Cell Delivery, and Molecular Materials", que presenta Julián Valero Moreno per a l'obtenció del títol de Doctor, ha estat realitzat sota la meva direcció a l'Institut Català d'Investigació Química i que acompleix els requeriments per poder optar a Menció Europea.

Tarragona 27 de setembre de 2011

El director

Prof. Javier de Mendoza Sans

UNIVERSITAT ROVIRA I VIRGILI
BICYCLIC GUANIDINIUM OLIGOMERS FOR RECOGNITION, CELL DELIVERY, AND MOLECULAR MATERIALS
Julián Valero Moreno
DL:T. 276-2012

Agradecimientos

Es cuando llegas al final del camino, cuando recuerdas a quién te ha acompañado durante el viaje, a quien te ha apoyado y ayudado incondicionalmente y con los que has pasado tantos y tan buenos momentos. Deseas que frente a los nuevos horizontes que se abren ante ti, sigan estando contigo y así poder disfrutar de nuevos instantes impagables junto a ellos. Sin ellos no hubiese llegado hasta aquí, ni las experiencias vividas hubiesen sido tan enriquecedoras.

El principal artífice de que hoy esté aquí, escribiendo estas líneas, es el profesor Javier de Mendoza. Tú me has inculcado la pasión por la química y por la investigación. Gracias por confiar en mí para este proyecto, por tus enseñanzas y por darme la libertad para desarrollar mis propias ideas y aportaciones.

Mención especial merecen mis "antepasados sintéticos oligoguanidínicos". A algunos de ellos sólo los conozco por sus trabajos, pero gran parte de esta tesis no hubiese sido posible sin sus aportaciones. A Jorge, Michiel y Ruth, gracias.

A mis compañeros de "labo" con quien he compartido tan buenos momentos, risas, discusiones científicas y de la vida en general. A la vieja guardia que tanto he echado de menos y a los que tanto me alegra volver a ver y saber de ellos: A Jesús "el chanantemaníaco" por su simpatía y por ser de Cuenca; Enrique "mi primer técnico" por sus consejos y sabiduría química; Vera "mi compi de escritorio" por compartir esos proyectos bio, todos estos años; Eric "infarrojo men" porque nadie reclamaba la hora del café como tú; Pascal, por lo buen tío que eres; Alla, por tu vitalidad y alegría; Pili "mi mama del labo" por preocuparte tanto por mi; Yong Yang and Min for being so nice; Matt "Chicago boy" for your recommendation about The Wire (and for giving me your car); la bella Caterina, por tu sonrisa; Augustin "mon ami" por ser tan "noble" y por tu sentido del humor; Gerald "mi modelo científico" porque nunca olvidaré ese viaje a las Vegas con Vittorio y Guzman; Fred "el gafe" perque finalment t'has retrobat amb la bona estrella; Simo "mi friki preferida", porque realmente no sé que estaremos haciendo en el año 2900 y pico; Eli, por todo lo que he aprendido gracias a ti y todo el

cariño que me has dado. Aritz y Margot, por ser mis pilares, mi apoyo y mis "consejeros" todos estos años, os aprecio de veras. A todos, gracias por estos y otros muchos recuerdos imborrables; por vuestra amistad.

Tampoco me querría olvidar de los últimos en llegar (la nueva hornada) y con los que he tenido el placer de compartir vitrina: Tim, Laura, Sara S., Sara P., Berta, Ondrej, Jéssica, Phillip, y Eva. Gracias por toda la ayuda y comprensión que me habéis prestado durante estos últimos años.

He de agradecer al ICIQ como institución el apoyo técnico y administrativo durante toda mi estancia, pero muy especialmente a la gente que trabaja y que mueve esos engranajes sin los cuales la investigación sería una tarea mucho más ardua y difícil de lo que es *per se*. Joan, Susana, Noemí, Alba, Kerman, Israel, Fernándo, Simo, Miguel, Eddy, Marta, Eduardo: muchas gracias no sólo por ayudarme con mis compuestos sino también por ser tan amables conmigo. En este sentido, merece especial atención la figura de "Conan el Cromatógrafo", alias Enrique con quien he compartido tantos buenos momentos y charlas, no sólo de "astrología química".

Sin duda, esta tesis no se podría haber llevado a cabo sin la ayuda de los muchos colaboradores que han participado de forma activa en la generación y comprensión de los resultados que aquí se exponen.

Asimismo, he de agradecer a los profesores Ernest Giralt y Carles Bo, por sus consejos y sus respectivas aportaciones en el Capítulo 1 sobre reconocimiento de p53 y en especial a Susana Gordo y Eva Santos por sus charlas, kilométricos e-mails e impagable ayuda.

I would like to thank Prof. Peter Nielsen, for making possible my stage in Copenhaguen and give me the opportunity to work in these amazing PNA projects. Moreover, I would like to mention the support and help received from the group, especially to Jolanta, Shirashi and Anu who have been actively working in those projects. Last but not least, I have to thank Peter B. for offering me his house and being so nice with me during these months.

Quisiera agradecer al Profesor Jose Luis Mascareñas por su inestimable ayuda en la

confección del Capítulo 3, relativo al reconocimiento selectivo de secuencias consenso de ADN y especialmente a Jesús Mosquera por su colaboración y por resolverme las dudas en un campo un tanto desconocido para mí.

I would also like to thank Prof. Guldi to afford new light into the photophysical properties of the complexes described in Chapter 5 and his co-workers, Bruno Grimm and Rafael Krick for the measurements and the data processing. Within this context, I would also like to mention the collaboration that we have just started with Prof. Hans Elemans which hopefully, will be very helpful in order to have a better insight into the aggregation behavior of those molecules by means of STM technique.

A Beatriu Escuder, por su activa colaboración en el capítulo de organogeles, por su entusiasmo y positivismo. Por ayudar a iniciarme en este campo tan interesante y por su paciencia para resolver todas las dudas que me iban surgiendo. Gracias.

No querría dejar pasar esta oportunidad para agradecer al Prof. Pau Ballester el compartir sus conocimientos y contagiarme algunas de sus inquietudes y manera de entender la química supramolecular.

Por último, nada de esto hubiese sido posible sin dos apoyos fundamentales en mi vida: amigos y familia.

A Cristina, por ayudarme todos estos años a formarme como músico, pero sobre todo por escucharme y dejar expresarme en ese diván con forma de banqueta de piano.

A mis amigos de siempre: Joan "juanitu", Ángel "good-good", Rosa "y su colección de tazas del viena" y Enric "vamos a correr?"; por hacerme olvidar aunque fuese por un momento de los problemas del laboratorio y pasar tan buenos ratos juntos. Y a los de la universidad: Ana M., Edu "el borde", Alex "maestro uni", Ruben, Eva, Nela y Joan "Zipi … o Zape?". Gracias a todos por vuestra amistad.

A mi familia. A mis padres y mi hermano, porque gran parte de lo que soy, de mis valores e ideales se lo debo a ellos. Gracias por cuidarme y preocuparos tanto por mí.

A tu Laia, perque sense tu aquest viatge no hagués sigut el mateix. Perque m'omples de felicitat cada día i em millores i complementes constantment. Perque em comprens. Gràcies.

UNIVERSITAT ROVIRA I VIRGILI
BICYCLIC GUANIDINIUM OLIGOMERS FOR RECOGNITION, CELL DELIVERY, AND MOLECULAR MATERIALS
Julián Valero Moreno
DL:T. 276-2012

"La originalidad consiste en el retorno al origen; así pues, original es aquello que vuelve a la simplicidad de las primeras soluciones."

Antoni Gaudí

UNIVERSITAT ROVIRA I VIRGILI
BICYCLIC GUANIDINIUM OLIGOMERS FOR RECOGNITION, CELL DELIVERY, AND MOLECULAR MATERIALS
Julián Valero Moreno
DL:T. 276-2012

A mi familia y a ti, Laia

UNIVERSITAT ROVIRA I VIRGILI
BICYCLIC GUANIDINIUM OLIGOMERS FOR RECOGNITION, CELL DELIVERY, AND MOLECULAR MATERIALS
Julián Valero Moreno
DL:T. 276-2012

List of Abbreviations

Amino acids:

Ala (A): alanine	Leu (L): leucine
Arg (R): arginine	Lys (K): lysine
Asn (N): asparagine	Met (M): methionine
Asp (D): aspartate	Phe (F): phenylalanine
Cys (C): cysteine	Pro (P): proline
Glu (E): glutamate	Ser (S): serine
Gln (Q): glutamine	Thr (T): threonine
Gly (G): glycine	Trp (W): tryptophan
His (H): hystidine	Tyr (Y): tyrosine
Ile (I): isoleucine	Val (V): valine

Nucleobases:

G: Guanine	C: Cytosine
A: Adenine	T: Thymine

A: acceptor
Ac: acetyl
ACC: Adrenal carcinoma
ACN: acetonitrile
Ar: aromatic
atm: atmosphere
Bn: benzyl
Boc: *tert*-butoxycarbonyl
tBu: *tert*-butyl
CD: circular dichroism
CF: carboxyfluorescein
CPP: cell penetrating peptide
CTV: cyclotriveratrylene
D: Donor
DCM: dichloromethane
Deca: decane
D*i*PEA: diisopropylethylamine
DMF: *N,N'*-dimethylformamide
DMSO: dimethylsulfoxide
DNA: deoxyribonucleic acid
DOSY: Diffusion Ordered Spectroscopy
EI-MS: Electron Impact Mass Spectrometry
Eq.: equivalent

ESI-MS: Electrospray Ionization Mass Spectrometry
Et: Ethyl
Et_3N: triethylamine
ex-TTF: Extended Tetrathiafulvalene
FAB-MS: Fast Atom Bombardment Mass Spectrometry
G: guanidine
GPC: Gel Permeation Chromatography
Hex/Hexa: hexane
HPLC :High Performance Liquid Chromatography
HRMS: High Resolution Mass Spectrometry
HSQC: heteronuclear single quantum correlation
ITC: isothermal titration calorimetry
MALDI: matrix-assisted laser desorption/ionization sprectrometry
MD: molecular dynamics
Me: methyl
MM: molecular modeling
Ms: methanesulfonyl or mesyl
MS-TOF: time of flight spectrometry
MW or μW: microwave reactor
NMM: *N*-methylmorpholine
LC-MS: liquid chromatography-mass spectroscopy
PG: protecting group
Ph: phenyl
PNA: peptide nucleic acid
ppm: part per million
p53DBD: p53 DNA-binding domain
p53TD: tetramerization domain of p53
p53R337H: p53 mutant R337H
Quant.: quantitative
r.t.: Room temperature
RMSD: root main square deviation
RNA: ribonucleic acid
mRNA: messenger RNA
RP: reverse phase
SN: nucleophilic substitution reaction
STM: Scanning Tunneling Microscopy
TFA: trifluoroacetic acid
TBAF: *tert*-butylammonium fluoride
TBDMS: *tert*-butyldimethylsilyl

TBDPS: *tert*-butyldiphenylsilyl
TCE: tetrachloroethane
Tf_2O: trifluoromethanesulfonic acid anhydride or triflic anhydride
THF: tetrahydrofurane
TLC: thin layer chromatography
UV-vis: Ultraviolet-visible
VT variable temperature
wt: wild type

UNIVERSITAT ROVIRA I VIRGILI
BICYCLIC GUANIDINIUM OLIGOMERS FOR RECOGNITION, CELL DELIVERY, AND MOLECULAR MATERIALS
Julián Valero Moreno
DL:T. 276-2012

Table of Contents

Chapter 3: Design and Synthesis of Peptide-Oligoguanidinium Conjugates for Specific DNA Sequence Recognition and Binding Enhancement

Chapter 4: A Tetraguanidinium Macrocycle for the Recognition and Cavity Expansion of Calix[4]arene Tetraoxoanions

Chapter 5: Guanidinium Bis-porphyrin Tweezers for the Complexation of Fullerene Carboxylate Derivatives

UNIVERSITAT ROVIRA I VIRGILI
BICYCLIC GUANIDINIUM OLIGOMERS FOR RECOGNITION, CELL DELIVERY, AND MOLECULAR MATERIALS
Julián Valero Moreno
DL:T. 276-2012

Objectives and Outline

Nature frequently uses guanidinium group (mainly found in the amino acid arginine) to bind *via* ion pairing and hydrogen bonding different anions (mostly oxoanions), thus facilitating interactions between macromolecules such as proteins or DNA. This anion coordination is also employed for specific recognition of substrates in enzymatic active sites or modulators in allosteric pockets.

Owing to these features, several artificial receptors based on guanidinium scaffold have been reported for binding a wide variety of anionic compounds. Within this context, our research group has extensively worked on a series of enantiomerically pure bicyclic guanidinium compounds (Figure 1) designed to complement different biomolecules such as amino acids, nucleotides or even proteins.

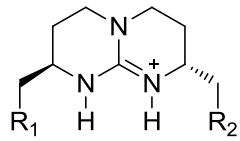

Figure 1. *General formula of bicyclic guanidinium compounds described in this manuscript.*

The aims of the work described in this thesis are: (i) to provide a robust and reliable synthetic methodology for the construction of bicyclic guanidinium oligomers of different lengths and functionalization degree, (ii) to gain a better insight into the biological activity of these compounds as ligands for the recognition of biomolecules (such as nucleic acids or peptide sequences) or as cell membrane carriers, (iii) to explore the use of the bicyclic guanidinium scaffold as a supramolecular building block for the construction of complex architectures, and finally (iv) to assess the physicochemical properties of these self-assembled systems for materials science applications.

This manuscript is divided into two clearly defined sections. The first one, including Chapters 1 to 3, is based on the binding properties of oligoguanidinium compounds with biologically relevant molecules such as p53 or targeted DNA sequences. Attributable to their cationic nature and hence similarity with cell penetrating peptides, bicyclic guanidinium oligomers are also known to interact and efficiently uptake cell membrane. Indeed, this feature is extensively studied in Chapter 2.

The second part explores the self-assembly of bicyclic guanidines for calix[4]arene complexation and expansion of their cavities (Chapter 4), multiporphyrin-fullerene dyad arrays (Chapter 5), and their properties and potential applications as organogelators (Chapter 6).

In particular, Chapter 1 describes different synthetic strategies towards oligoguanidinium ligands for the p53 tetramerization domain. A brief discussion about the design of those polycationic compounds and the mode of interaction with the protein arising from the NMR data is included.

Analogous bicyclic guanidinium oligomers are presented in Chapter 2 to allow cell uptake of covalently attached peptide nucleic acid (PNA) compounds. Assessment of their antisense activity by luciferase antisense assay directly relates to the internalization efficiency. Moreover, interpretations about the cellular uptake mechanism will be derived from aggregation studies of these conjugates. Antibacterial oligoguanidinium-PNA compounds targeting *E. coli* will be also evaluated.

In Chapter 3 the interaction of DNA with these polycationic molecules is studied. In combination with a miniaturized transcription factor peptide, oligoguanidines should promote a binding enhancement as the number of interactions with the specific oligonucleotide fragment increases. Binding affinities will be assessed by means of circular dichroism (CD) and electrophoretic mobility shift assays (EMSA).

Chapter 4 describes the design and synthesis of a macrocyclic tetraguanidium compound capable of strongly bind to oxoanionic calix[4]arenes even in highly polar media. This complexation results in the conformational stabilization and cavity

expansion of those calixarenes which will permit the inclusion of bulkier guests such as isoquinolinium salts.

Chapter 5 explores guanidinium-carboxylate dyads bearing electron donor-acceptor functionalities (namely, porphyrins and fullerenes). Contribution of the individual interactions and determination of the overall association constant will be studied by NMR and UV-vis titrations. Self-assembly of these robust complexes into multiporphyrin arrays will be addressed by a bidentate ligand as structural element.

Finally, the serendipitous finding on the gelation ability of some diguanidines is reported in Chapter 6. The role of chirality and the counterion on the gelation process will be further discussed. Indeed these gel-phase materials are anion responsive and moreover the use of enantiomeric mixtures results in the destabilization or complete disruption of the gel. The use of these gelators for controlled drug delivery applications is also explored.

UNIVERSITAT ROVIRA I VIRGILI
BICYCLIC GUANIDINIUM OLIGOMERS FOR RECOGNITION, CELL DELIVERY, AND MOLECULAR MATERIALS
Julián Valero Moreno
DL:T. 276-2012

UNIVERSITAT ROVIRA I VIRGILI
BICYCLIC GUANIDINIUM OLIGOMERS FOR RECOGNITION, CELL DELIVERY, AND MOLECULAR MATERIALS
Julián Valero Moreno
DL:T. 276-2012

Chapter 1

Who Guards the Guardian?

UNIVERSITAT ROVIRA I VIRGILI
BICYCLIC GUANIDINIUM OLIGOMERS FOR RECOGNITION, CELL DELIVERY, AND MOLECULAR MATERIALS
Julián Valero Moreno
DL:T. 276-2012

Chapter 1

New Bicyclic Guanidinium Oligomeric Ligands for the Tetramerization Domain of p53

1.1 Introduction

1.1.1 Protein p53: The Guardian of the Cell

Our cells are sensitive to many dangers including chemicals, viruses, the presence of oncogenes and ionizing radiation. When cells are damaged by these factors in sensitive places (e.g. on critical spots), the effects on some of the key regulatory elements which promote cell growth control can be disastrous. These regulatory elements may be blocked and the cell will rapidly multiply and grow into a tumor. Protein p53 acts as a "guardian" against this type of damage.[1,2]

Typically p53 is found at low levels but, as a response to DNA damage, the protein levels increase and a repair process is initiated through several independent mechanisms. p53 binds to specific regulatory sites in the genome and initiates the

[1] Lane, D. P. *Nature* **1992**, *358*, 15-16.
[2] Levine, A. J. *Cell* **1997**, *88*, 323-331.

synthesis of proteins that stop cell division until the normal function is restored. If this damage is too severe, p53 promotes cell death, or apoptosis, which directs the cell to commit suicide. In summary, p53 acts as a transcriptional factor, involved in cell-cycle regulation, the initiation of apoptotic cell death, and DNA repair.[3,4]

1.1.2 p53 Structure

p53 tumor suppressor is a flexible molecule composed of four identical protein chains. This flexibility is related to p53's ability to interact with different gene sequences and proteins. Each chain is composed by three main compact and globular domains with specific roles. A tetramerization domain (TD), that ties the four chains together, is located at the centre, defining the quaternary structure of the molecule. A long, flexible polypeptide region in each chain connects to the DNA-binding domain (DBD), responsible for the interaction with DNA to whom p53 binds through positively charged residues, mainly arginines, which allow contacts with the DNA phosphodiesters, and recognize specific regulatory sites on the gene sequence. Another flexible region connects this domain with the third stable domain, close to each arm, called the amino-terminal transactivation domain, which activates the DNA-reading machinery (Figure 1).[5]

[3] Vogelstein, B.; Lane, D.; Levine, A. J. *Nature* **2000**, *408*, 307-310.

[4] Goodsell, D. S. *The Oncologist* **1999**, *4*, 138-139.

[5] Römer, L.; Klein, C.; Dehner, A.; Kessler, H.; Buchner, J. *Angew. Chem. Int. Ed.* **2006**, *45*, 2-23.

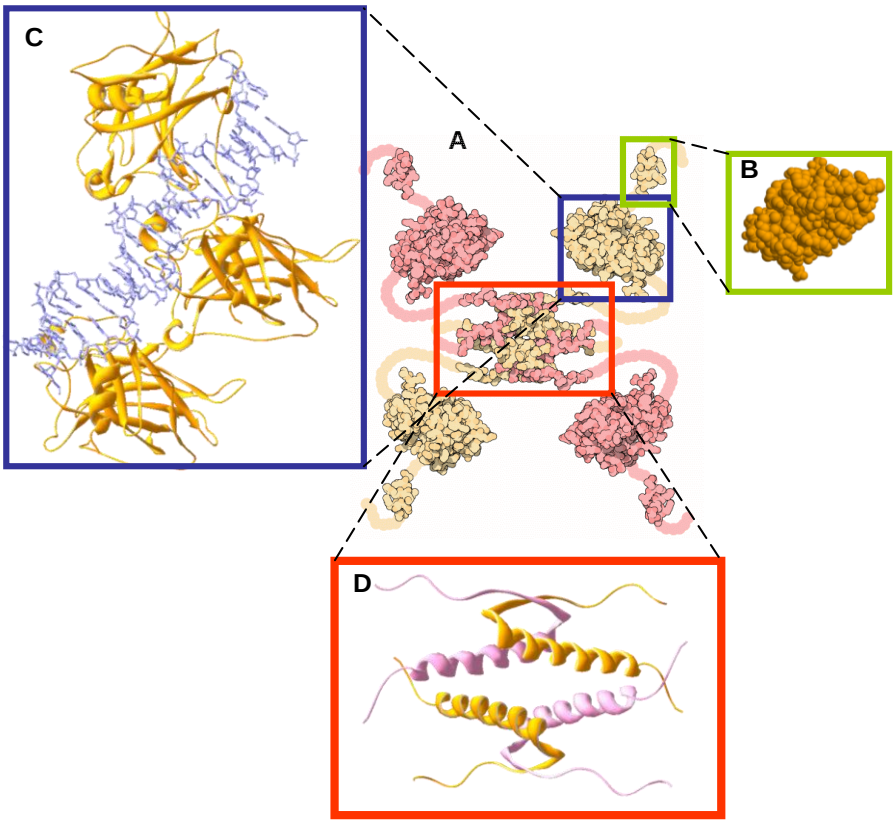

Figure 1. *(A) Schematic picture of the whole p53 protein.[4] (B) Transactivation domain crystal structure in space-fill representation, showing its globular shape. PDB (Protein Data Bank): 1YCQ. (C) Three DNA-binding domains co-crystallized with a DNA fragment (DNA is showed in stick display, meanwhile the DBD's are rendered in ribbon display). PDB: 1TUP. (D) Three-dimensional representation of oligomerization domain in ribbon display. PDB: 1OLG.*

Recently, Fersht *et al.* studied the quaternary structure of human p53 in solution, by combining small angle X-ray scattering (SAXS) data with NMR analysis.[6] Indeed, open and closed structures of the protein complexing DNA fragments were solved by means of electron microscopy together with the techniques above mentioned.

[6] Tidow, H.; Melero, R.; Mylonas, E.; Freund, S. M. V.; Grossmann, J. G.; Carazo, J. M.; Svergun, D. I.; Valle, M.; Fersht, A. L. *Proc. Natl. Acad. Sci. USA* **2007**, *104*, 12324-12329.

1.1.3 Functions of p53

Since the early 90s, it is known that target genes of p53 facilitate cell-cycle arrest[7] and DNA-repair mechanisms,[8,9,10] or apoptotic cell death[11] when DNA damage is too severe to be repaired.[12,13,14] Nowadays, new aspects involving p53 function with replicative senescense (in somatic cells only a limited amount of cell division can occur) and cell aging have been found.[15,16,17] Moreover, p53 also performs transcription reactions, as direct induction of apoptosis (Figure 2). [18,19]

[7] Ohki, R.; Nemoto, J.; Murasawa, H.; Oda, E.; Inazawa, J.; Tanaka, N.; Taniguchi, T. *J. Biol. Chem.* **2000**, *275*, 22627-22630.

[8] Tlsty, T. D. *Curr. Top. Microbiol. Immunol.* **1997**, *221*, 37-46.

[9] Wahl, G. M.; Linke, S. P.; Paulson, T. G.; Huang, L.-C. *Cancer Surv.* **1997**, *29*, 183-219.

[10] Tanaka, H. Arakawa, H.; Yamaguchi, T.; Shlralsh, K.; Fukuda, S.; Matsui, K.; Take, Y.; Nakamura, Y. *Nature* **2000**, *404*, 42-49.

[11] Vousden, K. H.; Lu, X. *Nat. Rev. Cancer* **2002**, *2*, 594-604.

[12] Adimoolam, S.; Ford J. M. *DNA Repair* **2003**, *2*, 947-954.

[13] Offer, H.; Wolkowicz, R.; Matas, D.; Blumenstein, S.; Livneh, Z.; Rotter, V. *FEBS Lett.* **1999**, *450*, 197-204.

[14] Zhou, J.; Ahn, J.; Wilson, S. H.; Prives, C. *EMBO J.* **2001**, *20*, 914-923.

[15] Tyner, S. D.; Venkatachalam, S.; Choi, J.; Jones, S.; Ghebranious, N.; Igelmann, H.; Lu, X.; Soron, G.; Cooper, B.; Brayton, C.; Hee, P. S.; Thompson, T.; Karsenty, G.; Bradley, A.; Donehower, L. A. *Nature* **2002**, *415*, 45-53.

[16] Garcia-Cao, I.; Garcia-Cao, M.; Martín-Caballero, J.; Criado, L. M.; Klatt, P.; Flores, J. M.; Weill, J. C.; Blasco, M. A.; Serrano, M. *EMBO J.* **2002**, *21*, 6225-6235.

[17] Campisi, J. *Nat. Rev. Cancer* **2003**, *3*, 339-349.

[18] Marchenko, N. D.; Zaika, A.; Moll, U. M. *J. Biol. Chem.* **2000**, *275*, 16202-16212.

[19] Mihara, M.; Moll, U. M. *Methods Mol. Biol.* **2003**, *234*, 203-209.

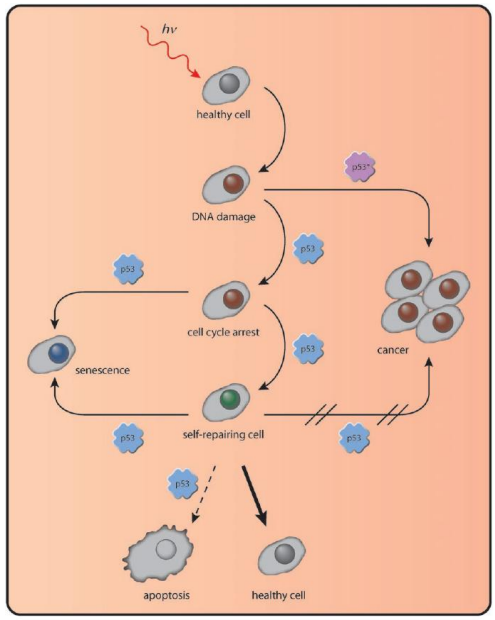

Figure 2. *Different cellular roles of p53 (reproduced from ref. 5). Influence of active p53 (blue) and mutant p53 (purple) on damaged eukaryotic cells.*[5]

1.1.4 p53 and DNA Binding

p53 binds specifically to a palindromic double-strand DNA-promotor consensus site, which may be up to 13 base pairs away from a second copy.[20] To form the stable DNA-p53 complex, the protein must be tetrameric.

The macromolecular association is illustrated in Figure 3. In this case, the tetramerization domain is seen behind the helix, tying the four chains together. The four transactivation domains are free and ready to activate the proteins involved in reading the DNA and regulating transcription of the corresponding target genes. The products of these genes are responsible for the induction of DNA repair mechanisms, or apoptosis.

[20] Cho, Y.; Gorina, S.; Jeffrey, P. D.; Pavletich, N. P. *Science* **1994**, *265*, 346-355.

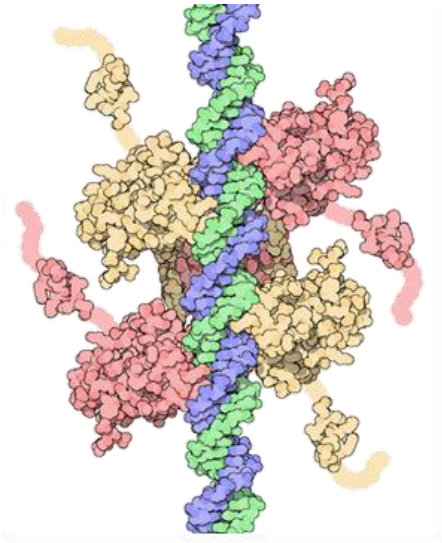

Figure 3. *Schematic representation of DNA-p53 binding.*

DNA binding of the DBD is highly cooperative,[21,22] even when excess DNA is present,[23] mainly because of the presence of inter-domain contacts in p53. In fact, a stabilizing dimerization interface (double salt bridge to residues E180 and R181) seems to be responsible for the observed cooperativity in DNA binding (Figure 4).[24]

[21] Klein, C.; Planker, E.; Diercks, T.; Kessler, H.; Kunkele, K. P.; Lang, K.; Hansen, S.; Schwaiger, M. *J. Biol. Chem.* **2001**, *276*, 49020-49027.

[22] Klein, C.; Georges, G.; Konkele, A. P.; Huber, R.; Engh, R. A.; Hansen, S. *J. Biol. Chem.* **2001**, *276*, 37390-37401.

[23] Rippin, T. M.; Freund, S. M. V.; Veprintsev, D. B.; Fersht, A. R. *J. Mol. Biol.* **2002**, *319*, 351-358.

[24] Dehner, A.; Klein, C.; Hansen, S.; Muller, L.; Buchner, J.; Schwaiger, M.; Kessler, H. *Angew. Chem. Int. Ed.* **2005**, *44*, 5247-5251.

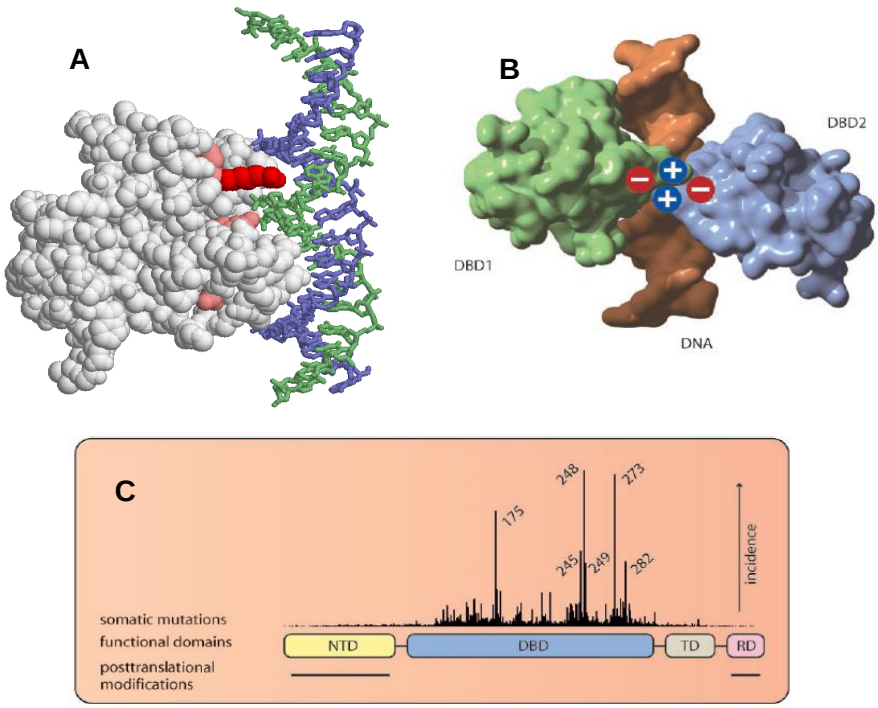

Figure 4. *(A) DNA-binding domain interacting with a DNA structure. In red, the residues interacting with the minor groove of the chain; in pink, other highly conserved arginines. (B) The dimerization interface between two DBDs (the model is based in 1TSR structure).*[5] *(C) Scheme showing the more common somatic mutations and the domains that are mainly post-translationally modified (reproduced from ref. 5).*

Inactivation of p53 is mainly due to mutations that interfere with the DNA-binding ability of the protein. A common mutation occurs on arginine 248. In Figure 4A, it can be observed how this residue snakes into the minor groove of the DNA, forming a strong stabilizing interaction. When it mutates to another amino acid, this interaction is lost and, as a result, p53 DNA binding ability disappears. Other frequently hot-spot mutations concern also arginine residues (colored in pink), including R175, R249, R273 and R282.[25] This highlights the importance of positively-charged residues in p53 to

[25] Olivier, M.; Eeles, R.; Hollstein, M.; Khan, M. A.; Harris, C. C.; Hainaut, P. *Hum. Mutat.* **2002**, *19*, 607-614.

efficiently interact with DNA or to position other DNA-binding amino acids.

1.1.5 Ripping p53 Tetramerization Domain

The structure of p53TD has been determined both by X-ray crystallography and by NMR.[26] The monomers of the tetramer are composed by a β-strand (residues 326 to 333) linked to an α-helix (residues 335 to 355) by a single residue (Gly334, a common amino acid localized in regions where a secondary structure change takes place). The monomer has a V-shape where each of the two secondary structures is a branch of the V (Figure 5). In addition, three amino acids (Ile332, Phe338 and Phe341) establish contacts to form a small hydrophobic core at the hinge region that highly stabilizes the monomeric structure.

Actually, p53TD is not a tetramer but a dimer of dimers.[26b,27] Two monomers associate via their β-strands to form an antiparallel double-stranded sheet and *via* antiparallel association of their helices to create a double-helical bundle, as shown in Figure 5. The formation of the antiparallel β-sheet leads to the creation of eight backbone hydrogen bonds. In addition, a hydrophobic cluster is generated at the interface between the monomers. This core is composed by Phe328, Leu330 and Ile332 of the β-strands and Phe338, Phe341 and Asn345 from the α-helices.[28] Arg337 also establishes a salt bridge with Asp352 across the helix-helix interface within dimer

[26] a) Clore, G. M.; Omichinski J. G.; Sakaguchi, K.; Zambrano, N.; Sakamoto, H.; Appella, E.; Gronenborn, A. M. *Science* **1994**, *265*, 386-391. b) Lee, W.; Harvey, T. S.; Yin, Y.; Yau, P.; Litchfield, D.; Arrowsmith, C. H. *Nat. Struct. Biol.* **1994**, *1*, 877-890. c) Clore, G. M.; Ernst, J.; Clubb, R.; Omichinski, J. G.; Kennedy, W. M.; Sakaguchi, K.; Appella, E.; Gronenborn, A. M. *Nat. Struct. Biol.* **1995**, *2*, 321-333. d) Jeffrey, P. D.; Gorina, S.; Pavletich, N. P. *Science* **1995**, *267*, 1498-1502. e) Miller, M.; Lubkowski, J.; Rao, J. K.; Danishefsky, A. T.; Omichinski, J. G.; Sakaguchi, K.; Sakamoto, H; Appella, E.; Gronenborn, A. M.; Clore, G. M. *FEBS Lett.* **1996**, *399*, 166-170. f) Chène, P.; Mittl, P.; Grutter, M. *J. Mol. Biol.* **1997**, *273*, 873-881. g) Mittl, P. R.; Chène, P.; Grutter, M. G. *Acta Crystallogr. D. Biol. Crystallogr.* **1998**, *54*, 86-89.

[27] Mateu, M. G.; Sánchez Del Pino, M. M.; Fersht, A. R. *Nat. Struct. Biol.* **1999**, *6*, 191-198.

[28] Mateu, M. G.; Fersht, A. R. *EMBO J.* **1998**, *17*, 2748-2758.

subunits, and it has been suggested that these ionic interactions are the driving force for dimerization and, subsequently, for tetramer formation. Therefore, mutations in these residues greatly influence the conformational stability of p53.

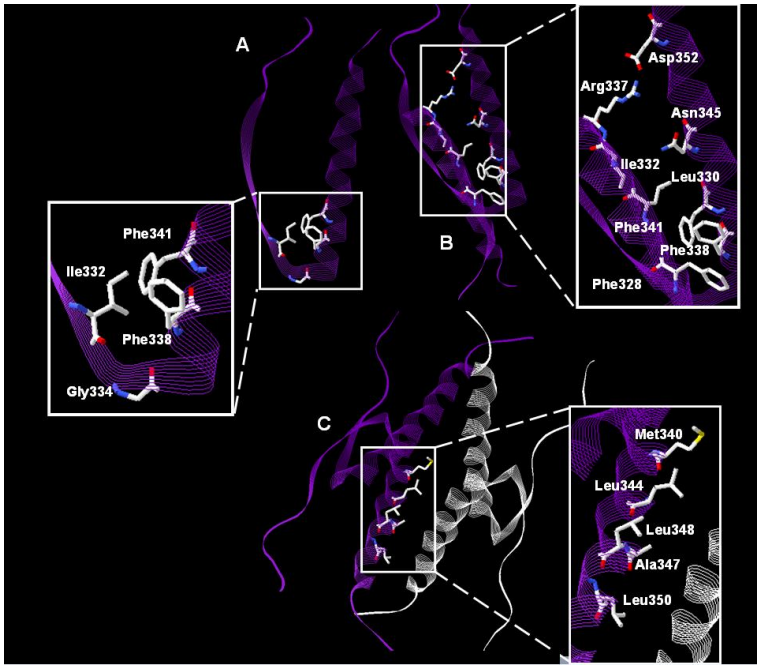

Figure 5. *Structure of tetramerization domain. (A) Ribbon representation of a monomer (residues 326-356); the residues involved in the stabilization are indicated. (B) Primary dimer formation; the residues involved in the stabilization are shown. (C) The four chains of a tetramer are represented forming a dimer of dimers; the residues involved in the hydrophobic contacts are indicated only in one of the chains.*

Two dimers interact via their α-helices, mainly involving hydrophobic residues like Met340, Leu344, Ala347, Leu348 and Leu350 (Figure 6).[29] The β-strands are on the outside of the tetramer and their residues are not directly related with the association between the two dimers. In addition, the presence of Arg342, Lys351 and four glutamates (Glu339, Glu343, Glu346 and Glu349) within the boundaries of the dimer-dimer interface can be observed. Only the pairs of complementary charged side chains

[29] Noolandi, J. *Macromol. Symp.* **2003**, *191*, 31-39.

close enough to form an intra-monomer salt bridge involve Lys351 with Glu343 and/or Glu346 (Figure 6). These residues can contribute four or more ionic interactions to p53's tetramer interface, favoring the stabilization and self-association of primary dimers.[30,31]

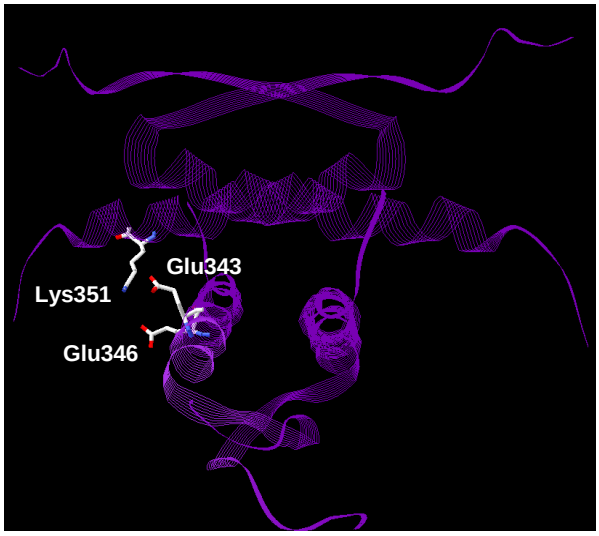

Figure 6. *Tetramerization domain view showing salt bridge interactions between two helices of different primary dimers.*

The hydrophobic residues mentioned before (between 340 and 351) form a nuclear export signal,[32] which is exposed on the surface of the protein when p53 is monomeric (at low cellular concentration), and buried beneath the surface when it is tetrameric (after accumulation), modifying the cellular localization of p53 by changes in its quaternary structure.

[30] Brokx, R. D.; Bolewska-Pedyczak, E.; Gariépy, J. *J. Biol. Chem.* **2003**, *278*, 2327-2332.

[31] Chène, P.; Bechter, E. *J. Mol. Biol.* **1999**, *286*, 1269-1276.

[32] Stommel, J. M.; Marchenko, N. D.; Jiménez, G. S.; Moll, U. M.; Hope, T. J.; Wahl, G. M. *EMBO J.* **1999**, *18*, 1660-1672.

1.1.6 p53 and Cancer: Who Guards the Guardian?

Due to its function, p53 plays an important role as a tumor suppressor and, consequently, it represents a natural defense against cancer. Typically, cancer cells contain two types of mutations: those which cause uncontrolled growth and multiplication of cells, and those which block the defenses that avoid unnatural growth. p53 mutations belong to the second group and that is the reason why mutations in the p53 gene are found in about 50% of the cases of human cancer.[5,33] Most of these are missense mutations, changing the information in the DNA at one position. This causes p53 to be expressed with an error, swapping an incorrect amino acid at one point, which prevents the protein to stop multiplication in the damaged cell, or to repair the DNA damage. Consequently, if other mutations affecting at the regulatory elements which control cell growth are present, this cell will develop into a tumor.

These are the key aspects of research on p53 which consists in the study of the activity of this protein and how altering it can have an influence on cancer development. As a result, different approaches have been established. Research on p53 focuses on its interaction with partner proteins, and how these associations may modify, enhance or inhibit its function. Many studies are related to proteins that promote post-transcriptional modifications[34,35] (phosphorylation,[36,37] acetylation,[38] ubiquitinylation[39,40] or sumoylation[41,42,43]) on p53 to modify its behavior (Figure 7).

---

[33] Soussi, T.; Legros, Y.; Lubin, R.; Ory, K.; Schlichtholz, B. *Int. J. Cancer* **1994**, *57*, 1-9.

[34] Brooks, C. L.; Gu, W. *Curr. Opin. Cell Biol.* **2003**, *15*, 164-171.

[35] Bode, A. M.; Dong, Z. *Nat. Rev. Cancer* **2004**, *4*, 793-805.

[36] Helt, C. E.; Wang, W.; Keng, P. C.; Bambara, R. A. *Cell Cycle* **2005**, *4*, 529-532.

[37] Caspari, T. *Curr. Biol.* **2000**, *10*, R315-R317.

[38] Prives, C.; Manley, J. L. *Cell* **2001**, *107*, 815-818.

[39] Jesenberger, V.; Jentsch, S. *Nat. Rev. Mol. Cell Biol.* **2002**, *3*, 112-121.

[40] Fang, S.; Jensen, J. P.; Ludwig, R. L.; Vousden, K. H.; Weissman, A. M. *J. Biol. Chem.* **2000**, *275*, 8945-8951.

[41] Rodríguez, M. S.; Desterro, J. M.; Lain, S.; Midgley, C. A.; Lane, D. P.; Hay, R. T. *EMBO J.*

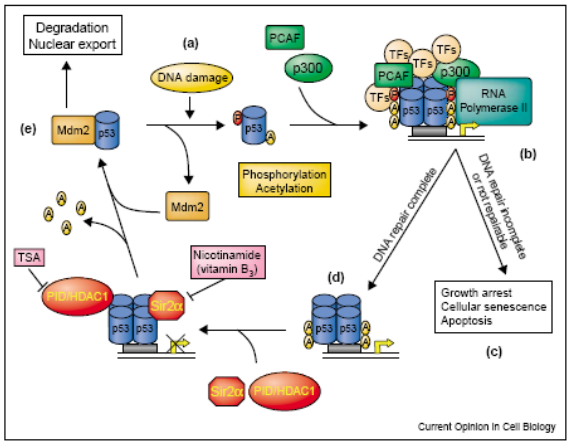

Figure 7. *Schematic representation (reproduced from ref. 34) of a mechanism for p53 transcriptional activation and, inherently, the changes in p53 function.*[34]

Another therapeutic strategy in p53 research is to reactivate and stabilize mutant[44] or inactive p53. Inhibition of p53 might be an interesting option to protect normal tissue from the harmful consequences of stroke or cancer treatment, because under those conditions p53 accumulates and activates in normal tissue,[45] being one of the reasons for neurodegeneration or the severe side effects observed with a conventional tumor therapy.[46] This can be done by small molecules, enzymes, or gene therapy.

To this aim, our proposal was to design a series of ligands able to interact with specific residues in the p53 tetramerization domain and consequently stabilize the

---

1999, *18*, 6455-6461.

[42] Gostissa, M.; Hengstermann, A.; Fogal, V.; Sandy, P.; Schwarz, S. E.; Scheffner, M.; Del Sal, G. *EMBO J.* **1999**, *18*, 6462-6471.

[43] Melchior, F.; Hengst, L. *Cell Cycle* **2002**, *1*, 245-249.

[44] Selivanova, G.; Kawasaki, T.; Ryabchenko, L.; Wiman, K. G. *Sem. Cancer Biol.* **1998**, *8*, 369-378.

[45] Lakkaraju, A.; Dubinsky, J. M.; Low, W. C.; Rahman, Y. E. *J. Biol. Chem.* **2001**, *276*, 32000-32007.

[46] Blagosklonny, M. V. *Int. J. Cancer* **2002**, *98*, 161-166.

structure of the whole protein, as p53 is only active as a tetramer.[47]

In addition, mutations in this domain can inactivate p53 preventing it to fold into the active form. One of these missense mutations takes places when Arg337 is replaced for histidine (R337H mutant) which prevents salt bridge formation between Asp352 and His337 when this residue is not protonated at lower physiological pH range.[48] As commented above, this interaction is crucial for the stability of the tetramer. In fact, this mutation has been linked to pediatric adrenal cortical carcinoma (ACC). Ribeiro and co-workers reported that in a localized population in southern Brazil, 97% of children that develop tumors in the adrenal gland harbor the p53-R337H mutation.[49] Stabilization of this mutated protein and, inherently, of the entire domain is one of the goals of our project.

[47] Chène, P. *Oncogene* **2001**, *20*, 2611-2617.

[48] DiGiammariono, E. L.; Lee, A. S.; Cadwell, C.; Zhang, W.; Bothner, B.; Ribeiro, R. C.; Zambetti, G.; Kriwacki, R. W. *Nat. Struct. Biol.* **2002**, *9*, 12-16.

[49] Ribeiro, R. C. Sandrini, F.; Figueiredo, B.; Zambetti, G. P.; Michalkiewicz, E.; Lafferty, A. R.; DeLacerda, L.; Rabin, M.; Cadwell, C.; Sampaio, G.; Cat, I.; Stratakis, C. A.; Sandrini, R. *Proc. Natl. Acad. Sci. USA* **2001**, *98*, 9330-9335.

1.2 Objectives. Designed Ligands for p53TD

1.2.1 Ligands Designed to Interact with p53TD

It has been reported by our laboratory and others that a bicyclic guanidinium[50,51] (Figure 8) binds with high affinity to carboxylates by ion-pairing and hydrogen bonding with both oxygen atoms of the carboxylate group. The guanidinium NH hydrogen atoms have defined *syn* directionality due to the bicyclic framework. This structural element also improves its solubility in apolar solvents, where hydrogen bonds are stronger.[52]

Hydrogen bonding is of a DD-AA type, which maximizes secondary interactions.[53] Transprotonation of the guanidinium-carboxylate would result in a non ionic, much weaker AD-DA guanidine-carboxylic acid interaction. However, transprotonation is unlikely, not only because of the weaker binding, but especially due to the large pK_a difference between the guanidinium and a carboxylic acid group (ΔpK_a *ca.* 9 in water).

[50] Echavarren, A. M.; Galán, A.; de Mendoza, J.; Salmerón, A.; Lehn, J.-M. *Helv. Chim. Acta* **1988**, *71*, 685-692.

[51] Kurzmeier, H.; Schmidtchen, F. P. *J. Org. Chem.* **1990**, *55*, 3749-3755.

[52] Blondeau, P.; Segura, M.; Pérez-Fernández, R.; de Mendoza, J. *Chem. Soc. Rev.* **2007**, *36*, 198-211.

[53] Jorgensen, W. L.; Pranata, J. *J. Am. Chem. Soc.* **1990**, *112*, 2008-2010.

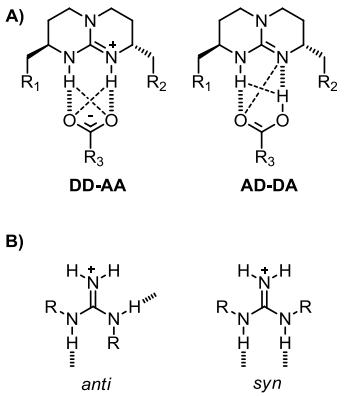

Figure 8. *A) Chiral bicyclic guanidinium receptor for carboxylate. B) Anti and syn conformations of guanidinium groups.*

Hydrogen-bonded salt bridges, such those involving guanidinium-carboxylate, are relevant contributors to α-helical stabilization and sometimes destabilization of peptides and proteins.[54] In fact, it has been demonstrated that bicyclic guanidinium oligomers can induce an increase of helicity to helical secondary protein structures with acidic residues at (*i, i+3*) distances and, consequently, enhance the stability of these helices.[55,56]

The sequence of one monomer of p53TD contains a highly conserved sequence of acidic residues (aspartic and glutamic acids) within *i+3* and *i+4* distances (Figure 9). Interaction studies with p53TD and symmetric tetraguanidinium oligomers were reported by our group, in collaboration with Prof. E. Giralt's group (IRB, Barcelona). An association constant K_a = 0.1 μM in 10% aqueous methanol and ^{1}H-^{15}N HSQC and STD NMR studies indicated that the tetraguanidinium ligand scrambled over the

[54] Luo, R.; David, L.; Hung, H.; Devaney, J.; Gilson, M. K. *J. Phys. Chem. B*, **1999**, *103*, 727-736.
[55] Peczuh, M. W.; Hamilton, A. D.; Sánchez-Quesada, J.; de Mendoza, J.; Haack, T.; Giralt, E. *J. Am. Chem. Soc.* **1997**, *119,* 9327-9328.
[56] Haack, T.; Peczuh, M. W.; Salvatella, X.; Sánchez-Quesada, J.; de Mendoza, J.;Hamilton, A. D.; Giralt, E. *J. Am. Chem. Soc.* **1999**, *121,* 11813-11820.

different positions of the six anionic residues of the helical patch.[57] Molecular dynamics simulations confirmed the different modes of binding between the tetracation and the hexaanionic patch.[58]

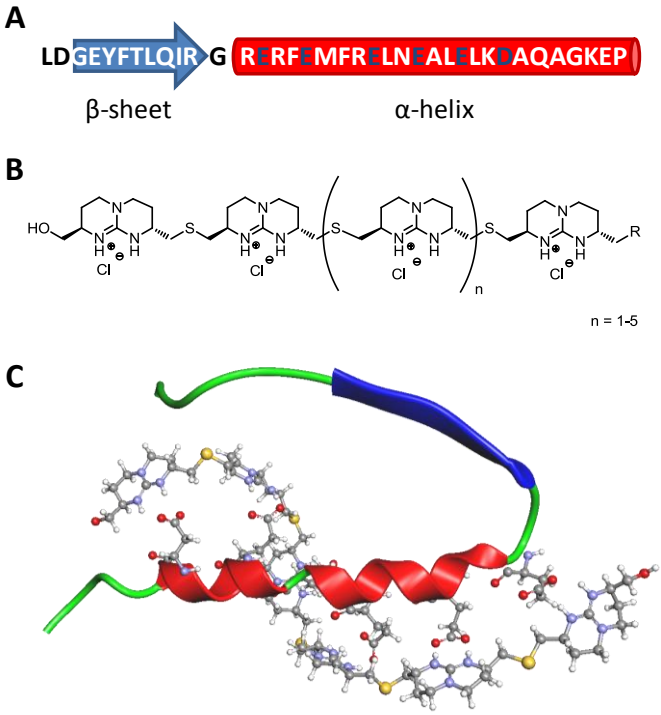

Figure 9. *(A) Monomer sequence; negative charged residues are depicted in blue. (B) General structure of oligoguanidinium ligands. (C) Molecular modeling of p53TD (ribbon representation) interacting with hexaguanidinium ligand (ball and stick display).*

Thus, a hexaguanidinium polycation might act as a perfect counterpart to match with the entire sequence (Figure 9C). Moreover, the interaction should be stronger by increasing the number of guanidinium-carboxylate salt bridges. Indeed, circular dicroism studies on the interaction between a polyglutamate and guanidinium

[57] Salvatella, X.; Martinell, M.; Gairí, M.; Mateu, M.; Feliz, M.; Hamilton, A. D.; de Mendoza, J.; Giralt, E. *Angew. Chem. Int. Ed.* **2004**, *43*, 196-198.

[58] Molecular dynamics calculations performed by E. Santos and C. Bo at the ICIQ.

oligomers of different lengths (Figure 10) were made in water at room temperature with hexafluorophosphate (PF_6^-) as counterion, revealing that a strong interaction occurs with the octamer (Figure 11).

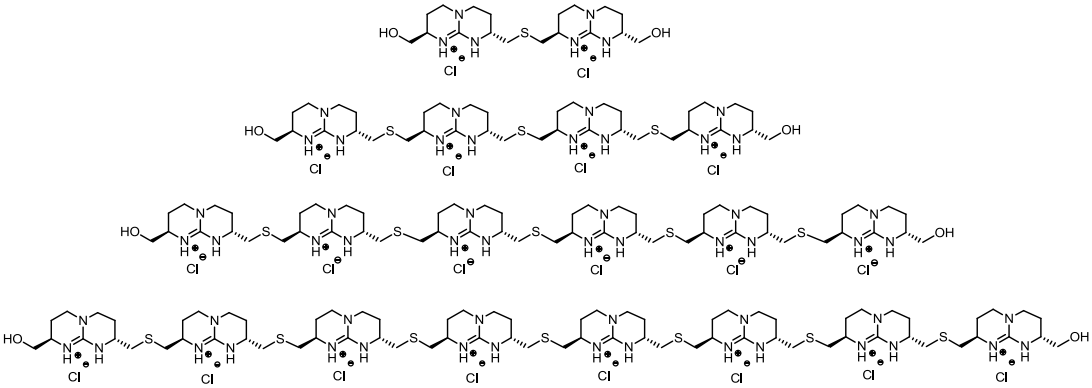

Figure 10. *Bicyclic guanidinium oligomers of different lengths.*

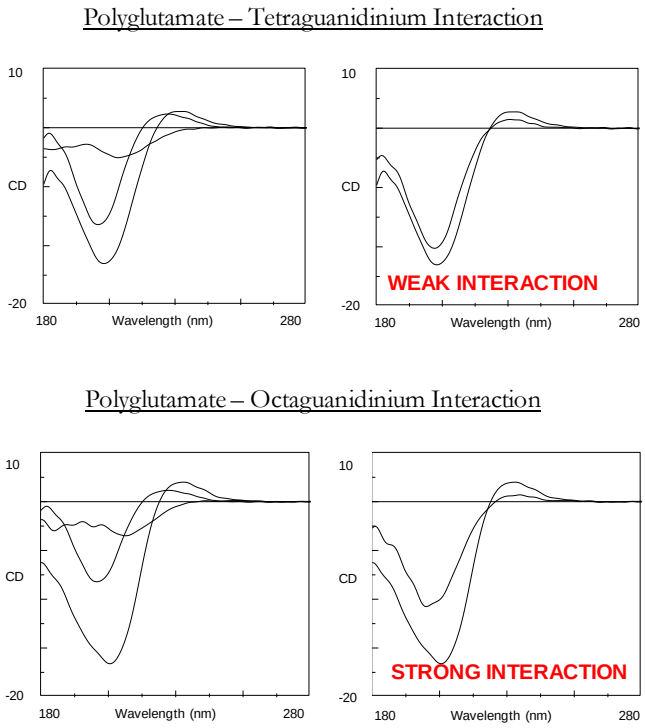

Figure 11. *Circular dichroism studies made by Giralt et al.*[59] *Left side curves represent the peptide, the guanidinium chain and the sum of both curves. The right side curves show the superposition of the addition curve with the experimental one.*

Therefore, we decided to synthesize and evaluate a series of new bicyclic guanidinium oligomers to get a deeper insight into the nature of the association with p53TD.

1.2.2 Theoretical Studies with the Hexaguanidinium and p53

To further understand the interaction between p53 and the guanidinium oligomers, computer modeling studies were done in collaboration with Dr. Eva Santos under the supervision of Prof. Carles Bo at the ICIQ. Molecular dynamics (MD) simulations with

[59] Salvatella, X.; Giralt, E.; Van Gool, M.; de Mendoza, J. *unpublished results.*

explicit water were performed on the following systems: (a) p53TD; (b) p53TD with four hexaguanidinium ligands, each of them bound to a monomer chain, to interact with residues E336, E339, E343, E346, E349, D352; (c) p53TD-R337H mutant; (d) p53TD-R337H mutant with four hexaguanidinium ligands located as in (b). Simulations (c) and (d) were carried out at 300K and 400K. This high temperature was applied to stress structural changes of the mutant protein at a reasonable time scale.

The relative stability of the protein was assessed by the dynamic analysis of the backbone's root mean square deviation (RMSD), as a measure of the inherent stability of the protein, along a 10 ns trajectory. This enables to evaluate the conformational stability of the protein. Typically, an increase of RMSD at the end of the trajectory means that the protein has not reached its most stable conformation. On the other hand, high RMSD values (beyond 2.5-3 Å) indicate significant deviations with respect to the initial structure.

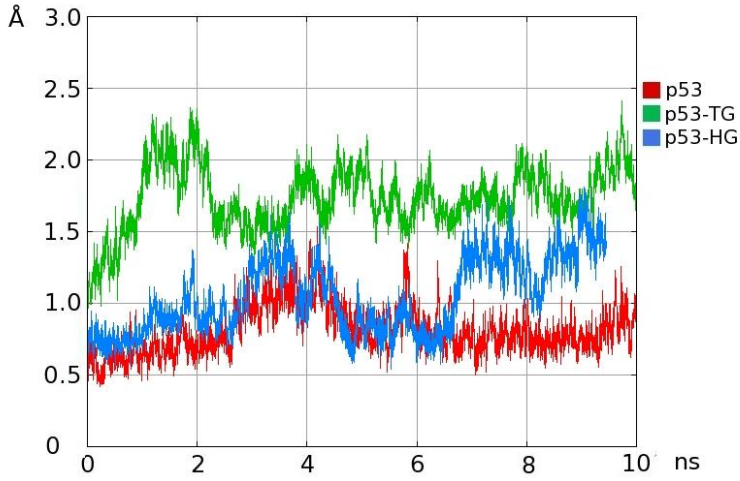

Figure 12. *RMSD vs. time curves of p53TD wild type, with and without ligands (TG = Tetraguanidinium, HG = Hexaguanidinium). MDs with explicit water calculations were made using Gromacs program, Amber94 force field, and a total time of 10 ns at 300K. Initial p53TD structure coordinates were taken from PDB: 1AIE.*

Figure 12 shows the curves for the p53TD (wild type) and the protein domain docked with tetraguanidinium (TG) and hexaguanidinium (HG) ligands. Starting from Glu336 (in the docking site), the RMSD value is lower in the presence of HG (in blue, RMSD < 1.5 Å) than of TG (in green). In both cases, the structure of the protein remains similar to the initial one suggesting that the conformation is not substantially disturbed by the ligands, although oscillations are stronger in the presence of tetraguanidinium. Nevertheless, all guanidinium-carboxylate interactions present in the initial system were progressively lost. At 4 ns, only half of the interactions remained and the complex continued losing protein-ligand interactions.

Molecular dynamics performed on the less stable mutant R337H showed an increased RMSD of the protein backbone relative to the wild-type structure, thus meaning a destabilization effect (Figure 13). As expected, the RMSD value of the mutant at 300 K (red line) was lower than at 400 K (green line), a temperature at which the protein thermally unfolds. At this high temperature a significant stabilizing effect of the hexaguanidinium ligands becomes evident (purple line).

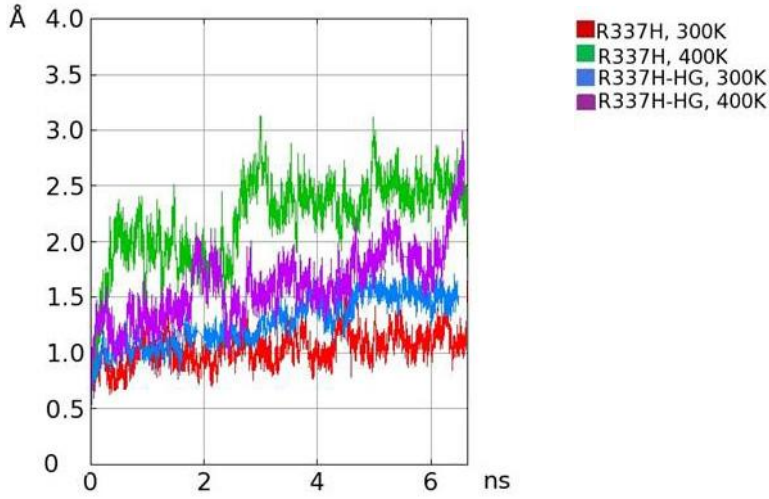

Figure 13. *RMSD vs. time curves of p53TD-R337H mutant, with and without hexaguanidinium ligand at different temperatures. MDs with explicit water; calculations were made using Gromacs program, Amber94 force field, and a total time of 6.5 ns.*

Simulations also revealed a successive loss of guanidinium-carboxylate interactions along the 6.5 ns trajectory. Thus, the initial protein-ligand complex did not reach stability during the whole trajectory. At 3 ns half of the interactions had already been lost. After 5 ns the RMSD of the mutant protein remained similar to the wild type one (Figure 14), although two hexaguanidines were not complexing and the other two were interacting through a new anionic patch between two different chains of the tetramerization domain with three and four anchorage points, respectively.

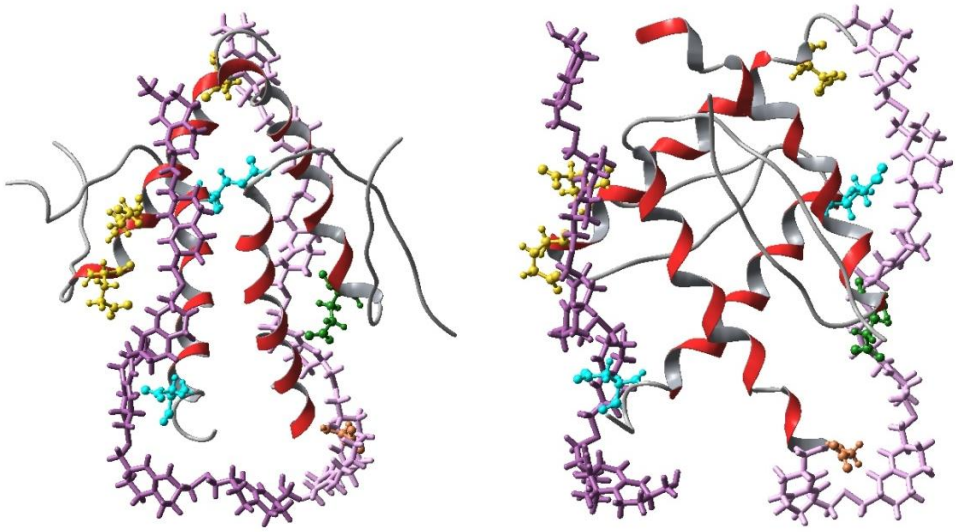

Figure 14. *Three-dimensional structures of p53TD-R337H mutant with hexaguanidinium ligand at 5 ns (Maestro program).*

In conclusion, the initial complex structures here considered turned out to be not stable. However, molecular dynamics show that guanidinium-carboxylate interactions of this nature can be effective in stabilizing the p53-R337H tetramer, which stress out the importance of testing ligands based on guanidinium moieties. Additional simulations are required, considering alternative stoichiometries (as 1:2 protein:ligand) and a correct arrangement of the ligands to reach more stable p53TD-HG complex structures.

1.3 Synthesis of Ligands for p53

1.3.1 Synthetic Attempts to Hexaguanidinium Oligomers

For the synthesis of hexaguanidinium ligand **15**, two different routes were explored.

The first one is based on the coupling of two non-symmetric monoprotected diguanidinium moieties on a central symmetric diguanidine. The reaction requires a nucleophilic attack of a thiol – formed from a thioacetate in the presence of cesium carbonate – on a mesylate leaving group, to generate the corresponding thioether. Within this route (2+2+2 path, Scheme 1), two different approaches were investigated:

1) Use the symmetric moiety as the electrophile.
2) Use the symmetric moiety as the nucleophile.

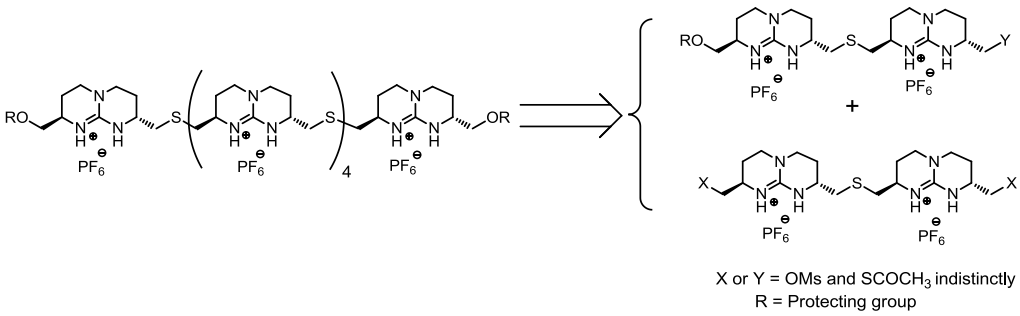

Scheme 1. *Retrosynthetic scheme of the symmetric (2+2+2) methodology.*

The second proposed synthetic route (4+2 path, Scheme 2) is based on the generation of the tetraguanidinium non-symmetric species, one-side protected with a TBDPS group and with a mesylate group on the other end, to allow the coupling with a thiol (from a thioacetate precursor) in one of the arms of a diguanidinium moiety which carries the protective TBDPS group in the other one.

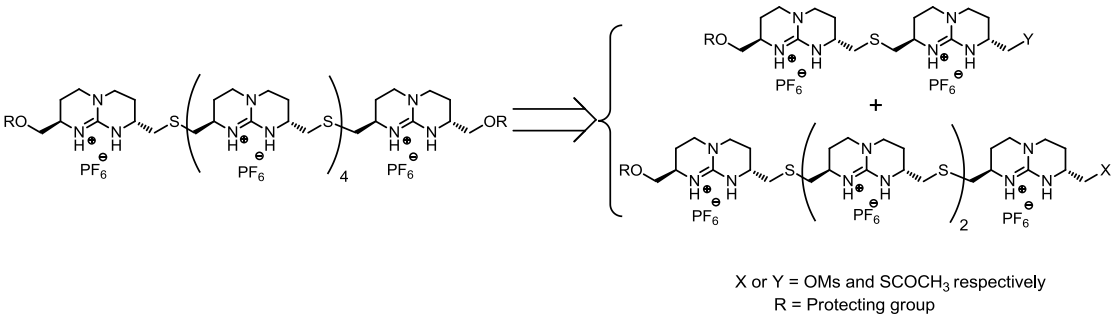

Scheme 2. *Retrosynthetic scheme of the non-symmetric (4+2) methodology.*

1.3.2 Synthesis of the Intermediates

Bicyclic guanidine **1** is the precursor for the synthesis of these oligomers. This compound was obtained on a multi-gram scale following the methodology described by Schmidtchen[51] and improved in our group at a multigram scale.[60] As precursors, D-asparagine and D-methionine were used, giving rise to the *R,R* enantiomer in nine steps with a 46% overall yield (Scheme 3).

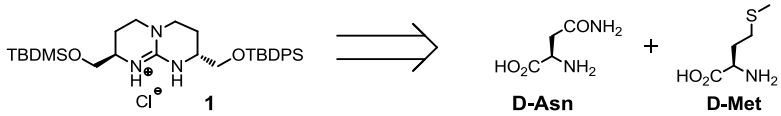

Scheme 3. *Retrosynthetic pathway for the preparation of* ***1****.*

The symmetric diguanidinium scaffold was synthesized using the methodology described in Scheme 4. First, the selective deprotection of the TBDMS group of **1** was performed, followed by activation of the corresponding alcohol as a methanosulfonate (mesylate) to generate a good leaving group. Then, reaction of a thioacetate group in the presence of a base leads to the formation of a nucleophilic thiolate, which reacts

[60] Sánchez-Quesada, J. *PhD Thesis*, Universidad Autónoma de Madrid, **1996**.

with compound **2** to give the symmetric diguanidinium molecule **4** with a thioether link. Deprotection of the TBDPS group takes place in good yields, generating a diol which was activated again as mesylate **6**. The mesylates were then replaced by thioacetates, to generate the corresponding thiolates, yielding compound **7**.

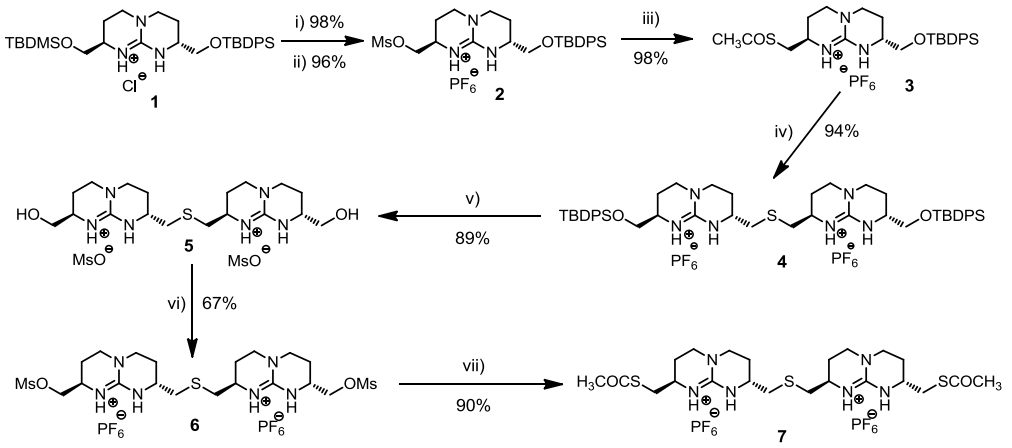

Scheme 4. *Synthesis of symmetric diguanidinium molecules. Conditions: i) H_2O, AcOH, THF; ii) Ms_2O, NMM, THF; iii) $KSCOCH_3$, THF/H_2O, reflux; iv) 1 eq.* ***2****, 2.5 eq. Cs_2CO_3, ACN/MeOH, v) 15 eq. MsOH, THF/H_2O, reflux; vi) Ms_2O, NMM, in dry CH_2Cl_2; vii) 7.5 eq. $KSCOCH_3$, MW, 140ºC, 15 min. ACN.*

Synthesis of non-symmetric diguanidinium compounds **10** and **11** is depicted in Scheme 5. Starting from compound **2** the corresponding disulfide **8** was formed. The disulfide bond was cleaved by reduction, generating the subsequent thiol which attacked mesylate **2**. As a result, the asymmetric guanidinium **9** was formed in good yield. The activation of the alcohol to the mesylate (**10**) and subsequent thioacetylation provided the nucleophilic precursor **11**.

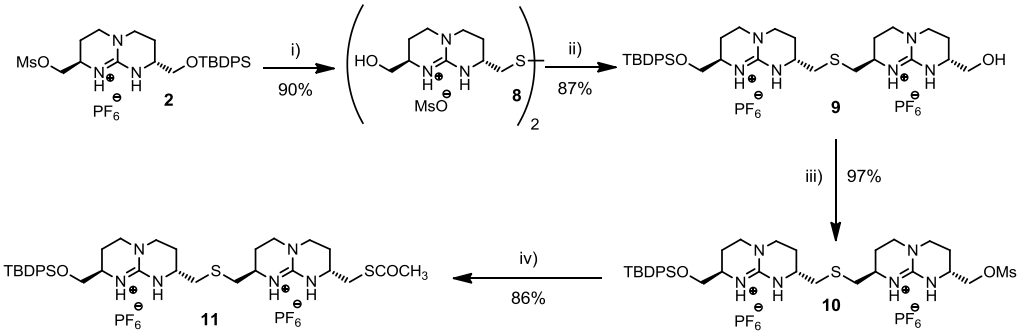

Scheme 5. *Synthesis of non-symmetric diguanidinium compounds. Conditions: i) $KSCOCH_3$, THF/H_2O, reflux; MsOH, THF/H_2O, reflux; ii)* ***2****, (^{t}Bu)$_2$PhP polystyrene, Cs_2CO_3, MeOH; iii) Ms_2O, NMM, THF; iv) $KSCOCH_3$, ACN, MW 140 ºC, 10 min.*

1.3.3 Synthesis of the Symmetric Tetraguanidinium Oligomer

In order to check the non-symmetric approach, the synthesis of model tetraguanidinium **12** was undertaken (Scheme 6).[61,62]

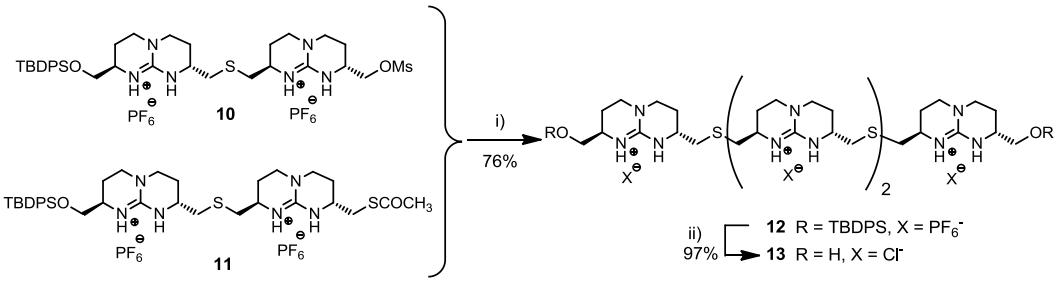

Scheme 6. *Synthesis of tetraguanidinium* ***12*** *and* ***13****. Conditions: i) 2.5 eq. Cs_2CO_3, (^{t}Bu)$_2$PhP polystyrene, ACN/MeOH; ii) ACN/3N HCl*

The nucleophilic attack of the thiol derivative on the activated methanesulfonate compound **10** produced tetraguanidine **12** in a 76% yield. Cleavage of the TBDPS

[61] Fernández-Carneado, J.; Van Gool, M.; Martos, V.; Castel, S.; Prados, P.; de Mendoza, J.; Giralt, E. *J. Am. Chem. Soc.* **2005**, *127*, 869-874.

[62] Pérez Fernández, R. *PhD Thesis*, Universidad Autónoma de Madrid, **2005**.

groups generated ligand **13** (Scheme 6).

This synthesis also provided additional amounts of this ligand to complete the reference binding studies with p53TD protein.

1.3.4 Synthesis of the Hexaguanidinium Oligomer

Despite its apparent simplicity, the formation of oligoguanidines linked by thioether bridges is not trivial. Although a thiolate is a quite reactive nucleophile, it easily oxidizes to the corresponding disulfide. Hence, the coupling reaction to generate the thioether link must be done under an inert atmosphere and in the presence of a reduction reagent, such as a phosphine.

Another key aspect in the synthesis is the decrease of reactivity as the length of the chain grows, likely due to the increasing steric hindrance, higher conformational flexibility, and polycationic nature of the higher oligomers.

As mentioned before, two approaches were followed. At first sight, the (2+2+2) symmetric route looks simpler and more convergent than the non-symmetric one. In addition, fewer steps are necessary.

However, the (4+2) non-symmetric approach, requiring the preparation of more complex structures such as non-symmetric tetraguanidinium compounds, was nevertheless pursued owing to the expected higher yields of the individual steps.[61,62]

1.3.4.1 Symmetric Approach

The first attempt using this methodology was performed with one equivalent of the bis-thioacetyl diguanidinium molecule **7** in the presence of 2.2 eq. of mesyl non-symmetric diguanidinium **10**, as it is shown in Scheme 7.

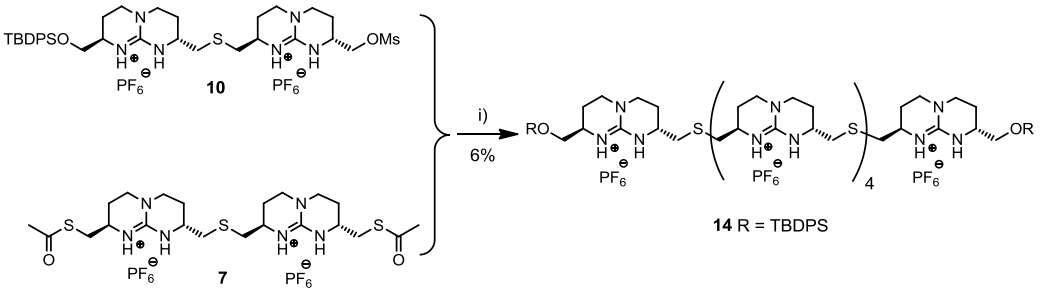

Scheme 7. *First attempt towards the hexaguanidinium oligomer using the symmetric approach. Conditions: i) 5 eq. Cs_2CO_3, ACN/MeOH, (^{t}Bu)$_2$PhP polystyrene, semi-preparative HPLC purification.*

HPLC-mass spectra showed that a small amount of the desired compound was present in the reaction crude. The product was isolated by semi-preparative HPLC, affording hexaguanidinium oligomer **14** in a modest 6% yield.

Owing to the low yield, another attempt was made, now using the dimesylated diguanidinium derivative and 2.2 eq. of the thioacetyl-containing non-symmetric one **11** (Scheme 8).

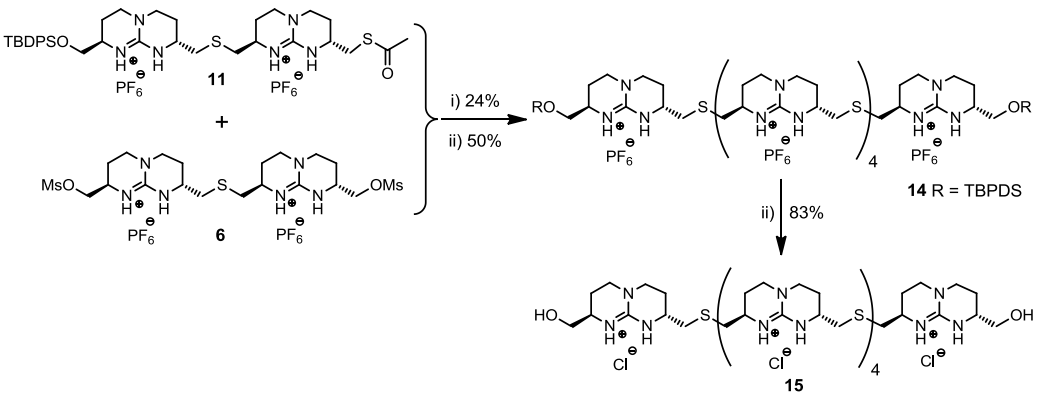

Scheme 8. *Second attempt towards the hexaguanidinium ligand using the symmetric approach. Conditions: i) 5 eq. Cs_2CO_3, ACN/MeOH, (^{t}Bu)$_2$PhP polystyrene; ii) Semi-prep. HPLC purification; iii) ACN/3N HCl.*

In this case, using similar reaction conditions as beforehand described, an overall yield of 10% was reached for the hexaguanidinium compound **15**. Likely, this increase in yield could be attributable to the relative stability of the thiol species formed during the reaction. In the initial attempt, a diguanidinium dithiol generated was able to partially oxidize giving rise to guanidinium oligomers and polymers linked by disulfide bridges. On the contrary, a single thiol function has less chance to get into intermolecular disulfide formation or polymerization.

Purification of the protected hexaguanidinium **14** was carried out on a silica PF_6^- chromatography column in a 24% yield. Although analytical chromatography did not reveal substantial impurities, only 50% of the initially isolated final product was recovered after semi-preparative HPLC purification.

Moreover, only 90% purity was reached after HPLC purification, due to the difficulty of separating the product from by-products. Subsequently, TBDPS cleavage afforded ligand **15** in 83% yield. The compound was pure enough, indeed, to perform some preliminary NMR binding studies with the p53 tetramerization domain.

1.3.4.2 Non-symmetric Approach

This synthetic strategy was attempted to improve the yields obtained in the symmetric route. The coupling between one tetraguanidinium and one diguanidinium should be more efficient than the coupling in the symmetric route, as it is based on a single reactive point.

The synthesis of the non-symmetrical tetraguanidinium was developed following the path shown in Scheme 9.

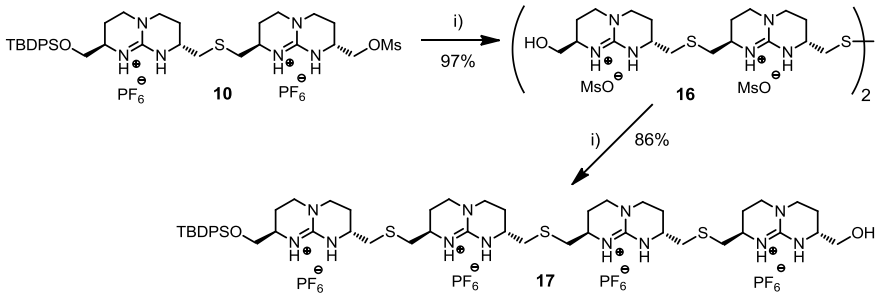

Scheme 9. *Non-symmetric synthesis of tetraguanidinium* ***17****. Conditions: i) $KSCOCH_3$, THF/H_2O, reflux; MsOH, THF/H_2O, reflux; ii)* ***10****, $(^tBu)_2PhP$ polystyrene, Cs_2CO_3, ACN/MeOH.*

The deprotected tetraguanidinium disulfide **16** was generated from compound **10**, and tetraguanidinium **17** was generated by reduction and subsequent nucleophilic attack of the diguanidinium thiol on **10**.

Subsequent activation of the alcohol as the mesylate intermediate took place in good yields and the coupling reaction between the non-symmetric diguanidinium **11** and **18** produced the symmetric protected hexaguanidinium in good yield (57%) (Scheme 10). Cleavage of the silyl groups under acidic conditions and purification by semi-preparative HPLC completed the synthesis of this ligand (93% purity). As a result of carrying out the purification after deprotection, an extra-step was necessary (ion-exchange column) to restore the chloride counterion, since the mobile phase used contains some trifluoroacetic acid to ensure the protonation of the guanidinium groups and to facilitate the isolation.

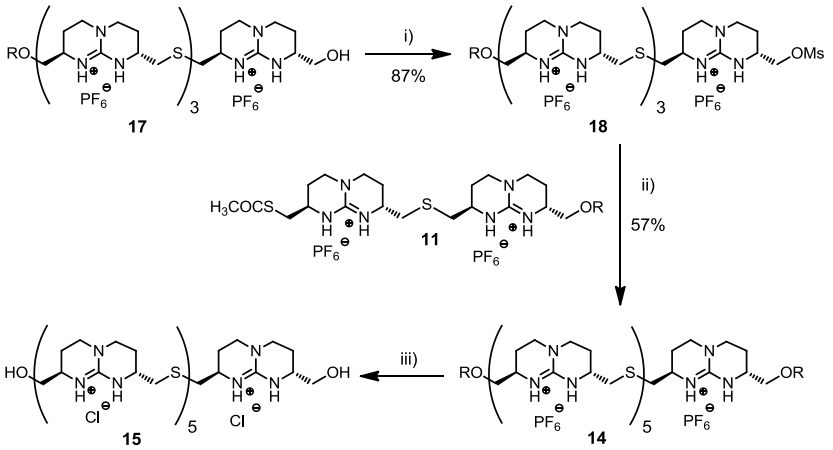

Scheme 10. *Non-symmetric synthesis of hexaguanidinium* ***15****. R = TBDPS. Conditions: i) dry* CH_2Cl_2*,* Ms_2O*, NMM; ii) (*^{t}*Bu)*$_2$*PhP polystyrene,* Cs_2CO_3*, MeOH iii) ACN/3N HCl.*

1.3.5 New Oligoguanidinium Compounds

New ligands were designed for protein p53TD surface recognition to better understand the position and orientation of the guanidinium residues in the protein surface, as well as their interaction features or stabilization/destabilization properties. Also, we wished to improve the association of these oligoguanidinium polycations with p53TD by introducing groups at the ends of the chain capable of altering its interaction mode.

Inspection of the three-dimensional structure of the tetramerization domain complexed with our oligoguanidines revealed that Asp352 is buried into the tetramer and therefore significantly less accessible than the remaining carboxylates (glutamates). In addition, as mentioned above, this residue forms a stabilizing salt bridge with Arg337.[63] Hence, removing or weakening this interaction could result in destabilization of the whole tetramer, thus justifying that the pentaguanidinium molecule **20** (Figure 15) might fit better in the helical patch of the protein.

[63] (a) Galea, C.; Bowman, P.; Kriwacki, R. *Prot. Sci.* **2005**, *14*, 2993-3003. (b) Bosshard, H. R.; Marti, D. N.; Jelesarov, I. *J. Mol. Recognit.* **2004**, *17*, 1-16.

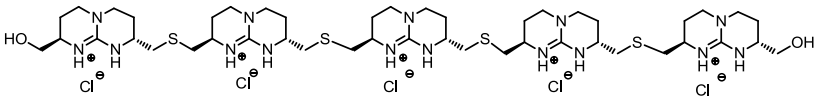

20

Figure 15. *Pentaguanidinium molecule* ***20****.*

Alternatively, functionalization of these polycationic molecules with aromatic groups such as naphthylmethyl and benzyl (molecules **28** and **35**, respectively, Figure 16) should provoke a preferred orientation of the ligand in allowing further contacts with the hydrophobic hairpin pocket of the domain (composed by residues Ile332, Phe338, Met340 and Phe341). These additional interactions would likely improve the binding and therefore stabilize the complex.

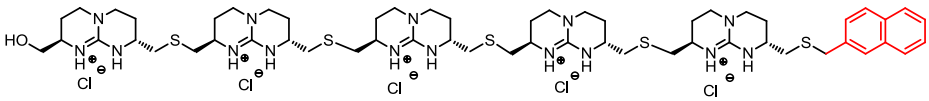

28

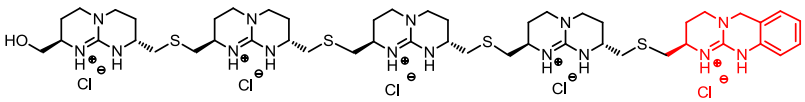

35

Figure 16. *Naphthylmethyl pentaguanidinium derivative* ***28*** *and pentaguanidinium* ***35****.*

Pentaguanidinium compound **35** bearing a terminal benzoguanidinium should show major avidity for p53TD due to the increased acidity of the benzoguanidinium protons.[64]

From the point of view of protein stabilization, the designed ligands should be able to embrace different monomers bringing them together and thus favoring

[64] Ratel, F. *DEA Report*, Universidad Autónoma de Madrid, **2005**.

tetramerization of the domain.[65] It is likely that the extended polycationic octaguanidinium ligand **38** (Figure 17), could interact simultaneously with more than one monomer in order to satisfy its complementary charge requirements.

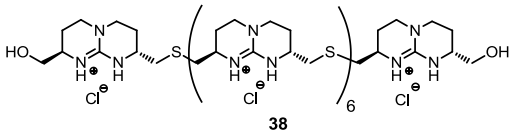

Figure 17. *Octaguanidinium compound* ***38****.*

Thus, the study of this complexation would bring into play the design of new highly multivalent ligands able to bind and stabilize different monomers or even consecutive domains of p53.

1.3.5.1 Synthesis of the Pentaguanidinium Oligomer 20

The synthesis of this new oligoguanidinium compound was performed following the non-symmetric (4+1) approach, since all starting compounds were already available (Scheme 11).

[65] (a) Gordo, S.; Martos, V.; Santos, E.; Menéndez, M.; Bo, C.; Giralt, E.; de Mendoza, J. *Proc. Nat. Acad. Sci.* **2008**, *105*, 16426-16431. (b) Gordo, S.; Martos, V.; Vilaseca, M.; Menéndez, M.; de Mendoza, J.; Giralt, E. *Chem. Asian J.* **2011**, *6*, 1463-1469.

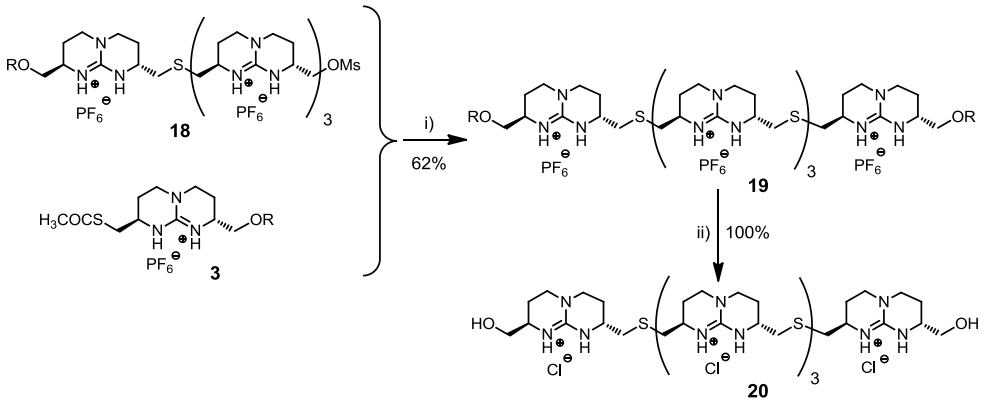

Scheme 11. *Synthesis of pentaguanidinium compound* ***20****. R=TBDPS. Conditions: i) (^{t}Bu)$_2$PhP polystyrene, Cs_2CO_3, ACN/MeOH; ii) ACN/3N HCl.*

Coupling of the activated methanesulfonate tetraguanidinium compound **18** with the monoguanidinium thioether **3**, yielded pentaguanidinium **19** in 62% yield after purification (Scheme 11). Cleavage of the R (TBDPS) groups gave rise to **20** quantitatively.

1.3.5.2 Synthesis of the Naphthylmethylpentaguanidinium Compound 28

To synthesize pentaguanidinium **28** *via* the non-symmetric approach, it was first necessary to prepare a guanidinium monomer with a naphthylmethyl group on one side and a reactive function on the other. To achieve this goal, the synthetic pathway shown in Scheme 12 was attempted.

Scheme 12. *First attempt towards methylnaphthalene monoguanidinium* ***21****. Conditions: i) (^{t}Bu)$_2$PhP polystyrene, Cs_2CO_3, ACN/MeOH; reflux.*

However, direct coupling of 2-(bromomethyl)naphthalene with guanidinium **3** was not successful because of the low reactivity of the aromatic species, even though the bromide is in a benzylic position.

Alternatively, the thioacetyl derivative **22** was prepared to improve the process (Scheme 13). The nucleophilic attack of this aromatic moiety with the monoguanidinium methanesulfonate derivative **2**, provided guanidinium **21** in a 72% yield. The reaction works well even without using the phosphine as a reducing agent, just keeping the inert atmosphere to avoid disulfide formation.

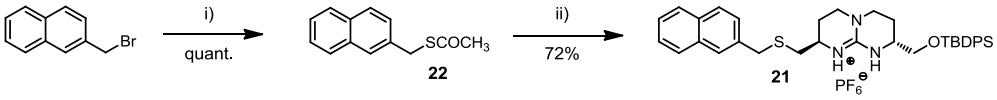

Scheme 13. *Second attempt towards methylnaphthalene monoguanidinium **21**. Conditions: i) $KSCOCH_3$, ACN, reflux; ii) **2**, Cs_2CO_3, MeOH/ACN.*

With compound **21** in hand, we focused at generating a reactive point to connect this molecule to a tetraguanidinium moiety to produce pentamer **28**. Firstly, cleavage of **21** was performed in the presence of hydrochloric acid to afford the corresponding alcohol **23**, which was activated as the chloride derivative **24**, since activation as a mesylate was not possible due to the presence of chloride anions that usually interfer in similar reactions with bicyclic guanidines. Unfortunately, thioacetylation of **24** did not occur so another synthetic route was developed. Thus, cleavage of **21** was carried out in the presence of methanesulfonic acid, generating an alcohol with mesylate as the counter ion. Formation of methanosulfonate **25** was achieved in an 87% yield. Finally, refluxing **25** with potassium thioacetate in acetonitrile yielded compound **26** (Scheme 14).

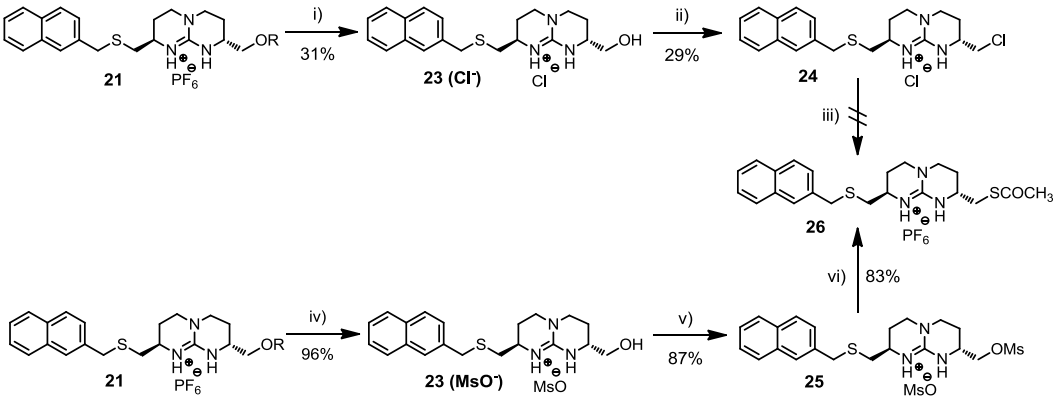

Scheme 14. *Synthetic pathways for compound* ***26****. R=TBDPS. Conditions: i) ACN/3N HCl; ii) thionyl chloride, DCM, reflux; iii) KSCOCH$_3$, ACN, reflux; iv) MsOH, reflux; v) Ms$_2$O, NMM, THF; vi) KSCOCH$_3$, ACN, reflux.*

Using again the (4+1) approach (Scheme 15), pentaguanidinium **27** was synthesized in a 71% yield, after which acidic conditions are required to obtain the related deprotected product **28**.

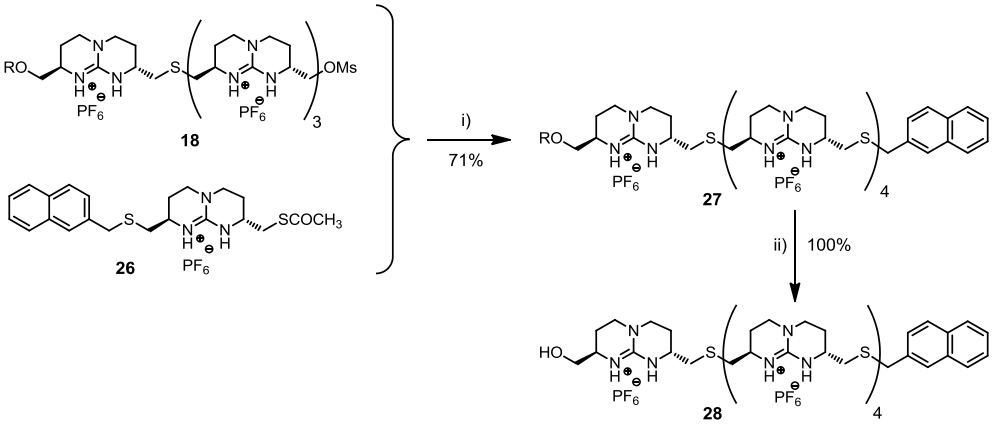

Scheme 15. *Synthesis of compound* ***28****. R=TBDPS. Conditions: i) (^{n}Bu)$_2$PhP polystyrene, Cs$_2$CO$_3$, ACN/MeOH; ii) ACN/3N HCl.*

1.3.5.3 Synthesis of Pentaguanidinium with a Benzoguanidinium (35)

For the formation of this oligomer, first benzoguanidinium **30** had to be prepared. This was done by the route outlined in Scheme 16, firstly developed in our group by Dr. Frédéric Ratel.

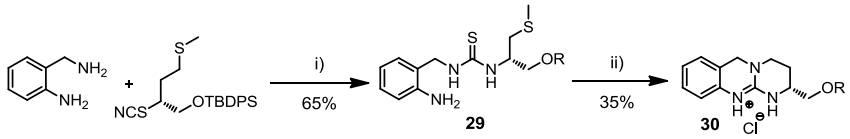

Scheme 16. *Synthesis of benzoguanidinium* ***30****.*[64] *R=TBDPS. Conditions: i) ACN, 3 days, r.t.; ii) MeOTf, DIPEA,* CH_2Cl_2*.*

Initially, 2-aminobenzylamine was reacted with the isothiocianate of the methionine derivative (a key intermediate in the synthesis of bicyclic guanidines), yielding thiourea **29**. Treatment of this compound with methyl triflate leads to methylation of both sulfur atoms, allowing the nucleophilic attack of the amines and the expected cyclization in the presence of DIPEA. Consequently, benzoguanidinium **30** was satisfactorily obtained by this procedure.

By cleaving the protective TBDPS group, the corresponding alcohol was formed and subsequently activated as a methanosulfonate derivative. Thioacetylation and coupling of this benzoguanidinium (**33**) to mesylated tetraguanidinium **18** afforded **35** as depicted in Scheme 17.

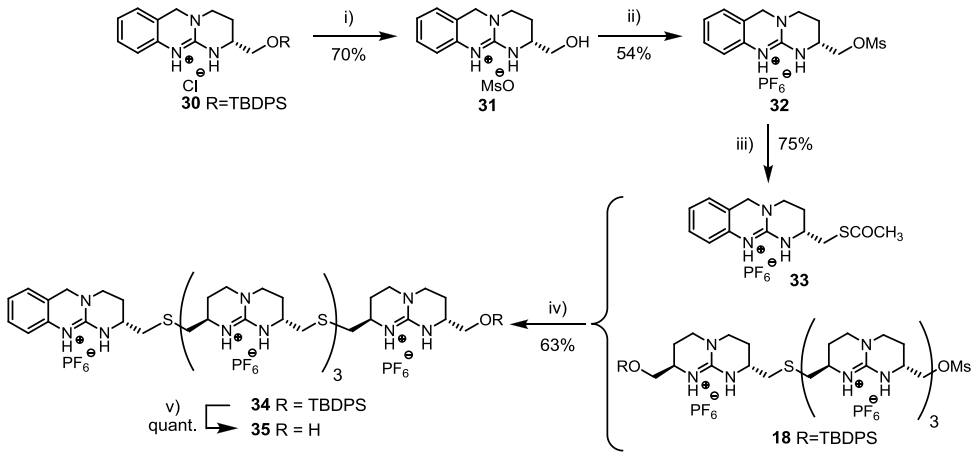

Scheme 17. *Synthesis of compound **35**. R=TBDPS. Conditions: i) MsOH, reflux; ii) NMM, Ms_2O; iii) ACN, $KSCOCH_3$, reflux; iv) Cs_2CO_3, (^{t}Bu)$_2$PhP polystyrene, ACN/MeOH; v) ACN/3N HCl.*

1.3.5.4 Synthesis of Octaguanidinium Compound 38

Following this synthetic methodology, octaguanidinium compound **38** was successfully prepared in 65% yield from tetramer **18** as described in Scheme 18.

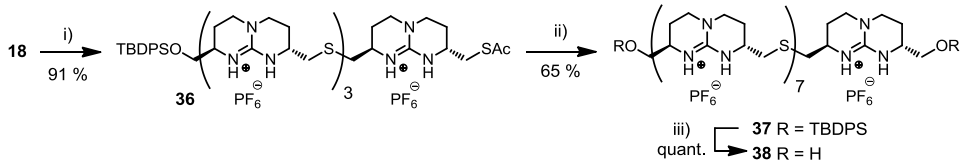

Scheme 18. *Synthesis of oligoguanidinium derivative **38**. Conditions: i) $KSCOCH_3$, ACN, reflux; ii) **18**, Cs_2CO_3, (^{t}Bu)$_2$PhP polystyrene, ACN/MeOH; iii) ACN/3N HCl.*

Deprotection of compound **37** in acidic media quantitavely afforded ligand **38**.

With these compounds in hand, we aimed to study their binding behavior in the presence of the tetramerization domain of p53. This work was performed in collaboration with Dr. Susana Gordo under the supervision of Prof. Ernest Giralt (IRB Barcelona).

1.4 NMR Binding Studies

The effect of the oligoguanidinium ligands on the amino acid sequence of p53 tetramerization domain was preliminary evaluated by NMR.[66] A ^{15}N-enriched sample of p53 tetramerization domain was titrated with ligands **13**, **15**, **20**, **28**, **35** and **38** and the titration was monitored by [^{1}H,^{15}N]-HSQC. These experiments were made with 0, 2 and 4 equivalents of each ligand with respect of monomer, for both the wild type and R337H mutant of p53TD.

As earlier reported,[57] binding of ligand **13** to the surface of p53TD causes significant changes in the ^{1}H and ^{15}N chemical shifts of some protein residues (Figure 19).

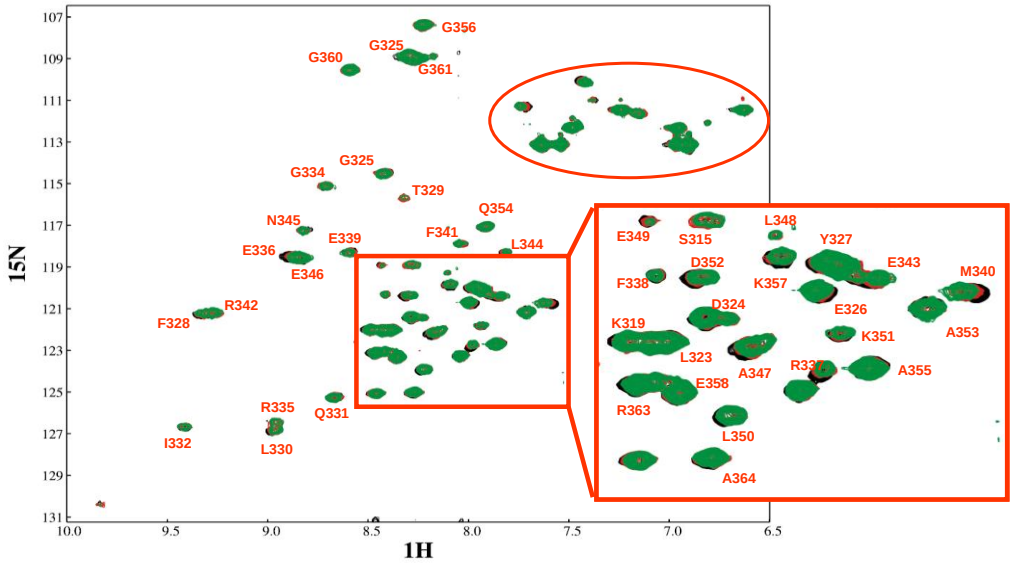

Figure 19. *[^{1}H,^{15}N]-HSQC spectrum of p53TD in the absence (black contours) and in the presence (red and green contours) of ligand* ***13*** *(2 and 4 eq, respectively). Signals in the [^{1}H, ^{15}N]-HSQC spectrum were assigned by ^{13}C-NMR.*

[66] Work performed by Dr. S. Gordo and Prof. E. Giralt at Parc Científic of Barcelona.

As expected, amino acids pertaining to the anionic patch are affected by the presence of the ligand. Nearby residues also experiment significant changes. The fact that a tetraguanidinium ligand affects all the six carboxylic amino acids in the sequence could be interpreted by scrambling of the ligand along the anionic patch.

For ligands **15**, **20**, and **35** the [^{1}H,^{15}N]-HSQC spectra were similar to the tetraguanidinium ligand **13** (Table 1). Ligand **28** produced relevant changes (Table 1), not only on the anionic patch but also on hydrophobic residues defining the hairpin pocket, accounting for the proximity of the aromatic naphthylmethyl moiety to the hairpin. Docking ligand **28** into the surface of a computer model of p53TD (Figure 20) showed that the naphthalene ring nicely fits between Arg337 and Met340, two of the most shifted amino acids in the sequence as shown in the chemical shift perturbation (CSP) plot (Table 1). Phe341 is also in close contact with the naphthalene group, interacting by π-stacking. Indeed, the strong chemical shift observed for these residues can be explained by a stable and robust interaction and by the anisotropic effect caused by the aromatic moiety. This proposed mode of binding justifies that Asp352 is affected by the ligand as one of its terminal bicyclic guanidines forms a salt bridge with this residue. On the contrary, chemical shift perturbation of Glu336 is probably influenced by the proximity of the aromatic naphthalene ring and not by the binding with a guanidinium moiety.

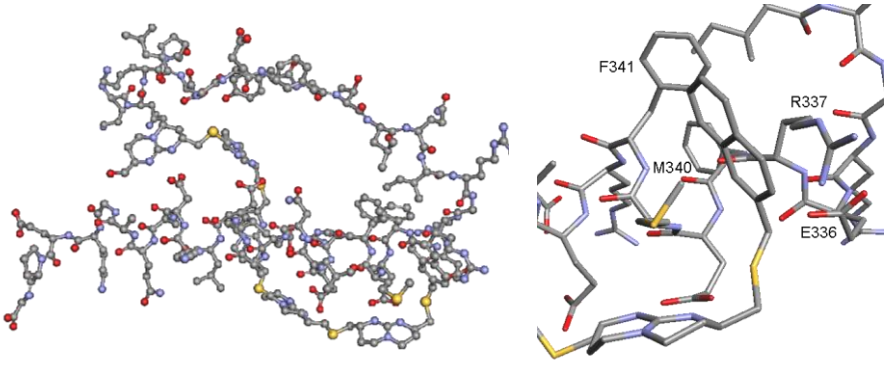

Figure 20. *(Left) Molecular modeling showing ligand* ***28*** *interacting with a monomer of p53TD. (Right) Detailed view of the contact between the naphthalene moiety and the hydrophobic pocket of the monomer.*

Octaguanidinium ligand **38** showed new chemical shifts accounting for the interaction with residues at the end of the α-helix (Leu350, Asp352 and Ala355), although several amino acids along the whole sequence were strongly affected by the presence of this ligand. This points out to an alternative mode of association where this molecule probably interacts with different monomers of the tetramerization domain in order to satisfy its charge complementarity and maximize the number of contacts with the protein.

Table 1. *[^{1}H, ^{15}N]-HSQC signals for the p53TD most representative chemical shifts in the presence of ligands* **13**, **15**, **20**, **28**, **35** and **38** *(for color codes, see Figure 19). CSP plots of the protein-ligand interaction are also attached for clarity.*

Ligand	Representative *[^{1}H, ^{15}N]-HSQC signals*			Chemical shift mapping
13	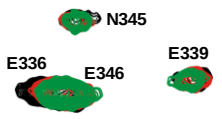	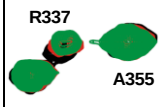	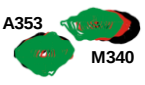	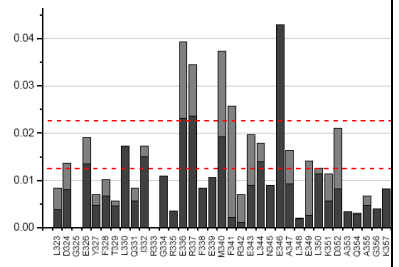
15	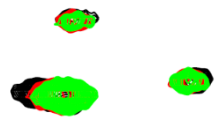	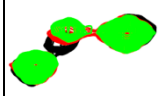	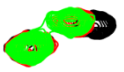	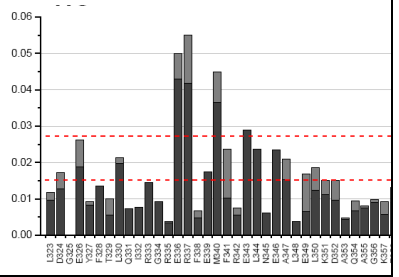
20	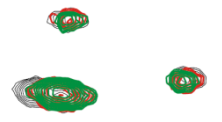	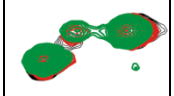	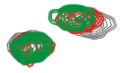	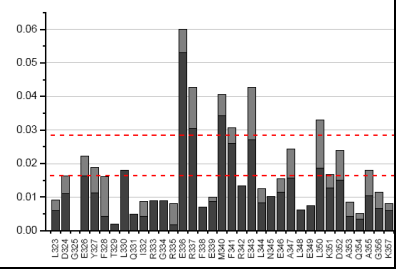

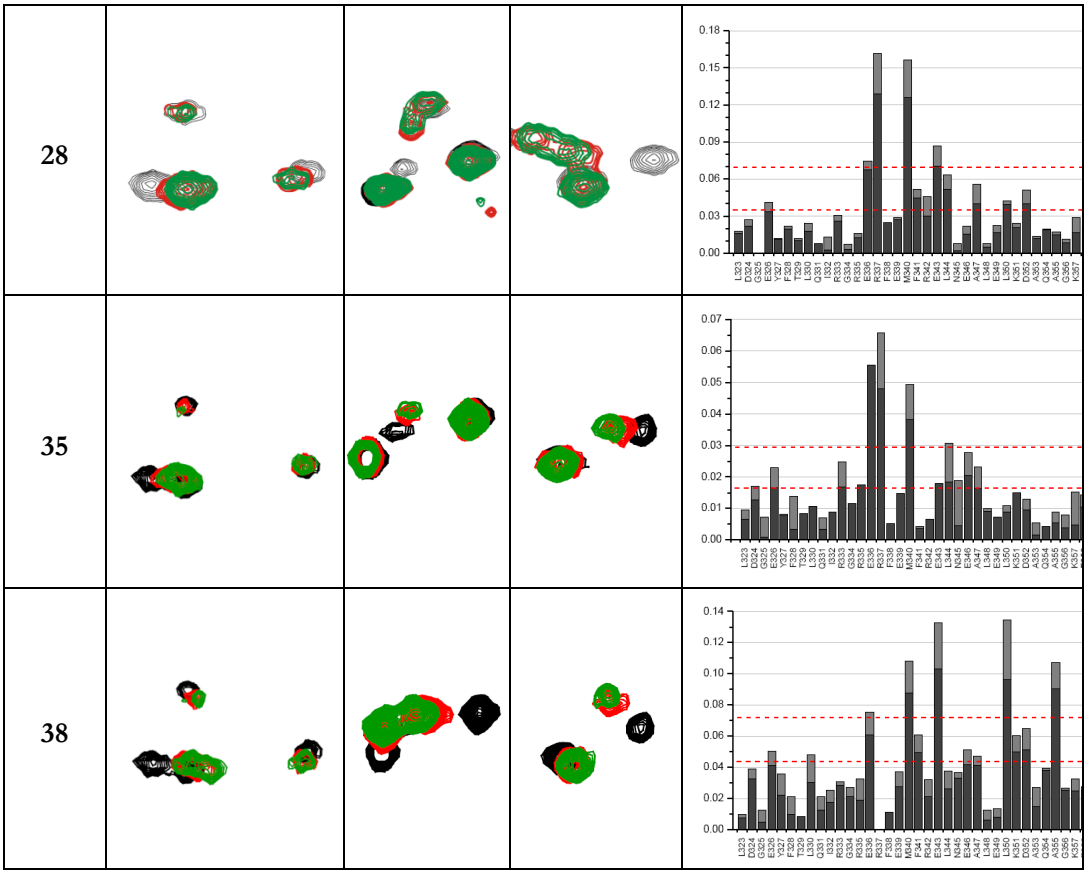

Qualitative information about the binding affinity can be assessed, assuming an analogous binding behavior of these ligands. Perturbation of Met340 was compared for all ligands (Figure 21). Ligands **13**, **15**, **20** and **35** shifted Met340 resonance similarly; interestingly, the shift increased with the number of guanidinium moieties (Δδ of **13** < **20** < **15** < **35**). That ligand 35 caused a strongest perturbation than ligand 15 despite having one guanidinium less could be explained by higher acidity of the benzoguanidinium NHs moiety,[67] and additional hydrophobic contacts with other residues of the protein. Finally, octaguanidinium ligand **38** and tetraguanidinium **28** induced the highest shift, suggesting a stronger binding to the protein. Anisotropic

[67] Ratel, F. *PhD Thesis*, Universidad Autónoma de Madrid, **2009**.

effects attributable to the interaction between the naphthyl aromatic moiety and residue Met340 should be also considered for the perturbations caused by ligand **28**.

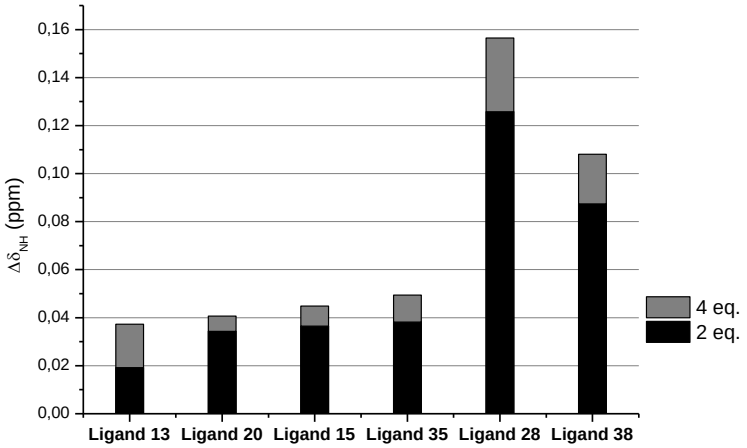

Figure 21. *Comparison of the chemical shifts observed for Met340 residue in the presence of the different oligoguanidinium ligands.*

Preliminar NMR experiments with p53TD R337H mutant in the presence of those ligands revealed new and unexpected shifts accounting for novel modes of binding. A more detailed study is however necessary to have a better insight into the interaction of these oligoguanidinium ligands with the mutant.[68]

[68] See Section 1.6 (Appendix) where most representative [^{1}H, ^{15}N]-HSQC spectra are available.

1.5 Experimental Section

1.5.1 General Procedures

Synthesis. All commercially available reagents (Aldrich, Fluka, Acros, NovaBiochem, Panreac) were used without further purification. Anhydrous solvents were obtained from a solvent purification system (SPS). All reactions were performed under nitrogen atmosphere unless specified. Chiral bicyclic guanidinium derivatives were synthesized in the *R*,*R* configuration.

Chromatography. Thin layer chromatography (TLC) was performed on pre-coated TLC-plates SIL G-25 UV_{254} (Macherey-Nagel) glass supported with detection by UV at 254 nm and/or bromocresol green stain (in EtOH and 1N NaOH mixture). Column chromatography was done using silica gel from SDS (Chromagel 60 ACC, 40-60 mm) and Scharlau (ASTM, 40-60 mm) following the procedure described by W. C. Still.[69] HPLC chromatograms were recorded on an Agilent Technologies 1100 (UV-detector) analytical HPLC C18 Symmetry300 and SunFire C18 columns (4.6 × 150 mm, 5 μm). For semi-preparative HPLC a LC 18 column Symmetry (10 × 150 mm, 5 μm) was used. The mobile phase consisted of CH_3CN/H_2O mixture containing 0.05 or 0.1% TFA. The solvents were provided by Scharlau and Carlo Erba (HPLC gradient grade).

Analysis. NMR spectra were performed on a Bruker Advance 400 (^1H: 400 MHz; ^{13}C: 100 MHz) equipped with a z-gradient 5 mm BBO probe with ATM Ultrashield spectrometer. Deuterated solvents used are indicated in each case. Chemicals shifts (δ) are expressed in ppm, and are referred to the residual peak of the solvent. Mass spectra were recorded in a Waters LCT Premier (ESI or APCI mode), Waters GCT (EI and CI ionization modes) or Bruker MALDI-TOF spectrometers.

[69] Still, W. C.; Kahn, M.; Mitra, A. *J. Org. Chem.* **1978**, *43*, 2923-2925.

Microwave specifications. A CEM Discover microwave reactor carrying a magnetron (2455 MHz) with a power output of 300 ± 10% W was employed.

1.5.2 Synthesis

(2*R*,8*R*)-2-(*tert*-Butyldiphenylsilanyloxymethyl)-8-(hydroxymethyl)-3,4,6,7,8,9-hexahydro-2*H*-pyrimido[1,2-*a*]pyrimidin-1-ium hexafluorophosphate.

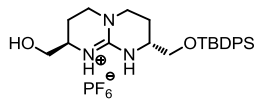

A solution of guanidinium **1** (5.00 g, 7.02 mmol) in H_2O/AcOH/THF (1:3:1, 125 mL) was stirred for 20 h at room temperature. After removing the solvent, the crude was dissolved in CH_2Cl_2 (125 mL) and washed subsequently with saturated solutions of Na_2CO_3 (100 mL) and NH_4Cl (3 × 100 mL). The organic phase was dried (Na_2SO_4) and after evaporating the solvent, the remaining oil was triturated with toluene/diethyl ether at 4 °C, resulting in the deprotected guanidinium as a white solid. The product was directly used in the next reaction step without further purification.

To exchange chloride for hexafluorophosphate, the compound was dissolved in CH_2Cl_2, washed with a 2N KOH solution (2 x 50 mL) and subsequently with 0.1N NH_4PF_6 (2 × 50 mL). Afterwards, the organic phase was filtered over cotton and evaporation of the solvent resulted in the desired product (PF_6^- salt). ^{1}H-NMR (400 MHz, $CDCl_3$) δ 7.67-7.64 (m, 4H, CH_{Ar}), 7.46-7.40 (m, 6H, CH_{Ar}), 6.15 (s, 1H, NH), 6.05 (s, 1H, NH), 3.86 (d, J = 12.5 Hz, 1H, CH_2OSi), 3.76 (dd, J = 5.4, 12.5 Hz, 1H, CH_2OSi), 3.67-3.47 (m, 4H, CH_2O, CH_α), 3.37-3.20 (m, 4H, $CH_{2\gamma}$), 2.15-1.85 (m, 5H, OH, $CH_{2\beta}$), 1.09 (s, 9H, $CH_{3t\text{-Bu}}$). ^{13}C-NMR (100 MHz, $CDCl_3$) δ 151.2 (C_{guan}) 135.5, 135.4, 132.6, 129.8, 128.9, 127.9 (C_{Ar}, CH_{Ar}), 65.3, 63.7 (CH_2O), 50.6, 49.3 (CH_α), 45.6, 44.6 ($CH_{2\gamma}$), 26.7 ($CH_{3t\text{-Bu}}$), 22.7 ($CH_{2\beta}$), 19.1 ($C_{t\text{-Bu}}$). ESI m/z 474.5 [$(M - PF_6^-)^+$, 100%].

(2*R*,8*R*)-2-(*tert*-Butyldiphenylsilanyloxymethyl)-8-methanesulfonyloxymethyl-3,4,6,7,8,9,-hexahydro-2*H*-pyrimido[1,2-*a*]-1-pyrimidinium hexafluorophosphate (2).

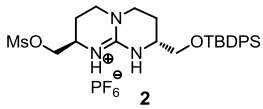

2

To a solution of mono-deprotected guanidine (PF_6^-) (4.67 g, 7.99 mmol) in dry THF (250 mL) a solution of Ms_2O (3.48 g, 19.98 mmol) in 50 ml of dry THF was added. The mixture was treated with NMM (3.55 mL, 31.97 mmol) and stirred for 4 h at room temperature. After evaporation of the solvent, the resulting solid was dissolved in CH_2Cl_2 (500 mL) and washed with a 0.1N NH_4PF_6 solution (2 × 250 mL). The organic layer was filtered over cotton and concentrated at reduced pressure. Purification by silica gel column chromatography (CH_2Cl_2/MeOH, 98:2) afforded mesylate **2** (4.74 g, 90%) as a white solid. ^{1}H-NMR (400 MHz, $CDCl_3$) δ 7.66 (m, 4H, CH_{Ar}), 7.46 (m, 6H, CH_{Ar}), 6.53 (s, 1H, NH), 6.31 (s, 1H, NH), 4.37 (m, 1H, CH_2OMs), 4.23 (m, 1H, CH_2OMs), 3.86 (m, 1H, CH_α), 3.72 (m, 2H, CH_2OSi), 3.63 (m, 1H, CH_α), 3.38 (m, 4H, $CH_{2\gamma}$), 3.17 (s, 3H, CH_{3MsO}), 2.20-1.91 (m, 4H, $CH_{2\beta}$), 1.01 (s, 9H, $CH_{3t\text{-}Bu}$). ^{13}C-NMR (100 MHz, $CDCl_3$) δ 150.6 (C_{guan}), 135.5, 132.5, 130.0, 128.9 (CH_{Ar}, C_{Ar}), 69.5 (CH_2OMs), 66.2 (CH_2OSi), 50.1, 47.7 (CH_α), 45.3, 44.9 ($CH_{2\gamma}$), 37.1 (CH_{3MsO}), 26.7 ($CH_{3t\text{-}Bu}$), 22.4, 21.9 ($CH_{2\beta}$), 19.1 ($C_{t\text{-}Bu}$). HRMS calcd. for $[C_{26}H_{38}N_3O_4SSi]^+$ 516.2352; found 516.2354.

(*2R,8R*)-2-Acetylsulfanylmethyl-8-(*tert*-butyldiphenylsilanyloxymethyl)-3,4,6,7,8,9-hexahydro-2*H*-pyrimido-[1,2-*a*]-1-pyrimidinium hexafluorophosphate (3).

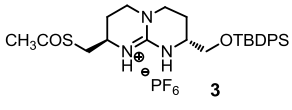

3

A solution of **2** (100 mg, 0.151 mmol) and potassium thioacetate (52 mg, 0.453 mmol) in CH_3CN (4 mL) was placed in a 6 mL microwave sealed tube. The reaction mixture was stirred and heated under microwaves for 10 min at 140 ºC. The resulting crude was allowed to cool to room temperature, the solvent was evaporated and the residue was dissolved in CH_2Cl_2 and washed with aqueous 0.1N NH_4PF_6 (2 × 10 mL). The organic phase was filtered over cotton and concentrated to dryness to give a crude residue which was purified by silica gel column chromatography (CH_2Cl_2/MeOH, 99.5:0.5 → 98:2), affording **3** as a brown-yellow oil. The experiment was repeated for three times in sealed tubes to afford a total amount of 380 mg (98%) of **3**. ^{1}H-NMR (400 MHz, $CDCl_3$) δ 7.66-7.63 (m, 4H, CH_{Ar}), 7.50-7.40 (m, 6H, CH_{Ar}), 6.57 (s, 1H, NH), 6.43 (s, 1H, NH), 3.76-3.64 (m, 2H, CH_2O), 3.63-3.56 (m, 2H, CH_α), 3.46-3.26 (m, 4H, $CH_{2\gamma}$), 3.10 (dd, J = 7.7, 14.2 Hz, 1H, CH_2S), 3.08 (dd, J = 7.8, 14.2 Hz, 1H, CH_2S), 2.41 (s, 3H, CH_3CO), 2.12-2.02 (m, 2H, $CH_{2\beta}$), 1.99-1.84 (m, 2H, $CH_{2\beta}$), 1.09 (s, 9H, $CH_{3t\text{-Bu}}$). ^{13}C-NMR (100 MHz, $CDCl_3$) δ 195.8 (CO), 150.8 (C_{guan}), 135.6, 134.4, 132.6, 130.1, 127.9 (CH_{Ar}, C_{Ar}), 65.4 (CH_2O), 49.7, 48.5 (CH_α), 45.1, 45.0 ($CH_{2\gamma}$), 32.5 (CH_2S), 30.5 (CH_3CO), 26.8 ($CH_{3t\text{-Bu}}$), 24.5, 22.7 ($CH_{2\beta}$), 19.2 ($C_{t\text{-Bu}}$). ESI-MS m/z 496.2 [(M - PF_6^-)$^+$, 100%]. HRMS calcd. for $[C_{27}H_{38}N_3O_2SSi]^+$ 496.2454; found 496.2429.

(2*R*,8*R*)-2-(*tert*-Butyldiphenylsilanyloxymethyl)-8-[(2*R*,8*R*)-8-(*tert*-butyldiphenylsilanyloxymethyl)-3,4,6,7,8,9-hexahydro-2*H*-pyrimido[1,2-*a*]-2-pyrimidin(methylsulfanylmethyl)-1-ium hexafluorophosphate]-3,4,6,7,8,9-hexahydro-2*H*-pyrimido[1,2-*a*]-1-pyrimidinium hexafluorophosphate (4).

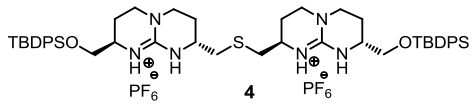

4

A mixture of compound **3** (214 mg, 0.334 mmol), mesylate **2** (221 mg, 0.334 mmol) and Cs_2CO_3 (304 mg, 0.930 mmol) was dissolved in 15 mL of degassed CH_3CN/MeOH (3:1) at 0 ºC under N_2 and the solution was stirred for 2 h. The

solvent was evaporated under vacuum at room temperature. The crude was dissolved in CH_2Cl_2 (20 mL) and washed with aqueous 1N NH_4PF_6 (2 × 10 mL). The organic phase was filtered over cotton and concentrated to dryness to give a crude residue which was purified by silica gel (with KPF_6) column chromatography (CH_2Cl_2/MeOH, 96:4), affording diguanidinium **4** (381 mg, 98%) as a white-yellow solid. ^{1}H-NMR (400 MHz, $CDCl_3$) δ 7.65-7.61 (m, 8H, CH_{Ar}), 7.49-7.37 (m, 12H, CH_{Ar}), 6.24 (s, 2H, NH), 6.10 (s, 2H, NH), 3.84-3.79 (m, 2H, CH_2O), 3.75-3.49 (m, 6H, CH_2O, CH_α), 3.48-3.18 (m, 8H, $CH_{2\gamma}$), 2.93-2.80 (m, 2H, CH_2S), 2.70-2.62 (m, 2H, CH_2S), 2.18-1.99 (m, 4H, $CH_{2\beta}$), 1.98-1.79 (m, 4H, $CH_{2\beta}$), 1.06 (s, 18H, $CH_{3t\text{-}Bu}$). ^{13}C-NMR (100 MHz, $CDCl_3$) δ 150.6 (C_{guan}), 135.6, 135.5, 132.8, 129.9, 127.9 (CH_{Ar}, C_{Ar}), 65.2 (CH_2O), 49.8, 47.7 (CH_α), 45.3, 44.9 ($CH_{2\gamma}$), 36.6 (CH_2S), 26.8 ($CH_{3t\text{-}Bu}$), 25.7, 22.5 ($CH_{2\beta}$), 19.2 ($C_{t\text{-}Bu}$). ESI-MS *m/z* 873.5 (M – HPF_6 - PF_6^-)$^+$, 437.3 (M – 2 PF_6^-)$^{2+}$. HRMS calcd. for $[C_{50}H_{69}N_6O_2SSi_2]^{2+}$ 873.4741; found 873.4731.

(2*R*,8*R*)-2-Hydroxymethyl-8-[(2*R*,8*R*)-8-hydroxymethyl-3,4,6,7,8,9-hexahydro-2*H*-pyrimido[1,2-*a*]-2-pyrimidinyl(methylsulfanylmethyl)-1-ium hexafluorophosphate]-3,4,6,7,8,9-hexahydro-2*H*-pyrimido[1,2-*a*]-1-pyrimidinium hexafluorophosphate (5).

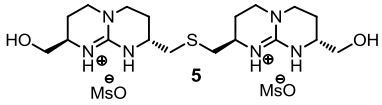

5

Procedure 1

A solution of **4** (385 mg, 0.330 mmol) and MsOH (24 μL, 0.400 mmol) in a mixture of THF/H_2O (3:1, 40 mL) was heated overnight at 76 ºC. The solvent was evaporated, the acid mixture diluted in water and washed with CH_2Cl_2 (2 × 50 mL). The aqueous phase was partially evaporated under reduced pressure. Afterwards $KHCO_3$ was added until a neutral pH was reached. The water was evaporated, and the crude was dissolved in a mixture of CH_2Cl_2/MeOH (1:20, 50 mL). The resulting precipitate was filtered off. The polarity of the solvent mixture was gradually reduced until pure CH_2Cl_2. The

solvent was then evaporated to afford compound **5** (173 mg, 89%) as a pale-yellow powder.

Procedure 2

A mixture of compound **4** (110 mg, 0.094 mmol) and Cs_2CO_3 (108 mg, 0.330 mmol) was dissolved in 30 mL of degassed CH_3CN/MeOH at room temperature and heated at 85 ºC overnight. The solvent was evaporated under vacuum. The crude was dissolved in CH_2Cl_2 (30 mL) and washed with water (2 × 10 mL). The aqueous phase was concentrated at reduced pressure to give a crude residue which was then dissolved in a mixture CH_2Cl_2/MeOH (1:20, 50 mL). The resulting precipitate was filtered off. The polarity of the solvent mixture was gradually reduced until pure CH_2Cl_2. The solvent was evaporated to afford compound **5** (36 mg, 56%) as a pale-yellow powder.

Procedure 3

Compound **4** (147 mg, 0.126 mmol) was dissolved in acetonitrile (20 mL) and CsF (115 mg, 0.76 mmol) was added to this solution. The mixture was stirred for 8 h at room temperature. The solvent was evaporated under vacuum and the resulting crude was dissolved in CH_2Cl_2 (25 mL) and washed with water (2 × 10 mL). The aqueous phase was evaporated to give a crude residue which was dissolved in a mixture of CH_2Cl_2/MeOH (1:20, 50 mL). The precipitate formed was filtered off. The polarity of the solvent mixture was reduced until pure CH_2Cl_2. The solvent was evaporated to afford compound **5** (26 mg, 30%) as pale-yellow powder.

Procedure 4

A solution of **4** (101 mg, 0.087 mmol) in a mixture of 3N HCl/CH_3CN (1:2, 20 mL) was stirred overnight at room temperature. The CH_3CN was evaporated, the acid mixture diluted with water and washed with ether (2 × 50 mL). The aqueous phase was

partially evaporated under reduced pressure. Afterwards $KHCO_3$ was added until a basic pH was reached. The water was evaporated, and the crude was dissolved in a mixture of CH_2Cl_2/MeOH (1:1, 50 mL). The resulting precipitate was filtered off. The polarity of the solvent mixture was gradually reduced until pure CH_2Cl_2. The solvent was evaporated to afford compound **5** (57 mg, quantitative) as a pale-yellow powder. ^{1}H-NMR (400 MHz, MeOD) δ 3.78-3.70 (m, 2H, CH_2O), 3.69-3.41 (m, 14H, CH_2O, CH_α, $CH_{2\gamma}$), 2.98 (dd, J = 5.2, 13.8 Hz, 2H, CH_2S), 2.75 (dd, J = 7.9, 13.8 Hz, 2H, CH_2S), 2.30-1.83 (m, 8H, $CH_{2\beta}$).^{13}C-NMR (100 MHz, MeOD) δ 152.1 (C_{guan}), 65.0 (CH_2O), 51.7 (CH_α), 46.4 ($CH_{2\gamma}$), 36.6 (CH_2S), 26.7, 23.5 ($CH_{2\beta}$). ESI-MS m/z 397.3 (M - HCl - Cl^-)$^+$, 199.1 (M – 2 Cl^-)$^{2+}$. HRMS calcd. for $[C_{18}H_{34}N_6O_2S]^+$ 397.2386; found 397.2392.

(2*R*,8*R*)-2-Methanesulfonyloxymethyl-8-[(2*R*,8*R*)-8-methanesulfonyloxymethyl-3,4,6,7,8,9-hexahydro-2*H*-pyrimido[1,2-*a*]-2-pyrimidinyl(methylsulfanylmethyl)-1-ium hexafluorophosphate]-3,4,6,7,8,9-hexahydro-2*H*-pyrimido[1,2-*a*]-1-pyrimidinium hexafluorophosphate (6).

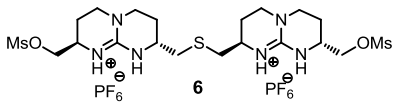

Compound **5** (100 mg, 0.17 mmol) and NMM (302 µL, 0.95 mmol) were mixed in dry CH_2Cl_2 (10 mL) under N_2 at 0 ºC and the mixture was stirred for 5-10 minutes. Then, a solution of Ms_2O (237 mg, 1.36 mmol) in dry CH_2Cl_2 (4 mL) was added and stirring was continued for 24 h. The solvent was evaporated under reduced pressure and the resulting crude dissolved in CH_2Cl_2 and washed with a 0.1N NH_4PF_6 solution (2 × 15 mL). The organic layer was filtered over cotton and left slowly to evaporate. A white precipitate was filtered affording **6** (95 mg, 67%) as a white solid. ^{1}H-NMR (400 MHz, CD_3CN) δ 6.51 (bs, 4H, NH), 4.33 (dd, J = 4.1, 10.7 Hz, 2H, CH_2O), 4.16 (dd, J = 7.4, 10.5 Hz, 2H, CH_2O), 3.85-3.76 (m, 2H, CH_α), 3.59-3.51 (m, 2H, CH_α), 3.43-3.30 (m, 8H, $CH_{2\gamma}$), 3.12 (s, 6H, CH_{3MsO}), 2.83 (dd, J = 5.04, 14.0 Hz, 2H, CH_2S), 2.58 (dd, J

= 8.6, 13.8 Hz, 2H, CH_2S), 2.13-2.04 (m, 4H, $CH_{2\beta}$), 1.93-1.78 (m, 4H, $CH_{2\beta}$). ^{13}C-NMR (100 MHz, CD_3CN) δ 150.4 (C_{guan}), 70.4 (CH_2O), 47.5, 47.4 (CH_α), 44.8, 44.4 ($CH_{2\gamma}$), 36.4 (CH_{3MsO}) 35.3 (CH_2S), 24.6, 21.3 ($CH_{2\beta}$). HRMS calcd. for $[C_{20}H_{38}N_6O_6S_3PF_6]^+$ 699.1657; found 699.1630.

(2*R*,8*R*)-2-(Acetylthiomethyl)-8-((((2*R*,8*R*)-8-(acetylthiomethyl)-2,3,4,6,7,8-hexahydro-1*H*-pyrimido[1,2-*a*]-9-pyrimidinium-2-yl)methylthio)methyl)-2,3,4,6,7,8-hexahydro-1*H*-pyrimido[1,2-*a*]-9-pyrimidinium hexafluorophosphate (7).

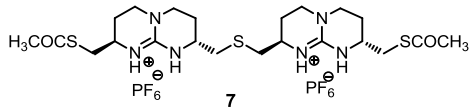

7

A mixture of **6** (91 mg, 0.101 mmol) and potassium thioacetate (27 mg, 0.250 mmol) in CH_3CN was stirred and refluxed for 9 h. Then, the solution was evaporated under vacuum, dissolved in CH_2Cl_2 and washed with a 0.1N NH_4PF_6 solution (2 × 20 mL). The organic layer was filtered over cotton and evaporated, affording **7** (78 mg, 90%) as a brownish powder. ^{1}H-NMR (400 MHz, $CDCl_3$) δ 6.50 (bs, 2H, NH), 3.72-3.60 (m, 4H, CH_2S), 3.54-3.34 (m, 8H, CH_α), 3.2-3.06 (m, 4H, CH_2S), 2.88 (dd, J =3.6, 13.5 Hz, 2H, CH_2S), 2.65 (m, 2H, CH_2S), 2.41 (s, 6H, CH_3COS), 2.20-2.09 (m, 4H, $CH_{2\gamma}$), 1.98-1.83 (m, 4H, $CH_{2\beta}$). ^{13}C-NMR (100 MHz, CD_3CN) δ 195.1 (SCO), 150.2 (C_{guan}), 47.6, 47.4 (CH_α), 44.8, 44.5 ($CH_{2\gamma}$), 37.5 (CH_2SCO), 35.3 (CH_2S), 30.8 (CH_3COS), 24.6, 21.5 ($CH_{2\beta}$). ESI m/z 659.4 $(M-PF_6^-)^+$, 513.6 $(M-PF_6^- -HPF_6)^+$.

(2*R*,8*R*)-2-(*tert*-Butyldiphenylsilanyloxymethyl)-8-[(2*R*,8*R*)-8-hydroxymethyl-3,4,6,7,8,9-hexahydro-2*H*-pyrimido[1,2-*a*]-2-pyrimidinyl(methylsulfanylmethyl)-1-ium hexafluorophosphate]-3,4,6,7,8,9-hexahydro-2*H*-pyrimido[1,2-*a*]-1-pyrimidinium hexafluorophosphate (9).

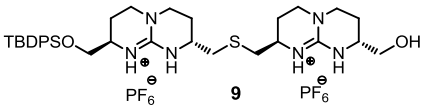

9

A solution of mesylate **2** (500 mg, 0.76 mmol) and potassium thioacetate (430 mg, 3.78 mmol) in a mixture of THF/H_2O (3:1, 40 mL) was refluxed for 7 h. After cooling to room temperature, MsOH (490 μL, 7.54 mmol) was added and the mixture was refluxed for 16 h. The reaction mixture was cooled to room temperature, 10 mL of Et_2O were added and then the aqueous phase was extracted and washed with $CHCl_3$ (2 × 20 mL) and finally with Et_2O (20 mL). After concentrating the aqueous layer to *ca.* 50%, $KHCO_3$ (607 mg, 9.06 mmol) was added and the solvent evaporated to dryness. Then, MeOH (50 mL) was added, the precipitate was removed by filtration and the solvent evaporated under reduced pressure. This procedure was repeated a few times increasing the amount of CH_2Cl_2 in the solvent mixture until pure CH_2Cl_2 was used, to afford the symmetric disulfide **8** (243 mg, 90%). ^{1}H-NMR (400 MHz, $CDCl_3$) δ 3.90-3.81 (bs, 2H, OH), 3.80-3.67 (m, 3H, CH_2O), 3.64-3.26 (m, 13H, CH_2O, CH_α, $CH_{2\gamma}$), 3.15 (dd, J = 5.2, 13.7 Hz, 2H, CH_2S), 2.87-2.78 (m, 2H, CH_2S), 2.28-2.20 (m, 2H, $CH_{2\beta}$), 1.96-1.79 (m, 6H, $CH_{2\beta}$).

To a solution of **8**, Cs_2CO_3 (250 mg, 0.77 mmol) in MeOH (5 mL) and PBu_2Ph polystyrene resin (617 mg, 0.58 mmol) were added and the mixture was stirred for 40 min. Then a solution of guanidine mesylate **2** (512 mg, 0.77 mmol) in THF (12 mL) was added and the mixture was stirred for 4 h. After evaporation of the solvent, the crude residue was dissolved in CH_2Cl_2 (25 mL) and washed with a 0.1N NH_4PF_6 solution (2 × 20 mL). The organic layer was filtered over cotton and concentrated at reduced pressure. Purification by silica gel column chromatography (CH_2Cl_2/MeOH, 96:4 → 94:6) afforded **9** (220 mg, 87%) as a white solid. ^{1}H-NMR (400 MHz, $CDCl_3$) δ

7.69-7.63 (m, 4H, CH_{Ar}), 7.49-7.39 (m, 6H, CH_{Ar}), 6.59 (s, 1H, NH), 6.50 (s, 2H, NH), 6.39 (s, 1H, NH), 3.82-3.13 (m, 16H, CH_2O, CH_α, $CH_{2\gamma}$), 2.95-2.82 (m, 2 H, CH_2S), 2.72 (dd, J = 3.6, 13.2 Hz, 1H, CH_2S), 2.59 (dd, J = 3.6, 13.2 Hz, 1H, CH_2S), 2.54 (dd, J = 3.8, 13.6 Hz, 1H, CH_2S), 2.18-1.79 (m, 8H, $CH_{2\beta}$), 1.08 (s, 9H, $CH_{3t\text{-}Bu}$). ^{13}C-NMR (100 MHz, $CDCl_3$) δ 150.7 (C_{guan}), 150.3 (C_{guan}), 135.2, 132.7, 132.5, 129.8, 127.7 (CH_{Ar}, C_{Ar}), 65.4, 65.2 (CH_2OSi, CH_2O), 50.1, 49.8, 47.7, 47.6 (CH_α), 45.3, 44.8 ($CH_{2\gamma}$), 36.0, 35.7 (CH_2S), 26.7 ($CH_{3t\text{-}Bu}$), 26.5, 25.8, 22.4, 22.2 ($CH_{2\beta}$), 19.1 ($C_{t\text{-}Bu}$). HRMS calcd. for $[C_{34}H_{52}N_6O_2SSi]^{2+}$ 318.1821; found 318.1816.

(2*R*,8*R*)-8-[(2*R*,8*R*)-8-*tert*-Butyldiphenylsilanyloxymethyl-3,4,6,7,8,9-hexahydro-2*H*-pyrimido[1,2-*a*]-2-pyrimidinyl(methylsulfanylmethyl)-1-ium hexafluorophosphate]-2-methanesulfonyloxymethyl-3,4,6,7,8,9-hexahydro-2*H*-pyrimido[1,2-*a*]-1-pyrimidinium hexafluorophosphate (10).

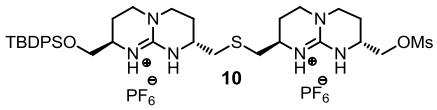

To a solution of alcohol **9** (180 mg, 0.19 mmol) and NMM (173 μL, 1.55 mmol) in dry CH_2Cl_2 (10 mL) a solution of Ms_2O (169 mg, 0.97 mmol) in CH_2Cl_2 (4 mL) was added and the mixture was stirred for 4 h. The solvent was evaporated under reduced pressure and the resulting crude dissolved in CH_2Cl_2 and washed with a 0.1N NH_4PF_6 solution (2 × 30 mL). The organic layer was filtered over cotton and concentrated to dryness. Purification by silica gel (with KPF_6) column chromatography (CH_2Cl_2/MeOH, 96:4) afforded **10** (191 mg, 98%) as a white solid. ^{1}H-NMR (400 MHz, $CDCl_3$) δ 7.67-7.63 (m, 4H, CH_{Ar}), 7.48-7.39 (m, 6H, CH_{Ar}), 6.55 (s, 1H, NH), 6.45 (s, 2H, NH), 6.39 (s, 1H, NH), 4.27 (dd, J = 4.9, 10.4 Hz, 1H, CH_2O), 4.21 (dd, J = 6.1, 10.4 Hz, 1H, CH_2O), 3.86-3.22 (m, 16H, CH_2O, CH_α, $CH_{2\gamma}$), 3.07 (s, 3H, CH_{3MsO}), 2.91-2.83 (m, 2H, CH_2S), 2.69-2.53 (m, 2H, CH_2S), 2.12-1.79 (m, 8H, $CH_{2\beta}$), 1.06 (s, 9H, $CH_{3t\text{-}Bu}$). ^{13}C-NMR (100 MHz, $CDCl_3$) δ 151.4 (C_{guan}), 151.2 (C_{guan}), 135.8, 132.7, 132.8, 130.3, 127.7 (CH_{Ar}, C_{Ar}), 68.4, 65.6 (CH_2OSi, CH_2O), 50.1, 49.8, 47.7,

47.4 (CH_{α}), 45.7, 44.8 ($CH_{2\gamma}$), 37.5 (CH_2S), 37.0 (CH_{3MsO}) 36.9 (CH_2S), 26.7 ($CH_{3t\text{-}Bu}$), 26.5, 25.9, 22.6, 22.4 ($CH_{2\beta}$), 19.2 ($C_{t\text{-}Bu}$). HRMS calcd. for $[C_{35}H_{53}N_6O_4S_2Si]^+$ 713.3339; found 713.3344.

(2*R*,8*R*)-2-(Acetylsulfanylmethyl)-8-[(2R,8*R*)-8(*tert*-butyldiphenylsilanyloxymethyl)-3,4,6,7,8,9-hexahydro-2*H*-pyrimido[1,2-*a*]-2-pyrimidinyl(methylsulfanylmethyl)-1-ium hexafluorophosphate]-3,4,6,7,8,9-hexahydro-2*H*-pyrimido[1,2-*a*]-1-pyrimidinium hexafluorophosphate (11).

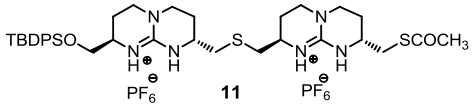

11

Procedure 1

A solution of **10** (318 mg, 0.316 mmol) and potassium thioacetate (90 mg, 0.79 mmol) in CH_3CN (4 mL) was placed in a 6 mL sealed reactor vessel. The mixture was irradiated in the microwave oven at 200 W for 10 min at 140 ºC. After cooling to room temperature the solvent was removed. The residue was dissolved in CH_2Cl_2 (50 mL) and washed with a 0.1N NH_4PF_6 solution (3 × 50 mL). The organic layer was filtered over cotton and concentrated at reduced pressure. Purification by silica gel (with KPF_6) column chromatography (CH_2Cl_2/MeOH, 95:5) afforded **11** (231 mg, 75%) as a light brown solid.

Procedure 2

Compound **10** (150 mg, 0.140 mmol) and potassium thioacetate (51 mg, 0.45 mmol) were dissolved in CH_3CN (10 mL) and the mixture was refluxed and stirred overnight. After cooling it to room temperature, the solvent was removed and the crude dissolved in CH_2Cl_2. Then, the solution was washed with a 0.1N NH_4PF_6 solution (3 × 40 mL). The organic phase was filtered over cotton and concentrated to dryness. Purification was performed as described in Procedure 1, yielding **11** (125 mg, 86%). ^{1}H-NMR (400

MHz, $CDCl_3$) δ 7.69-7.59 (m, 4H, CH_{Ar}), 7.49-7.37 (m, 6H, CH_{Ar}), 6.27 (s, 2H, NH), 6.15 (s, 1H, NH), 6.08 (s, 1H, NH), 3.82-3.67 (m, 2H, CH_2O), 3.65-3.54 (m, 4H, CH_α), 3.49-3.20 (m, 8H, $CH_{2\gamma}$), 3.14-2.96 (m, 2H, CH_2S), 2.93-2.80 (m, 2H, CH_2S), 2.76-2.57 (m, 2H, CH_2S), 2.34 (s, 3H, CH_3CO), 2.20-2.07 (m, 4H, $CH_{2\beta}$), 1.99-1.80 (m, 4H, $CH_{2\beta}$), 1.08 (s, 9H, $CH_{3t\text{-}Bu}$). ^{13}C-NMR (100 MHz, $CDCl_3$) δ 183.0 (CO), 150.6 (C_{guan}), 135.6, 135.5, 129.9, 127.9 (CH_{Ar}, C_{Ar}), 65.2 (CH_2O), 49.8, 47.7 (CH_α), 45.3, 45.4 ($CH_{2\gamma}$), 36.6, 36.4 (CH_2S), 30.5 (CH_3CO), 26.8 ($CH_{3t\text{-}Bu}$), 25.7, 22.5 ($CH_{2\beta}$), 19.2 ($C_{t\text{-}Bu}$). ESI-MS m/z 839.3 (M - PF_6^-)$^+$. HRMS calcd. for $[C_{36}H_{54}N_6O_2SSi_2PF_6]^+$ 839.3161; found 839.3155.

Compound 12

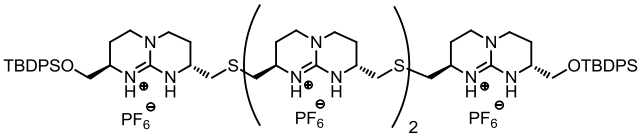

12

A mixture of **11** (174 mg, 0.177 mmol), mesylate **10** (195 mg, 0.194 mmol) and Cs_2CO_3 (144 mg, 0.442 mmol) was dissolved in 25 mL of degassed CH_3CN/MeOH at 25 ºC under N_2 and stirred for 6 h. The solvent was evaporated at reduced pressure at room temperature. The crude was dissolved in CH_2Cl_2 (30 mL) and washed with 1N NH_4PF_6 (2 × 30 mL). The organic phase was filtered over cotton and concentrated at reduced pressure to give a crude which was purified on silica gel (with KPF_6) column chromatography (CH_2Cl_2/MeOH, 92:8), affording **12** (PF_6) (234 mg, 72%) as a white solid. ^{1}H-NMR (400 MHz, $CDCl_3$) δ, 7.72-7.60 (m, 8H, CH_{Ar}), 7.51-7.38 (m, 12H, CH_{Ar}), 6.33-5.84 (bs, 7H, NH), 3.86-48 (m, 12H, CH_2O, CH_α), 3.47-3.18 (m, 16H, $CH_{2\gamma}$), 2.95-2.75 (m, 6H, CH_2S), 2.74-2.50 (m, 6H, CH_2S), 2.28-1.99 (m, 8H, $CH_{2\beta}$), 1.98-1.75 (m, 8H, $CH_{2\beta}$), 1.07 (s, 18H, $CH_{3t\text{-}Bu}$). ^{13}C-NMR (100 MHz, $CDCl_3$) δ 151.2 (C_{guan}), 135.6, 135.5, 132.8, 129.9, 127.9 (CH_{Ar}, C_{Ar}), 65.2 (CH_2O), 49.3, 48.2 (CH_α), 45.4, 44.9 ($CH_{2\gamma}$), 37.2, 37.0 (CH_2S), 26.8 ($CH_{3t\text{-}Bu}$), 25.7, 22.5 ($CH_{2\beta}$), 19.2 ($C_{t\text{-}Bu}$). ESI-

MS m/z 1267.69 $(M - PF_6^- - 3HPF_6^-)^+$.

Compound 13

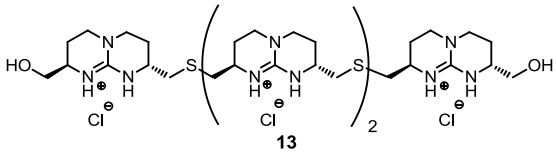

13

A solution of **12** (145 mg, 0.077 mmol) in 12N HCl/CH_3CN (1:1, 5 mL) was stirred for 12 h at room temperature. The solvent was removed and the resulting crude dissolved in distilled water (10 mL) and washed with CH_2Cl_2 (3 × 10 mL). The aqueous phase was evaporated to dryness, yielding **13** (71 mg, 98%) as a white solid. ^{1}H-NMR (400 MHz, MeOD) δ 3.74-3.64 (m, 8H, CH_2O, CH_α), 3.62-3.47 (m, 20H, CH_α, $CH_{2\gamma}$), 3.04-2.92 (m, 6H, CH_2S), 2.85-2.73 (m, 6H, CH_2S), 2.31-1.86 (m, 16H, $CH_{2\beta}$). ^{13}C-NMR (100 MHz, MeOD) δ 151.2 (C_{guan}), 65.2 (CH_2O), 49.3, 48.2 (CH_α), 45.4, 44.9 ($CH_{2\gamma}$), 37.1, 37.0 (CH_2S), 26.4, 22.5 ($CH_{2\beta}$). ESI-MS m/z 901.3 $(M - Cl^-)^+$. HRMS calcd. for $[C_{36}H_{66}N_{12}O_2S_3Cl_3]^+$ 899.3659; found 899.3698.

Compound 14

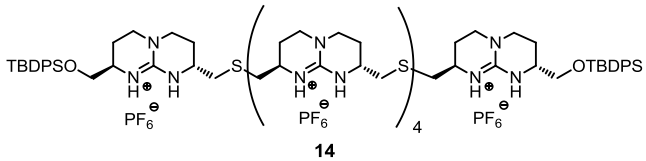

14

Procedure 1 (first symmetrical trial)

To a solution of **7** (52 mg, 0.065 mmol) and Cs_2CO_3 (105 mg, 0.323 mmol) in dry MeOH (15 mL), $(^nBu)_2$PhP polystyrene (178 mg, 0.155 mmol) was added and the mixture was stirred for 2 h. Then a solution of guanidine mesylate **10** (143 mg, 0.142 mmol) in dry CH_3CN (10 mL) was added and the mixture was stirred for 3 days at room temperature under N_2. After evaporation of the solvent at room temperature, the crude residue was dissolved in CH_2Cl_2 (25 mL) and washed with a 0.1N NH_4PF_6

solution (2 × 20 mL). The organic layer was filtered over cotton and concentrated to dryness. Purification by semi-preparative HPLC (Analytical conditions: Column: SunFire C18 5 μm, 150 x 4.6 mm, Purification Method: CH_3CN (0.1% TFA)/H_2O (0.05% TFA), Gradient: 5-55% CH_3CN (0.1% TFA) in 30 min, Flow: 1 mL/min, room temperature) afforded product **14** (9 mg, 6%) as a yellowish solid.

Procedure 2 (second symmetrical trial)

A mixture of compound **6** (54 mg, 0.034 mmol), PBu_2Ph polystyrene (140 mg, 0.160 mmol) and Cs_2CO_3 (103 mg, 0.317 mmol) was dissolved in 10 mL of dry MeOH at 25 ºC under N_2. After 15 min, compound **11** (152 mg, 0,139 mmol) was added and the solution was stirred for 2 days. The solvent was evaporated under vacuum at room temperature. The crude was dissolved in CH_2Cl_2 (30 mL) and washed with 0.1N NH_4PF_6 (2 × 20 mL). The organic phase was filtered over cotton and concentrated to dryness to give a crude which was purified by silica gel (with KPF_6) column chromatography (CH_2Cl_2/MeOH, 98:2 → 94:6), yielding **14** (PF_6) (40 mg, 24%). A further semi-preparative HPLC column was necessary to fully purify the product, affording **14** (CF_3COO^-) (18 mg, 12%) as a white solid.

Procedure 3 (non-symmetrical trial)

Compound **11** (89 mg, 0.090 mmol) was dissolved in MeOH (10 mL). Then, PBu_2Ph polystyrene (103 mg, 0.090 mmol) and Cs_2CO_3 (65 mg, 0.200 mmol) were added to the solution and the mixture was stirred for 20 min under N_2. Afterwards, compound **17** (127 mg, 0.075 mmol) was added and the mixture was further stirred for 2 days. The solvent was evaporated under vacuum, dissolved in CH_2Cl_2 (30 mL) and washed with 0.1N NH_4PF_6 (2 × 20 mL). The organic layer was filtered over cotton and concentrated at reduced pressure. Purification by silica gel (with KPF_6) column chromatography (CH_2Cl_2/MeOH, 98:2 → 94:6) afforded **14** (108 mg, 57%) as a light yellow solid. ^{1}H-NMR (400 MHz, CD_3CN) δ 8.35, 8.15, 8.12 (s, 10H, NH), 7.72-7.61

(m, 8H, CH_{Ar}), 7.43-7.37 (m, 12H, CH_{Ar}), 6.32 (s, 2H, NH), 5.80 (s, 2H, NH), 3.70 (dd, J = 4.3, 10.2 Hz, 4H, CH_2O), 3.63-3.48 (m, 12H, CH_α), 3.45-3.19 (m, 24H, $CH_{2\gamma}$), 2.87-2.19 (m, 20H, CH_2S), 2.22-1.75 (m, 24H, $CH_{2\beta}$), 1.06 (s, 18H, $CH_{3t\text{-}Bu}$). ^{13}C-NMR (100 MHz, CD_3CN) δ 150.94 (C_{guan}), 135.6, 135.5, 134.8, 129.9, 127.9, 127.7 (CH_{Ar}, C_{Ar}), 65.4 (CH_2O), 49.1, 47.9 (CH_α), 45.4, 44.9 ($CH_{2\gamma}$), 36.8 (CH_2S), 26.7 ($CH_{3t\text{-}Bu}$), 25.5, 22.7 ($CH_{2\beta}$), 19.1 ($C_{t\text{-}Bu}$). ESI-MS m/z 2232.0 $(M - TFA^-)^+$, 1059.5 $(M - 2\ TFA^-)^{2+}$.

Compound 15

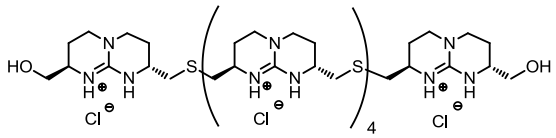

15

A solution of **14** (18 mg, 0.008 mmol) in 3N HCl/CH_3CN (1:1, 5 mL) was stirred for 36 h at room temperature. The solvent was removed and the resulting crude dissolved in distilled water (10 mL) and washed with CH_2Cl_2 (3 × 10 mL). The aqueous phase was evaporated to dryness, yielding **15** (10 mg, 88%) as a white solid. ^{1}H-NMR (400 MHz, D_2O) δ 3.67-3.43 (m, 16H, CH_2O, CH_α), 3.42-3.24 (m, 24H, $CH_{2\gamma}$), 2.88-2.75 (m, 10H, CH_2S), 2.62 (dd, J = 8.2, 13.8 Hz, 10H, CH_2S), 2.12-1.70 (m, 24H, $CH_{2\beta}$). ^{13}C-NMR (100 MHz, D_2O) δ 150.9 (C_{guan}), 65.4 (CH_2O), 49.1, 47.9 (CH_α), 45.4, 44.9 ($CH_{2\gamma}$), 36.8 (CH_2S), 25.5, 22.7 ($CH_{2\beta}$). ESI-MS m/z 1755.8 ($M\text{-}PF_6^-$). HRMS calcd. for $[C_{54}H_{96}N_{18}O_2S_5]^{4+}$ 297.1636; found 297.1648.

Compound 16

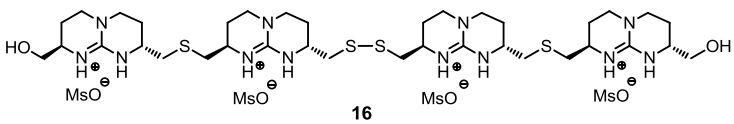

16

A solution of mesylate **10** (280 mg, 0.279 mmol) and potasium thioacetate (159 mg, 1.39 mmol) in a mixture THF/H_2O (3:1, 40 mL) was refluxed for 7 h. After cooling to

room temperature, MsOH (270 μL, 4.18 mmol) was added and the mixture was refluxed overnight. The reaction mixture was cooled to room temperature, evaporated to dryness and the crude was dissolved in water (30 mL). Then, 10 mL of Et_2O were added and the aqueous phase was extracted and washed with $CHCl_3$ (2 × 20 mL) and finally with Et_2O (20 mL). After concentration of about 50% of the aqueous layer, $KHCO_3$ (474 mg, 4.74 mmol) was added and the solvent evaporated to dryness. Afterwards, MeOH (50 mL) was added, the precipitate was removed by filtration and the solvent evaporated at reduced pressure. This procedure was repeated for a few times increasing the amount of CH_2Cl_2 in the solvent mixture until pure CH_2Cl_2, to afford the symmetric disulfide **16** (165 mg, 97%). This compound was immediately used in the next synthetic step. ^{1}H-NMR (400 MHz, MeOD) δ 3.86-3.72 (m, 2H, CH_2O), 3.70-3.47 (m, 10H, CH_2O, CH_α), 3.46-3.35 (m, 16H, $CH_{2\gamma}$), 3.05 -2.82 (m, 6H, CH_2S), 2.79-2.62 (m, 2H, CH_2S), 2.21-1.78 (m, 16H, $CH_{2\beta}$).

Compound 17

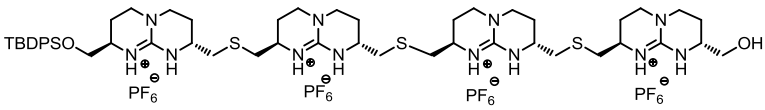

17

To a solution of feshly prepared **16** (218 mg, 0.180 mmol), Cs_2CO_3 (118 mg, 0.361 mmol) in MeOH (15 mL), PBu_2Ph polystyrene (332 mg, 0.289 mmol) was added and the mixture was stirred for 1 h. Then a solution of diguanidine mesylate **10** (327 mg, 0.325 mmol) in THF (10 mL) was added and the mixture was stirred for 6 h. After evaporation of the solvent, the crude residue was dissolved in CH_2Cl_2 (25 mL) and washed with a 0.1N NH_4PF_6 solution (2 × 20 mL). The organic layer was filtered over cotton and concentrated at reduced pressure. Purification by silica gel column chromatography (CH_2Cl_2/MeOH, 99:1 → 95:5) afforded **17** (280 mg, 96%) as a white solid. ^{1}H-NMR (400 MHz, CD_3CN) δ 7.69-7.63 (m, 4H, CH_{Ar}), 7.49-7.39 (m, 6H, CH_{Ar}), 6.59 (s, 1H, NH), 6.50 (s, 2H, NH), 6.39 (s, 1H, NH), 3.82-3.13 (m, 16H,

CH_2O, CH_α, $CH_{2\gamma}$), 2.95-2.82 (m, 2 H, CH_2S), 2.72 (dd, J = 3.6, 13.2 Hz, 1H, CH_2S), 2.59 (dd, J = 3.6, 13.2 Hz, 1H, CH_2S), 2.54 (dd, J = 3.8, 13.6 Hz, 1H, CH_2S), 2.18-1.79 (m, 8H, $CH_{2\beta}$), 1.08 (s, 9H, $CH_{3t\text{-Bu}}$). ^{13}C-NMR (100 MHz, CD_3CN) δ 151.3, 151.2 (C_{guan}), 135.7, 133.2, 133.1, 130.3, 128.2 (CH_{Ar}, C_{Ar}), 66.3, 64.4 (CH_2OSi, CH_2O), 51.1, 50.6, 48.2, 48.1, 48.0 (CH_α), 45.7, 45.5, 45.4, 45.3 ($CH_{2\gamma}$), 36.3, 36.2, 36.1 (CH_2S), 26.6 ($CH_{3t\text{-Bu}}$), 26.0, 25.8, 25.7, 22.8, 22.7 ($CH_{2\beta}$), 19.2 ($C_{t\text{Bu}}$). HRMS calc for $[C_{52}H_{81}N_{12}O_2S_3Si]^+$ 1029.5537 found 1029.5512.

Compound 18

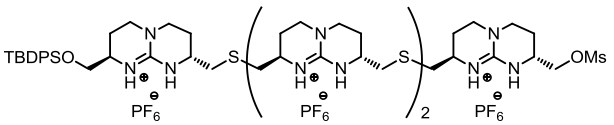

18

To a solution of alcohol **17** (150 mg, 0.093 mmol) and NMM (83 μL, 0.744 mmol) in dry CH_2Cl_2 (10 mL) a solution of Ms_2O (81 mg, 0.495 mmol) in CH_2Cl_2 (4 mL) was added and the mixture was stirred for 4 h. The solvent was evaporated under reduced pressure and the resulting crude dissolved in CH_2Cl_2 and washed with a 0.1N NH_4PF_6 solution (2 × 30 mL). The organic layer was filtered over cotton and concentrated to dryness. Purification on silica gel (with KPF_6) column chromatography (CH_2Cl_2/MeOH, 96:4) afforded **18** (137 mg, 87%) as a white solid. ^{1}H-NMR (400 MHz, CD_3CN) δ 7.67-7.63 (m, 4H, CH_{Ar}), 7.48-7.39 (m, 6H, CH_{Ar}), 6.55 (s, 1H, NH), 6.45 (s, 2H, NH), 6.39 (s, 1H, NH), 4.27 (dd, J = 4.9, 10.4 Hz, 1H, CH_2O), 4.21 (dd, J = 6.1, 10.4 Hz, 1H, CH_2O), 3.86-3.22 (m, 16H, CH_2O, CH_α, $CH_{2\gamma}$), 3.07 (s, 3H, CH_{3MsO}), 2.91-2.83 (m, 2H, CH_2S), 2.69-2.53 (m, 2H, CH_2S), 2.12-1.79 (m, 8H, $CH_{2\beta}$), 1.06 (s, 9H, $CH_{3t\text{-Bu}}$). ^{13}C-NMR (100 MHz, CD_3CN) δ 151.9, 151.8 (C_{guan}), 136.3, 136.2, 133.7, 133.6, 130.9, 128.8 (CH_{Ar}, C_{Ar}), 71.7 (CH_2OMs), 66.9 (CH_2OSi), 51.2, 48.7, 48.6 (CH_α), 46.0, 45.9, 45.5 ($CH_{2\gamma}$), 37.2, 36.6 (CH_3, CH_2S), 27.2 ($CH_{3t\text{-Bu}}$), 26.3, 26.2, 23.2, 22.6 ($CH_{2\beta}$), 19.7 ($C_{t\text{-Bu}}$). HRMS calcd. for $[C_{53}H_{85}F_{12}N_{12}O_4P_2S_4Si]^{2+}$ 700.2421; found 700.2412.

Compound 19

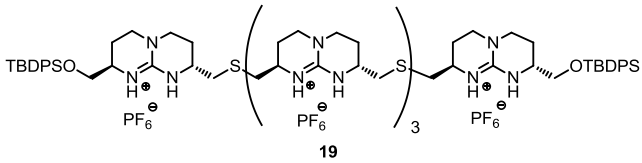

19

Compound **3** (46 mg, 0.071 mmol) was dissolved in MeOH (10 mL). Then, PBu_2Ph polystyrene (68 mg, 0.059 mmol) and Cs_2CO_3 (51 mg, 0.158 mmol) were added to the solution and the mixture was stirred for 20 min under N_2 at room temperature. Afterwards, a solution of compound **18** (100 mg, 0.059 mmol) in CH_3CN (15 mL) was added to the mixture and stirred for 2 days. The solvent was evaporated under vacuum, dissolved in CH_2Cl_2 (30 mL) and washed with 0.1N NH_4PF_6 (2 × 20 mL). The organic layer was filtered over cotton and concentrated to dryness. Purification on silica gel (with KPF_6) column chromatography (CH_2Cl_2/MeOH, 98:2 → 94:6) afforded **19** (80 mg, 62%) as a white solid. ^{1}H-NMR (400 MHz, CD_3CN) δ 7.74-7.67 (m, 8H, CH_{Ar}), 7.56-7.44 (m, 12H, CH_{Ar}), 6.44-6.11 (bs, 8H, NH), 3.81-3.47 (m, 14H, CH_2O, CH_α), 3.44-3.27 (m, 20H, $CH_{2\gamma}$), 2.90-2.19 (m, 16H, CH_2S), 2.26-1.75 (m, 20H, $CH_{2\beta}$), 1.09 (s, 18H, $CH_{3t\text{-}Bu}$). ^{13}C-NMR (100 MHz, MeOD) δ 150.8 (C_{guan}), 135.7, 135.4, 134.5, 129.8, 127.8, 127.5 (CH_{Ar}, C_{Ar}), 65.5 (CH_2O), 48.9, 47.7 (CH_α), 45.4, 45.1 ($CH_{2\gamma}$), 36.6 (CH_2S), 26.8 ($CH_{3t\text{-}Bu}$), 25.4, 22.6 ($CH_{2\beta}$), 19.3 ($C_{t\text{-}Bu}$). HPLC-MS: Conditions: Column: SunFire C18 5 μm, 150 x 4.6 mm, CH_3CN (0.1% TFA)/H_2O (0.05% TFA), Gradient: 10-100% CH_3CN (0.1% TFA) in 25 min, Flow: 1 mL/min, room temperature. Retention time: 14.5 min. ESI-MS m/z 1921.8 (M – TFA-)$^+$, 903.9 (M – 2 TFA-)$^{2+}$, 564.9 (M – 3 TFA-)$^{3+}$, 395.7 (M – 4 TFA-)$^{4+}$.

Compound 20

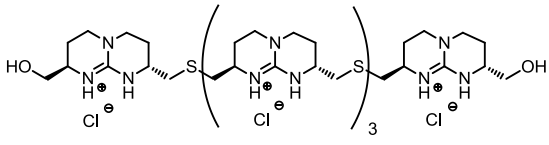

20

A solution of **19** (79 mg, 0.034 mmol) in 3N HCl/CH_3CN (1:1, 10 mL) was stirred for 36 h at room temperature. The solvent was removed and the resulting crude was dissolved in distilled water (15 mL) and washed with CH_2Cl_2 (3 × 15 mL). The aqueous phase was evaporated to dryness, affording **20** (45 mg, quantitative) as a white solid. Afterwards this solid was purified by semi-preparative HPLC (Analytical conditions: Column: SunFire C18 5 μm, 150 x 4.6 mm, MP: CH_3CN (0.1% TFA)/H_2O (0.05% TFA), Gradient: 10-40% CH_3CN (0.1% TFA) in 30 min, Flow: 1 mL/min, room temperature) yielding **20** (41 mg, 91%). ^{1}H-NMR (400 MHz, MeOD) δ 3.69-3.40 (m, 14H, CH_2O, CH_α), 3.39-3.22 (m, 20H, $CH_{2\gamma}$), 2.84-2.75 (m, 8H, CH_2S), 2.65-2.56 (m, 8H, CH_2S), 2.10-1.70 (m, 20H, $CH_{2\beta}$). ^{13}C-NMR (400 MHz, MeOD) δ 150.9 (C_{guan}), 65.4 (CH_2O), 49.1, 47.9 (CH_α), 45.4, 44.9 ($CH_{2\gamma}$), 36.8 (CH_2S), 25.5, 22.7 ($CH_{2\beta}$). HRMS calcd. for $[C_{45}H_{81}N_{15}O_2S_4]^{4+}$ 247.8896; found 247.8881.

***S*-(2-Naphthylmethyl)ethanethioate (22).**

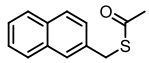

22

2-(Bromomethyl)naphthalene (210 mg, 0.91 mmol) and potassium thioacetate (312 mg, 2.74 mmol) were dissolved in CH_3CN (15 mL) and the mixture was refluxed and stirred overnight. After cooling to room temperature the solvent was removed and the residue was dissolved in CH_2Cl_2. Then, the solution was washed with a 0.1N NH_4PF_6 solution (3 x 40 mL). The organic phase was filtered over cotton and concentrated to dryness. Purification by silica gel column chromatography (CH_2Cl_2/MeOH, 99:1 → 97:3) afforded **22** (198 mg, quantitative) as a brownish oil. ^{1}H-NMR (400 MHz, $CDCl_3$) δ 7.92-7.75 (m, 4H, CH_{Ar}), 7.57-7.47 (m, 2H, CH_{Ar}) 7.43 (d, J = 8.3 Hz, 1H, CH_{Ar}), 4.34 (s, 2H, CH_2), 2.40 (s, 3H, CH_3COS). ^{13}C-NMR (100 MHz, $CDCl_3$) δ 194.0 (SCO), 133.1, 131.8 (C_{Ar}), 127.7, 127.6, 127.3, 127.0, 126.9, 126.0, 125.1 (CH_{Ar}), 33.4 (CH_2), 30.3 (CH_3).

(2*R*,8*R*)-2-[(*tert*-Butyldiphenylsilyloxy)methyl]-8-[(2-naphthylmethylthio)methyl]-2,3,4,6,7,8-hexahydro-1*H*-pyrimido[1,2-*a*].9-pyrimidinium hexafluorophosphate (21).

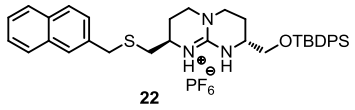

22

To a solution of compound **22** (100 mg, 0.454 mmol) in MeOH (10 mL), Cs_2CO_3 (394 mg, 1.209 mmol) was added and the mixture was stirred for 15 min under N_2 at room temperature. Then a solution of **2** (200 mg, 0.302 mmol) in CH_3CN (15 mL) was added and the mixture was stirred for 4 h. Afterwards the solvent was evaporated to dryness and then dissolved in CH_2Cl_2. The solution was washed with a 0.1 N NH_4PF_6 solution (3 × 25 mL). The organic phase was filtered over cotton and concentrated at reduced pressure to give a crude which was purified by silica gel (with KPF_6) column chromatography (CH_2Cl_2/MeOH, 98:2 → 94:6), yielding **21** (160 mg, 72%) as a yellow solid. ^{1}H-NMR (400 MHz, $CDCl_3$) δ 7.92-7.77 (m, 4H, CH_{Ar}), 7.67-7.58 (m, 4H, CH_{Ar}), 7.54-7.40 (m, 9H, CH_{Ar}), 6.15 (s, 1H, NH), 5.93 (s, 1H, NH), 3.93 (s, 2H, $C_{Ar}CH_2S$), 3.72-3.60 (m, 2H, CH_2O), 3.51-3.36 (m, 2H, CH_α), 3.29-3.12 (m, 4H, $CH_{2\gamma}$), 2.74 (dd, J = 5.8, 13.7 Hz, 1H, CH_2S), 2.58 (dd, J = 7.8, 13.7 Hz, 1H, CH_2S), 2.07-1.75 (m, 4H, $CH_{2\beta}$), 1.07 (s, 9H, $CH_{3t\text{-Bu}}$). ^{13}C-NMR (100 MHz, $CDCl_3$) δ 151.2 (C_{guan}) 135.5, 135.4, 133.1, 132.6, 131.8, 129.8, 128.9, 127.9, 127.8, 127.6, 127.4, 127.1, 126.9, 126.2, 125.3 (C_{Ar}, CH_{Ar}), 65.3 (CH_2O), 50.6, 49.3 (CH_α), 45.6, 44.6 ($CH_{2\gamma}$), 35.8, 33.4 (CH_2S), 26.7 ($CH_{3t\text{-Bu}}$), 22.7 ($CH_{2\beta}$), 19.1 ($C_{t\text{-Bu}}$).

(2*R*,8*R*)-2-(Hydroxymethyl)-8-[(2-naphthylmethylthio)methyl]-2,3,4,6,7,8-hexahydro-1*H*-pyrimido[1,2-*a*]-9-pyrimidinium mesylate (23).

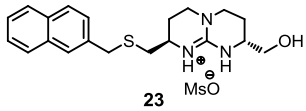

23

Procedure 1

Compound **21** (160 mg, 0.216 mmol) was dissolved in 3N HCl/CH_3CN (1:1, 15 mL) and stirred for 24 h at room temperature. The solvent was removed and the resulting crude dissolved in distilled water (15 mL) and washed with CH_2Cl_2 (3 × 15 mL). The aqueous phase was evaporated to dryness, yielding **23 (Cl^-)** (33 mg, 30%) as a white solid.

Procedure 2

To a solution of **21** (175 mg, 0.237 mmol) in THF/H_2O (2:1, 25 mL), MsOH (0.230 mL, 3.553 mmol) was slowly added at room temperature. The mixture was stirred and refluxed overnight. The solvent was evaporated to dryness and then dissolved in water (20 mL). The aqueous layer was washed with Et_2O (25 mL), $CHCl_3$ (3 × 15 mL) and Et_2O (15 mL). Afterwards the aqueous phase was concentrated over 50%. $KHCO_3$ (474 mg, 4.74 mmol) was added and the solvent was removed. MeOH (50 mL) was added, the precipitate was removed by filtration and the solvent evaporated at reduced pressure. This step was repeated a few times increasing the amount of CH_2Cl_2 until pure CH_2Cl_2 to afford **23 (MsO^-)** (81 mg, 96%). ^{1}H-NMR (400 MHz, $CDCl_3$) δ 7.88-7.69 (m, 4H, CH_{Ar}), 7.55-7.43 (m, 3H, CH_{Ar}), 3.92 (s, 2H, $C_{Ar}CH_2S$), 3.72-3.62 (m, 2H, CH_2O), 3.50-3.34 (m, 2H, CH_α), 3.28-3.07 (m, 4H, $CH_{2\gamma}$), 2.70 (dd, J = 5.7, 13.3 Hz, 1H, CH_2S), 2.51 (dd, J = 7.7, 13.3 Hz, 1H, CH_2S), 2.07-1.72 (m, 4H, $CH_{2\beta}$). ^{13}C-NMR (100 MHz, $CDCl_3$) δ 151.2 (C_{guan}) 133.1, 131.8, 127.9, 127.8, 127.6, 127.4, 127.1, 126.9, 126.2, 125.3 (C_{Ar}, CH_{Ar}), 64.5 (CH_2O), 50.5, 49.5 (CH_α), 45.6, 43.9 ($CH_{2\gamma}$), 35.7, 33.5 (CH_2S), 22.7 ($CH_{2\beta}$).

(2*R*,8*R*)-2-(Chloromethyl)-8-[(naphthalen-2-ylmethylthio)methyl]-2,3,4,6,7,8-hexahydro-1*H*-pyrimido[1,2-*a*]pyrimidin-9-ium chloride (24).

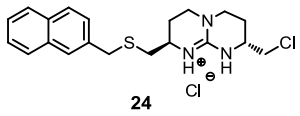

24

To a solution of compound **23** (33 mg, 0.066 mmol) in CH_2Cl_2 (10 mL), thionyl chloride (48 μL, 0.659 mmol) was added dropwise. Then the reaction mixture was stirred and refluxed for 5 h. The solvent was evaporated to dryness and the residue was dissolved in CH_2Cl_2 (20 mL). The solution was washed with Et_2O (2 × 15 mL) and a 0.1N NH_4Cl solution. The organic layer was filtered over cotton and concentrated at reduced pressure to give a crude which was purified by silica gel column chromatography (CH_2Cl_2/MeOH, 98:2 → 94:6), affording **24** (10 mg, 29%) as a yellow solid. ^{1}H-NMR (400 MHz, $CDCl_3$) δ 9.25 (s, 1H, NH), 8.92 (s, 1H, NH), 7.90-7.67 (m, 4H, CH_{Ar}), 7.55-7.44 (m, 3H, CH_{Ar}), 3.97 (s, 2H, $C_{Ar}CH_2S$), 3.79-3.64 (m, 2H, CH_2O), 3.54-3.44 (m, 2H, CH_α), 3.34-3.13 (m, 4H, $CH_{2\gamma}$), 2.84 (dd, J = 4.8, 13.5 Hz, 1H, CH_2S), 2.57 (dd, J = 8.36, 13.5 Hz, 1H, CH_2S), 2.15-1.84 (m, 4H, $CH_{2\beta}$). ^{13}C-NMR (100 MHz, $CDCl_3$) δ 151.2 (C_{guan}), 133.1, 131.8, 127.9, 127.8, 127.6, 127.4, 127.1, 126.9, 126.2, 125.3 (C_{Ar}, CH_{Ar}), 50.5, 49.5 (CH_α), 45.6, 45.3, 43.9 ($CH_{2\gamma}$, CH_2Cl), 35.5, 33.5 (CH_2S), 22.7 ($CH_{2\beta}$).

(2*R*,8*R*)-2-[(Methylsulfonyloxy)methyl]-8-[(2-naphthalylmethylthio)methyl]-2,3,4,6,7,8-hexahydro-1*H*-pyrimido[1,2-*a*]-9-pyrimidinium hexafluorophosphate (25).

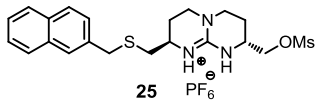

25

To a solution of alcohol **23** (MsO^-) (81 mg, 0.179 mmol) and NMM (160 μL, 1.44 mmol) in dry CH_2Cl_2 (15 mL) was added Ms_2O (156 mg, 0.898 mmol) and the mixture was stirred for 6 h. The solvent was evaporated at reduced pressure and the resulting

crude dissolved in CH_2Cl_2 (20 mL) and washed with a 0.1N NH_4PF_6 solution (2 × 20 mL). The organic layer was filtered over cotton and concentrated to dryness. Purification by silica gel (with KPF_6) column chromatography (CH_2Cl_2/MeOH, 97:3) afforded **25** (91 mg, 87%) as a clear yellowish solid. ^{1}H-NMR (400 MHz, $CDCl_3$) δ 7.93-7.87 (m, 3H, CH_{Ar}) 7.81 (s, 1H, CH_{Ar}), 7.58-7.50 (m, 3H, CH_{Ar}), 6.39 (s, 1H, NH), 6.33 (s, 1H, NH), 4.31-4.24 (m, 1H, CH_2OMs), 4.12 (dd, J = 7.4, 10.5 Hz, 1H, CH_2OMs), 3.97 (s, 2H, $C_{Ar}CH_2S$), 3.73 (m, 1H, CH_α), 3.53 (m, 1H, CH_α), 3.35-3.23 (m, 4H, $CH_{2\gamma}$), 3.12 (s, 3H, CH_{3MsO}), 2.70 (dd, J = 5.4, 13.8 Hz, 1H, CH_2S), 2.53 (dd, J = 8.3, 13.8 Hz, 1H, CH_2S), 2.12-1.73 (m, 4H, $CH_{2\beta}$). ^{13}C-NMR (100 MHz, $CDCl_3$) δ 150.6 (C_{guan}), 133.1, 131.8, 127.9, 127.8, 127.6, 127.4, 127.1, 126.9, 126.2, 125.3 (CH_{Ar}, C_{Ar}), 69.5 (CH_2OMs), 50.1, 47.7 (CH_α), 45.3, 44.9 ($CH_{2\gamma}$), 37.1 (CH_{3MsO}), 35.5, 33.8 (CH_2S), 22.4, 21.9 ($CH_{2\beta}$).

(2*R*,8*R*)-2-(Acetylthiomethyl)-8-[(2-naphthylmethylthio)methyl]-2,3,4,6,7,8-hexahydro-1*H*-pyrimido[1,2-*a*]-9-pyrimidinium hexafluorophosphate (26).

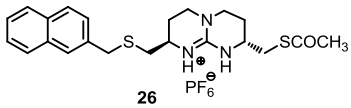

26

Compound **25** (90 mg, 0.154 mmol) and potassium thioacetate (91 mg, 0.622 mmol) were dissolved in CH_3CN (20 mL) and the mixture was refluxed and stirred for 7 h. After cooling it to room temperature the solvent was removed and then dissolved in CH_2Cl_2 (20 mL). Then, the solution was washed with a 0.1N NH_4PF_6 solution (3 × 20 mL). The organic phase was filtered over cotton and concentrated to dryness. Purification by silica gel column chromatography (CH_2Cl_2/MeOH, 99:1 → 95:5) afforded **26** (73 mg, 84%) as a brownish oil. ^{1}H-NMR (400 MHz, $CDCl_3$) δ 7.87-7.78 (m, 3H, CH_{Ar}) 7.75 (s, 1H, CH_{Ar}), 7.53-7.41 (m, 3H, CH_{Ar}), 6.21 (s, 1H, NH), 6.16 (s, 1H, NH), 3.88 (s, 2H, $C_{Ar}CH_2S$), 3.53-3.40 (m, 2H, CH_α), 3.39-3.14 (m, 4H, $CH_{2\gamma}$), 2.99 (d, J = 6.5 Hz, 2H, CH_2S), 2.58 (d, J = 6.5 Hz, 2H, CH_2S), 2.37 (s, 3H, CH_3CO), 2.07-1.95 (m, 2H, $CH_{2\beta}$), 1.83-1.69 (m, 2H, $CH_{2\beta}$). ^{13}C-NMR (100 MHz, $CDCl_3$) δ

195.8 (CO), 150.2 (C_{guan}), 135.2, 133.3, 132.5, 128.6, 127.9, 127.6, 127.1, 126.4, 126.0 (CH_{Ar}, C_{Ar}), 48.6, 47.9 (CH_{α}), 45.3, 45.0 ($CH_{2\gamma}$), 36.7, 35.7, 32.6 (CH_2S), 30.5 (CH_3CO), 25.2, 24.5 ($CH_{2\beta}$). ESI-MS *m/z* 414.2 $(M\text{-}PF_6^-)^+$.

Compound 27

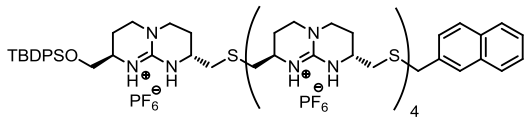

27

Cs_2CO_3 (56 mg, 0.174 mmol) and PBu_2Ph polystyrene (94 mg, 0.078 mmol) were added to a solution of **26** (44 mg, 0.078 mmol) in MeOH (10 mL). The mixture was stirred for 30 min under N_2 at room temperature. Afterwards, a solution of compound **18** (110 mg, 0.065 mmol) in CH_3CN (15 mL) was added and the mixture was stirred for 2 days. The solvent was evaporated under vacuum, dissolved in CH_2Cl_2 (30 mL) and washed with 0.1N NH_4PF_6 (2 × 20 mL). The organic layer was filtered over cotton and concentrated to dryness. Purification by silica gel (with KPF_6) column chromatography (CH_2Cl_2/MeOH, 98:2 → 94:6) afforded **27** (90 mg, 71%) as a yellowish solid. ^{1}H-NMR (400 MHz, CD_3CN) δ 7.94-7.87 (m, 3H, CH_{Ar}) 7.81 (s, 1H, CH_{Ar}), 7.73-7.68 (m, 4H, CH_{Ar}), 7.59-7.43 (m, 9H, CH_{Ar}), 6.47-6.05 (bs, 5H, NH), 3.97 (s, 2H, $C_{Ar}CH_2S$), 3.80-3.44 (m, 12H, CH_2O, CH_{α}), 3.43-3.22 (m, 20H, $CH_{2\gamma}$), 2.93-2.42 (m, 18H, CH_2S), 2.20-1.70 (m, 20H, $CH_{2\beta}$), 1.09 (s, 9H, $CH_{3t\text{-}Bu}$). HPLC-MS: Conditions: Column SunFire C18 5 μm, 4.6x150 mm. Gradient H_2O/ACN (0.1%TFA) 95% →100% ACN in 34 min. Retention time: 18.07 min. ESI-MS *m/z* 1838.5 $(M\text{-}TFA^-)^+$.

Compound 28

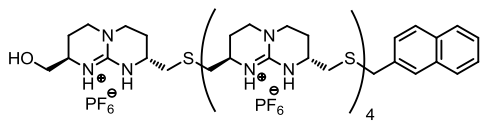

28

A solution of **27** (90 mg, 0.046 mmol) in 3N HCl/CH_3CN (1:1, 10 mL) was stirred for 2 days at room temperature. The solvent was removed and the resulting crude was dissolved in distilled water (15 mL) and washed with CH_2Cl_2 (3 × 15 mL). The aqueous phase was evaporated to dryness, yielding **28** as a yellowish oil. Afterwards this oil was purified by semi-preparative HPLC (Analytical conditions: Column: SunFire C18 5 μm, 150 x 4.6 mm, MP: CH_3CN (0.05% TFA)/H_2O (0.05% TFA), Gradient: 30-45% CH_3CN (0.05% TFA) in 30 min, Flow: 1 mL/min, room temperature) and lyophilized, yielding **28** (13 mg, 21%). ^{1}H-NMR (400 MHz, MeOD) δ 3.95 (s, 2H, $C_{Ar}CH_2S$), 3.71-3.43 (m, 12H, CH_2O, CH_α), 3.45-3.24 (m, 20H, $CH_{2\gamma}$), 2.84-2.65 (m, 9H, CH_2S), 2.62-2.49 (m, 9H, CH_2S), 2.21-1.70 (m, 20H, $CH_{2\beta}$). HPLC-MS: Conditions: Column SunFire C18 5 μm, 4.6x150 mm. Gradient H_2O/ACN (0.1%TFA) 5% →100% ACN in 25 min. Retention time: 11.1 min. ESI-MS m/z 1600.5 (M - $TFA^-)^+$, 743.8 (M – 2 $TFA^-)^{+2}$. HRMS calcd. for $[C_{56}H_{90}N_{15}O_2S_5]^{3+}$ 328.1961; found 328.1942.

(*R*)-1-(2-Aminobenzyl)-3-[1-(*tert*-butyldiphenylsilyloxymethyl)-4-(methylthio)-2-butyl] thiourea (29).

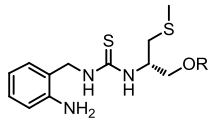

29

A solution of (2*R*)-1-(*tert*-butyldiphenylsilyloxy)-5-thia-2-hexyl isothiocyanate (3.91 g, 9.45 mmol) and 2-aminobenzylamine (1.27 g, 11.34 mmol) in CH_3CN (15 mL) was stirred for 3 days at room temperature. Solvent was eliminated at reduced pressure and the crude was purified by silica gel column chromatography (Et_2O/hexane, 70:30 → 55:45), affording **29** (3.21 g, 65%). ^{1}H-NMR (400 MHz, $CDCl_3$) δ 7.63-7.59 (m, 4H, Ph-Si), 7.45-7.35 (m, 6H, Ph-Si), 7.10 (dt, J = 1.6, 8.0 Hz, 1H, H_a), 7.02 (d, J = 7.6 Hz, 1H, H_d), 6.67 (t, J = 7.6 Hz, 1H, H_c), 6.63 (d, J = 8.0 Hz, 1H, H_b), 6.40-5.95 (m, 3H, NH, NH_2), 4.82 (bs, 1H, NH), 4.52 (dd, J = 14.0, 3.2 Hz, 1H, CH_α), 4.14 (bs, 2H,

Ar*CH*$_2$), 3.69 (m, 2H, CH_2OSi), 2.40 (t, J = 6.8 Hz, 2H, $CH_{2\gamma}$), 2.00-1.75 (m, 5H, SCH_3, $CH_{2\beta}$), 1.06 (s, 9H, $CH_{3t\text{-}Bu}$). ^{13}C-NMR (400 MHz, $CDCl_3$) δ 180.3 (C=S), 144.6 (C_{Ar}-NH_2), 134.6, 131.8, 129.5, 129.0, 128.4, 126.9, 119.7, 116.9, 114.8 (CH_{Ar}, C_{Ar}), 64.5 (CH_2O), 53.3 (CH_α), 46.4 (ArCH_2NH), 29.6 ($CH_{2\beta}$, $CH_{2\gamma}$), 25.9 ($CH_{3t\text{-}Bu}$), 18.2 ($C_{t\text{-}Bu}$), 14.1 (SCH_3).

(*R*)-2,3,4,6-Tetrahydro-2-(*tert*-butyldiphenylsilyloxymethyl)-1*H*-pyrimido[2,1-*b*]quinazolinium hydrochloride (30).

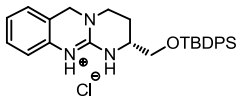

30

To a solution of **29** (2.54 g, 4.73 mmol) in dry CH_2Cl_2 were added diisopropylethylamine (DIPEA) (286 µL, 1.630 mmol) and methyl trifluoromethanesulfonate (1.1 mL, 10.402 mmol) at low temperature and under argon. The mixture was stirred for 2 h at room temperature and more DIPEA (6.84 mL, 38.99 mmol) was added dropwise and the mixture was refluxed for 12 h. Solvent was eliminated at reduced pressure and the residue was distributed between 1N NaOH (5 mL) and diethyl ether (10 mL). The organic phase was washed with 1N NaOH (50 mL) and water (50 mL). The organic phase was then collected in a flask and a solution of 1N NH_4Cl was added to allow the product to precipitate *via* vigorous agitation. Compound **30** was filtered off (819 mg, 35%) and the organic phase was dried over Na_2SO_4. After elimination of the solvent a yellow oil was obtained, which was purified by silica gel column chromatography (CH_2Cl_2/MeOH, 100 → 95:5). The isolated compound was still impure and did not precipitate in diethyl ether. Therefore, purification still needs improvement. ^{1}H-NMR (400 MHz, $CDCl_3$) δ 11.67 (bs, 1H, Ph-NH), 9.39 (s, 1H, NH), 7.71-7.63 (m, 4H, CH_{Ar}), 7.50-7.38 (m, 6H, CH_{Ar}), 7.28-7.23 (m, 1H, CH_{Ar}), 7.14-6.97 (m, 3H, CH_{Ar}), 4.43 (ABX system, 2H, $CH_{2\gamma}C_{Ar}$), 3.93-3.87 (dd, J = 4.1, 10.3 Hz, 2H, CH_2O), 3.78-3.63 (m, 2H, CH_α), 3.38-3.23 (m, 2H, $CH_{2\gamma}$), 2.24-2.02 (m, 2H, $CH_{2\beta}$), 1.10 (s, 9H, $CH_{3t\text{-}Bu}$). ^{13}C-NMR (400 MHz, $CDCl_3$) δ 149.7

(C_{guan}), 135.5, 135.4, 132.5, 132.4, 129.9, 128.9, 127.8, 125.3, 123.8, 115.6, 115.5 (CH_{Ar}, C_{Ar}), 65.1 (CH_2O), 49.6 (Ph*C*H_2N), 49.2 (CH_α), 44.4 ($CH_{2\gamma}$), 26.8 ($CH_{3t\text{-}Bu}$), 22.5 ($CH_{2\beta}$), 19.0 ($C_{t\text{-}Bu}$). HRMS calcd. for $[C_{28}H_{34}N_3OSi]^+$ 456.2471; found 456.2472.

(*R*)-2-(Hydroxymethyl)-2,3,4,6-tetrahydro-1*H*-pyrimido[2,1-*b*]-11-quinazolinium mesylate (31).

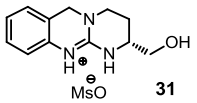

31

To a solution of **30** (256 mg, 0.520 mmol) in THF/H_2O (2:1, 25 mL), MsOH (675 μL, 10.41 mmol) was slowly added at room temperature. The mixture was stirred and refluxed overnight. The solvent was evaporated to dryness and then dissolved in water (20 mL). The aqueous layer was washed with Et_2O (25 mL), $CHCl_3$ (3 × 15 mL) and Et_2O (15 mL). Afterwards the aqueous phase was concentrated over 50% and $KHCO_3$ (1.04 g, 10.41 mmol) was added and the solvent was removed completely. MeOH (50 mL) was added, the precipitate was removed by filtration and the solvent evaporated at reduced pressure. This step was repeated for a few times increasing the amount of CH_2Cl_2 until pure CH_2Cl_2 was reached, affording **31** (114 mg, 70%) as an oil. ^{1}H-NMR (400 MHz, $CDCl_3$) δ 7.11 (t, J = 7.2 Hz, 1H, CH_{Ar}), 6.92-6.78 (m, 3H, CH_{Ar}), 4.37 (ABX system, 2H, $CH_{2\gamma}C_{Ar}$), 3.81-3.72 (m, 2H, CH_2O), 3.69-3.58 (m, 1H, CH_α), 3.53-3.43 (m, 1H, CH_α), 3.28 (td, J = 4.1, 11.6 Hz, 1H, $CH_{2\gamma}$), 3.22-3.13 (m, 1H, $CH_{2\gamma}$), 2.05-1.94 (m, 1H, $CH_{2\beta}$), 1.82-1.67 (m, 1H, $CH_{2\beta}$). ^{13}C-NMR (400 MHz, $CDCl_3$) δ 149.7 (C_{guan}), 135.5, 129.9, 128.9, 128.2, 127.8, 126.0 (CH_{Ar}, C_{Ar}), 63.9 (CH_2O), 49.6 (Ph*C*$H_{2\beta}$), 49.2 (CH_α), 44.4 ($CH_{2\gamma}$), 22.5 ($CH_{2\beta}$). ESI-MS m/z 218.1 $(M\text{-}MsO^-)^+$. HRMS calcd. for $[C_{12}H_{16}N_3O]^+$ 218.1293; found 218.1296.

(*R*)-2-[(Methylsulfonyloxy)methyl]-2,3,4,6-tetrahydro-1*H*-pyrimido[2,1-*b*]-11-quinazolinium hexafluorophosphate (32).

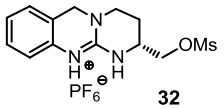

32

To a solution of compound **31** (MsO^-) (113 mg, 0.362 mmol) and NMM (322 μL, 2.90 mmol) in dry CH_2Cl_2 (15 mL) was added Ms_2O (315 mg, 1.81 mmol) and the mixture was stirred for 6 h. The solvent was evaporated under reduced pressure and the resulting crude was dissolved in CH_2Cl_2 (20 mL) and washed with a 0.1N NH_4PF_6 solution (2 × 20 mL). The organic layer was filtered over cotton and concentrated at reduced pressure. Purification by silica gel (with KPF_6) column chromatography (CH_2Cl_2/MeOH, 99:1 → 95:5) afforded **32** (90 mg, 57%) as a white solid. ^{1}H-NMR (400 MHz, CD_3CN) δ 7.34-7.28 (m, 1H, CH_{Ar}), 7.20-7.14 (m, 2H, CH_{Ar}), 6.95 (d, J = 7.9 Hz, 1H, CH_{Ar}), 4.59 (s, 2H, $CH_{2\gamma}C_{Ar}$), 4.40-4.34 (dd, J = 4.5, 10.6 Hz, 1H, CH_2OMs), 4.23 (dd, J = 7.0, 10.7 Hz, 1H, CH_2OMs), 3.98-3.90 (m, 1H, CH_α), 3.52-3.41 (m, 2H, $CH_{2\gamma}$), 3.14 (s, 3H, CH_{3MsO}), 2.15-1.82 (m, 4H, $CH_{2\beta}$).^{13}C-NMR (400 MHz, CD_3CN) δ 150.9 (C_{guan}), 135.3, 129.5, 128.7, 128.2, 127.6, 125.8 (CH_{Ar}, C_{Ar}), 60.5 (CH_2O), 49.6 (Ph*C*$H_{2\beta}$), 49.2 (CH_α), 44.4 ($CH_{2\gamma}$), 39.2 (CH_{3MsO}), 22.5 ($CH_{2\beta}$).

(*R*)-2-((Acetylthio)methyl)-2,3,4,6-tetrahydro-1H-pyrimido[2,1-*b*]-11-quinazolinium hexafluorophosphate (33)

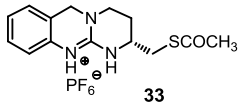

33

Compound **32** (91 mg, 0.205 mmol) and potassium thioacetate (82 mg, 0.716 mmol) were dissolved in CH_3CN (15 mL) and the mixture was refluxed and stirred overnight. After cooling to room temperature, the solvent was removed and the crude was dissolved in CH_2Cl_2 (20 mL). Then, the solution was washed with a 0.1N NH_4PF_6 solution (3 × 20 mL). The organic phase was filtered over cotton and concentrated to

dryness. Purification by silica gel column chromatography (CH_2Cl_2/MeOH, 100:0 → 95:5) afforded **33** (65 mg, 75%) as a brownish oil. ^{1}H-NMR (400 MHz, $CDCl_3$) δ 8.40 (s, 1H, NH), 7.27-7.21 (m, 1H, CH_{Ar}), 7.13-7.00 (m, 2H, CH_{Ar}), 6.93 (d, J = 7.9 Hz, 1H, CH_{Ar}), 6.71 (s, 1H, NH), 4.55 (s, 2H, $CH_{2\gamma}C_{Ar}$), 3.81-3.69 (m, 1H, CH_α), 3.56-3.40 (m, 2H, $CH_{2\gamma}$), 3.20-3.06 (m, 2H, CH_2S), 2.39 (s, 3H, CH_3CO), 2.26-2.12 (m, 2H, $CH_{2\beta}$). ^{13}C-NMR (100 MHz, $CD_3CN/CDCl_3$) δ 195.5 (CO), 148.8 (C_{guan}), 128.9, 126.1, 124.5, 118.9 (CH_{Ar}), 49.1 ($CH_{2\gamma}$), 48.7 (CH_α), 44.5 ($CH_{2\gamma}$), 32.3 (CH_2S), 29.9 (CH_3CO), 23.9 ($CH_{2\beta}$). ESI-MS m/z 276.1 (M – PF_6^-)$^+$. HRMS calcd. for $[C_{14}H_{18}N_3OS]^+$ 276.1171; found 276.1177.

Compound 34

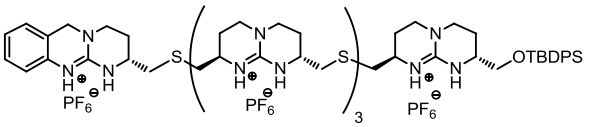

34

To a solution of **33** (27 mg, 0.065 mmol) in MeOH (5 mL), Cs_2CO_3 (51 mg, 0.158 mmol) and PBu_2Ph polystyrene (78 mg, 0.065 mmol) were added and stirred for 30 min. under N_2 at room temperature. Afterwards, a solution of compound **18** (100 mg, 0.059 mmol) in CH_3CN (15 mL) was added to the mixture and stirred overnight. The solvent was evaporated under vacuum, dissolved in CH_2Cl_2 (30 mL) and washed with 0.1N NH_4PF_6 (2 × 20 mL). The organic layer was filtered over cotton and concentrated to dryness. Purification by silica gel (with KPF_6) column chromatography (CH_2Cl_2/MeOH, 98:2 → 94:6) afforded **34** (73 mg, 63%) as a yellowish solid. ^{1}H-NMR (400 MHz, CD_3CN) δ 8.36 (s, 1H, NH), 7.74-7.67 (m, 4H, CH_{Ar}), 7.56-7.44 (m, 6H, CH_{Ar}), 7.32 (t, J = 7.4 Hz, 1H, CH_{Ar}), 7.22-7.13 (m, 2H, CH_{Ar}), 6.94 (d, J = 7.9 Hz, 1H, CH_{Ar}), 6.58 (s, 1H, NH), 6.23 (s, 7H, NH), 4.59 (s, 2H, $CH_{2\gamma}C_{Ar}$), 3.76 (dd, J = 4.3, 10.2 Hz, 1H, CH_2O), 3.73-3.50 (m, 10H, CH_2O, CH_α), 3.49-3.28 (m, 18H, $CH_{2\gamma}$), 2.94-2.77 (m, 8H, CH_2S), 2.71-2.52 (m, 8H, CH_2S), 2.14-2.07 (m, 10H, $CH_{2\beta}$), 1.91-1.77 (m, 8H, $CH_{2\beta}$), 1.09 (s, 9H, $CH_{3t\text{-}Bu}$). ^{13}C-NMR (100 MHz, CD_3CN) δ 150.8, 150.7, 150.6

(C_{guan}), 135.5, 135,4, 132.4 (C_{Ar}), 130.1, 128.9, 128.0, 126.2, 124.4, 114.9 (CH_{Ar}), 65.9 (CH_2O), 50.1 (CH_α), 49.1 ($CH_{2\gamma}$), 47.8, 47.7 (CH_α), 45.1, 45.0, 44.8 ($CH_{2\gamma}$), 36.0, 35.9, 35.8, 35.7 (CH_2S), 26.2 (CH_3), 25.2, 25.1, 24.8, 22.1 ($CH_{2\beta}$), 18.8 ($C_{t\text{-}Bu}$). HPLC-MS: Conditions: Column SunFire C18 5 μm, 4.6x150 mm. Gradient H_2O/ACN (0.1%TFA) 5% →100% ACN in 20 min. Retention time: 10.40 min. ESI-MS *m/z* 1700.794 $(M - TFA^-)^+$.

Compound 35

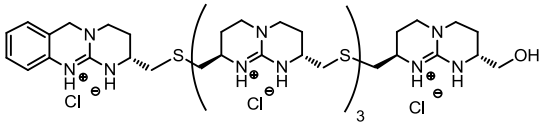

35

Compound **34** (37 mg, 0.019 mmol) was dissolved in 3N HCl/CH_3CN (1:1, 10 mL) and stirred for 2 days at room temperature. The solvent was removed and the resulting crude dissolved in distilled water (15 mL) and washed with CH_2Cl_2 (3 × 15 mL). The aqueous phase was evaporated to dryness, yielding **35** (22 mg, quantitative) as a yellowish oil. Analytical conditions: Column: Symmetry300 C18 5 μm, 150 x 4.6 mm, MP: CH_3CN (0.05% TFA)/H_2O (0.05% TFA), Gradient: 5-100% CH_3CN (0.05% TFA) in 20 min, Flow: 1 mL/min, room temperature, wavelength 220 nm. Retention time: 8.7 min. HRMS calcd. for $[C_{48}H_{76}N_{15}OS_4]^+$ 1006.5235; found 1006.4870.

Compound 36

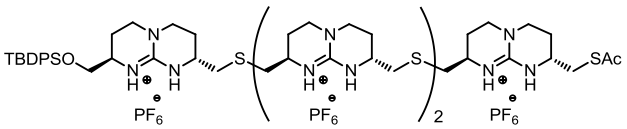

36

Compound **18** (10 mg, 0.006 mmol) and potassium thioacetate (2.7 mg, 0.024 mmol) were dissolved in CH_3CN (2 mL) and the mixture was refluxed and stirred overnight. After cooling it to room temperature, the solvent was removed and the crude dissolved

in CH_2Cl_2. Then, the solution was washed with a 0.1N NH_4PF_6 solution (2 × 10 mL). The organic phase was filtered over cotton and concentrated to dryness. Compound **36** (9 mg, 91%) was characterized by NMR and used directly in the next synthetic step without further purification. ^{1}H-NMR (400 MHz, CD_3CN) δ 7.76-7.67 (m, 4H, CH_{Ar}), 7.56-7.39 (m, 6H, CH_{Ar}), 3.83 (dd, J = 4.3, 9.8 Hz, 1H, CH_2O), 3.68 (dd, J = 7.3, 9.8 Hz, 1H, CH_2O), 3.65-3.41 (m, 6H, CH_α), 3.40-3.20 (m, 18H, CH_α, $CH_{2\gamma}$), 2.97-2.54 (m, 12H, CH_2S), 2.48-2.42 (m, 2H, CH_2S), 2.76-2.57 (m, 2H, CH_2S), 2.35 (s, 3H, CH_3CO), 2.12-2.02 (m, 8H, $CH_{2\beta}$), 1.91-1.65 (m, 8H, $CH_{2\beta}$), 1.05 (s, 9H, $CH_{3t\text{-}Bu}$). ^{13}C-NMR (100 MHz, CD_3CN) δ 135.5, 135.4, 130.0, 128.1, 128.0 (C_{Ar}), 65.3 (CH_2O), 49.3, 48.8, 48.3, 47.5 (CH_α), 44.9, 44.5, 44.3 ($CH_{2\gamma}$), 36.4, 36.3, 36.2 (CH_2S), 30.0 (*CH_3*CO), 26.2 ($CH_{3t\text{-}Bu}$), 25.4, 25.1, 22.4 ($CH_{2\beta}$).

Compound 37

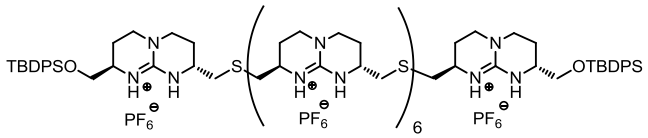

37

To a solution of **36** (74 mg, 0.044 mmol) in MeOH (5 mL), Cs_2CO_3 (30 mg, 0.092 mmol) and PBu_2Ph polystyrene (53 mg, 0.044 mmol) were added and stirred for 5 min under N_2 at room temperature. Afterwards, a solution of compound **18** (100 mg, 0.059 mmol) in CH_3CN (5 mL) was added to the mixture and stirred overnight. The solvent was evaporated under vacuum and the crude was triturated with 0.1N NH_4PF_6 (2 × 20 mL) and filtered. Purification by reverse phase–C18 column chromatography (H_2O/CH_3CN: 40/60 → 30/70) afforded **37** (93 mg, 65%) as a yellowish solid. ^{1}H-NMR (400 MHz, acetone-d_6) δ 7.74-7.69 (m, 8H, CH_{Ar}), 7.56-7.45 (m, 12H, CH_{Ar}), 7.23 (s, 1H, NH), 7.18 (bs, 6H, NH), 7.05 (s, 1H, NH), 3.87-3.70 (m, 20H, CH_2O, CH_α), 3.60-3.48 (m, 32H, $CH_{2\gamma}$), 3.05-2.96 (m, 14H, CH_2S), 2.78-2.70 (m, 14H, CH_2S), 2.29-2.15 (m, 16H, $CH_{2\beta}$), 2.06-1.90 (m, 16H, $CH_{2\beta}$), 1.08 (s, 18H, $CH_{3t\text{-}Bu}$). ^{13}C-NMR

(100 MHz, acetone-d_6) δ 151.4, 151.3, 151.2 (C_{guan}), 135.9, 135.8, 133.3, 133.2, 130.5, 130.4, 128.3 (CH_{Ar}, C_{Ar}), 66.4 (CH_2O), 50.6, 48.3, 48.2 (CH_α), 45.6, 45.5 ($CH_{2\gamma}$), 36.3, 36.2 (CH_2S), 26.7 ($CH_{3t\text{-}Bu}$), 25.9, 25.8, 22.8 ($CH_{2\beta}$), 19.3 ($C_{t\text{-}Bu}$). HRMS calcd. for $[C_{104}H_{166}F_{36}N_{24}O_2P_6S_7Si]^{+2}$ 1466.4525; found 1466.4358.

Compound 38

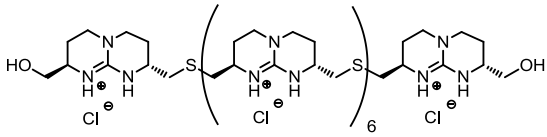

38

Compound **37** (55 mg, 0.017 mmol) was dissolved in 3N HCl/CH_3CN (1:1, 10 mL) and stirred for 2 days at room temperature. The solvent was removed and the resulting crude dissolved in distilled water (15 mL) and washed with CH_2Cl_2 (3 × 15 mL). The aqueous phase was evaporated to dryness, yielding **38** (33 mg, quant.) as a yellowish oil. ^{1}H-NMR (400 MHz, D_2O) δ 3.67-3.44 (m, 20H, CH_2O, CH_α), 3.42-3.26 (m, 32H, $CH_{2\gamma}$), 2.89-2.76 (m, 14H, CH_2S), 2.62 (dd, J = 8.0, 13.8 Hz, 14H, CH_2S), 2.15-1.93 (m, 16H, $CH_{2\beta}$), 1.92-1.72 (m, 16H, $CH_{2\beta}$). ^{13}C-NMR (100 MHz, D_2O) δ 62.2 (CH_2O), 48.8, 46.6, 46.4, 46.2 (CH_α), 43.6, 43.4 ($CH_{2\gamma}$), 34.6, 34.5 (CH_2S), 23.8, 20.9 ($CH_{2\beta}$). HPLC-MS: Conditions: Column SunFire C18 5 μm, 150 x 4.6 mm, MP: CH_3CN (0.05% TFA)/H_2O (0.05% TFA), Gradient: 5-100% CH_3CN (0.05% TFA) in 20 min, Flow: 1 mL/min, room temperature, wavelength 214 nm). Retention time: 6.0 min. ESI-MS m/z 2379.0 (M – $TFA^-)^+$. HRMS calcd. for $[C_{72}H_{130}Cl_5N_{24}O_2S_7]^{+3}$ 587.2426; found 587.2390.

1.6 Appendix

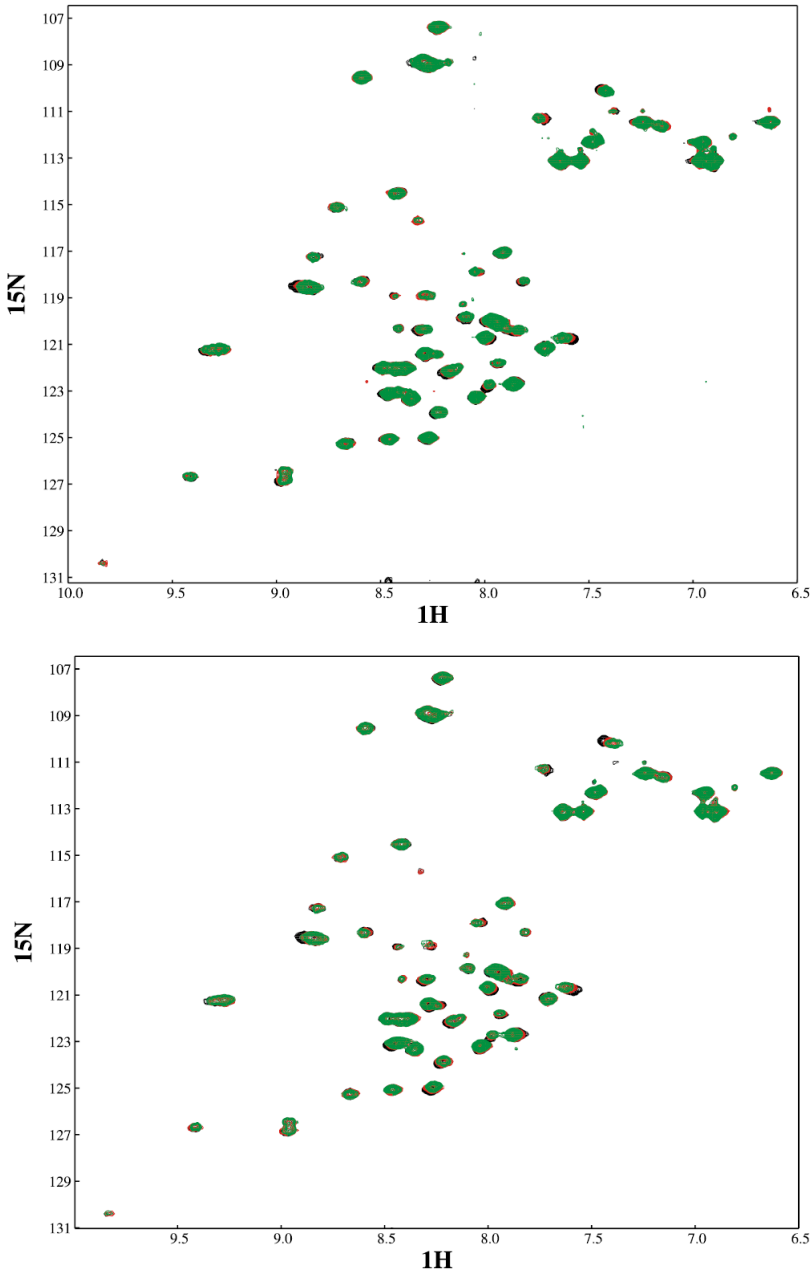

Figure 22. *[^{1}H, ^{15}N]-HSQC spectrum of p53TD wild type in the absence (black contours) and in the presence (2 and 4 eq. in red and green contours, respectively) of ligand* ***13*** *(top) and* ***20*** *(bottom).*

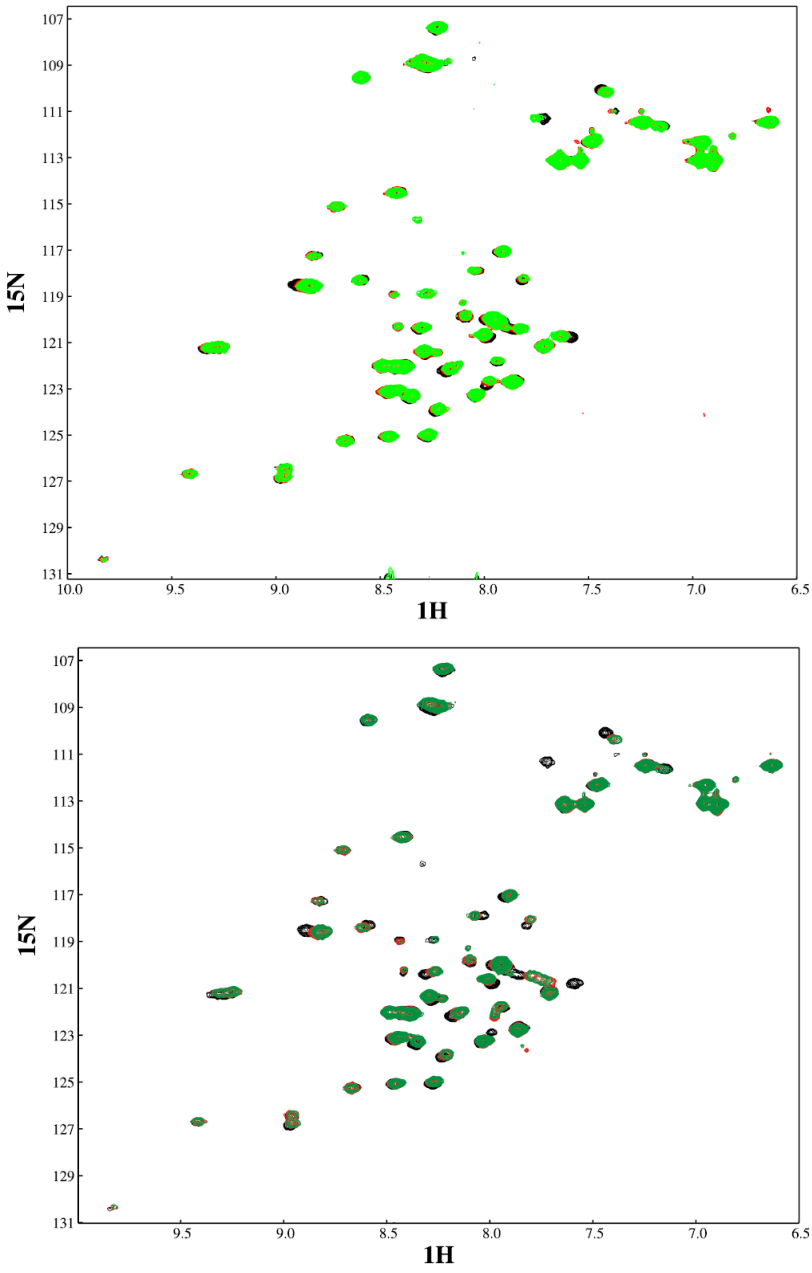

Figure 23. *[^{1}H, ^{15}N]-HSQC spectrum of p53TD wild type in the absence (black contours) and in the presence (2 and 4 eq. in red and green contours, respectively) of ligand* ***15*** *(top) and* ***28*** *(bottom).*

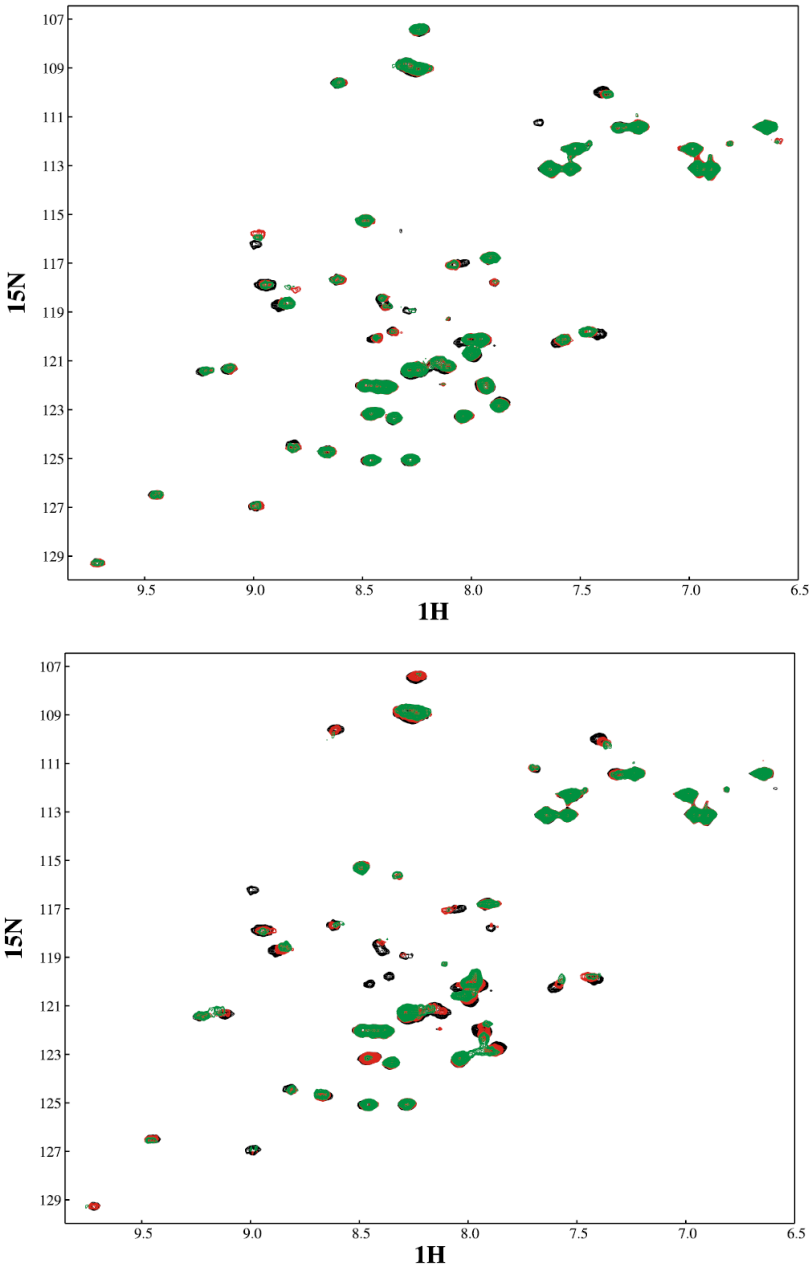

Figure 24. *[^{1}H, ^{15}N]-HSQC spectrum of p53TD R337H mutant in the absence (black contours) and in the presence (2 and 4 eq. in red and green contours, respectively) of ligand* ***13*** *(top) and* ***20*** *(bottom).*

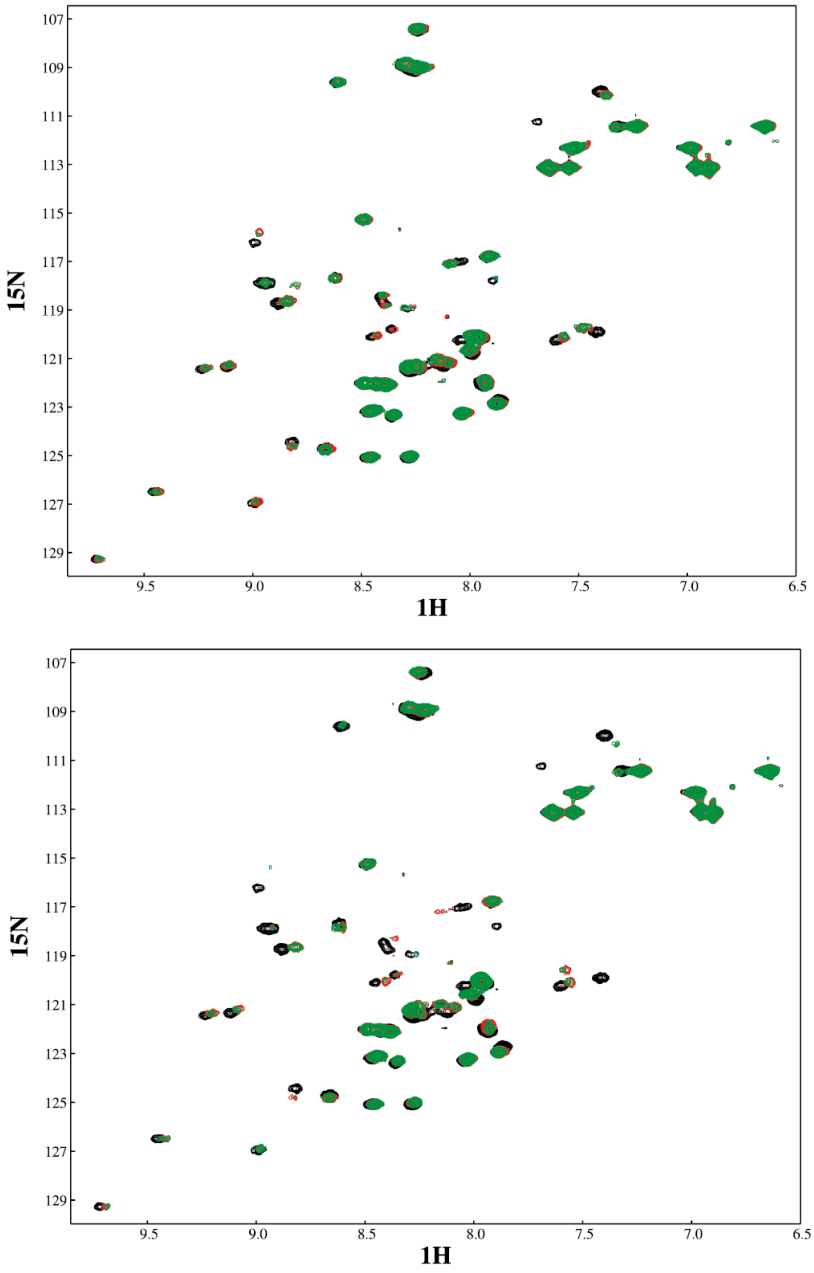

Figure 25. *[^{1}H, ^{15}N]-HSQC spectrum of p53TD R337H mutant in the absence (black contours) and in the presence (2 and 4 eq. in red and green contours, respectively) of ligand* ***15*** *(top) and* ***28*** *(bottom).*

UNIVERSITAT ROVIRA I VIRGILI
BICYCLIC GUANIDINIUM OLIGOMERS FOR RECOGNITION, CELL DELIVERY, AND MOLECULAR MATERIALS
Julián Valero Moreno
DL:T. 276-2012

Chapter 2

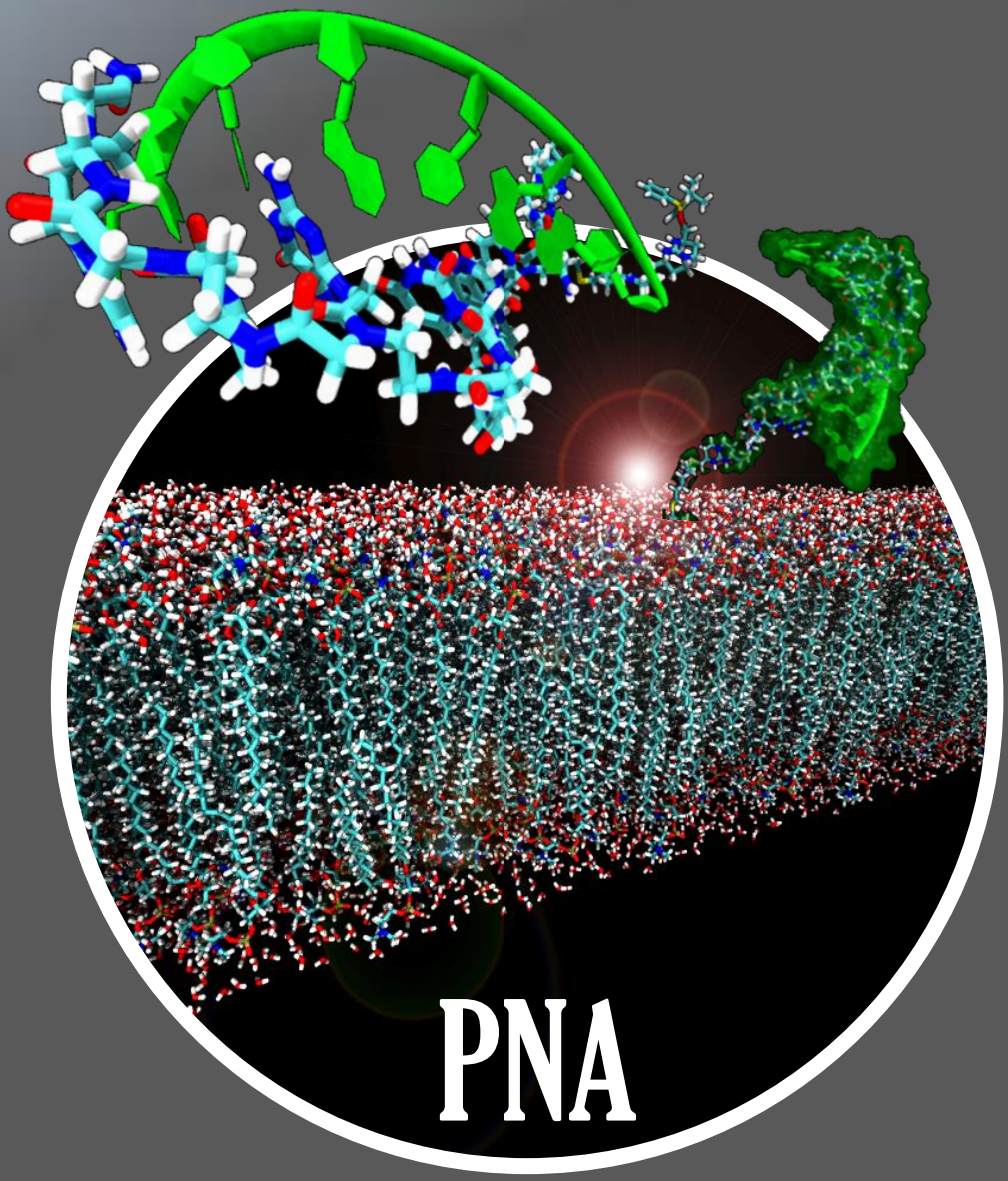

Cellular Uptake

UNIVERSITAT ROVIRA I VIRGILI
BICYCLIC GUANIDINIUM OLIGOMERS FOR RECOGNITION, CELL DELIVERY, AND MOLECULAR MATERIALS
Julián Valero Moreno
DL:T. 276-2012

Chapter 2

PNA-Oligoguanidinium Conjugates as Potential Tools for Gene Therapy

2.1 Introduction and Objectives

Peptide nucleic acids (PNAs) are oligonucleotide mimics whose nucleobases are attached through a pseudo-peptide backbone typically composed by *N*-(2-aminoethyl)glycine (aeg) subunits (Figure 1).[1] Different backbone modifications have been explored over the last decade. However, they have shown inferior selectivity and hybridization properties than the simplest aegPNA, although some of these backbone modifications have demonstrated specific improved features.[2] This DNA mimic combines the ability to store genetic information with the chemical robustness of peptides. Conceptually, a PNA can be considered as a hybrid structure between a regular oligonucleotide (nucleobase) and a peptide (amide-based backbone) and

[1] (a) Nielsen, P.E.; Egholm, M.; Berg, R.H.; Buchardt, O. *Science* **1991**, *254*, 1497-1500. (b) Nielsen, P. E. *Acc. Chem. Res.* **1999**, *32*, 624-630.

[2] (a) Ganesh, K. N.; Nielsen, P. E. *Curr. Org. Chem.* **2000**, *4*, 931-943. (b) Pensato, S.; Saviano M.; Romanelli, A. *Expert Opin. Biol. Ther.* **2007**, *7*, 1219-1232.

therefore exhibits properties from both worlds. Thus, the molecules are not degraded in the cell by nucleases (RNases or DNases), which is in contrast with natural exogenous oligonucleotides. The PNA molecule also displays higher chemical stability than the corresponding natural oligonucleotides. In contrast to DNA, which depurinates on treatment with strong acids, PNAs are completely acid stable.[3] In addition, due to their inherent flexibility and the lack of charge repulsion between phosphodiester groups commonly found in DNA or RNA backbone, PNA molecules show efficient and sequence-specific binding to both single stranded RNA and DNA as well as to double stranded DNA.[1c,4]

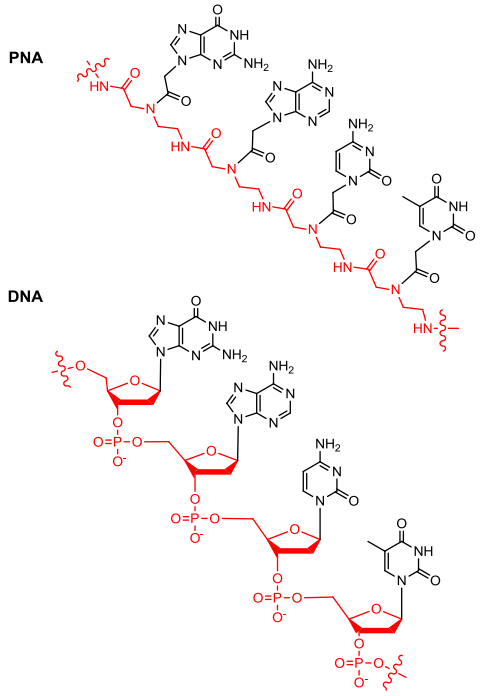

Figure 1. *Differences between the DNA structure and aegPNA.*

[3] Dueholm, K. L.; Egholm, M.; Behrens, C.; Christensen, L.; Hansen, H. F.; Vulpius, T.; Petersen, K. H.; Berg, R. H.; Nielsen, P. E.; Buchardt, O. *Org. Chem.* **1994**, *59*, 5767-5773.

[4] For reviews see: (a) Nielsen, P. E.; Haaima, G. *Chem. Soc. Rev.* **1997**, *26*, 73-78. (b) Uhlmann, E.; Peyman, A.; Breipohl, G.; Will, D. W. *Angew. Chem. Int. Ed.* **1998**, *37*, 2796-2823. (c) Nielsen, P. E *Chem. Biodivers.* **2010**, *7*, 786-803.

Indeed, PNA was initially designed to bind double stranded DNA *via* major groove triplex formation, through Hoogsteen base pairing (T-A-T and C^+-G-C). However, in addition to triple helix formation with natural oligonucleotides, PNA follows the Watson-Crick rules on hybridization with complementary DNA and RNA, thus favoring helix disruption and strand invasion both forming duplex or triplex structures.[5] Therefore, the PNA scaffold opens the possibility towards other hybridization modes and complex structures, with a high dependence on the explored sequences (Figure 2).

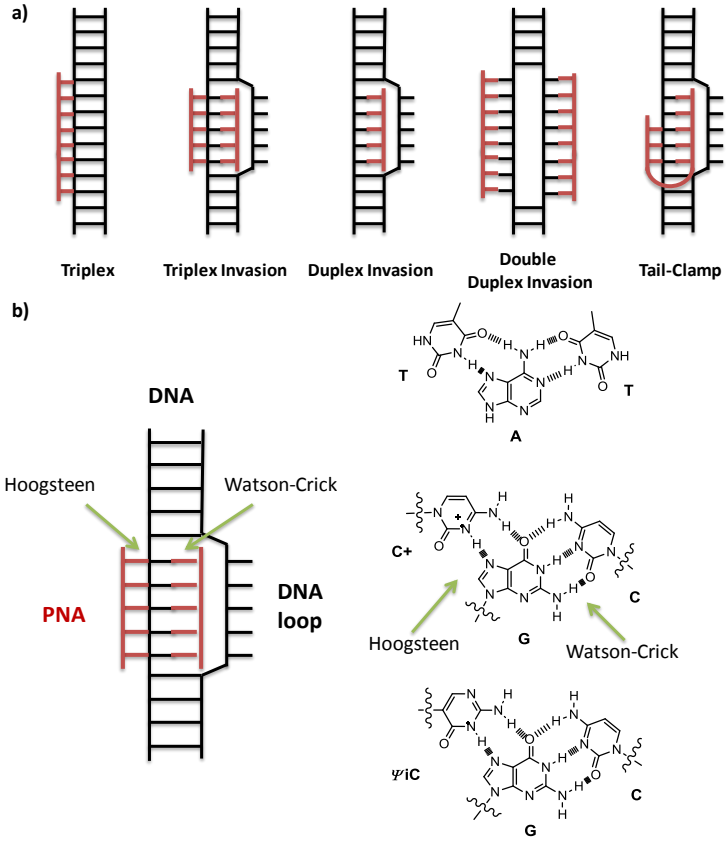

Figure 2. *(a) Different hybridization modes of PNA. (b) Detail of the Hoogsteen and Watson-Crick base pairing possibilities of PNA constructs.*

[5] Egholm, M.; Buchardt, O.; Christensen,L.; Behrens,C.; Freier, S. M.; Driver, D. A.; Berg, R. H.; Kim, S. K.; Norden, B.; Nielsen, P. E. *Nature* **1993**, *365*, 566-568.

Peptide nucleic acids do not only show astonishing specificity but also high binding affinity towards DNA and RNA sequences. In fact, antiparallel PNA/DNA hybrids are more stable than the corresponding double stranded DNA and RNA sequences (average T_m increase of 1K and 1.5K/base *ca.*, respectively).[6] PNA complexes showed remarkable stability at very low ionic strength due to their uncharged framework (no cation shielding of the phosphodiester backbone is required).[7] The introduction of non-standard (or alternative) nucleobases and the effect of base-pairing mismatches have been extensively studied to further assess the binding properties and sequence discrimination of these biological constructions.[8]

2.1.1 Potential Applications

Owing to their unique physicochemical properties and the inherent similarities with regular oligonucleotides, PNAs have been developed in view of their medical, biomolecular and nanobiotechnological potential applications.

Antisense drug approaches have been explored over the last decade, either by mRNA or by rRNA targeting. PNA can effectively inhibit the translation process by blocking both the elongation and the initiation phase (Figure 3).[9] In addition, splice junctions show to be very sensitive targets for antisense PNAs.[10] By interfering with exon-intron junctions, alternative splicing can occur with the consequent skipping of the exons and/or non-splicing of the introns. Hence, targeting mRNA during splicing as an alternative antisense strategy may afford interesting applications and opens new perspectives in drug discovery. Indeed, alternative splice redirection has been

[6] (a) Rose, D. J. *Anal. Chem.* **1993**, *65*, 3545-3549. (b) Jesen, K. K.; Oerum, H.; Nielsen, P. E.; Norden, B. *Biochemistry* **1997**, *36*, 5072-5077.

[7] Tomac, S.; Sarkar, M.; Ratilainen, T.; Wittung, P.; Nielsen, P. E.; Norden, B.; Gralund, A. *J. Am. Chem. Soc.* **1996**, *118*, 5544-5552.

[8] Wojciechowski, F.; Hudson, R. H. *Curr. Top. Med. Chem.* **2007**, *7*, 667-679.

[9] Knudsen, H.; Nielsen, P. E. *Nucleic Acids Res.* **1996**, *24*, 494-500.

[10] Karras, J. G.; Maier, M. A.; Lu, T.; Watt, A.; Manoharan, M. *Biochemistry* **2001**, *40*, 7853-7859.

successfully applied with promising results in both *in vitro* and *in vivo* models for muscular dystrophy.[11] Recent developments on targeting and inhibition of micro-RNAs (MiRs) by PNAs have also been reported as an alternative antisense strategy.[12] Since these MiRs are known to play a crucial role on gene regulation, this approach offers significant possibilities in drug discovery.

PNA has also been used as an antigene agent to control gene expression at DNA level by inhibiting transcription processes (Figure 3). Inhibition occurs *via* triple helix formation or strand invasion. These hybridization motifs block the access of DNA binding proteins such as transcription factors or DNA methylases. Elongation of DNA primers by DNA polymerases and thus DNA replication can also be inhibited through PNA helix invasion. Indeed, efficient arresting of replication in mitochondrial DNA (predominantly single stranded during replication) has been reported using this PNA technology.[13]

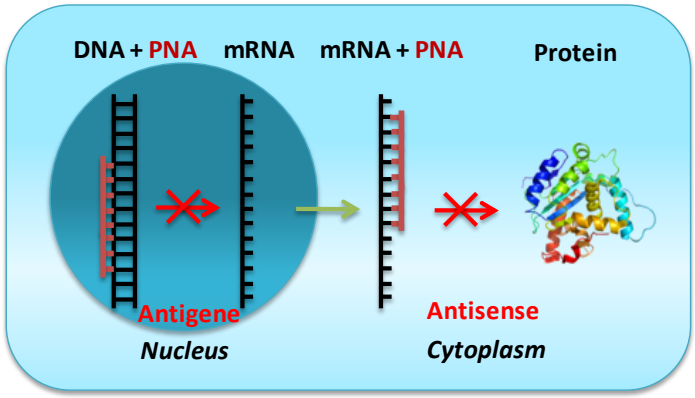

Figure 3. *Antigene and antisense PNA interference mechanisms.*

[11] Yin, H.; Lu, Q.; Wood, M. *Mol. Ther.* **2008**, *16*, 38-45.

[12] (a) Fabani, M. M.; Gait, M. J. *RNA* **2008**, *14*, 336-346. (b) Oh, S. Y.; Ju, Y.; Park, H. A.; *Mol. Cell.* **2009**, *28*, 341-345.

[13] Taylor, R. W.; Chinnery, P. F.; Turnbull, D. M.; Lightowlers, R. N. *Nat. Genet.* **1997**, *15*, 212-215.

More interesting is the ability of PNA to activate transcription (Figure 4). Initiation of transcription from double stranded DNA to RNA involves formation of an open DNA complex, in which *ca.* 12 base pairs stay single stranded for hybridization with the synthesized RNA. This structure is equivalent to the P-loop formed upon triplex invasion of a double stranded PNA with the corresponding DNA template.[14] This complex is effectively detected by RNA polymerases, and thus RNA transcription is initiated in the P-loop structure formed by this artificial PNA-based "transcription factor".[15]

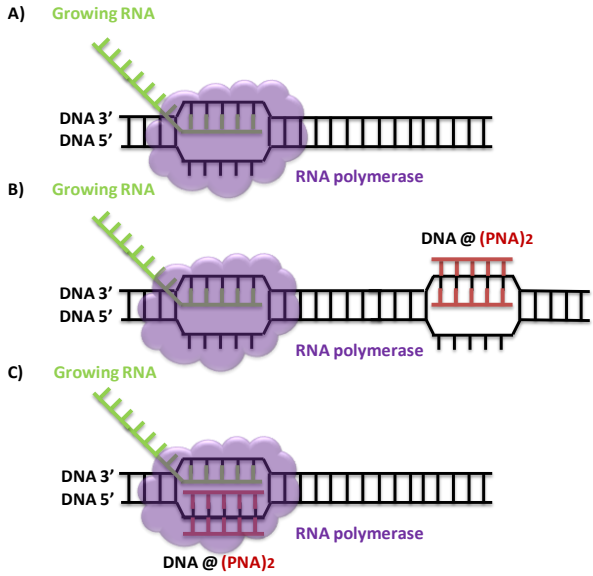

Figure 4. *(A) Normal transcription mechanism through formation of an open promoter complex. (B) Inhibition of transcription via PNA strand invasion and triple helix formation. (C) Activation of transcription by PNAs.*

[14] (a) Cherny, D. Y.; Belotserkovskii, B. P.; Frank-Kamenetskii, M. D.; Egholm, M.; Buchardt, O.; Berg, R. H.; Nielsen, P. E. *Proc. Natl. Acad. Sci. USA* **1993**, *90*, 1667-1670. (b) Nielsen, P. E.; Egholm, M.; Buchardt, O. *J. Mol. Recognit.* **1994**, *7*, 165-170. (c) Demidov, V. V.; Yavnilovich, M. V.; Belotserkovskii, B. P.; Frank-Kamenetskii, M. D.; Nielsen P. E. *Proc. Natl. Acad. Sci. USA* **1995**, *92*, 2637-2641.

[15] Mollegaard, N. E.; Buchardt, O.; Egholm, M.; Nielsen, P. E. *Proc. Natl. Acad. Sci. USA* **1994**, *91*, 3892-3895.

One of the most promising applications of peptide nucleic acids is related to targeting gene repair. For instance, correction of a thalassemia-associated β-globin mutation was recently assessed by targeting proximal genome sites to the mutated site with a homopurine rich pseudo-complementary PNA sequence.[16]

PNAs have also been used as scaffolds to template different reactions and DNA ligations.[17] In addition, some examples reported by Winssinger *et al.*[18] have shown the potential application of PNAs as sequence tags in peptide combinatorial libraries. These libraries are encoded with PNAs and self-assemble into an organized microarray through hybridization to generate DNA arrays. This technology has been successfully applied to screen and profile different kinases[19] and proteases, as well as to identify protease inhibitors.

The use of PNAs in diagnostics and bioanalytics has been widely explored over the last decade. In contrast with DNA, PNA is not a substrate for DNA polymerase and therefore cannot act as a primer in PCR. Instead, PNAs behave as highly effective blockers of PCR amplification as they showed competitive binding with DNA primers for the DNA template. PNA sequence specificity can allow the discrimination and detection of single mismatch sequences and genetic mutations such as the CFTR gene in cystic fibrosis.[20] Thereby, discrimination of single point mutations in the Ki-*ras* gene has been achieved using PCR clamping.[21]

---

[16] (a) Chin, J. Y.; Kuan, J. Y.; Lonkar, P. S.; Krause, D. S.; Seidman, M. M.; Peterson, K. R.; Nielsen, P. E.; Kole, R.; Glazer, P. M. *Proc. Natl. Acad. Sci. U.S.A.* **2008**, *105*, 13514-13519. (b) Lonkar, P.; Kim, K. H.; Kuan, J. Y.; Chin, J. Y.; Rogers, F. A.; Knauert, M. P.; Kole, R.; Nielsen, P. E.; Glazer, P. M. *Nucleic Acids Res.* **2009**, *37*, 3635-3644.

[17] Grossmann, T. N.; Seitz, O. *Chem. Eur. J.* **2009**, *15*, 6723-6730.

[18] (a) Winssinger, N.; Damoiseaux, R.; Tully, D. C.; Geierstanger, B. H.; Burdick, K.; Harris, J. L. *Chem. Biol.* **2004**, *11*, 1351-1360. (b) Urbina, H. D.; Winssinger, N. *Chem. Eur. J.* **2005**, *11*, 6792-6801. (c) Urbina, H. D.; Debaene, F.; Jost, B.; Bole-Feysot, C.; Mason, D. E.; Kuzmic, P.; Harris, J. L.; Winssinger, N. *ChemBioChem* **2006**, *7*, 1790-1797.

[19] Pouchain, D.; Diaz-Mochon, J. J.; Bialy, L.; Bradley, M. *ACS Chem. Biol.* **2007**, *2*, 810-818.

[20] Carlsson, C.; Jonsson, M.; Norden, B.; Dulay, M. T.; Zare, R. N.; Noolandi, J.; Nielsen, P. E.;

Additionally, several PNA probes have been used by means of Fluorescence *in situ* Hybridization (FISH) assays on quantitative measurements of telomere length,[22] chromosome painting techniques[23] and detection of viruses and bacteria.[24] Furthermore, replacement of DNA with PNA as a more robust biomolecular probe for the development of new nanobiosensors and microarrays has raised high expectations in the field. This PNA-based technology can be applied to areas such as molecular genetic diagnosis and cytogenetics, among other pharmacological purposes.[25]

2.1.2 Antibacterial/Antimicrobial PNAs

PNAs have been widely reported as antibiotic agents due to their antisense properties. Some of the traditional antibiotics directly affect the microbial protein synthesis by blocking bacterial translation through binding to ribosomes and ribosomal RNA. Nielsen *et al.* described a bis-PNA able of targeting the α-sarcin loop of 23S ribosomal RNA, hence inhibiting the growth of *E. coli*.[26] However, it was shown that the antibacterial activity of these constructs was limited by their poor cellular uptake.[27]

Tsui, L-C.; Zielenski, J. *Nature*, **1996**, *380*, 207.

[21] Bayerdörffer, T. C.; Blasczyk, E.; Wittig, R.; Neubauer, B. *Nucleic Acids Res.* **1996**, *24*, 983-984.

[22] Lansdorp, P. M.; Verwoerd, N. P.; van de Rijke, F. M.; Dragowska, V.; Little, M-T.; Dirks, R. W.; Raap, A. K.; Tanke, H. J. *Hum. Mol. Genet.* **1996**, ***5,*** 685-691.

[23] Chen, C.; Wu, B. L.; Wei, T.; Egholm, M.; Strauss, W. M. *Mamm. Genome* **2000**, *11*, 384-391.

[24] (a) Drobniewski, F. A.; More, P. G.; Harris, G. S. *J. Clin. Microbiol.* **2000**, *38*, 444-447. (b) Worden, A. Z.; Chisholm, S. W.; Binder, B. *J. Appl. Environ. Microbiol.* **2000**, *66*, 284-289. (c) Hongmanee, P.; Stender, H, Rasmussen, O. F. *J. Clin. Microbiol.* **2001**, *39*, 1032-1035. (d) Stender, H.; Oliveira, K.; Rigby, S.; Bragoot, F. Coull, J. *J. Microbiol. Methods* **2001**, *45*, 31-39.

[25] (a) Brandt, O.; Hoheisel J. D. *Trends Biotechnol.* **2004**, 22, 618-622. (b) Singh, R. P.; Oh, B-K.; Choi, J-W. *Bioelectrochemistry* **2010**, *79*, 153-161.

[26] (a) Good, L.; Nielsen, P. E. *Proc. Natl. Acad. Sci. USA* **1998**, *95*, 2073-2076. (b) Good, L.; Nielsen, P. E. *Nat. Biotechnol.* **1998**, *16*, 355-358.

[27] (a) Nikaido, H. *Science* **1994**, *264*, 382-388. (b) Good, L. M; Sandberg, R.; Larsson, O.; Nielsen, P. E.; Wahlestedt, C. *Microbiology* **2000**, *146*, 2665-2670.

Conjugation of PNAs to a peptide sequence, known to interact with the anionic membrane lipopolysaccharides and thus to cross bacterial cell wall, increased the potency of PNAs targeting both α-sarcin loop as well as essential *acp*P gene.[28] Moreover, work on PNA targeting HIV RNA has demonstrated the potential application of PNA oligomers for antisense-HIV drugs.[29]

2.1.3 Cell Delivery Strategies

PNA oligomers are large, uncharged, hydrophobic molecules with limited antisense activity without a support or technique to assist bypassing the cell membrane. Over the last decade, major efforts have been devoted to promote efficient internalization and thus enhancement of the intracellular effect of PNA.[30] For example, cellular uptake of unmodified PNAs has been developed using different techniques and strategies such as microinjection,[31] electroporation,[10,32] co-transfection with DNA[33] or direct delivery

[28] (a) Good, L.; Awasthi, S. K.; Dryselius, R.; Larsson, O.; Nielsen, P. E. *Nat. Biotechnol.* **2001**, *19*, 360-364. (b) Eriksson, M.; Nielsen, P. E.; Good, L. *J. Biol. Chem.* **2002**, *277*, 7144-7147. (c) Tan, X. X.; Actor, J. K.; Chen, Y. *Antimicrob. Agents Chemother.* **2005**, *49*, 3203-3207. (d) Nikravesh, A.; Dryselius, R.; Faridani, O. R.; Goh, S.; Sadeghizadeh, M.; Behmanesh, M.; Ganyu, A.; Jan Klok, E.; Zain, R.; Good, L. *Mol. Ther.* **2007***, 15*, 1537-1542.

[29] (a) Tripathi, S.; Chaubey, B.; Ganguly, S.; Harris, D.; Casale, R. A.; Pandey, V. N. *Nucleic Acids Res.* **2005**, *33*, 4345-4356. (b) Chaubey, B.; Tripathi, S.; Ganguly, S.; Harris, D.; Casale, R. A.; Pandey, V. N. A. *Virology* **2005**, *331*, 418-428. (c) Tripathi, S.; Chaubey, B.; Barton, B. E.; Pandey, V. N. A. *Virology* **2007**, *363*, 91-103.

[30] For reviews see: (a) Koppelhus, U.; Nielsen, P. E. *Adv. Drug. Deliv. Rev.* **2003**, *55*, 267-280. (b) Nielsen, P. E. *Q. Rev. Biophys.* **2005**, *38*, 345-350. (c) Shiraishi, T.; Nielsen, P. E. *Delivery Technologies for Biopharmaceuticals: Peptides, Proteins, Nucleic Acids and Vaccines* **2009**, Ed. John Wiley & Sons, 305-338.

[31] Hamilton, S. E.; Simmons, C. G.; Kathiriya, I. S.; Corey, D. R. *Chem. Biol.* **1999**, *6*, 343-351.

[32] (a) Shammas, M. A.; Simmons, C. G.; Corey, D. R.; Shmookler-Reis, R. J. *Oncogene* **1999**, *18*, 6191-6200. (b) Wang, G.; Xu, X.; Pace, B.; Dean, D. A.; Glazer, P. M.; Chan, P.; Goodman, S. R.; Shokolenko, I. *Nucleic Acids Res.* **1999**, *27*, 2806-2813.

(showing low antisense activity).[26,34] However, new and more efficient methods have been developed to allow cell permeability of PNA molecules by their own without external stimuli. This usually requires modification of the PNA structure by anchoring auxiliary molecular vectors to allow entry into the cell.

Most work in the field is related to the so-called "Trojan peptides" or cell penetrating peptides (CPPs). These peptides are mainly composed of positively charged and hydrophobic residues, which allow interaction with the anionic surface of the cell membrane and therefore cellular uptake.

Several examples of PNA cellular uptake have been described by attachment of CPPs to the PNA oligomers. Some have shown promising results and applicability both for *in vitro* and *in vivo* systems.[35] A systematic study reported by Nielsen *et al.* describes the covalent incorporation of several CPPs to PNA and the evaluation of their antisense potency. Interestingly, attachment of lipid moieties to the sequences, referred to as "CatLip domains" results in an increase of their antisense activity.[36] Improved cellular delivery and hence antisense activity of these CPP-PNAs has been achieved by photochemical internalization.[37] Thus, cell penetrating peptides and their

---

[33] (a) Faruqi, A. F.; Egholm, M.; Glazer, P. M. *Proc. Natl. Acad. Sci. USA* **1998**, *95*, 1398-1403. (b) Doyle, D. F.; Braasch, D. A.; Simmons, C. G.; Janowski, B. A.; Corey, D. R. *Biochemistry* **2001**, *40*, 53-64.

[34] Sei, S.; Yang, Q. E.; O'Neill, D.; Yoshimura, K.; Nagashima, K.; Mitsuya, H. *J. Virol.* **2000**, *74*, 4621-4633.

[35] (a) Pooga, M.; Soomets, U.; Hällbrink, M.; Valkna, A.; Saar, K.; Rezaei, K.; Kahl, U.; Hao, J. X.; Xu, X. J.; Wisenfeld-Hallin, Z.; Hökfelt, T.; Bartfai, T.; Langel, Ü. *Nat. Biotechnol.* **1998**, *16*, 857-861. (b) Bendifallah, N.; Rasmussen, F. W.; Zachar, V.; Ebbesen, P.; Nielsen, P. E.; Koppelhus, U. *Bioconjugate Chem.* **2006**, *17*, 750-758. (c) Ivanova, G. D.; Arzumanov, A.; Abes, R.; Yin, H.; Wood, M. J.; Lebleu, B.; Gait, M. J. *Nucleic Acids Res.* **2008**, *36*, 6418-6428.

[36] Koppelhus, U.; Shiraishi, T.; Zachar, V.; Pankratova, S.; Nielsen, P. E. *Bioconjugate Chem.* **2008**, *19*, 1526-1534.

[37] (a) Shiraishi, T.; Nielsen, P. E. *FEBS Lett.* **2006***, 580*, 1451-1456. (b) Shiraishi, T.; Nielsen, P. E. *Cell-Penetrating Peptides: Methods and Protocols*, Methods in Molecular Biology, **2011** Ed. Springer Science, *683*, 391-397.

derivatives may be developed for *in vivo* medical application as efficient PNA transporters. However, endosomal trapping of these conjugates is known to hamper their activity inside the cell and remains one of the major obstacles for enhancing the effectiveness of this strategy.[38]

Another synthetic modification of a PNA sequence aimed at improving cellular uptake consists of introduction of negatively charged groups to allow transfection *via* the widespread commercially available cationic lipids (such as lipofectamine™). These cationic transfection reagents are originally employed for DNA transfection. Charge neutral PNA cannot interact (or at least not efficiently) with these cationic reagents. Therefore, PNAs were either complexed with DNA (consequently formed PNA/DNA heteroduplex) or chemically modified with lipidic ligands or phosphonate ligands to form transfectional complexes with these reagents through hydrophobic/electrostatic interactions. Conjugation of phosphonate glutamine and *bis*-phosphonate lysine amino acid derivatives to the PNA scaffold, in combination with lipofectamine, afforded subnanomolar antisense activity.[39] However, this strategy is limited to *in vitro* studies owing to the toxicity of the transfection agents.

Finally, use of crosslinked cationic nanoparticles,[40] or polymers such as polyethyleneimine (PEI)[41] have been reported, showing interesting results for the efficient cellular permeability of PNAs.

---

[38] (a) Koppelhus, U.; Awasthi, S. K.; Zachar, V.; Holst, H. U.; Ebbesen, P.; Nielsen, P. E. *Antisense Nucleic Acid Drug Dev.* **2002**, *12*, 51-63. (b) Shiraishi, T.; Pankratova, S.; Nielsen, P. E. *Chem. Biol.* **2005**, *12*, 923-929. (c) Abes, S.; Williams, D.; Prevot, P.; Thierry, A.; Gait, M. J.; Lebleu, B. *J. Control. Release* **2006**, *110*, 595-604.

[39] Shiraishi, T.; Hamzavi, R.; Nielsen, P. E. *Nucleic Acids Res.* **2008**, *36*, 4424-4432.

[40] (a) Zhang, K.; Fang, H.; Shen, G.; Taylor, J-S. A.; Wooley, K. L. *Proc. Am. Thorac. Soc.* **2009**, *6*, 450-457. (b) Fang, H.; Zhang, K.; Shen, G.; Wooley, K. L.; Taylor, J-S. A. *Mol. Pharm.* **2009**, *6*, 615-626.

[41] Berthold, P. R.; Shiraishi, T.; Nielsen, P. E. *Bioconjug. Chem.* **2010**, *21*, 1933-1938.

2.1.4 Objectives

Our focus is based on the employment of bicyclic guanidinium oligomers as new efficient transporters for PNA delivery. Guanidinium (or arginine)-containing cell penetrating peptides have been widely used in cellular uptake of biologically relevant cargos. Previous studies by Wender *et al.* highlighted the importance of the length, the number of arginine residues, and the spacer between the guanidinium groups to allow efficient internalization.[42] In our group, we have explored the cell penetrating properties of TBDPS protected tetraguanidinium oligomer as a non-peptide carrier. By attaching a fluorescence probe, confocal microscopy experiments confirmed the preferential cellular localization and accumulation of this molecular vector in mitochondria (Figure 5). Moreover, these molecules showed more efficient translocation through HeLa membranes than the corresponding Tat or Antp peptides.[43] Further studies using terbium complexes attached to this tetraguanidinium carrier confirmed mitochondrial targeting.[44] This paves the way to the attachment of drugs to this tetraguanidinium transporter, to target mitochondria. Indeed, it was recently reported that attachment of Gamitrinibs, a molecule designed to target and inhibit Hsp90, to our tetraguanidinium vector results in the efficient inhibition of Hsp90 ATPase activity, therefore showing mithocondrial accumulation.[45]

---

[42] (a) Goun, E. A.; Pillow, T. H.; Jones, L. R.; Rothbard, J. B.; Wender, P. A. *ChemBioChem* **2006**, *7*, 1497-1515. (b) Wender, P. A.; Galliher, W. C.; Goun, E. A.; Jones, L. R.; Pillow, T. H. *Adv. Drug Deliver. Rev.* **2008**, *60*, 452-472.

[43] Fernández-Carneado, J.; Van Gool, M.; Martos, V.; Castel, S.; Prados, P.; de Mendoza, J.; Giralt, E. *J. Am. Chem. Soc.* **2005**, *127*, 869-874.

[44] Kielar, F.; Congreve, A.; Law, G.; New, E. J.; Parker, D.; Wong, K-L.; Castreño, P.; de Mendoza, J. *Chem. Commun.* **2008**, 2435-2437.

[45] Kang, B. H.; Plescia, J.; Song, H. Y.; Meli, M.; Colombo, G.; Beebe, K.; Scroggins, B.; Neckers, L.; Altieri, D. C. *J. Clin. Invest.* **2009**, *119*, 454-464.

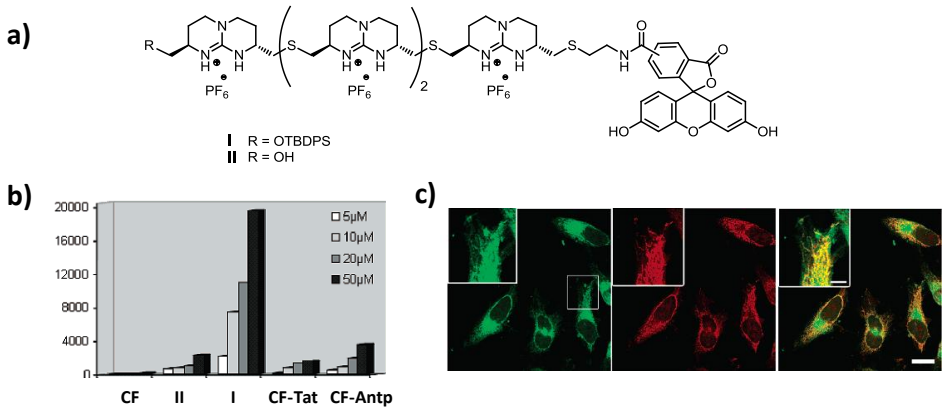

Figure 5. *(a) Structure of the fluorescein-labelled tetraguanidinium vectors. (b) Fluorescence measurements in HeLa cells incubated with these non-peptide vectors* ***I*** *and* ***II****, compared with Tat and Antp peptide vectors. (c) Cellular localization of vector* ***I*** *showing accumulation in mitochondria.*

The goal of this project is not only to improve the internalization of PNA by conjugation with oligoguanidinium molecules, but also to study in detail which structural factors of these oligomers are essential for cellular uptake. Several experiments were thus designed to gain some insight into the internalization mechanism of these conjugates. Furthermore, the application of these oligoguanidinium-PNA conjugates as antibacterial agents have been explored.

2.2 Synthesis of PNA-Oligoguanidinium Conjugates

A series of oligoguanidinium-PNA conjugates were prepared in order to evaluate their internalization and antisense activity properties. The construction of the oligoguanidinium fragment was achieved using an iterative synthetic strategy as described in Chapter 1. Bicyclic guanidinium monomers were bound together through thioether linkages by means of the nucleophilic attack of the corresponding thiolate species to the electrophile (mesylate). The thiolate species can be formed *in situ, via* thioacetate cleavage or *via* a disulfide reduction, using a polymer-bound phosphine. These two synthetic approaches were explored to afford polycationic oligomers (**44a-e**, **10**, **18**, **46** and **48**) in moderate to high yields, and were subsequently coupled with the PNA construct (see details in the experimental section).

The number of bicyclic guanidinium subunits and the nature of the lipophilic group were evaluated to optimize the cellular uptake (Scheme 1). Thus, mono-, di-, tri-, tetra-, and pentaguanidinium-PNA oligomers bearing a TBDPS silyl group were synthesized and studied.

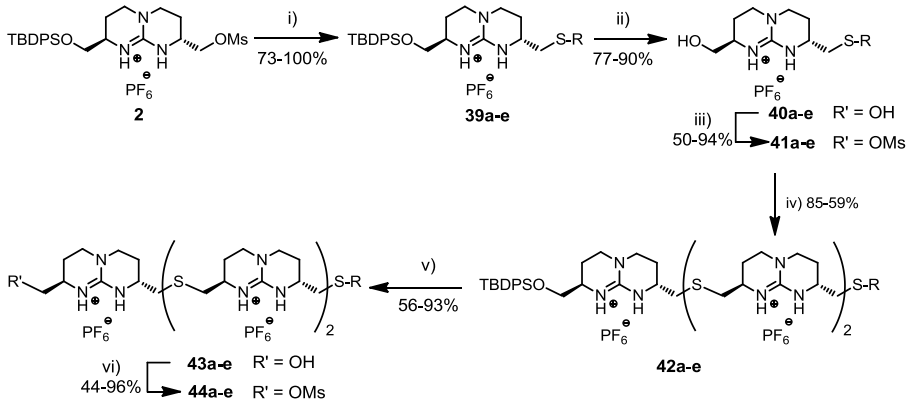

Scheme 1. *Synthetic path for triguanidinium-PNA conjugates* ***44****;* ***a*** *R = hexyl,* ***b*** *R = decyl,* ***c*** *R = tetradecyl,* ***d*** *R = cholesteryl and* ***e*** *R = triethylene glycol chains. Conditions: i) (****a-d****) 2 eq. of corresponding alkylthiol, 2,5 eq. of ^{t}BuOK in acetone at r.t., under N_2; i) (****e****) 2,5 eq. of Cs_2CO_3 in ACN/MeOH, 4 h at r.t. under N_2; ii) (****a-c****, ****e****) TBAF in THF, 4 h at r.t.; ii) (****d****) HF/pyr 70%, o.n.; iii) 2,5 eq. of NMM, 4 eq. of Ms_2O in CH_2Cl_2; iv) 1 eq. of* ***11****, 2,5 eq. of Cs_2CO_3 in ACN/MeOH, 3 h at r.t. under N_2; v) TBAF in THF, o.n. at r.t.; vi) 4 eq. of NMM, 6 eq. of Ms_2O in THF.*

Several lipophilic (R) groups were attached to the bicyclic guanidinium mesylate **2** by nucleophilic substitution. Cleavage of the silyl protecting group with TBAF, followed by mesylation of the resulting alcohol afforded compounds **41a**-**e**. Subsequent coupling to a thioacetyl diguanidinium derivative (**11**), which was obtained by treatment of diguanidinium mesylate **10** with potassium thioacetate, afforded the desired triguanidinium compounds **42a**-**e**. These molecules were again submitted to deprotection and mesylation, to obtain compounds **44a**-**e** in moderate to good yields.

For the construction of the oligoguanidinium compounds bearing the TBDPS protecting group, the synthesis was based on the generation of a thiolate species from the corresponding disulfide by reduction (Scheme 2).

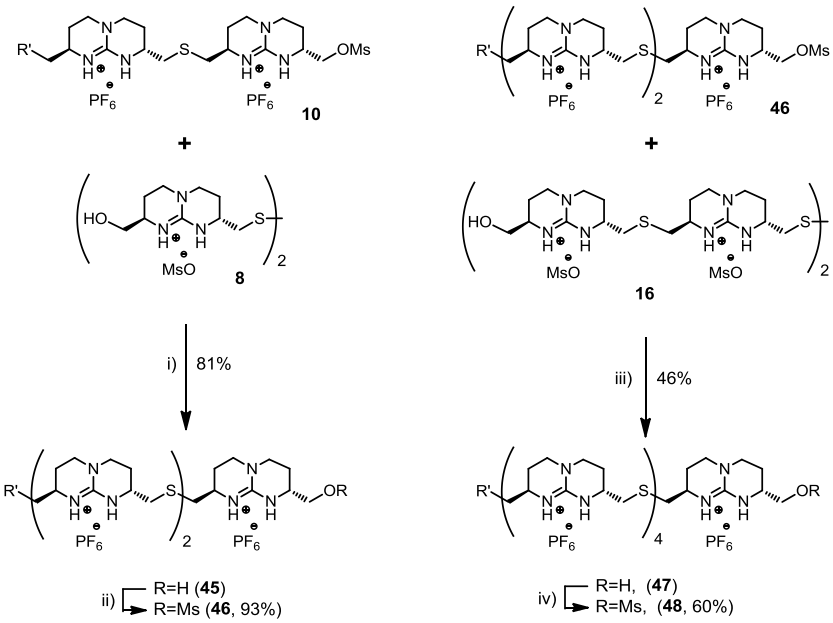

Scheme 2*. Synthesis of TBDPS-protected oligoguanidinium molecules* ***46*** *and* ***48*** *(R'=OTBDPS). Conditions: i) 1 eq. of* ***8****, 2 eq. of* ***10****, 2,5 eq. of Cs_2CO_3 and 1.3 eq. of $^n(Bu)_2PhP$ polystyrene resin, in ACN/MeOH, 5 h at r.t. under N_2; ii) 2,5 eq. of NMM, 4 eq. of Ms_2O in CH_2Cl_2; iii) 1 eq. of* ***16****, 2 eq. of* ***46****, 2,5 eq. of Cs_2CO_3 and 1.3 eq. of $^n(Bu)_2PhP$ polystyrene resin, in ACN/MeOH, 5 h at r.t. under N_2; iv) 4 eq. of NMM, 6 eq. of Ms_2O in THF.*

Thus, disulfide **8** was generated by thioacetylation of mesylate **2**, cleavage of the TBDPS groups and subsequent treatment with base. The disulfide bond of compound **8** was then reduced with $^nBu(Ph)_2P$ polymeric resin, allowing the nucleophilic attack of the resulting thiolate over mesylate **10**, to afford triguanidinium **45**. This strategy was used for the synthesis of the di-, tetra- (both described in Chapter 1, see Experimental Section) and pentaguanidinium oligomers bearing the silyl protecting group at the end, by varying the length (number of bicyclic guanidinium groups) of the starting compounds. Hence, this synthetic strategy successfully allowed linear growth of these molecules.

Two different synthetic approaches were considered to link these oligoguanidinium compounds to the biologically active PNA sequences, both based on the use of the

mesylate oligomers as electrophiles to be coupled with the PNA moiety. Monoguanidinium compound **2** was employed as a model for the screening and optimization of the reaction conditions.

Firstly, direct *N*-alkylation to the *N-terminus* of the PNA (Scheme 3) was tested using previously reported methodologies[46] (Table 1), and the reaction was monitored by HPLC analysis. This strategy does not require further modifications of the PNA or the guanidinium scaffold. However, no product was obtained and only low conversions were achieved using phosphate buffer at pH =11 as a base. Moreover, isolation of the product was not successful.

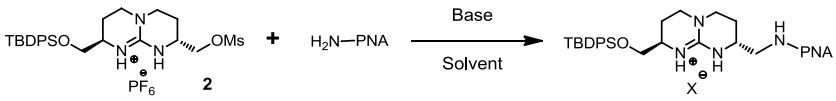

Scheme 3. *N-alkylation model reaction between the N-terminus of PNA and the monoguanidinium mesylate* ***2****.*

Table 1. *Reaction conditions for N-alkylation between PNA and monoguanidinium molecule* ***2****.*

#	Solvent	Base	Eq. of base or conc./pH	Eq. of Mesylate 1	Temp. (ºC)	Additional info.	Conversion (%)
1	DMSO/H_2O	LiOH	3 eq.	4 eq.	r.t.	---	No product
2	DMF/MeOH	CsOH	5 eq.	5 eq.	25 → 80	MS 4Å	---
3	ACN/MeOH/DMF	Cs_2CO_3	5 eq.	5 eq.	25 → 60	---	---
4	ACN/MeOH	phosphate	0,1 M / 11	5 eq.	25 → 60	---	9 %

The second approach was based on the *S*-alkylation of a modified PNA bearing an *N*-acetylated cysteine at the end of the sequence (Scheme 4).

[46] Salvatore, R. N.; Nagle, A. S.; Jung K. W. *J. Org. Chem.* **2002**, *67,* 674-683.

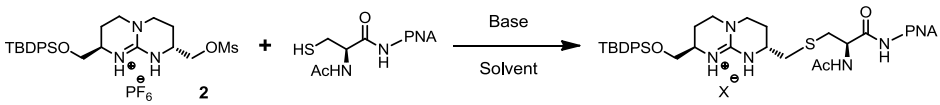

Scheme 4. *S-alkylation between the terminal cysteine of PNA and monoguanidinium mesylate* ***2****.*

Different conditions were tested to perform this reaction (Table 2). Parameters such as the nature of the base, the number of equivalents of electrophile or the temperature were screened to optimize the reaction and thus improve conversions. Reducing agents such as DTT or polymer bound $^{n}(Bu)_2PhP$ to prevent disulfide formation were also examined. The best conversion rate (56%) was obtained using 0.1M phosphate buffer at pH=10, with five equivalents of mesylate and heating at 60 ºC overnight under an inert atmosphere (entry 15).

Table 2. *Reaction conditions for coupling cysteine-PNA to the monoguanidinium molecule* ***2****.*

#	Solvent	Base	Eq. of base or conc./pH	Eq. of 1	Temp. (ºC)	Additional info.	Conversion (%)
1	DMSO	---	---	1 → 10 eq.	r.t.	---	No product
2	DMSO/H_2O	K_2CO_3	2,5 eq.	1 → 10 eq.	r.t.	---	No product
3	DMF/MeOH	Cs_2CO_3	5 eq.	5 eq.	r.t.	Inert atmosfere (N_2)	---
4	ACN/MeOH	K_2CO_3	5 eq.	10 eq.	r.t.	---	(6-8%)
5	ACN/H_2O	DIPEA	3 eq.	5 eq.	r.t.	Inert atmosfere (N_2)	---
6	ACN/H_2O	DIPEA	3 eq.	5 eq.	r.t.	15 eq. DTT in NH_4HCO_3	39- 43%
7	ACN/H_2O	DIPEA	3 eq.	5 eq.	r.t.	15 eq. DTT in NH_4HCO_3 with sephadex separation	5%
8	ACN/H_2O	Cs_2CO_3	3 eq.	10 eq.	r.t.	1,5 eq. $(^{n}Bu)_2PhP$ pol.	---
9	ACN/H_2O	phosphate	10 mM / 7,7	2 → 12 eq.	r.t.	Inert atmosfere (N_2)	19%
10	ACN/H_2O	phosphate	0,1 M / 8	2 → 12 eq.	r.t.	Inert atmosfere (N_2)	37%
11	ACN/H_2O	phosphate	0,1 M / 8	20 eq.	r.t.	Inert atmosfere (N_2)	13%
12	ACN/H_2O	phosphate	0,1 M / 8	5 eq.	r.t.	Inert atmosfere (N_2)	14%
13	ACN/H_2O	phosphate	0,1 M / 9	5 eq.	25 →60	---	14%
14	ACN/H_2O	phosphate	0,1 M / 9	5 eq.	60	Inert atmosfere (N_2)	38 %
15	ACN/H_2O	phosphate	0,1 M / 10	5 eq.	60	Inert atmosfere (N_2)	56 %

Under these reaction conditions, oligoguanidinium-PNA conjugates (**49a-e** and **50** to **56**) were successfully synthesized (Scheme 5) from moderate to high conversion rates (Table 3). The compounds were purified by preparative HPLC and lyophilized to obtain a white solid in almost all the cases. HPLC purification of these PNA molecules was performed in collaboration with Ms. Jolanta Barbara Ludvigsen (Prof. Nielsen's group). With these compounds in hand, biological assays were set up to evaluate their antisense activity and thus their cellular uptake.

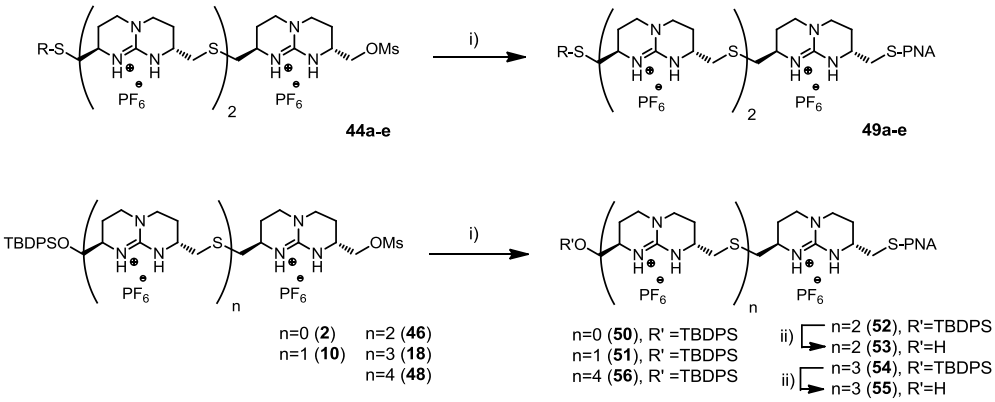

Scheme 5. *Coupling of oligoguanidinium molecules to PNA. For definitions of residues R in* **a-e** *see Scheme 1. Conditions: i) 0.1M phosphate buffer pH 10 in water/ACN mixture at 60ºC during 2 days; ii) (1:1:1) H_2O/TFA/ACN, overnight.*

Table 3. *List of conjugates synthesized with their corresponding molecular weight and conversions. *From acid hydrolysis of the protecting group in ACN/H_2O 15% TFA.*

PNA #	Name	Mass found (Calcd)	Conv. (%)	Purity (%)
49a	**Hexa-$(BG)_3$-PNA**	5588 (5587)	28%	90+
49b	**Deca-$(BG)_3$-PNA**	5643 (5643)	22%	90+
49c	**Tetradeca-$(BG)_3$-PNA**	5708 (5699)	14%	90+
49d	**cholesterol-$(BG)_3$-PNA**	5879 (5873)	13%	95+
49e	**eg-$(BG)_3$-PNA**	5661 (5660)	22%	90+
50	**TBDPSO-(BG)-PNA**	5330 (5330)	56%	95+
51	**TBDPSO-$(BG)_2$-PNA**	5522 (5528)	37%	95+
52	**TBDPSO-$(BG)_3$-PNA**	5730 (5727)	36%	95+
53	**HO-$(BG)_3$-PNA**	5492 (5489)	100%*	80+
54	**TBDPSO-$(BG)_4$-PNA**	5930 (5925)	66%	95+
55	**HO-$(BG)_4$-PNA**	5691 (5688)	100%*	90+
56	**TBDPSO-$(BG)_5$-PNA**	6124 (6120)	31%	95+

2.3 Internalization and Antisense Properties Determined by Luciferase Antisense Assays

Antisense splice correction assays for luciferase protein were performed to quantitatively assess the antisense activity of the PNA-oligoguanidinium conjugates previously described.[47] This work was done in collaboration with Dr. Takehiko Shiraishi (Prof. Nielsen's group).

Thus, the antisense splice correction of the aberrant globin intron was determined by measuring luciferase activity in HeLa pLuc 705 cells. This intron insertion to luciferase gene comes from a naturally occurring mutation in salacemia patients. In normal splicing, pre-mRNA introns are removed and the exons are joined. This gives rise to the final mRNA, which contains the information to be translated into the corresponding protein. HeLa pLuc 705 cells carry a luciferase gene interrupted with a mutated β-globin intron, which causes aberrant splicing of luciferase mRNA, and subsequently prevents translation of luciferase. Selective targeting of this aberrant intron using the complementary oligonucleotide sequence induces the correct splicing and thus leads to recovery of the luciferase activity (Figure 6). The amount of luciferase protein after incubation (measured luminescent activity by using the enzyme substrate luciferin) is directly related with the splice correction, and thus with the antisense activity of the PNA-oligoguanidinium conjugate. The targeting PNA sequence used for the splice correction was CCT CTT ACC TCA GTT ACA.[36,39]

[47] (a) Kang, S. H.; Cho, M. J.; Kole, R. *Biochemistry* **1998**, *37*, 6235-6239. (b) Kang, S. H.; Zirbes, E. L.; Kole, R. *Antisense Nucleic Acid Drug Dev.* **1999**, *9*, 497-505.

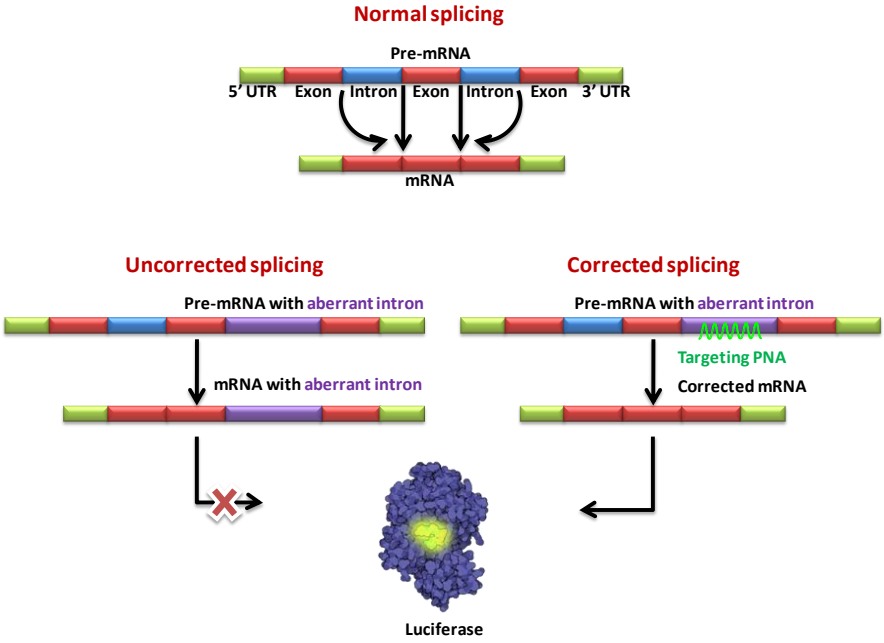

Figure 6. *Mechanism of normal cellular splicing, abnormal splicing and splicing correction mediated by PNA recognition.*

Initially, a range of oligoguanidinium-PNA conjugates were tested by varying the number of bicyclic guanidinium moieties (from 1 to 4), and with each bearing the highly hydrophobic TBPDS protecting group. These conjugates were compared with an octaarginine-PNA construct (a CPP commonly used for transfection) and with a more hydrophilic triguanidinium-PNA conjugate bearing a triethyleneglycol chain at the end of the oligomer. As observed in Figure 7, tetraguanidinium-PNA conjugate **54** showed the highest antisense activity, about 5-fold superior than the octaarginine-PNA (R_8-PNA). As the number of guanidines increases in the sequence, the antisense activity also rises. The triguanidinium-PNA conjugate **49e** with the terminal triethyleneglycol was noticeably less active than the corresponding TBDPS protected one. This suggests that not only the number of bicyclic guanidinium moieties affects in the cellular uptake of these constructs, but also its hydrophobicity.

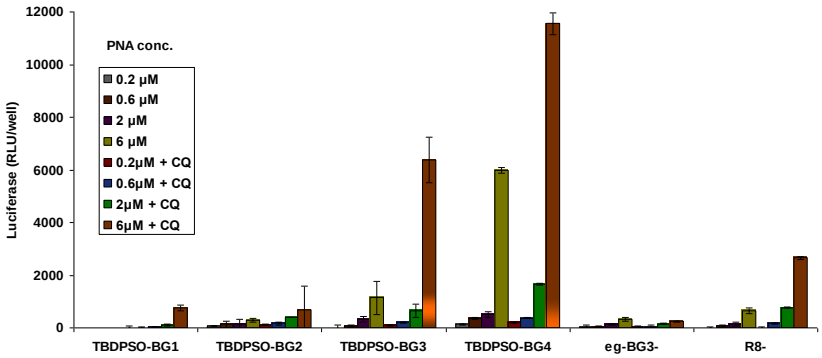

Figure 7. *Relative cellular luciferase antisense activity in HeLa pLuc705 cells of oligoguanidinium-PNA conjugates with different number of bicyclic guanidinium monomers.*

The experiments were also performed in presence of chloroquine (CQ), a well-known endosomal disrupting agent (Figure 7). As expected, the antisense activity of the corresponding PNA-conjugates increased upon addition of chloroquine, although for tetraguanidinium-PNA **54** the effect was less pronounced (only 2-fold increase, as compared with the antisense activity in absence of chloroquine). This likely indicates that this conjugate facilitates endosomal escape by its own or it crosses the membrane through a non-endosomal pathway. The octaarginine-PNA reference compound showed a higher activity enhancement upon chloroquine addition, confirming that cellular entry mechanism for this cell penetrating peptide is mainly endosomal.

As the cellular uptake trend clearly indicates a higher antisense activity upon increasing the number of guanidinium moieties, it seemed feasible that TBDPS protected pentaguanidinium-PNA **56** shows higher luciferase activity than the corresponding tetraguanidinium one. However, when comparing the different oligoguanidinium-PNA conjugates bearing the TBDPS protecting group, the tetraguanidinium-PNA still showed the highest activity (Figure 8). Cell viability experiments (Figure 9) demonstrated that the pentaguanidinium-PNA conjugate was toxic at higher concentrations (6 µM), thus explaining the decrease in antisense activity.

These oligoguanidinium-based PNA conjugates were compared to the Tat-Deca-PNA conjugate, which contains Tat peptide (a well-known cell penetrating peptide) bound to the PNA oligomer and a decanoic acid coupled to the ε-amine of a central lysine. This type of cationic peptide-lipid hybrid (CatLip) has been reported to improve cellular uptake of PNA and enhance its antisense activity. In fact, this specific conjugate was evaluated along with other CPP-PNA and CatLip-PNA conjugates, showing superior luciferase activity.[36] As depicted in Figure 6, the tetraguanidinium-PNA conjugate exhibits higher antisense activity than the corresponding Tat-Deca-PNA conjugate. Hence, oligoguanidinium vectors can be considered as promising internalizing carriers for the cellular uptake of peptide nucleic acids with antisense activity.

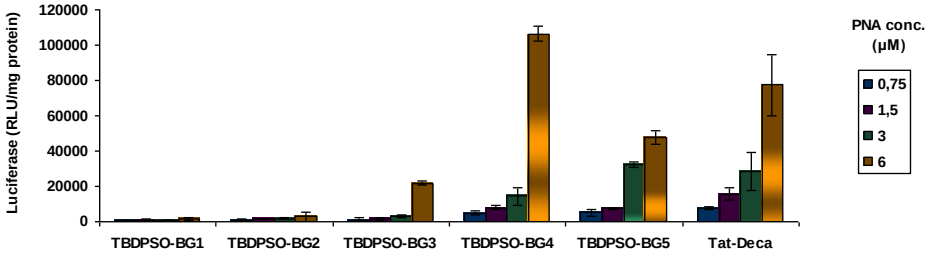

Figure 8. *Relative cellular luciferase antisense activity in HeLa pLuc705 cells of oligoguanidinium-PNA conjugates with different number of bicyclic guanidinium monomers.*

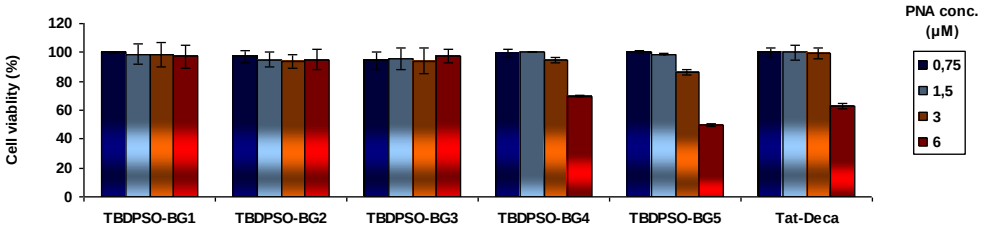

Figure 9. *Cellular viabilities analyzed by MTS assay (Promega) (values normalized to the average value of non-PNA treated sample).*

RT-PCR (Reverse Transcription PCR) measurements were performed to quantitatively assess the amount of mRNA corrected by the antisense activity of the PNA conjugates (Figure 10). This technique is based on the separation and the reverse transcription of the RNA present in the cell into DNA. Subsequently, this DNA is amplified by PCR, analyzed by gel electrophoresis and quantified. As a result, the splicing correction ratio and thus the efficiency of the process are assessed by measuring the amount of corrected and uncorrected mRNA.

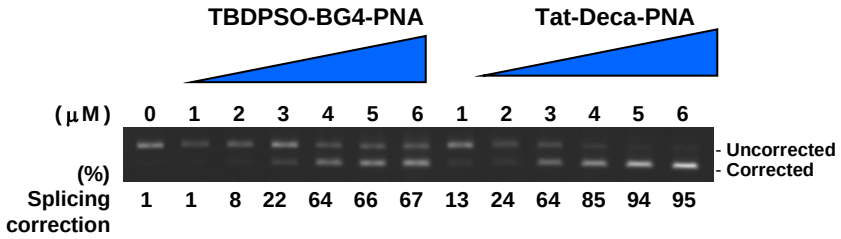

Figure 10. *Antisense activities of Tat-Deca-PNA and TBDPSO-BG4-PNA (**54**) measured by RT-PCR.*

As shown in Figure 10, splice correction with Tat-Deca-PNA appears to be more efficient than with the tetraguanidinium-PNA conjugate **54**. Nevertheless, melting temperatures (T_m) of the corresponding DNA/PNA hybrids indicated that Tat-Deca-PNA shows higher affinity for the target DNA sequence than the unmodified PNA sequence or the tetraguanidinium-PNA conjugate (Table 4). This suggests that the affinity for targeting the corresponding DNA or RNA sequence increases upon increasing the number of positive charges present in the sequence (8 charges for Tat peptide *vs.* 4 for the tetraguanidinium molecule). Hence, we possibly overestimate the splicing correction efficiency, since these PNA sequences, and especially Tat-Deca-PNA, can strongly bind to the uncorrected mRNA and DNA sequence and inhibit its reverse transcription and PCR amplification, respectively.

Table 4. *Melting temperatures of the PNA hybrids with its complemetary sequence.*

PNA	Tm (ºC)
Unmodified PNA	68.0
TBDPS-BG4-PNA	72.1
Tat-Deca-PNA	78.2

To assess the influence of hydrophobic groups at the end of oligoguanidinium-PNA conjugates, the antisense activity of a range of triguanidinium-PNA compounds was evaluated and compared with **54** and Tat-Deca-PNA. These conjugates only differed in the group attached at the end of the oligomer. As illustrated in Figure 11, the best luciferase activity was reached for the triguanidinium compound bearing a terminal decyl chain (**49b**). Indeed, at lower concentrations the deca-triguanidinium-PNA showed higher activity than the TBDPS protected one at 6 μM. However, upon increasing the concentration to 4 μM, the antisense activity drops, thus suggesting an increase in cytotoxicity.

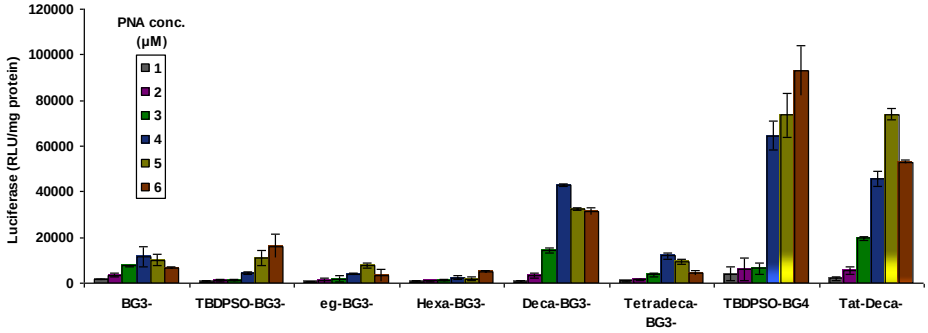

Figure 11. *Relative luciferase antisense activity of oligoguanidinium-PNA conjugates with different lipophilic substituents.*

In conclusion, we have been able to determine and optimize some structural parameters essential in the cellular uptake by measuring the antisense activity of a set of oligoguanidinium-PNA conjugates. Four bicyclic guanidinium subunits seem to be the optimal length to afford an efficient internalization without compromising cell viability. On the other hand, hydrophobic groups such as TBDPS are required for the efficient cellular entry of these molecules, although a decyl alkyl chain appears to be a good alternative as shown with the triguanidinium-PNA series. Therefore, tetraguanidinium-PNA conjugates bearing a decyl alkyl chain could be good future candidates to achieve higher antisense activity at lower concentrations.

2.4 Aggregation Studies and Internalization Mechanistic Interpretations

Luciferase activity assays reveal a concentration dependence of the activities of the TBDPS-$(BG)_4$-PNA conjugate. At 2 μM, the compound showed almost no activity in contrast with the experiment run at 6 μM concentration. In a more detailed study from 0 to 6 μM (Figure 12), the Tat-Deca-PNA conjugate showed typical concentration *vs.* activity response compared with other conjugates previously reported, whereas the tetraguanidinium conjugate **54** exhibited an abrupt increase in activity. These antisense splice correction assays pointed to a cooperative mechanism in the internalization of these conjugates. Since these TBDPSO-oligoguanidinium-PNA oligomers are amphiphilic compounds able to self-assemble, the formation of higher aggregates could explain the anomalous increment in activity observed in the 0-6 μM range (Figure 10). Indeed, this effect has been previously described for similar modified PNAs with analogous physicochemical properties.[48]

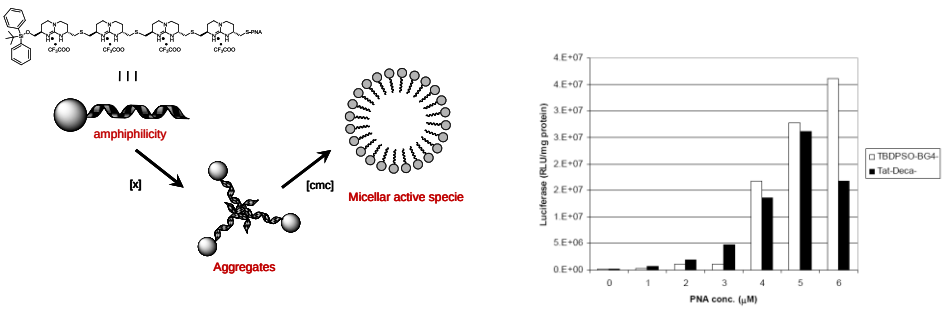

Figure 12. *Proposed aggregation mechanism for oligoguanidinium-PNA conjugates (left). Antisense activity jump in the concentration range studied (right).*

[48] (a) Lau, C.; Bitton, R.; Bianco-Peled, H.; Schultz, D. G.; Cookson, D. J.; Grosser, S. T.; Schneider, J. W. *J. Phys. Chem. B* **2006**, *1110*, 9027-9033. (b) Shen, G.; Fang, H.; Song, Y.; Bielska, A. A.; Wang, Z.; Taylor, J-S. A. *Bioconjugate. Chem.* **2009**, *20*, 1729-1736.

A series of experiments were setup for studying both the formation and the properties of these complexes. Dynamic light scattering (DLS) experiments were performed to measure the diffusion coefficient and thus the hydrodynamic radius of the particles formed by aggregation of the TBDPSO-$(BG)_4$-PNA conjugate **54** (Figure 13).

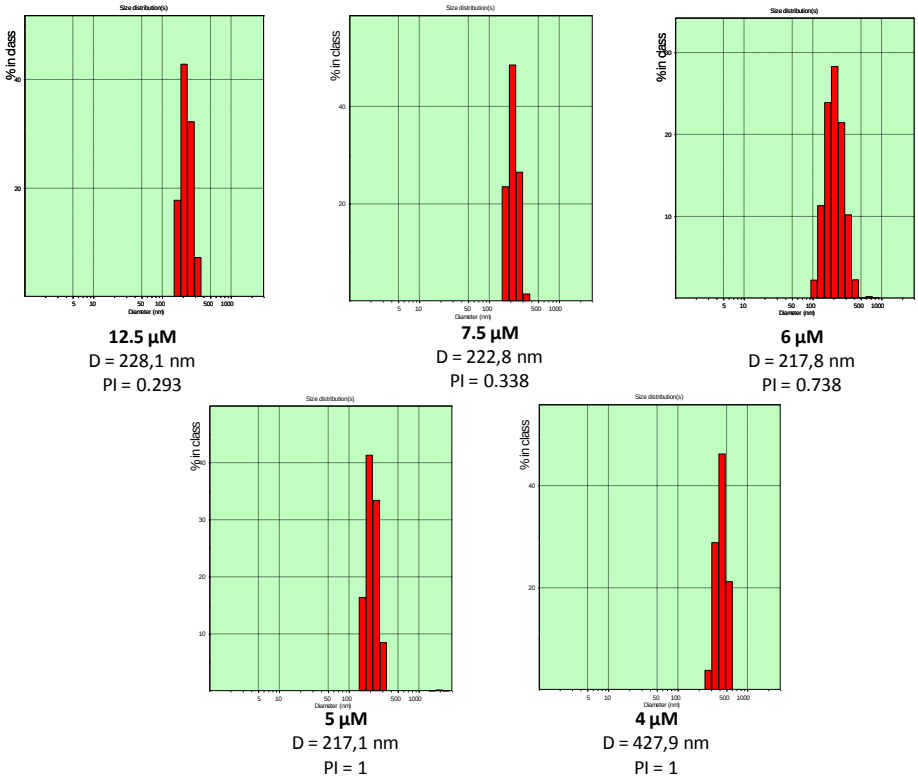

Figure 13. *Particle size distribution histograms of the oligoguanidinium-PNA conjugate* ***54*** *at different concentrations. PI refers to the polydispersity index.*

Concentration dependent experiments with aqueous solutions of **54** (from 2-12 µM) were analyzed by dynamic light scattering. Large particles were observed in samples with concentrations higher than 4 µM (Figure 13). Upon increasing the concentration, the polydispersity index drops, giving rise to well-defined aggregates with an average diameter of *ca.* 220 nm. Below this critical concentration, no aggregate or particle with

a considerable size could be detected. Indeed, at this concentration range the tetraguanidinium-PNA conjugate showed an increased antisense activity, suggesting a cooperative cellular uptake mechanism where the oligoguanidinium-PNA molecules interact and self-assemble, forming a supramolecular aggregate, which could be responsible for promoting efficient cell entry.

Transmission electron microscopy (TEM) was used to study these tetraguanidinium-PNA aggregates in more detail. This technique has enough resolution to distinguish the nanoparticles previously detected by DLS. A concentrated aqueous solution was deposited on a copper conducting film and allowed to slowly evaporate to dryness. The film was stained with ammonium phosphomolybdate as contrasting agent to improve the sharpness of the images. As shown in Figure 14, some micelle-like spherical aggregates of different sizes were formed. The larger ones (between 600 and 1000 nm in diameter) differ from the values obtained in solution by dynamic light scattering. However, there are also smaller aggregates (between 150 and 250 nm) of more consistent sizes with our data (Figure 13). These differences in size could be explained by the loss of solvent during the deposition process. Under such conditions, the sample concentration, which is an essential factor for the formation of these supramolecular structures, is not controlled. Thus, it is expected that more heterogeneous aggregates are formed.

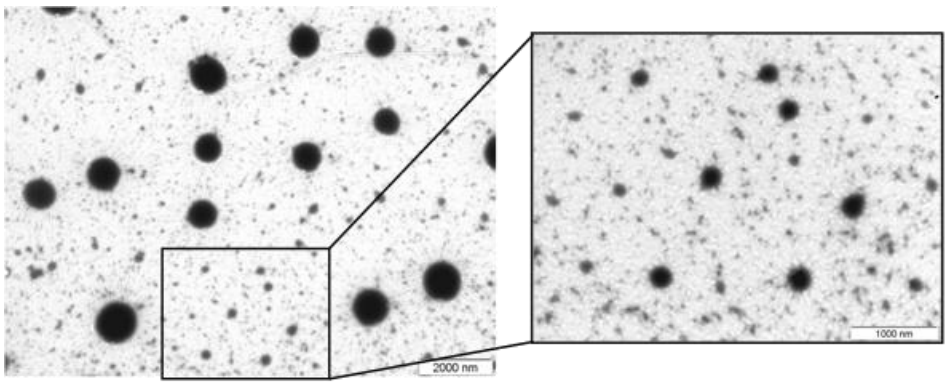

Figure 14. *TEM images of the micellar-like aggregates using phosphomolybdate as a contrast agent. The two predominant particle sizes are shown in the expansion.*

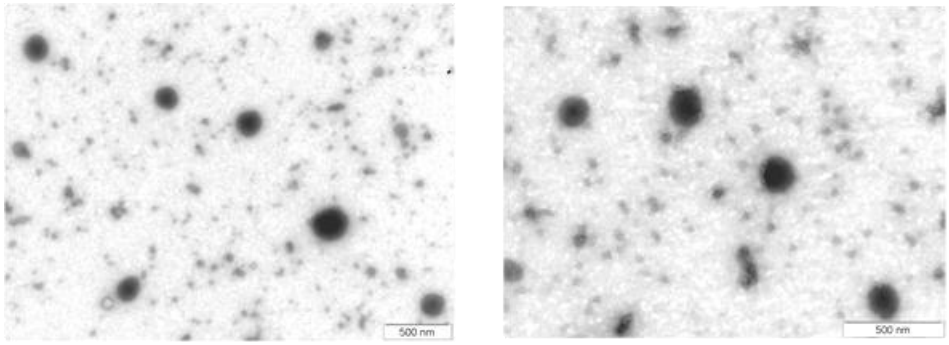

Figure 15. *TEM pictures of the smaller micellar aggregates.*

In summary, the formation of spherical micellar-like aggregates by the interaction and self-association of a TBDPS-$(BG)_4$-PNA compound has been demonstrated, both by dynamic light scattering (DLS) and TEM imaging. The diameter of these particles is *ca.* 200 nm in aqueous media in the concentration range studied. At lower concentrations ($\leq$ 3.5 μM) aggregation does not occur, in agreement with the data from the antisense activity tests. This could explain the cellular uptake mechanism for the tetraguanidinium-PNA conjugate, thus justifying the gap in activity previously observed at certain concentrations.

2.5 Novel Chiral Bicyclic Guanidinium Monomer for Solid-Phase Synthesis

In view of the encouraging results obtained with these oligoguanidinium-PNA conjugates, we proposed to expand the number of these hybrids with the intention of improving their activity as antisense agents. Inspired by previous attempts in our research group[49] and owing to PNA constructs are traditionally synthesized through solid-phase synthesis,[4b,50] we designed compound **57**, which can be used as a "unnatural amino acid" monomer for solid-phase synthesis. With this molecule in hand, we would be able to easily afford bicyclic guanidinium oligomers directly attached to PNAs (or any peptide in general). In contrast with the original oligoguanidinium salts, the bicyclic guanidinium moiety is not linearly oriented but stays branched which respect to the linear peptide sequence as a non-natural side-chain amino acid. Within this context, it can be considered as an artificial Boc-arginine analog. This new class of oligomers would present different properties and thus they may improve the internalization of the corresponding PNA conjugates. Moreover, it would allow the facile and sequential introduction of different spacers, functionalities and other amino acids, increasing exponentially the synthetic possibilities.

The synthesis of this new bicyclic guanidinium monomer is based on the attachment of a Boc-cysteine with mesylate **2** in the presence of Cs_2CO_3, giving rise to **57** in gram scale and good yields (Scheme 6).

[49] Martos, V.; Castreño, P.; Royo, M.; Albericio, F.; de Mendoza, J. *J. Comb. Chem.* **2009**, 11, 410-421.

[50] de Koning, M. C.; van der Marel, G. A.; Overhand, M. *Curr. Op. Chem. Biol.* **2003**, *7*, 734-740.

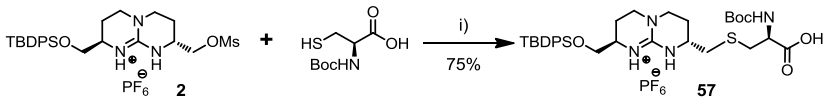

Scheme 6. *Synthesis of bicyclic guanidinium monomer* ***57****. Conditions: i) 3 eq. of* Cs_2CO_3*, 1.3 eq. of Boc-cysteine in THF/MeOH (3:1), under* N_2*.*

One of the inconveniences of this synthesis relies on the removal of the TBDPS group upon cleavage of the polymeric resin support with trifluoroacetic acid. As previously commented, silyl protected oligoguanidinium-PNA conjugates showed higher antisense activity than the non-protected ones. However, this can be easily fixed by the introduction of non-labile lipophylic groups. Indeed, this synthetic strategy not only can be applied on the TBDPS protected monoguanidinium molecule but also with other functionalized monoguanidines and oligoguanidinium compounds by attaching them to a Boc-cysteine.

To conclude, bicyclic guanidinium monomer **57** has been successfully used for the solid-phase synthesis of new PNA conjugates bearing up to seven of these guanidinium subunits with and without linkers (6-aminohexanoic acid) connecting the monomers. This work has been performed by Ms. Jolanta Barbara Ludvigsen under the supervision of Prof. Peter E. Nielsen. Determination of the antisense activity of these new oligoguanidinium-PNA conjuguates is currently under evaluation.

2.6 Antibacterial Oligoguanidinium-PNA Conjugates

Peptide nucleic acids have been widely studied as gene targeting therapeutic agents, able to inhibit or enhance gene expression by both antigene and antisense mechanisms (affecting transcription or translation processes, respectively).[51] One promising application is bacterial growth inhibition by targeting mRNA and ribosomal RNA.[52]

Antisense inhibition requires efficient cellular uptake, and delivery across bacterial cell walls constitutes one of the major drawbacks for these oligonucleotides mimics.[27] To explore the antisense activity of oligoguanidinium-PNA conjugates in bacteria, a range of constructs targeting an essential mRNA sequence for *E. coli* was synthesized. The PNA compounds were designed to bind strongly to the mRNA sequence of the *acpP* gene (Figure 16), inhibiting its correct translation and thus the biosynthesis of molecules such as fatty acids, crucial for bacterial development.

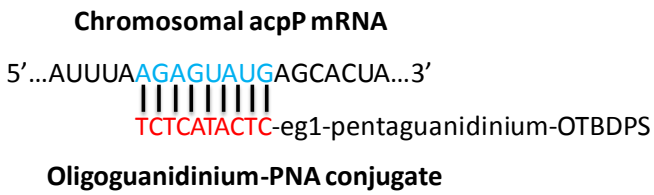

Figure 16. *PNA sequence alignment with chromosomal acpP mRNA target.*

2.6.1 Synthesis of the Antibacterial Oligoguanidinium-PNA Conjugates

A series of TBDPS protected oligoguanidinium molecules were successfully attached to the PNA oligomer, which targets the mRNA of the *acpP* gene. These PNA compounds differed in the nature of the linker between the bicyclic guanidinium

[51] For reviews see: (a) Nielsen, P. E. *Pharm. Toxicol.* **2000**, *86*, 3-7. (b) Zaffaroni, N.; Villa, R.; Folini, M. *Lett. Pept. Sci.* **2004**, *10*, 287-296. (c) Braasch, D. A.; Corey, D. R. *Biochemistry* **2009**, *41*, 4503-4510.

[52] Hatamoto, M.; Ohashi, A.; Imachi, H. *Appl. Microbiol. Biotechnol.* **2010**, *86*, 397-402.

oligomer and the peptide nucleic acid (from a simple ethyleneglycol linker (eg1) to an extended one with phenylalanine and glycine (Phe-Gly-eg1)). Mismatch PNA compounds were also linked to the corresponding oligoguanidinium vectors to determine sequence-specificity inhibition. These mismatch conjugates would serve as controls to evaluate possible side effects caused by the oligoguanidinium moiety on *E. coli* and to further support the antisense inhibitory mechanism.

Therefore, TBDPS-protected tri-, tetra- and pentaguanidinium molecules were attached to the terminal cysteine residue present in the antibacterial PNA sequence by using the same synthetic strategy and reaction conditions as previously shown. Semi-preparative-HPLC purification and subsequent lyophilization of the polar solvent mixture afforded compounds **58** to **67**.

2.6.2 Antibacterial Activity Evaluation of the Conjugates Targeting E. coli

The antibacterial potency of the oligoguanidinium-PNA conjugates targeting chromosomal *acpP* mRNA in *E. coli* was evaluated (Table 5). This work was performed by Mr. Anubrata Ghosal under the supervision of Prof. Peter E. Nielsen. MIC (Minimum Inhibitor Concentration) values, determined for each of the conjugates, clearly confirmed efficient antibacterial activity. As expected, mismatch conjugates showed almost no activity. By increasing the number of bicyclic guanidine moieties from tri- to pentaguanidinium oligomer, the activity also increases. This antibacterial effect enhancement suggested more efficient cellular uptake for the PNA conjugates bearing longer guanidinium oligomers. As for luciferase antisense assays, previously described, these molecular vectors efficiently assist the internalization of the PNA conjugates. In those assays, a decrease in activity was observed for the pentaguanidinium conjugates with respect to the tetraguanidinium analogous, probably due to their inherent increase in toxicity (see Figure 9, in section 2.3). Nonetheless, different cellular systems have been examined in each case (HeLa cells and *E. coli*, respectively), suggesting also different internalization mechanisms and toxicity. In addition, lower concentrations were required to induce the antibacterial effect (beyond

the minimum oligoguanidinium-PNA concentration necessary to induce toxicity for HeLa cells, Figure 9, in section 2.3). MIC values from the oligoguanidinium-PNA mismatch conjugates accounted for sequence-specificity inhibition and thus the antibacterial effect observed is driven by the specific PNA targeting and not by the guanidinium oligomer or the mismatch PNA sequence. Finally, conjugates containing longer linkers between the PNA sequence and the tetraguanidinium moiety showed lower MIC values than those with the ethyleneglycol connection (0.1 and 0.3 μM, respectively). This antibacterial enhancement can be attributable to two factors: a better cellular uptake and/or a stronger sequence affinity for the target mRNA.

Table 5. *Oligoguanidinium-PNA sequences tested and MIC values for E. coli. PNA (Target) CTC ATA CTC T; PNA (Mismatch) CTC TTA CAC T.*

PNA #	PNA sequence	Gene Target	Bacteria Target	MIC (μM)
58	**TBDPSO-$(BG)_3$-eg1-PNA (Target)**	acpP	E. Coli (MG1655)	>0.5
59	**TBDPSO-$(BG)_3$-eg1-Phe-Gly-PNA (Target)**	acpP	"	0.5
60	**TBDPSO-$(BG)_4$-eg1-PNA (Target)**	acpP	"	0.5
61	**TBDPSO-$(BG)_4$-eg1-PNA (Mismatch)**	---	"	>0.5
62	**TBDPSO-$(BG)_4$-eg1-Phe-Gly-PNA (Target)**	acpP	"	0.3
63	**TBDPSO-$(BG)_4$-eg1-Phe-Gly-PNA (Mismatch)**	---	"	>0.5
64	**TBDPSO-$(BG)_5$-eg1-PNA (Target)**	acpP	"	0.1
65	**TBDPSO-$(BG)_5$-eg1-PNA (Mismatch)**	---	"	>0.5
66	**TBDPSO-$(BG)_5$-eg1-Phe-Gly-PNA (Target)**	acpP	"	0.1
67	**TBDPSO-$(BG)_5$-eg1-Phe-Gly-PNA (Mismatch)**	---	"	>0.5

Representative growth curves accounting for the antibacterial response of pentaguanidinium-PNA conjugates towards *E. coli* are depicted below (Figure 17). No growth inhibition was observed using the scrambled PNA control conjugate (**67**), whereas the anti-acyl carrier protein (ACP) pentaguanidinium-PNA clearly showed complete growth inhibition upon addition of 300 nM of the corresponding conjugate.

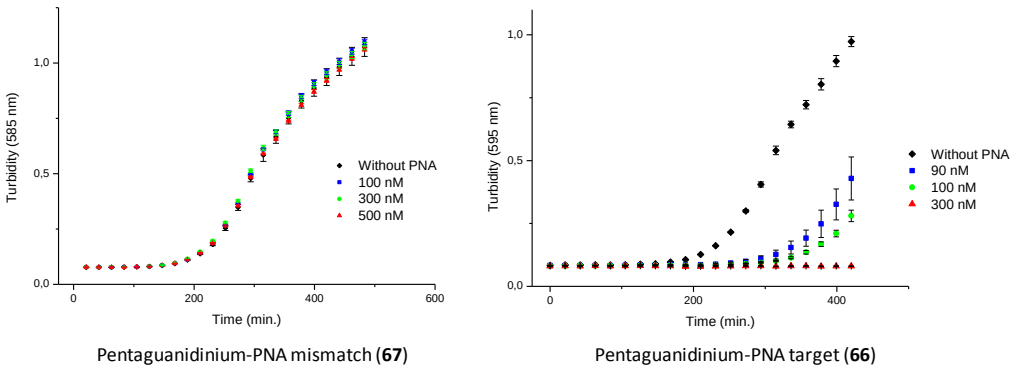

Figure 17. *Growth curves of E. coli K12 treated with pentaguanidinium-PNA conjugates incorporating the mismatch (left) and the target (right) sequences.*

Compared with a similar antibacterial anti-*acp*P peptide-PNA (MIC value of 0.8 μM) which contains a cationic cell penetrating peptide (KFFKFFKFFK),[28a,b,d] the oligoguanidinium-PNA conjugates here described showed lower MIC values (*ca.* 0.1 μM) and have thus more potent antibacterial effect in full-strength Mueller-Hilton (MH) broth.

In conclusion, we have demonstrated the practical use of oligoguanidinium-PNA conjugates as antibacterial agents with promising gene therapeutic antisense applications. They show remarkably higher antibacterial activity than the peptide-PNA conjugates reported to date. Issues concerning their bioavailability, human and animal toxicity, and pharmacokinetic behavior remain to be addressed. Nevertheless, this opens the possibility towards the use of these PNA-based vectors not only for targeting bacterial growth but also for other biologically relevant systems.

2.7 Experimental Section

General procedure for compounds 39 a-c. Compound 39b

To a stirred solution of 1-decanethiol (130 μL, 0.61 mmol) in dry MeOH (5 mL) *t*-BuOK (85 mg, 0.76 mmol) was added under N_2, and subsequently **2** (200 mg, 0.30 mmol) in dry THF (10 mL). The resulting mixture was stirred for 4 h at room temperature. The solvent was removed and the solid residue was dissolved in CH_2Cl_2 (30 mL) and washed with a solution of 0.1N NH_4PF_6 (2 × 30 mL). The organic phase was filtered over cotton and concentrated *in vacuo* to give a crude residue which was purified by silica gel column chromatography (CH_2Cl_2/MeOH, 100:0 →98:2), affording **39b** (226 mg, quantitative) as a white solid.

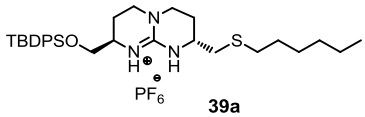

39a

(**39a**): ^{1}H-NMR (400 MHz, $CDCl_3$) δ 7.67-7.61 (m, 4H, CH_{Ar}), 7.50-7.41 (m, 6H, CH_{Ar}), 6.29 (s, 1H, NH), 6.14 (s, 1H, NH), 3.77-3.65 (m, 2H, CH_2OSi), 3.61-3.50 (m, 2H, CH_α), 3.41-3.26 (m, 4H, $CH_{2\gamma}$), 2.76 (dd, J = 5.7, 13.8 Hz, 1H, CH_2S), 2.64 (dd, J = 8.0, 13.8 Hz, 1H, CH_2S), 2.57 (t, J = 7.4 Hz, 2H, SCH_{2hex}), 2.24-2.14 (m, 1H, $CH_{2\beta}$), 2.07-1.88 (m, 3H, $CH_{2\beta}$), 1.59-1.55 (m, 2H, CH_{2hex}), 1.43-1.24 (m, 6H, CH_{2hex}), 1.09 (s, 9H, $CH_{3t\text{-}Bu}$), 0.90 (t, J = 6.8 Hz, 3H, CH_{3hex}). ^{13}C-NMR (100 MHz, $CDCl_3$) δ 150.4 (C_{guan}), 135.6, 135.5 (CH_{Ar}), 132.6, 132.5 (C_{Ar}), 130.1, 128.0 (CH_{Ar}), 65.5 (CH_2OSi), 50.2, 48.5 (CH_α), 45.6, 45.3 ($CH_{2\gamma}$), 36.3 (CH_2S), 32.6 (SCH_{2hex}), 31.4, 29.5, 28.4 (CH_{2hex}), 26.8 ($CH_{3t\text{-}Bu}$), 25.2 ($CH_{2\beta}$), 22.6, 22.5 ($CH_{2\beta}$), 19.2 ($C_{t\text{-}Bu}$), 14.0 (CH_{3hex}). HRMS calcd. for $[C_{31}H_{48}N_3OSSi]^+$ 538.3290; found 538.3292.

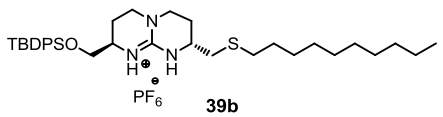

39b

(**39b**): ^{1}H-NMR (400 MHz, $CDCl_3$) δ 7.68-7.62 (m, 4H, CH_{Ar}), 7.50-7.40 (m, 6H, CH_{Ar}), 6.23 (s, 1H, NH), 6.07 (s, 1H, NH), 3.76-3.65 (m, 2H, CH_2OSi), 3.61-3.49 (m,

2H, CH_{α}), 3.40-3.26 (m, 4H, $CH_{2\gamma}$), 2.75 (dd, J = 5.5, 13.5 Hz 1H, CH_2S), 2.63 (dd, J = 8.1, 13.5 Hz 1H, CH_2S), 2.56 (t, J = 7.5 Hz, 2H, SCH_{2dec}), 2.25-2.14 (m, 1H, $CH_{2\beta}$), 2.09-1.87 (m, 3H, $CH_{2\beta}$), 1.63-1.55 (m, 2H, CH_{2dec}), 1.46-1.26 (m, 14H, CH_{2dec}), 1.09 (s, 9H, $CH_{3t\text{-}Bu}$), 0.90 (t, J = 6.8 Hz, 3H, CH_{3dec}). ^{13}C-NMR (100 MHz, $CDCl_3$) δ 150.4 (C_{guan}), 135.6, 135.5 (CH_{Ar}), 132.6, 132.6 (C_{Ar}), 130.1, 130.1, 128.0 (CH_{Ar}), 65.5 (CH_2OSi), 50.2, 48.5 (CH_{α}), 45.6, 45.3 ($CH_{2\gamma}$), 36.4 (CH_2S), 32.6 (SCH_{2dec}), 31.9, 29.6, 29.6, 29.5, 29.3, 29.2, 28.8 (CH_{2dec}), 26.8 ($CH_{3t\text{-}Bu}$), 25.2 ($CH_{2\beta}$), 22.7, 22.6 ($CH_{2\beta}$), 19.2 ($C_{t\text{-}Bu}$), 14.1 (CH_{3dec}). HRMS calcd. for $[C_{35}H_{56}N_3OSSi]^+$ 594.3916; found 594.3895.

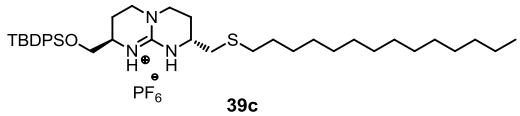

39c

(**39c**): ^{1}H-NMR (400 MHz, $CDCl_3$) δ 7.67-7.60 (m, 4H, CH_{Ar}), 7.49-7.37 (m, 6H, CH_{Ar}), 6.29 (s, 1H, NH), 6.14 (s, 1H, NH), 3.75-3.63 (m, 2H, CH_2OSi), 3.60-3.48 (m, 2H, CH_{α}), 3.40-3.23 (m, 4H, $CH_{2\gamma}$), 2.75 (dd, J = 5.7, 13.6 Hz, 1H, CH_2S), 2.62 (dd, J = 8.2, 13.5 Hz, 1H, CH_2S), 2.55 (t, J = 7.4 Hz, 2H, $SCH_{2tetradec}$), 2.23-2.12 (m, 1H, $CH_{2\beta}$), 2.06-1.86 (m, 3H, $CH_{2\beta}$), 1.56-1.52 (m, 1H, $CH_{2tetradec}$), 1.43-1.20 (m, 23H, $CH_{2tetradec}$), 1.07 (s, 9H, $CH_{3t\text{-}Bu}$), 0.88 (t, J = 6.8 Hz, 3H, $CH_{3tetradec}$). ^{13}C-NMR (100 MHz, DEPTQ, $CDCl_3$) δ 150.4 (C_{guan}), 135.6, 135.5 (CH_{Ar}), 132.6, 132.6 (C_{Ar}), 130.1, 130.0, 128.0 (CH_{Ar}), 65.5 (CH_2OSi), 50.2, 48.5 (CH_{α}), 45.6, 45.3 ($CH_{2\gamma}$), 36.3 (CH_2S), 32.6 ($SCH_{2tetradec}$), 31.9, 29.7, 29.7, 29.6, 29.6, 29.5, 29.4, 29.2, 28.8 ($CH_{2tetradec}$), 26.8 ($CH_{3t\text{-}Bu}$), 25.1 ($CH_{2\beta}$), 22.7, 22.6 ($CH_{2\beta}$), 19.1 ($C_{t\text{-}Bu}$), 14.1 ($CH_{3tetradec}$). HRMS calcd. for $[C_{39}H_{64}N_3OSSi]^+$ 650.4537; found 650.4537.

Compound 39d

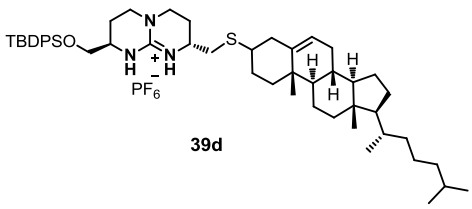

39d

To a stirred solution of **2** (300 mg, 0.45 mmol) in dry THF (40 mL) a solution of thiocholesterol (270 mg, 0.68 mmol) and *t*-BuOK (76 mg, 0.68 mmol) in THF/MeOH (2:1, 15 mL) was added. The resulting mixture was stirred for 4 h at room temperature. The solvent was removed and the residue was dissolved in CH_2Cl_2 and washed with a solution of 0.1N NH_4PF_6. The organic phase was filtered over cotton and concentrated *in vacuo*. Purification by silica gel column chromatography (CH_2Cl_2/MeOH, 100:0 →99:1) afforded **39d** (410 mg, 93%) as a white solid. ^{1}H-NMR (400 MHz, COSY, $CDCl_3$) δ 7.69-7.62 (m, 4 H, CH_{Ar}), 7.49-7.39 (m, 6H, CH_{Ar}), 6.48 (s, 1H, NH), 6.29 (s, 1H, NH), 5.39-5.33 (m, 1H, CH_{chol}), 3.74-3.62 (m, 2H, CH_2OSi), 3.60-3.43 (m, 2H, CH_α), 3.38-3.26 (m, 4H, $CH_{2\gamma}$), 2.79 (dd, J = 5.7, 13.6 Hz, 1H, CH_2S), 2.66 (dd, J = 6.2, 13.6 Hz, 1H, CH_2S), 2.63-2.53 (m, 1H, CHS_{chol}), 2.30-2.23 (m, 2H, CH_2CH_{chol}), 2.22-2.14 (m, 2H, $CH_{2\beta}$), 2.08-1.78 (m, 8H, $CH_{2\beta}$, CH_{chol}, CH_{2chol}), 1.65-1.11 (m, 17H, CH_{2chol}, CH_{chol}, CH_2CH), 1.08 (s, 9H, $CH_{3t\text{-}Bu}$), 1.00 (s, 3H, CH_{3chol}), 1.00-0.90 (m, 1H, CH_{chol}), 0.93 (d, J = 6.6 Hz, 3H, CH_3), 0.89 (dd, J = 1.7, 6.6 Hz, 6H, CH_3), 0.69 (s, 3H, CH_3). ^{13}C-NMR (100 MHz, HSQC-DEPTQ, $CDCl_3$) δ 150.4 (C_{guan}) 141.2 (C=CH), 135.6, 135.5, 132.6, 132.6, 130.1, 128.0, (C_{Ar}, CH_{Ar}), 121.4 (CH=C), 65.5 (CH_2O), 56.7, 56.2 (CH_{chol}), 50.2, 50.1 (CH_α), 48.9 (CH_{chol}), 45.6, 45.2 ($CH_{2\gamma}$), 45.0, 42.3 (CH_{chol}), 40.0, 39.7 (CH_{2chol}), 39.5, 39.4 (CH_2), 36.8 (CH), 36.2 (CH_2), 35.8 (CH), 34.0, 31.9 (CH_2), 31.8 (CH), 29.7 (CH_2), 28.2 (CH), 28.0 (CH_2), 26.8 ($CH_{3t\text{-}Bu}$), 25.1, 24.3, 23.9 (CH_2), 22.8 (CH_3), 22.6 (CH_2), 22.6 (CH_3), 20.9 (CH_2), 19.3 (CH_3), 19.2 ($C_{t\text{-}Bu}$), 18.7, 11.9 (CH_3). ESI-MS m/z 822.7 (M - PF_6^-)$^+$. HRMS calcd. for $[C_{52}H_{80}N_3OSSi]^+$ 822.5791; found 822.5779.

Compound 39e

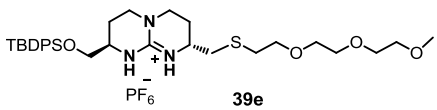

39e

To a stirred solution of triethyleneglycol monomethyl tioacetate (202 mg, 0.91 mmol) and Cs_2CO_3 (221 mg, 0.68 mmol) in dry MeOH (10 mL) was added a solution of **2** (300 mg, 0.45 mmol) in acetonitrile (20 mL). The resulting mixture was stirred for 4 h at room temperature. The solvent was removed, and the solid residue dissolved in CH_2Cl_2 (30 mL) and washed twice with a solution of 0.1N NH_4PF_6 (2 x 30 ml). The organic phase was filtered over cotton and concentrated *in vacuo*. Purification by silica gel column chromatography (CH_2Cl_2/MeOH, 100:0 →98:2) afforded **39e** (330 mg, 98%) as a yellowish oil. ^{1}H-NMR (400 MHz, $CDCl_3$) δ 7.67-7.62 (m, 4H, CH_{Ar}), 7.58-7.38 (m, 6H, CH_{Ar}), 6.86 (s, 1H, NH), 6.42 (s, 1H, NH), 3.79-3.49 (m, 14H, CH_2OSi, CH_2O_{gly}, CH_3O_{gly}, CH_α), 3.43-3.27 (m, 9H, CH_2O_{gly} $CH_{2\gamma}$), 2.93-2.69 (m, 4H, CH_2S, SCH_{2gly}), 2.12-1.98 (m, 2H, $CH_{2\beta}$), 1.95-1.83 (m, 2H, $CH_{2\beta}$), 1.09 (s, 9H, $CH_{3t\text{-}Bu}$). ^{13}C-NMR (100 MHz, $CDCl_3$) δ 150.6 (C_{guan}), 135.5, 135.5 (CH_{Ar}), 132.7, 132.6 (C_{Ar}), 130.1, 130.1, 128.0, 127.9 (CH_{Ar}),71.9, 71.3, 70.9, 69.6, 69.6 (CH_2O_{gly}), 65.8 (CH_2OSi), 58.5 (OCH_{3gly}) 50.3, 48.8 (CH_α), 45.5, 45.2 ($CH_{2\gamma}$), 37.1 (CH_2S), 32.2 (SCH_{2gly}), 26.8 ($CH_{3t\text{-}Bu}$), 25.4 ($CH_{2\beta}$), 22.6 ($CH_{2\beta}$), 19.2 ($C_{t\text{-}Bu}$). ESI-MS m/z 600.3 $(M - PF_6^-)^+$.

General procedure for compounds 40 a-c. Compound 40a

Compound **39a** (155 mg, 0.23 mmol) was dissolved in dry THF (15 mL). Then, 1M THF TBAF solution (680 μL, 0.68 mmol was added and the mixture was stirred overnight under inert atmosphere. The solvent was removed under vacuum and the compound was redissolved in CH_2Cl_2 (25 mL) and washed with a solution of 0.1N NH_4PF_6 (15 mL). The aqueous phase was extracted back with CH_2Cl_2 (2 x 20 mL) and $CHCl_3$ (20 mL). The organic phases were mixed and filtered over cotton, and then concentrated *in vacuo* to give a crude residue which was purified by silica gel column chromatography (CH_2Cl_2/MeOH, 100:0 →95:5), to give **40a** (90 mg, 89%) as a yellowish oil.

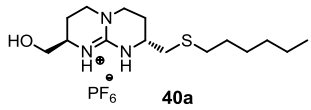

40a

(**40a**): ^{1}H-NMR (400 MHz, $CDCl_3$) δ 6.60 (s, 1H, NH), 6.38 (s, 1H, NH), 3.71-3.60 (m, 2H, CH_2OSi), 3.58-3.43 (m, 2H, CH_α), 3.40-3.19 (m, 4H, $CH_{2\gamma}$), 2.75 (dd, J = 6.0, 13.6 Hz, 1H, CH_2S), 2.60 (dd, J = 7.8, 13.6 Hz, 1H, CH_2S), 2.51 (t, J = 7.5 Hz, 2H, SCH_{2hex}), 2.21-2.00 (m, 2H, $CH_{2\beta}$), 1.95-1.80 (m, 2H, $CH_{2\beta}$), 1.63-1.56 (m, 2H, CH_{2hex}), 1.33-1.27 (m, 4H, CH_{2hex}), 0.91 (t, J = 6.8 Hz, 3H, CH_{3hex}). ^{13}C-NMR (100 MHz, DEPTQ, $CDCl_3$) δ 151.1 (C_{guan}), 64.4 (CH_2OH), 50.6, 48.3 (CH_α), 45.7, 45.4 ($CH_{2\gamma}$), 36.8 (CH_2S), 32.7 (SCH_{2hex}), 31.4, 30.9, 29.6, 28.5 (CH_{2hex}), 25.5 ($CH_{2\beta}$), 22.7 ($CH_{2\beta}$), 22.5 (CH_{2hex}), 14.0 (CH_{3hex}). HRMS calcd. for $[C_{15}H_{30}N_3OS]^+$ 300.2110; found 300.2114.

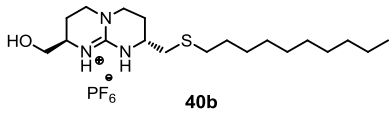

40b

(**40b**): ^{1}H-NMR (400 MHz, $CDCl_3$) δ 6.62 (s, 1H, NH), 6.38 (s, 1H, NH), 3.85 (d, J = 7.8 Hz, 1H, CH_2OH), 3.67-3.30 (m, 7H, CH_2OH, CH_α, $CH_{2\gamma}$), 2.73 (dd, J = 6.0, 13.7 Hz, 1H, CH_2S), 2.62 (dd, J = 7.9, 13.7 Hz, 1H, CH_2S), 2.55 (t, J = 7.5 Hz, 2H, SCH_{2dec}), 2.19-2.00 (m, 2H, $CH_{2\beta}$), 1.96-1.77 (m, 2H, $CH_{2\beta}$), 1.62-1.55 (m, 2H, CH_{2dec}), 1.39-1.28 (m, 14H, CH_{2dec}), 0.90 (t, J = 6.8 Hz, 3H, CH_{3dec}). ^{13}C-NMR (100 MHz, DEPTQ, $CDCl_3$) δ 151.0 (C_{guan}), 64.4 (CH_2OH), 50.5, 48.2 (CH_α), 45.7, 45.4 ($CH_{2\gamma}$), 36.7 (CH_2S), 32.6 (SCH_{2dec}), 31.9, 29.7, 29.6, 29.3, 29.3, 28.8 (CH_{2dec}), 25.5 ($CH_{2\beta}$), 22.7 (CH_{2dec}), 22.7 ($CH_{2\beta}$), 14.1 (CH_{3dec}). HRMS calcd. for $[C_{19}H_{38}N_3OS]^+$ 356.2736; found 356.2753.

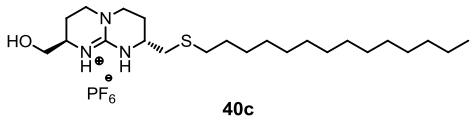

40c

(**40c**): ^{1}H-NMR (400 MHz, $CDCl_3$) δ 6.61 (s, 1H, NH), 6.42 (s, 1H, NH), 3.75-3.63 (m, 2H, CH_2OSi), 3.60-3.48 (m, 2H, CH_α), 3.40-3.23 (m, 4H, $CH_{2\gamma}$), 2.75 (dd, J = 5.7,

13.6 Hz, 1H, CH_2S), 2.62 (dd, J = 8.2, 13.5 Hz, 1H, CH_2S), 2.55 (t, J = 7.4 Hz, 2H, $SCH_{2tetradec}$), 2.23-2.12 (m, 1H, $CH_{2\beta}$), 2.06-1.86 (m, 3H, $CH_{2\beta}$), 1.56-1.52 (m, 1H, $CH_{2tetradeca}$), 1.43-1.20 (m, 23H, $CH_{2tetradeca}$), 1.07 (s, 9H, $CH_{3t\text{-}Bu}$), 0.88 (t, J = 6.8 Hz, 3H, $CH_{3tetradeca}$). ^{13}C-NMR (100 MHz, DEPTQ, $CDCl_3$) δ 151.0 (C_{guan}), 64.4 (CH_2OH), 50.5, 48.3 (CH_α), 46.0 ($CH_{2\gamma}$), 36.9 (CH_2S), 32.7 ($SCH_{2tetradeca}$), 31.9, 29.7, 29.7, 29.6, 29.4, 29.3, 29.2, 29.1, 28.9 ($CH_{2tetradeca}$), 26.2 ($CH_{2\beta}$), 22.7 ($CH_{2\beta}$), 14.2 ($CH_{3tetradeca}$). HRMS calcd. for $[C_{23}H_{46}N_3OS]^+$ 412.3362; found 412.3369.

Compound 40d

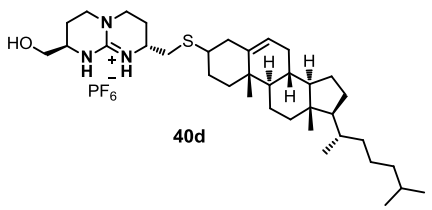

40d

To a solution of **39d** (200 mg, 0.21 mmol) in dry THF (20 mL) HF/Py (70%, 1.3 mL) was added dropwise at 0ºC. The resulting mixture was stirred overnight at room temperature. The solvent was removed and the crude was redissolved in CH_2Cl_2. After neutralization with an aqueous saturated solution of Na_2CO_3, the organic phase was collected, filtered over cotton and evaporated again. The final residue was purified by silica gel column chromatography (CH_2Cl_2/MeOH, 97:3 → 95:5), affording **40d** (136 mg, 90%) as a yellowish oil. ^{1}H-NMR (500 MHz, COSY, $CDCl_3$) δ 6.79 (s, 1H, NH), 6.57 (s, 1H, NH), 5.35 (d, J = 5.1 Hz, 1H, CH_{chol}), 3.80 (br s, 1H, OH), 3.58 (dd, J = 7.6, 18.7 Hz, 2H, CH_2OH), 3.49-3.41 (m, 2H, CH_α), 3.40-3.20 (m, 4H, $CH_{2\gamma}$), 2.76 (dd, J = 6.6, 13.5 Hz, 1H, CH_2S), 2.70 (dd, J = 7.2, 13.5 Hz, 1H, CH_2S), 2.57 (m, 1H, CHS_{chol}), 2.28-2.14 (m, 4H, CH_2CH_{chol}), 2.01-1.77 (m, 12H, $CH_{2\beta}$, CH_{2chol}), 1.55-1.20 (m, 11H, CH_2CH_{chol}, CH_{2chol}, CH_{chol}), 1.18-1.09 (m, 1H, CH_{chol}), 1.00-0.92 (m, 4H, CH_{2chol}, CH_{chol}), 0.98 (s, 3H, CH_3), 0.91 (d, J = 6.5 Hz, 3H, CH_3), 0.87 (d, J = 6.6 Hz, 3H, CH_3), 0.86 (d, J = 6.6 Hz, 3H, CH_3), 0.66 (s, 3H, CH_3). ^{13}C-NMR (125 MHz, DEPT, $CDCl_3$) δ 150.7 (C_{guan}) 141.1 (C=CH), 121.4 (C*H*=C), 64.6 (CH_2O), 56.7

(CH_{chol}), 56.2 (CH_{chol}), 50.2 (CH_{α}), 48.5 (CH_{chol}), 45.6, 45.4 ($CH_{2\gamma}$), 44.8, 42.3 (CH_{chol}), 39.8, 39.7 (CH_{2chol}), 39.5, 39.4 (CH_2), 36.8 (CH), 36.2 (CH_2), 35.8 (CH), 34.6, 31.8 (CH_2), 31.7 (CH), 29.8 (CH_2), 28.2 (CH), 28.0, 25.5, 24.3, 23.8 (CH_2), 22.7 (CH_3), 22.5 (CH_2), 22.46 (CH_3), 20.9, 19.3 (CH_2), 18.7, 11.8 (CH_3). ESI-MS m/z 584.5 $(M - PF_6^-)^+$. HRMS calcd.for $[C_{36}H_{62}N_3OS]^+$ 584.4613; found 584.4633.

Compound 40e

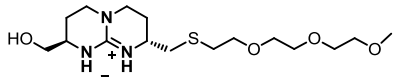

40e

A solution of **39e** (330 mg, 0.34 mmol) and TBAF (1M THF solution, 1.02 mL, 1.02 mmol) in THF (20 mL) was stirred overnight. The solvent was removed and the crude dissolved in CH_2Cl_2 (30 mL) and washed with a 1N NH_4PF_6 (10 mL) solution. The organic phase was filtered over cotton and concentrated *in vacuo* to give a crude residue which was purified by silica gel column chromatography (CH_2Cl_2/MeOH, 100:0 → 96:4), giving rise to **40e** (135 mg, 78%) as a yellowish oil. ^{1}H-NMR (400 MHz, $CDCl_3$) δ, 6.82 (s, 1H, NH), 6.76 (s, 1H, NH), 3.84-3.53 (m, 15H, CH_2OSi, CH_2O_{gly}, CH_3O_{gly}, CH_{α}), 3.52-3.32 (m, 8H, CH_2O_{gly} $CH_{2\gamma}$), 2.86 (dd, J = 5.0, 14.0 Hz, 1H, CH_2S), 2.79 (q, J = 5.0 Hz, 2H, SCH_{2gly}), 2.71 (dd, J = 8.2, 14.1 Hz, 1H, CH_2S) 2.21-2.11 (m, 1H, $CH_{2\beta}$), 2.07-1.98 (m, 1H, $CH_{2\beta}$), 1.96-1.82 (m, 2H, $CH_{2\beta}$). ^{13}C-NMR (100 MHz, CD_3OD) δ 150.6 (C_{guan}), 71.6, 70.9, 69.8, 69.7, 69.1 (CH_2O_{gly}), 63.8 (CH_2OH), 57.8 (OCH_{3gly}) 50.3, 48.1 (CH_{α}), 45.2, 45. ($CH_{2\gamma}$), 36.7 (CH_2S), 31.5 (SCH_{2gly}), 25.5 ($CH_{2\beta}$), 22.5 ($CH_{2\beta}$). ESI-MS m/z 362.2 $(M - PF_6^-)^+$.

General procedure for compounds 41 a-c. Compound 41b

To a solution of **40b** (118 mg, 0.24 mmol) and NMM (157 μL, 1.41 mmol) in dry THF (15 mL) was added Ms_2O (164 mg, 0.94 mmol). The reaction mixture was stirred for 4 h at room temperature. After evaporating the solvent, the resulting crude was dissolved in CH_2Cl_2 (30 mL) and washed with a 0.1N NH_4PF_6 solution (2 x 20 mL). The organic layer was filtered over cotton and concentrated *in vacuo*. Purification by silica gel column chromatography (CH_2Cl_2/MeOH, 100:0 → 96:4) afforded **41b** (118 mg, 86%) as a yellowish oil.

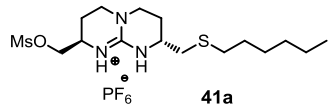

41a

(**41a**): ^{1}H-NMR (400 MHz, $CDCl_3$) δ 6.82 (s, 1H, NH), 6.69 (s, 1H, NH), 4.41-4.32 (m, 1H, CH_2OMs), 4.24-4.11 (m, 1H, CH_2OMs), 3.93-3.84 (m, 1H, CH_α), 3.63-3.32 (m, 5H, CH_α, $CH_{2\gamma}$), 3.17 (s, 3H, CH_{3MsO}), 3.02-2.78 (m, 2H, CH_2S), 2.73-2.67 (m, 1H, CH_2S), 2.58 (t, J = 7.4 Hz, 1H, SCH_2), 2.23-2.11 (m, 2H, $CH_{2\beta}$), 2.10-1.88 (m, 2H, $CH_{2\beta}$), 1.51-1.40 (m, 2H, CH_{2hex}), 1.39-1.29 (m, 6H, CH_{2hex}), 0.91 (t, J = 7.0 Hz, 3H, CH_{3hex}). ^{13}C-NMR (100 MHz, HSQC-DEPT, $CDCl_3$) δ 150.7 (C_{guan}), 70.3 (CH_2OMs), 47.7, 45.7 (CH_α), 44.9, 44.1 ($CH_{2\gamma}$), 37.1 (CH_{3MsO}), 36.5 (CH_2S), 33.3 (SCH_{2hex}), 32.4, 31.9, 31.4, 29.7 (CH_{2dec}), 28.4 ($CH_{2\beta}$), 22.7 ($CH_{2\beta}$), 14.1 (CH_{3hex}). HRMS calcd. for $[C_{16}H_{32}N_3O_3S_2]^+$ 378.1885; found 378.1883.

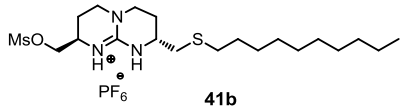

41b

(**41b**): ^{1}H-NMR (400 MHz, $CDCl_3$) δ 6.21 (s, 1H, NH), 6.17 (s, 1H, NH), 4.28 (dd, J = 4.3, 10.5 Hz, 1H, CH_2OMs), 4.10 (dd, J = 6.7, 10.5 Hz, 1H, CH_2OMs), 3.82-3.76 (m, 1H, CH_α), 3.49-3.45 (m, 1H, CH_α), 3.40-3.26 (m, 4H, $CH_{2\gamma}$), 3.07 (s, 3H, CH_{3MsO}), 2.60-2.58 (m, 2H, CH_2S), 2.47 (t, J = 7.4 Hz, 2H, SCH_{2dec}), 2.16-2.05 (m, 2H, $CH_{2\beta}$), 1.96-1.80 (m, 2H, $CH_{2\beta}$), 1.52-1.46 (m, 2H, CH_{2dec}), 1.30-1.19 (m, 14H, CH_{2dec}), 0.81 (t, J = 6.8 Hz, 3H, CH_{3dec}). ^{13}C-NMR (125 MHz, HSQC-DEPT, $CDCl_3$) δ 151.0 (C_{guan}),

70.1 (CH_2OMs), 48.8, 48.2 (CH_α), 46.2, 45.4 ($CH_{2\gamma}$), 37.7 (CH_{3MsO}), 36.8 (CH_2S), 33.0 (SCH_{2dec}), 32.3, 30.0, 29.9, 29.7, 29.6, 29.2 (CH_{2dec}), 25.6 ($CH_{2\beta}$), 23.1 (CH_{2dec}), 22.4 ($CH_{2\beta}$), 14.5 (CH_{3dec}). HRMS calcd. for $[C_{20}H_{40}N_3O_3S_2]^+$ 434.2511; found 434.2510.

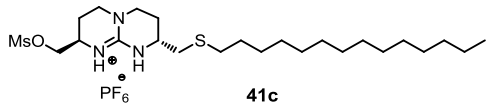

41c

(**41c**): ^{1}H-NMR (400 MHz, $CDCl_3$) δ 6.84 (s, 1H, NH), 6.71 (s, 1H, NH), 4.40-4.32 (m, 1H, CH_2OMs), 4.25-4.11 (m, 1H, CH_2OMs), 3.85-3.84 (m, 1H, CH_α), 3.64-3.32 (m, 5H, CH_α, $CH_{2\gamma}$), 3.17 (s, 3H, CH_{3MsO}), 3.00-2.80 (m, 2H, CH_2S), 2.74-2.67 (m, 1H, CH_2S), 2.57 (t, J = 7.5 Hz, 1H, SCH_2), 2.37-2.11 (m, 2H, $CH_{2\beta}$), 2.09-1.89 (m, 2H, $CH_{2\beta}$), 1.53-1.42 (m, 2H, $CH_{2tetradec}$), 1.41-1.20 (m, 22H, $CH_{2tetradec}$), 0.90 (t, J = 7.0 Hz, 3H, $CH_{3tetradec}$). ^{13}C-NMR (125 MHz, HSQC-DEPT, $CDCl_3$) δ 151.2 (C_{guan}), 70.7 (CH_2OMs), 48.1, 47.8 (CH_α), 46.1, 45.0 ($CH_{2\gamma}$), 37.4 (CH_{3MsO}), 37.0 (CH_2S), 32.4 ($SCH_{2tetradeca}$), 32.2, 30.0, 29.9, 29.88, 29.81, 29.7, 29.6, 29.5, 29.1 ($CH_{2tetradeca}$), 26.1 ($CH_{2\beta}$), 23.0 ($CH_{2tetradeca}$), 22.2 ($CH_{2\beta}$), 14.3 ($CH_{3tetradeca}$). HRMS calcd. for $[C_{24}H_{48}N_3O_3S_2]^+$ 490.3137; found 490.3141.

Compound 41d

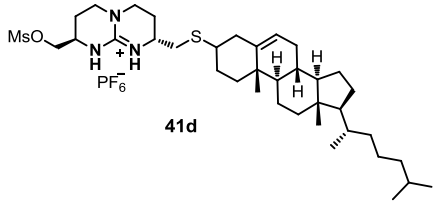

41d

To a solution of **40d** (136 mg, 0.19 mmol) and NMM (83 μL, 0.75 mmol) in dry THF (10 mL) Ms_2O (98 mg, 0.56 mmol) in dry THF (5 mL) was added. The reaction mixture was stirred for 4 h at room temperature. After evaporating the solvent, the resulting crude was dissolved in CH_2Cl_2 and washed with a 0.1N NH_4PF_6 solution.

The organic layer was filtered over cotton and concentrated *in vacuo*. Purification by silica gel column chromatography (CH_2Cl_2/MeOH, 96:4) afforded **41d** (140 mg, 93%) as a white solid. ^{1}H-NMR (500 MHz, COSY, $CDCl_3$) δ 7.22 (s, 1H, NH), 7.09 (s, 1H, NH), 5.36 (s, 1H, CH_{chol}), 4.32-4.17 (m, 2H, CH_2OMs), 3.60-3.35 (m, 6H, CH_α, $CH_{2\gamma}$), 3.15 (s, 3H, CH_{3MsO}), 2.88-2.63 (m, 2H, CH_2S), 2.60-2.57 (m, 1H, CHS_{chol}), 2.35-2.10 (m, 4H, CH_2CH_{chol}, $CH_{2\beta}$), 2.04-1.86 (m, 10H, CH_2CH_{chol}, CH_{2chol}, $CH_{2\beta}$), 1.68-1.43 (m, 9H, CH_{2chol}, CH_{chol}), 1.22-1.07 (m, 5H, CH_2, CH), 0.99 (s, 3H, CH_3), 0.91 (d, J = 6.4 Hz, 3H, CH_3), 0.87 (d, J = 6.6 Hz, 3H, CH_3), 0.86 (d, J = 6.6 Hz, 3H, CH_3), 0.67 (s, 3H, CH_3). ^{13}C-NMR (125 MHz, $CDCl_3$) δ 150.7 (C_{guan}) 141.2 (*C*=CH), 121.4 (*C*H=C), 69.8 (CH_2O), 56.7 (CH_{chol}), 56.2 (CH_{chol}), 50.2, 49.0 (CH_α), 47.5 (CH_{chol}), 45.6, 45.2 ($CH_2\gamma$), 44.8, 42.3 (CH_{chol}), 39.8, 39.7 (CH_{2chol}), 39.5, 39.4 (CH_2), 37.2 (CH_3), 36.8, 36.2 (CH_2), 35.8 (CH), 34.1, 31.8 (CH_2), 31.78, 29.9, 29.7 (CH), 28.2, 28.0, 25.0, 24.3, 23.8 (CH_2), 22.8, 22.5 (CH_3), 21.0 (CH_2), 19.3, 18.7, 11.8 (CH_3). FAB/LSIMS m/z 662.3 [(M - PF_6^-)$^+$, 100%]. HRMS calcd. for $[C_{37}H_{64}N_3O_3S_2]^+$ 662.4389; found 662.4388.

Compound 41e

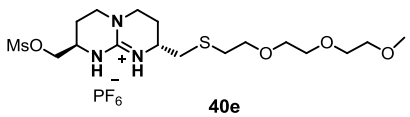

40e

To a solution of **40e** (135 mg, 0.27 mmol) in dry THF (15 mL) was added Ms_2O (139 mg, 0.80 mmol). The mixture was treated with NMM (118 μL, 1.06 mmol) and stirred for 4 h at room temperature. After evaporating the solvent, the resulting solid was dissolved in CH_2Cl_2 (60 mL) and washed with a 0.1M NH_4PF_6 solution (2 × 30 mL). The organic layer was filtered over cotton and concentrated *in vacuo*. Purification by silica gel column chromatography (CH_2Cl_2/MeOH, 97:3) afforded **41e** (157 mg, 94%) as a yellowish oil. ^{1}H-NMR (400 MHz, $CDCl_3$) δ, 7.07 (s, 1H, NH), 6.95 (s, 1H, NH), 4.38 (dd, J = 4.5, 10.3 Hz, 1H, CH_2OMs), 4.25 (dd, J = 7.0, 10.3 Hz, 1H, CH_2OMs), 3.92-3.60 (m, 13H, CH_2OSi, CH_2O_{gly}, CH_3O_{gly}, CH_α), 3.58-3.31 (m, 8H, CH_2O_{gly} $CH_{2\gamma}$), 3.12 (s, 1H, CH_{3OMs}), 2.85-2.71 (m, 4H, CH_2S), 2.29-2.12 (m, 2H,

$CH_{2\beta}$), 2.10-1.99 (m, 1H, $CH_{2\beta}$), 1.94-1.82 (m, 2H, $CH_{2\beta}$). ^{13}C-NMR (100 MHz, HSQC-DEPTQ $CDCl_3$) δ 150.9 (C_{guan}), 71.9, 71.5, 70.9, 70.3 (CH_2O_{gly}), 70.0 (CH_2OMs), 69.7 (CH_2O_{gly}), 58.8 (OCH_{3gly}) 48.5, 47.6 (CH_α), 45.7, 44.9 ($CH_{2\gamma}$), 37.3 (CH_{3MsO}), 37.2 (CH_2S), 32.1 (SCH_{2gly}), 25.4 ($CH_{2\beta}$), 22.1 ($CH_{2\beta}$). ESI-MS m/z 440.2 (M - PF_6^-)$^+$.

General procedure for compounds 42 a-c. Compound 42a

A mixture of diguanidinium tioacetate compound **11** (55 mg, 0.06 mmol), mesylate **41a** (32 mg, 0.06 mmol) and Cs_2CO_3 (46 mg, 0.14 mmol) was dissolved in 20 mL of degassed CH_3CN/MeOH at room temperature under N_2 and stirred for 4 h. The solvent was evaporated and the crude was dissolved in CH_2Cl_2 (30 mL) and washed with 1N NH_4PF_6 (2 × 10 mL). The organic phase was filtered over cotton and concentrated *in vacuo* to give a crude residue which was purified by silica gel column chromatography (CH_2Cl_2/MeOH, 100:0 → 96/4), affording **42a** (58 mg, 75%) as a yellowish oil.

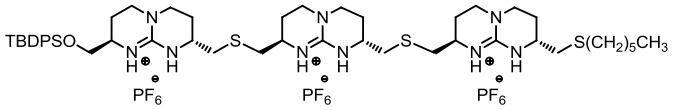

42a

(**42a**): ^{1}H-NMR (400 MHz, $CDCl_3$) δ 7.69-7.63 (m, 4H, CH_{Ar}), 7.49-7.40 (m, 6H, CH_{Ar}), 6.75-6.13 (bs, 2H, NH), 3.86-3.20 (m, 20H, CH_2OSi, CH_α,$CH_{2\gamma}$), 2.93-2.49 (m, 10H, CH_2S), 2.28-2.01 (m, 6H, $CH_{2\beta}$), 1.99-1.78 (m, 6H, $CH_{2\beta}$), 1.57-1.54 (m, 2H, CH_{2hex}), 1.44-1.24 (m, 8H, CH_{2hex}), 1.07 (s, 9H, $CH_{3t\text{-}Bu}$), 0.90 (t, J = 6.8 Hz, 3H, CH_{3hex}). ^{13}C-NMR (100 MHz, $CDCl_3$) δ 150.7, 150,6, 150.5 (C_{guan}), 135.6, 135.5 (CH_{Ar}), 132.8, 132.7 (C_{Ar}), 130.0, 128.8, 128.0 (CH_{Ar}), 65.4 (CH_2OSi), 50.1, 49.6, 48.5, 47.7, 47.5, 47.1 (CH_α), 45.6, 45.5, 45.4, 45.3, 45.2, 45.0 ($CH_{2\gamma}$), 36.4, 36.3, 36.2 (CH_2S), 32.6 (SCH_{2hex}), 31.4, 29.6, 28.5 (CH_{2hex}), 26.8 ($CH_{3t\text{-}Bu}$), 25.7, 25.6, 25.1 ($CH_{2\beta}$), 22.5 ($CH_{2\beta}$), 19.2 ($C_{t\text{-}Bu}$), 14.1 (CH_{3hex}). HRMS calcd. for $[C_{49}H_{79}F6N_9OPS_3Si]^+$ 1078.4909; found 1078.4908.

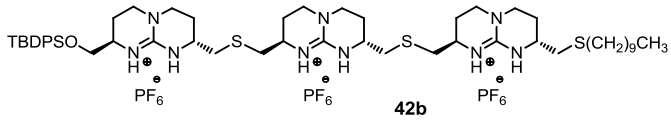

42b

(**42b**): ^{1}H-NMR (400 MHz, $CDCl_3$) δ 7.73-7.65 (m, 4H, CH_{Ar}), 7.51-7.42 (m, 6H, CH_{Ar}), 6.65-6.03 (bs, 3H, NH), 3.87-3.16 (m, 20H, CH_2OSi, CH_{α},$CH_{2\gamma}$), 2.91-2.45 (m, 10H, CH_2S), 2.34-1.74 (m, 12H, $CH_{2\beta}$), 1.59-1.55 (m, 2H, SCH_{2deca}), 1.43-1.21 (m, 14H, CH_{2deca}), 1.08 (s, 9H, $CH_{3t\text{-}Bu}$), 0.89 (t, J = 7.0 Hz, 3H, CH_{3dec}). ^{13}C-NMR (100 MHz, $CDCl_3$) δ 150.7 (C_{guan}), 135.6, 135.5 (CH_{Ar}), 132.7, 132.6 (C_{Ar}), 130.0, 127.9 (CH_{Ar}), 65.4 (CH_2OSi), 53.5, 50.1, 49.5, 47.8, 47.7, 47.3 (CH_{α}), 45.6, 45.5, 45.4, 45.3, 45.0 ($CH_{2\gamma}$), 36.5, 36.4, 36.2 (CH_2S), 32.6 (SCH_{2deca}), 31.9, 29.7, 29.6, 29.5, 29.3, 29.2, 28.8, 28.7 (CH_{2deca}), 26.8 ($CH_{3t\text{-}Bu}$), 26.0, 25.7, 25.6, 25.1 ($CH_{2\beta}$), 22.7, 22.5 ($CH_{2\beta}$), 18.9 ($C_{t\text{-}Bu}$), 14.1 (CH_{3deca}). HRMS calcd. for $[C_{53}H_{86}N_9OS_3Si]^+$ 988.5881, found 988.5795.

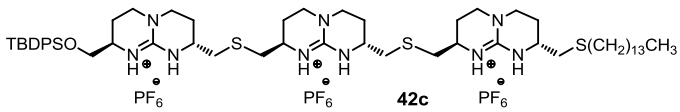

42c

(**42c**): ^{1}H-NMR (400 MHz, $CDCl_3$) δ 7.70-7.62 (m, 4H, CH_{Ar}), 7.49-7.39 (m, 6H, CH_{Ar}), 6.58-5.82 (bs, 3H, NH), 3.83-3.15 (m, 20H, CH_2OSi, CH_{α},$CH_{2\gamma}$), 2.93-2.48 (m, 10H, CH_2S), 2.31-1.77 (m, 12H, $CH_{2\beta}$), 1.57-1.54 (m, 2H, $CH_{2tetradeca}$), 1.43-1.18 (m, 22H, $CH_{2tetradeca}$), 1.08 (s, 9H, $CH_{3t\text{-}Bu}$), 0.90 (t, J = 7.0 Hz, 3H, $CH_{3tetradec}$). ^{13}C-NMR (100 MHz, $CDCl_3$) δ 150.6 (C_{guan}), 135.6, 135.5 (CH_{Ar}), 132.8, 132.7 (C_{Ar}), 130.0, 128.0 (CH_{Ar}), 65.4 (CH_2OSi), 50.1, 49.7, 48.5, 47.5, 47.1, 46.9 (CH_{α}), 45.5, 45.4, 45.3, 45.2, 45.0 ($CH_{2\gamma}$), 36.5, 36.3, 36.2 (CH_2S), 32.7 ($SCH_{2tetradeca}$) 31.9, 29.7, 29.65, 29.6, 29.4, 29.3, 29.2, 28.9, 28.7 ($CH_{2tetradeca}$), 26.8 ($CH_{3t\text{-}Bu}$) 25.8, 25.7, 25.1 ($CH_{2\beta}$), 22.7, 22.5 ($CH_{2\beta}$), 19.0 ($C_{t\text{-}Bu}$), 14.1 ($CH_{3tetradeca}$). HRMS calcd. for $[C_{57}H_{96}F_6N_9OPS_3Si]^{2+}$ 595.8155; found 595.8193.

Compound 42d

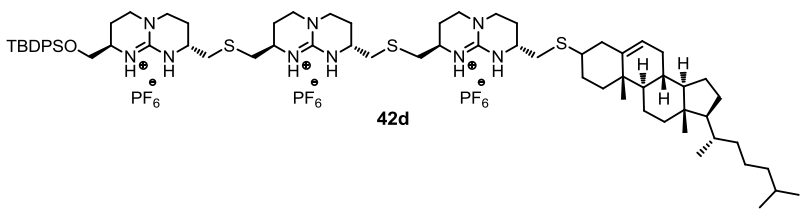

Diguanidinium tioacetate compound **11** (78 mg, 0.08 mmol) was dissolved in dry MeOH (10 ml) in the presence of Cs_2CO_3 (64 mg, 0.18 mmol) and the mixture was stirred for 5 minutes. Then a solution of mesylated guanidinium **41d** (64 mg, 0.08 mmol) in dry acetonitrile was added and the mixture was stirred for 4 h under N_2 atmosphere at room temperature. The solvent was evaporated under low pressure. The crude was dissolved in CH_2Cl_2 (30 mL) and washed with a 1N NH_4PF_6 solution (2 × 10 mL). The organic phase was filtered over cotton and concentrated *in vacuo* to give a crude residue which was purified by silica gel column chromatography (CH_2Cl_2/MeOH, 100:0 → 96:4), affording **42d** (92 mg, 71%) as a yellowish oil. ^{1}H-NMR (400 MHz, $CDCl_3$) δ 7.70-7.63 (m, 4H, CH_{Ar}), 7.50-7.39 (m, 6H, CH_{Ar}), 6.64-5.85 (bs, 4H, NH), 5.36 (s, 1H, CH_{chol}), 3.89-3.22 (m, 20H, CH_2OSi, CH_α,$CH_{2\gamma}$), 2.93-2.74 (m, 5H, CH_2S), 2.73-2.53 (m, 6H, CH_2S, CHS_{chol}), 2.37-1.73 (m, 22H, $CH_{2\beta}$, CH_2CH_{chol}, CH_{2chol}), 1.62-1.25 (m, 12H, CH_2, CH_{2chol}, CH_{chol}), 1.22-1.11 (m, 5H, CH_2, CH), 1.07 (s, 9H, $CH_{3t\text{-}Bu}$), 1.00 (s, 3H, CH_3), 0.93 (d, J = 6.5 Hz, 3H, CH_3), 0.89 (dd, J = 1.1, 6.6 Hz, 6H, CH_3), 0.69 (s, 3H, CH_3). ^{13}C-NMR (100 MHz, HSQC-DEPTQ, $CDCl_3$) δ 150.4 (C_{guan}) 141.2 (*C*=CH), 135.6, 135.5, 130.0, 128.0 (C_{Ar}, CH_{Ar}), 121.3 (*C*H=C), 65.4 (CH_2O), 56.7, 56.1 (CH_{chol}), 50.2, 50.1, 50.0 (CH_α), 48.5 (CH_{chol}), 45.5, 45.3, 45.0 ($CH_{2\gamma}$), 42.5, 42.3 (CH_{chol}), 40.0, 39.8, 39.7 (CH_{2chol}), 39.5, 39.4 (CH_2), 37.4 (CH), 36.8, 36.5, 36.2 (CH_2), 35.8 (CH), 34.1, 31.9 (CH_2), 31.8 (CH), 29.7, 28.2 (CH_2), 28.0 (CH), 26.8 ($CH_{3t\text{-}Bu}$), 25.5, 25.3, 25.0, 24.8, 24.3, 23.9 (CH_2), 22.8 (CH_3), 22.6 (CH_3), 22.5 (CH_2), 21.2 (CH), 20.9 (CH_2), 19.2 ($C_{t\text{-}Bu}$), 19.3, 18.7, 11.9 (CH_3). ESI-MS m/z 1216.7 $(M - PF_6^- - 2HPF_6)^+$.

Compound 42e

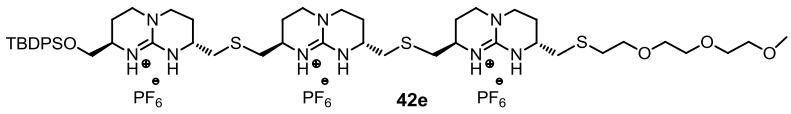

A mixture of diguanidinium thioacetate compound **11** (100 mg, 0.1 mmol), mesylate **41e** (65 mg, 0.11 mmol) and Cs_2CO_3 (82 mg, 0.25 mmol) was dissolved in 20 mL of degassed CH_3CN/MeOH at room temperature under N_2 and stirred for 3 h. The solvent was removed and the resulting crude was dissolved in CH_2Cl_2 (30 mL) and washed with a 1N NH_4PF_6 solution (2 × 20 mL). The organic phase was filtered over cotton and concentrated *in vacuo* to give a crude residue which was purified by silica gel column chromatography (CH_2Cl_2/MeOH, 100:0 → 96:4), affording **42e** (86 mg, 59%) as a yellowish oil. ^{1}H-NMR (400 MHz, $CDCl_3$) δ 7.69-7.63 (m, 4H, CH_{Ar}), 7.49-7.40 (m, 6H, CH_{Ar}), 6.80-6.00 (bs, 3H, NH), 3.81-3.54 (m, 19H, CH_2OSi, CH_2O_{gly}, CH_3O_{gly}, CH_α), 3.53-3.22 (m, 14H, CH_2O_{gly} $CH_{2\gamma}$), 2.93-2.54 (m, 12H, CH_2S), 2.31-1.79 (m, 12H, $CH_{2\beta}$), 1.08 (s, 9H, $CH_{3t\text{-}Bu}$). ^{13}C-NMR (100 MHz, C-DEPTQ, HSQC, CD_3CN) δ 150.7, 150.6 (C_{guan}), 135.5, 135.4 (CH_{Ar}), 132.7, 132.6 (C_{Ar}), 130.1, 127.9 (CH_{Ar}), 71.6, 71.4, 70.5, 69.8, 69.5, 68.9 (CH_2O_{gly}) 65.9 (CH_2OSi), 57.9 (OCH_{3gly}), 50.3, 48.3, 47.8, 47.7 (CH_α), 45.3, 45.2, 45.1 ($CH_{2\gamma}$), 38.6, 36.7 35.7, 35.6 (CH_2S), 31.5 (SCH_2), 26.2 ($CH_{3t\text{-}Bu}$), 25.3, 25.2, 25.1 ($CH_{2\beta}$), 22.1 ($CH_{2\beta}$), 20.1 ($C_{t\text{-}Bu}$). ESI-MS *m/z* 1096.3 (M - PF_6^- - HPF_6)$^+$, 950.3 (M - PF_6^- - 2 HPF_6)$^+$, 475.7 (M - PF_6^- - 2 HPF_6)$^{2+}$.

General procedure for compounds 43 a-c. Compound 43b

A solution of **42a** (64 mg, 0.05 mmol) and TBAF (1M THF solution, 137 μL, 0.14 mmol) in THF (20 mL) was stirred overnight. The solvent was removed and the crude dissolved in CH_2Cl_2 (30 mL) and washed with a 1N NH_4PF_6 (10 mL) solution. The organic phase was filtered over cotton and concentrated *in vacuo* to give a crude residue which was purified by silica gel (with KPF_6) column chromatography (CH_2Cl_2/MeOH, 100:0 → 92:8), giving rise to **43b** (42 mg, 79%) as a white solid, which was directly

used in the next step without further characterization.

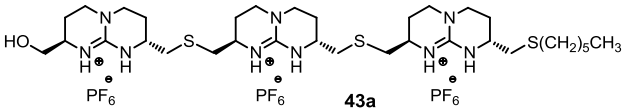

43a

(**43a**): ^{1}H-NMR (400 MHz, CD_3CN) δ 7.37-6.89 (bs, 5H, NH), 3.66 (dd, J = 3.8, 10.5 Hz, 1H, CH_2OH), 3.60-3.29 (m, 19H, CH_2O, CH_α,$CH_{2\gamma}$), 2.97-2.86 (m, 3H, CH_2S), 2.77 (dd, J = 5.6, 13.8 Hz, 1H, CH_2S), 2.64-2.51 (m, 6H, CH_2S), 2.16-2.07 (m, 6H, $CH_{2\beta}$), 1.88-1.78 (m, 6H, $CH_{2\beta}$), 1.65-1.54 (m, 2H, SCH_{2hex}), 1.45-1.27 (m, 8H, CH_{2hex}), 0.92 (t, J = 6.9 Hz, 3H, CH_{3hex}).

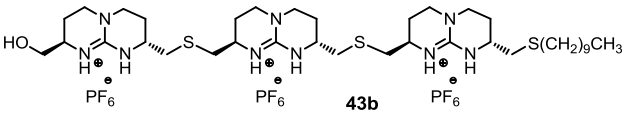

43b

(**43b**): ^{1}H-NMR (400 MHz, CD_3CN) δ 7.25-7.06 (bs, 2H, NH), 6.98-6.77 (bs, 3H, NH), 3.66 (dd, J = 3.7, 10.4 Hz, 1H, CH_2OH), 3.62-3.29 (m, 19H, CH_2O, CH_α,$CH_{2\gamma}$), 2.94-2.87 (m, 3H, CH_2S), 2.78 (dd, J = 5.3, 13.7 Hz, 1H, CH_2S), 2.66-2.50 (m, 6H, CH_2S), 2.18-2.05 (m, 6H, $CH_{2\beta}$), 1.88-1.69 (m, 6H, $CH_{2\beta}$), 1.67-1.52 (m, 2H, SCH_{2dec}), 1.44-1.26 (m, 16H, CH_{2dec}), 0.91 (t, J = 6.9 Hz, 3H, CH_{3dec}).

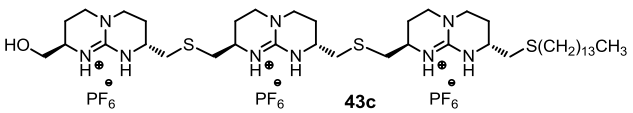

43c

(**43c**): ^{1}H-NMR (400 MHz, CD_3CN) δ 7.30-6.75 (bs, 5H, NH), 3.67 (dd, J = 3.7, 10.5 Hz, 1H, CH_2OH), 3.63-3.28 (m, 19H, CH_2O, CH_α,$CH_{2\gamma}$), 2.95-2.85 (m, 3H, CH_2S), 2.76 (dd, J = 5.5, 13.8 Hz, 1H, CH_2S), 2.63-2.49 (m, 6H, CH_2S), 2.19-2.04 (m, 6H, $CH_{2\beta}$), 1.85-1.71 (m, 6H, $CH_{2\beta}$), 1.65-1.53 (m, 2H, $SCH_{2tetradec}$), 1.45-1.27 (m, 24H, $CH_{2tetradec}$), 0.91 (t, J = 6.8 Hz, 3H, $CH_{3tetradec}$).

General procedure for compounds 44 a-c. Compound 44a

To a solution of alcohol **43a** (38 mg, 0.03 mmol) and NMM (22.3 μL, 0.20 mmol) in dry THF (10 mL) was added Ms_2O (23 mg, 0.13 mmol) and the mixture was stirred for 4 h. The solvent was evaporated under reduced pressure and the resulting crude was dissolved in CH_2Cl_2 and washed with a 0.1N NH_4PF_6 solution (2 × 30 mL). The organic layer was filtered over cotton and concentrated *in vacuo*. Purification by silica gel (with KPF_6) column chromatography (CH_2Cl_2/MeOH, 94:6) afforded **44a** (21 mg, 52%) as a white solid.

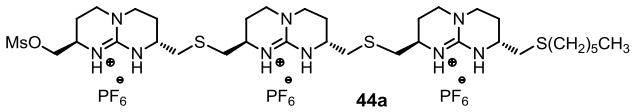

44a

(**44a**): ^{1}H-NMR (400 MHz, CD_3CN) δ 7.15-6.64 (bs, 4H, NH), 4.32 (dd, J = 4.2, 10.6 Hz, 1H, CH_2OMs), 4.18-4.11 (m, 1H, CH_2OMs), 3.80 (m, 1H, CH_α), 3.60-3.29 (m, 17H, CH_α,$CH_{2\gamma}$), 3.13 (s, 3H, CH_{3MsO}), 2.94-2.84 (m, 3H, CH_2S), 2.82-2.75 (dd, J = 5.0, 13.6 Hz, 1H, CH_2S), 2.63-2.52 (m, 6H, CH_2S), 2.15-2.03 (m, 6H, $CH_{2\beta}$), 1.89-1.74 (m, 6H, $CH_{2\beta}$), 1.65-1.54 (m, 2H, SCH_{2hex}), 1.45-1.27 (m, 8H, CH_{2hex}), 0.92 (t, J = 6.6 Hz, 3H, CH_{3hex}). ^{13}C-NMR (100 MHz, C-DEPT, CD_3CN) δ 150.1, 150.0 (C_{guan}), 70.7 (CH_2OMs), 47.6, 47.5, 47.5, 47.3 (CH_α), 45.3, 45.2, 45.2, 44.8, 44.6 ($CH_{2\gamma}$), 36.7 (CH_{3MsO}), 36.0, 35.9, 35.9, 35.7 (CH_2S), 31.1 (SCH_{2hex}), 29.4, 28.2, 28.0 (CH_{2hex}), 25.7, 25.6, 25.4 ($CH_{2\beta}$), 24.5 (CH_{2hex}), 22.1, 21.7, 21.5 ($CH_{2\beta}$), 13.3 (CH_{3hex}). HRMS calcd. for $[C_{34}H_{64}F_{12}N_9O_3P_2S_4]^+$ 1064.3255; found 1064.3269.

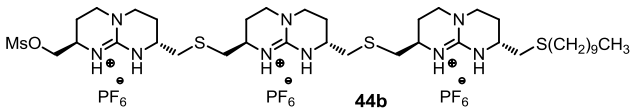

44b

(**44b**): ^{1}H-NMR (400 MHz, CD_3CN) δ 7.25-6.55 (bs, 4H, NH), 4.32 (dd, J = 3.8, 10.3 Hz, 1H, CH_2OMs), 4.19-4.09 (m, 1H, CH_2OMs), 3.86-3.76 (m, 1H, CH_α), 3.65-3.27 (m, 17H, CH_α,$CH_{2\gamma}$), 3.13 (s, 3H, CH_{3MsO}), 2.99-2.83 (m, 3H, CH_2S), 2.78 (dd, J = 5.2, 13.9 Hz, 1H, CH_2S), 2.66-2.49 (m, 6H, CH_2S), 2.16-2.05 (m, 6H, $CH_{2\beta}$), 1.90-1.73 (m, 6H, $CH_{2\beta}$), 1.66-1.51 (m, 2H, SCH_{2dec}), 1.46-1.24 (m, 16H, CH_{2dec}), 0.91 (t, J = 6.7 Hz,

3H, CH_{3dec}). ^{13}C-NMR (100 MHz, HSQC-DEPTQ, CD_3OD) δ 150.0 (C_{guan}), 70.1 (CH_2OMs), 48.0, 47.5, 47.5 (CH_α), 45.1, 44.9, 44.7, 44.4 ($CH_{2\gamma}$), 36.0 (CH_{3MsO}), 36.1, 36.0 (CH_2S), 31.7 (SCH_{2dec}), 29.3, 29.2, 29.2, 29.1, 29.0, 28.4 (CH_{2dec}), 25.3, 25.2, 25.1, 25.0 ($CH_{2\beta}$), 22.4 (CH_{2dec}), 22.2, 21.9 ($CH_{2\beta}$), 13.1 (CH_{3dec}). HRMS calcd. for $[C_{38}H_{71}F_6N_9O_3PS_4]^+$ 974.4227; found 974.4218

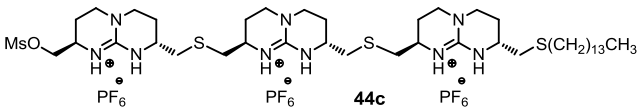

44c

(**44c**): ^{1}H-NMR (400 MHz, CD_3CN) δ 7.03-6.59 (bs, 4H, NH), 4.32 (dd, J = 4.4, 10.5 Hz, 1H, CH_2OMs), 4.16 (dd, J = 7.2, 10.5 Hz, 1H, CH_2OMs), 3.86-3.76 (m, 1H, CH_α), 3.62-3.47 (m, 5H, CH_α), 3.46-3.28 (m, 12H, $CH_{2\gamma}$), 3.13 (s, 3H, CH_{3MsO}), 2.93-2.82 (m, 3H, CH_2S), 2.78 (dd, J = 5.4, 13.9 Hz, 1H, CH_2S), 2.68-2.51 (m, 6H, CH_2S), 2.16-2.07 (m, 6H, $CH_{2\beta}$), 1.91-1.75 (m, 6H, $CH_{2\beta}$), 1.67-1.53 (m, 2H, $SCH_{2tetradec}$), 1.45-1.23 (m, 24H, $CH_{2tetradec}$), 0.91 (t, J = 6.8 Hz, 3H, $CH_{3tetradec}$). ^{13}C-NMR (100 MHz, CD_3CN) δ 150.1, 150.0 (C_{guan}), 70.8 (CH_2OMs), 47.6, 47.5, 47.5, 47.3 (CH_α), 45.3, 45.2, 44.7 ($CH_{2\gamma}$), 36.6 (CH_{3MsO}), 36.0, 35.9, 35.9, 35.7 (CH_2S), 31.7 ($SCH_{2tetradec}$), 29.9, 29.4, 29.3, 29.3, 29.2, 29.1, 28.4, 28.3 ($CH_{2tetradec}$), 25.7, 25.6, 25.4 ($CH_{2\beta}$), 25.0, 24.4 ($CH_{2tetradec}$), 22.1, 21.7, 21.5 ($CH_{2\beta}$), 13.4 ($CH_{3tetradec}$). HRMS calcd. for $[C_{42}H_{79}F_6N_9O_3PS_4]^+$ 1030.4831; found 1030.4791

Compound 44d

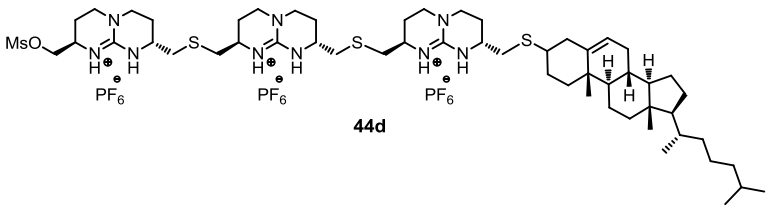

44d

A solution of **42d** (89 mg, 0.05 mmol) and TBAF (1M THF solution, 161 µL, 0.16 mmol) in THF (15 mL) was stirred overnight. The solvent was removed and the crude was dissolved in CH_2Cl_2 (30 mL) and washed with a 1N NH_4PF_6 solution (10 mL).

The organic phase was filtered over silica first with pure CH_2Cl_2 to elute the tetrabutylammonium salts formed and then with a mixture CH_2Cl_2/MeOH (96:4) to obtain product **43d** as a yellowish oil (93%, 70 mg), which was directly used in the next step without further purification. To a solution of alcohol **43d** (70 mg, 0.05 mmol) and NMM (44 μL, 0.40 mmol) in dry THF (15 mL) was added Ms_2O (52 mg, 0.3 mmol) and the mixture was stirred for 5 h. The solvent was evaporated under reduced pressure and the resulting crude was dissolved in CH_2Cl_2 and washed with a 0.1N NH_4PF_6 solution (2 × 20 mL). The organic layer was filtered over cotton and concentrated *in vacuo*. Purification by silica gel (with KPF_6) column chromatography (CH_2Cl_2/MeOH, 96:4) afforded **44d** (33 mg, 44 %) as a yellow oil. ^{1}H-NMR (400 MHz, CD_3CN) δ 7.13-6.54 (bs, 5H, NH), 5.39 (s, 1H, CH_{chol}), 4.32 (dd, J = 4.2, 10.3 Hz, 1H, CH_2OMs), 4.15 (dd, J = 7.5, 10.3 Hz, 1H, CH_2OMs), 3.86-3.77 (m, 1H, $CH_{\alpha,}CH_{2\gamma}$), 3.66-3.30 (m, 16H, $CH_{\alpha,}CH_{2\gamma}$), 3.14 (s, 3H, CH_{3MsO}), 3.13-3.10 (m, 1H, CHS_{chol}), 2.95-2.80 (m, 5H, CH_2S), 2.67-2.52 (m, 5H, CH_2S), 2.41-2.01 (m, 14H, $CH_{2\beta}$, CH_2CH_{chol}, CH_{2chol}), 1.93-1.75 (m, 7H, $CH_{2\beta}$, CH_2CH_{chol}, CH_{2chol}), 1.65-1.08 (m, 19H, CH_2, CH_{2chol}, CH_{chol}), 1.03 (s, 3H, CH_3), 0.96 (d, J = 6.6 Hz, 3H, CH_3), 0.89 (dd, J = 1.6, 6.5 Hz, 6H, CH_3), 0.73 (s, 3H, CH_3). ^{13}C-NMR (100 MHz, HSQC-DEPTQ CD_3CN) δ 150.8, 150.8, 150.7 (C_{guan}) 141.7 (*C*=CH), 121.0 (*C*H=C), 70.7 (CH_2O), 56.7 (CH_{chol}), 56.1 (CH_{chol}), 50.3(CH_{chol}), 48.6, 47.7, 47.6, 47.4, 47.4 (CH_α), 45.3, 45.3, 45.1, 44.6 ($CH_2\gamma$), 44.4 (CH_{chol}), 39.8, 39.7 (CH_{2chol}), 39.4, 39.2 (CH_2), 36.7 (CH_{3MsO}), 36.0 (CH_2), 35.7 35.7, 35.6 (SCH_2), 35.4 (CH), 34.1 (SCH_2), 31.7 (CH), 31.6, 29.8, 28.0 (CH_2), 27.7 (CH), 25.4, 25.4, 25.3(CH_2), 25.0 (CH_3), 24.0, 23.5 (CH_2), 22.0, 21.8 (CH_3), 21.7, 20.7 (CH_2), 18.8, 18.2, 11.3 (CH_3). ESI-MS m/z 1348.1 (M -PF_6^-)$^+$, 1202.2 (M - PF_6^- - HPF_6)$^+$, 1056.3 (M - PF_6^- - 2 HPF_6)$^+$, 601.6 (M – 2 PF_6^-)$^{2+}$, 528.7 (M – 2 PF_6^- - HPF_6)$^{2+}$.

Compound 44e

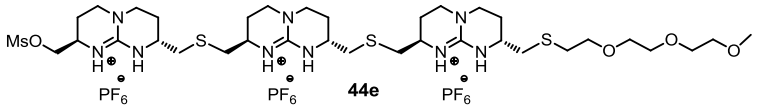

44e

A solution of **42e** (86 mg, 0.06 mmol) and TBAF (1M THF solution, 180 μL, 0.18 mmol) in THF (15 mL) was stirred overnight. The solvent was removed and the crude was dissolved in CH_2Cl_2 (30 mL) and washed with a 1N NH_4PF_6 solution (10 mL). The organic phase was filtered over silica, first with CH_2Cl_2 to elute the tetrabutylammonium salts formed and then with a mixture CH_2Cl_2/MeOH (94:6) to elute the corresponding product **43e** (91%, 65 mg), which was directly used in the next step without further purification. To a solution of alcohol **43e** (65 mg, 0.05 mmol) and NMM (24 μL, 0.21 mmol) in dry THF (15 mL) was added Ms_2O (28 mg, 0.16 mmol) and the mixture was stirred for 5 h. The solvent was evaporated under reduced pressure and the resulting crude was dissolved in CH_2Cl_2 and washed with a 0.1N NH_4PF_6 solution (2 × 20 mL). The organic layer was filtered over cotton and concentrated *in vacuo*. Purification by silica gel (with KPF_6) column chromatography (CH_2Cl_2/MeOH, 95:5) afforded **44d** (41 mg, 60 %) as an oil. ^{1}H-NMR (400 MHz, CD_3CN) δ 7.20 (bs, 4H, NH), 4.46 (dd, J = 4.3, 10.4 Hz, 1H, CH_2OMs), 4.28 (dd, J = 7.4, 10.5 Hz, 1H, CH_2OMs), 4.03-3.93 (m, 1H, CH_α), 3.80-3.46 (m, 27H, CH_2O_{gly}, CH_α,$CH_{2\gamma}$), 3.33 (s, 3H, CH_3O_{gly}), 3.19 (s, 3H, CH_{3MsO}), 3.07-2.93 (m, 6H, CH_2S), 2.82-2.68 (m, 6H, CH_2S), 2.31-2.19 (m, 6H, $CH_{2\beta}$), 2.02-1.87 (m, 6H, $CH_{2\beta}$). ^{13}C-NMR (100 MHz, C-DEPT, CD_3CN) δ 150.8, 150.7 (C_{guan}), 71.5, 70.7 (CH_2O_{gly}), 70.5 (CH_2OMs), 69.8, 69.7, 69.5 (CH_2O_{gly}), 57.9 (OCH_{3gly}), 48.2, 48.1, 47.7, 47.7, 47.6, 47.6 (CH_α), 45.2, 45.2, 45.1, 45.1, 45.0, 44.6 ($CH_{2\gamma}$), 36.7 (CH_2S), 36.6 (CH_{3MsO}), 35.8, 35.7, 35.6, 31.3 (CH_2S),25.3, 25.2, 25.2, 25.1 ($CH_{2\beta}$), 21.6 ($CH_{2\beta}$). ESI-MS m/z 1126.0 $(M\text{-}PF_6^-)^+$, 980.1 $(M\text{-}PF_6^-\text{-}HPF_6)^+$, 834.1 $(M\text{-}PF_6^-\text{-}2\,HPF_6)^+$, 490.5 $(M-2\,PF_6^-)^{2+}$, 417.6 $(M-2\,PF_6^-\text{-}HPF_6)^{2+}$.

Compound 45

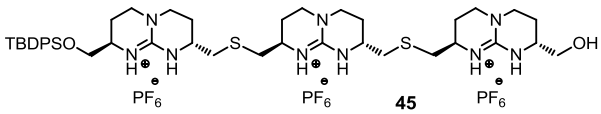

45

To a solution of disulfide **8** (50 mg, 0.08 mmol) in MeOH (3 mL), Cs_2CO_3 (52 mg, 0.16 mmol) and P(^{n}Bu)$_2$Ph polystyrene (110 mg, 0.10 mmol) was added and the mixture was stirred for 40 min. Then a solution of **10** (145 mg, 0.15 mmol) in THF (10 mL) was added and the mixture was stirred for 3 h. After evaporation of the solvent, the crude residue was dissolved in CH_2Cl_2 (20 mL) and washed with a 0.1N NH_4PF_6 solution (2 × 30 mL). The organic layer was filtered over cotton and concentrated *in vacuo*. Purification by silica gel column chromatography (CH_2Cl_2/MeOH, 98:2 → 94:6) afforded **45** (148 mg, 81%) as a white solid. ^{1}H-NMR (400 MHz, $CDCl_3$) δ 7.64-7.24 (m, 4H, CH_{Ar}), 7.43-7.38 (m, 6H, CH_{Ar}), 6.47 (s, 2H, NH), 6.35 (s, 2H, NH), 6.23 (s, 2H, NH), 3.72-3.23 (m, 22H, CH_2O, CH_α, $CH_{2\gamma}$), 2.86-2.50 (m, 8H, CH_2S), 2.65-2.63 (m, 2H, CH_2S), 2.12-1.81 (m, 12H, $CH_{2\beta}$), 1.05 (s, 9H, $CH_{3t\text{-}Bu}$). ^{13}C-NMR (100 MHz, CD_3CN) δ 150.8, 150.7 (C_{guan}), 135.5, 135.4, 130.1, 128.0, 127.9 (CH_{Ar}, C_{Ar}), 65.9, 63.7 (CH_2OSi, CH_2O), 50.5, 50.2, 47.8, 47.7, 47.6 (CH_α), 45.4, 45.1, 45.0 ($CH_{2\gamma}$), 35.7, 35.6 (CH_2S), 26.2 ($CH_{3t\text{-}Bu}$), 25.4, 25.2, 22.2, 22.1 ($CH_{2\beta}$), 19.0 ($C_{t\text{-}Bu}$). HRMS calcd. for $[C_{43}H_{68}N_9O_2F_6PS_2Si]^{2+}$ 489.7180; found 489.7166.

Compound 46

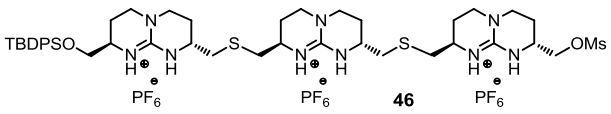

46

To a solution of alcohol **45** (148 mg, 0.12 mmol) and NMM (64 μL, 0.58 mmol) in dry CH_2Cl_2 (10 mL) was added Ms_2O (81 mg, 0.47 mmol) and the mixture was stirred for 4 h. The solvent was evaporated under reduced pressure and the resulting crude

was dissolved in CH_2Cl_2 and washed with a 0.1N NH_4PF_6 solution (2 × 30 mL). The organic layer was filtered over cotton and concentrated *in vacuo*. Purification by silica gel column chromatography (CH_2Cl_2/MeOH, 100:0 → 96:4) afforded **46** (145 mg, 93%) as a white solid. ^{1}H-NMR (400 MHz, $CDCl_3$) δ 7.68-7.66 (m, 4H, CH_{Ar}), 7.43-7.38 (m, 6H, CH_{Ar}), 6.37 (s, 2H, NH), 6.28 (s, 2H, NH), 6.22 (s, 2H, NH), 4.22-4.01 (m, 2H, CH_2O), 3.72-3.68 (m, 2H, CH_2O), 3.47-3.23 (m, 18H, CH_α, $CH_{2\gamma}$), 3.10 (s, 3H, CH_{3MsO}), 2.84-2.52 (m, 8H, CH_2S), 2.13-1.79 (m, 12H, $CH_{2\beta}$), 1.06 (s, 9H, $CH_{3t\text{-}Bu}$). ^{13}C-NMR (100 MHz, $CDCl_3$) δ 150.8, 150.8, 150.7 (C_{guan}), 135.5, 135,4, 133.0, 132.8, 130.1, 128.0 (CH_{Ar}, C_{Ar}), 70.7 (CH_2OMs), 65.9 (CH_2OSi), 50.2, 47.7, 47.7, 47.6, 47.5 (CH_α), 45.2, 45.1, 45.0, 44.6 ($CH_{2\gamma}$), 36.6 (CH_{3MsO}), 35.7, 35.7, 35.6 (CH_2S), 26.2 ($CH_{3t\text{-}Bu}$), 25.3, 25.2, 25.1, 22.2, 21.6 ($CH_{2\beta}$), 18.8 ($C_{t\text{-}Bu}$). HRMS calcd. for $[C_{44}H_{69}F_6N_9O_4PS_3Si]^+$ 1056.4044; found 1056.4033.

Compound 47

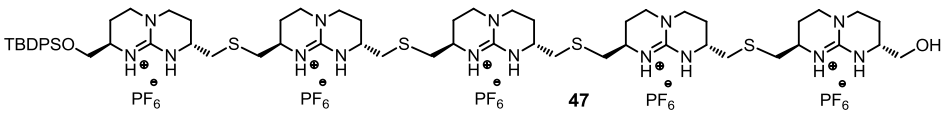

To a solution of disulfide **16** (75 mg, 0.05 mmol) in MeOH (3 mL), Cs_2CO_3 (33 mg, 0.10 mmol) and $P(^nBu)_2Ph$ polystyrene (71 mg, 0.07 mmol) was added and the mixture was stirred for 40 min. Then a solution of **46** (132 mg, 0.10 mmol) in THF (10 mL) was added and the mixture was stirred for 5 h. After evaporation of the solvent, the crude residue was dissolved in CH_2Cl_2 (20 mL) and washed with a 0.1N NH_4PF_6 solution (2 × 30 mL). The organic layer was filtered over cotton and concentrated *in vacuo*. Purification by silica gel (with KPF_6) column chromatography (CH_2Cl_2/MeOH, 98:2 → 90:10) afforded **47** (105 mg, 46%) as a white solid. ^{1}H-NMR (400 MHz, CD_3CN) δ 7.74-7.68 (m, 4H, CH_{Ar}), 7.55-7.44 (m, 6H, CH_{Ar}), 7.03-6.40 (bs, 8H, NH), 3.79-3.46 (m, 14H, CH_2O, CH_α), 3.44-3.28 (m, 20H, $CH_{2\gamma}$), 2.92-2.82 (m, 8H, CH_2S), 2.65-2.50 (m, 8H, CH_2S), 2.17-2.05 (m, 10H, $CH_{2\beta}$), 1.89-1.69 (m, 10H, $CH_{2\beta}$), 1.08 (s, 9H, $CH_{3t\text{-}Bu}$). ^{13}C-NMR (100 MHz, CD_3CN) δ 150.8, 150.7, 150.6 (C_{guan}), 135.5, 135.4,

130.0, 128.0, 127.9 (CH_{Ar}, C_{Ar}), 65.7, 63.9 (CH_2OSi, CH_2O), 50.5, 50.2, 47.8, 47.8, 47.7, 47.6 (CH_α), 45.4, 45.1, 45.0, 44.9 ($CH_{2\gamma}$), 35.7, 35.6, 35.5 (CH_2S), 26.1 ($CH_{3t\text{-}Bu}$), 25.4, 25.3, 25.2, 22.2, 22.1 ($CH_{2\beta}$), 19.1 ($C_{t\text{-}Bu}$). HRMS calcd. for $[C_{61}H_{100}F_{24}N_{15}O_2P_4S_4Si]^+$ 1810.5398; found 1810.5701.

Compound 48

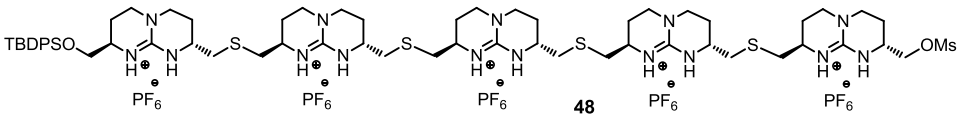

48

To a solution of alcohol **47** (40 mg, 0.02 mmol) and NMM (18 μL, 0.16 mmol) in dry THF/CH_3CN (15 mL, 1:0.1) was added Ms_2O (21 mg, 0.12 mmol) and the mixture was stirred for 4 h. The solvent was evaporated under reduced pressure and the resulting crude was dissolved in CH_2Cl_2 and washed with a 0.1N NH_4PF_6 solution (2 × 30 mL). The organic layer was filtered over cotton and concentrated *in vacuo*. Purification by silica gel (with KPF_6) column chromatography (CH_2Cl_2/MeOH, 100:0 → 92:8) afforded **48** (25 mg, 60%) as a white solid. ^{1}H-NMR (400 MHz, CD_3CN) δ 7.73-7.67 (m, 4H, CH_{Ar}), 7.54-7.43 (m, 6H, CH_{Ar}), 7.13-6.49 (bs, 9H, NH), 4.35-4.29 (m, 1H, CH_2O), 4.15 (dd, J = 7.4, 10.0 Hz, 1H, CH_2O), 3.84-3.64 (m, 2H, CH_2O), 3.62-3.46 (m, 10H, CH_α), 3.47-3.29 (m, 20H, $CH_{2\gamma}$), 3.13 (s, 3H, CH_{3MsO}) 2.91-2.80 (m, 8H, CH_2S), 2.65-2.52 (m, 8H, CH_2S), 2.15-2.07 (m, 10H, $CH_{2\beta}$), 1.90-1.76 (m, 10H, $CH_{2\beta}$), 1.09 (s, 9H, $CH_{3t\text{-}Bu}$). ^{13}C-NMR (100 MHz, CD_3CN) δ 150.8, 150.7, 150.7 (C_{guan}), 135.5, 135,4, 130.1, 130.1, 128.0, 127.9 (CH_{Ar}, C_{Ar}), 70.7 (CH_2OMs), 65.9 (CH_2OSi), 50.2, 47.8, 47.7, 47.7, 47.6 (CH_α), 45.2, 45.1, 45.0, 44.6 ($CH_{2\gamma}$), 36.6 (CH_{3MsO}), 36.0, 35.9, 35.9, 35.8, 35.7 (CH_2S), 26.2 ($CH_{3t\text{-}Bu}$), 25.3, 25.3, 25.2, 22.2, 21.6 ($CH_{2\beta}$), 18.8 ($C_{t\text{-}Bu}$). HRMS calcd. for $[C_{62}H_{102}F_{24}N_{15}O_4P_4S_5Si]^+$ 1888.5174; found 1888.5498.

Compound 57

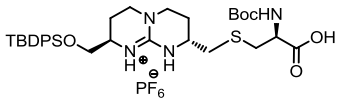

57

To a stirred solution of Boc-cysteine (494 mg, 2.231 mmol) and Cs_2CO_3 (1.51 g, 4.65 mmol) in dry MeOH (15 mL) was added a solution of **2** (1.23 mg, 1.86 mmol) in dry THF (30 mL). The resulting mixture was stirred for 4 h at room temperature. The solvent was removed, and the solid residue dissolved in CH_2Cl_2 (30 mL) was washed twice with an aqueous solution of 0.1N NH_4PF_6 (2 x 30ml). The organic phase was filtered over cotton and concentrated *in vacuo*. Purification by silica gel column chromatography (CH_2Cl_2/MeOH, 100:0 →95:5) afforded **57** (1.1 g, 75%) as a white solid. ^{1}H-NMR (400 MHz, $CDCl_3$) δ 7.67-7.62 (m, 4H, CH_{Ar}), 7.48-7.38 (m, 6H, CH_{Ar}), 5.89 (s, 1H, NH), 4.25 (s, 1H, CHCO) 3.80 (dd, J = 3.3, 9.5 Hz, 1H, CH_2OSi), 3.57 (m, 3H, CH_2OSi, CH_α), 3.33 (d, J = 13.5 Hz, 1H, SCH_2), 3.26-3.09 (m, 5H, $CH_{2\gamma}$, CH_2S), 3.02 (d, J = 13.5 Hz, 1H, SCH_2), 2.55-2.44 (m, 1H, CH_2S), 2.16-1.82 (m, 4H, $CH_{2\beta}$), 1.43 (s, 9H, $NHCH_{3t\text{-}Bu}$), 1.08 (s, 9H, $CH_{3t\text{-}Bu}$). ^{13}C-NMR (100 MHz, $CDCl_3$) δ 178.5, 175.5 (CO), 151.1 (C_{guan}), 135.6, 135,5, 133.0, 132.9, 129.9, 127.8 (CH_{Ar}, C_{Ar}), 65.5 (CH_2OSi), 55.2 (CHN), 49.1, 48.4 (CH_α), 45.2, 44.8 ($CH_{2\gamma}$), 37.7, 36.0, 35.9 (CH_2S), 28.5 (CH_{3Boc}), 26.9 ($CH_{3t\text{-}Bu}$), 24.5, 23.0 ($CH_{2\beta}$), 19.2 ($C_{t\text{-}Bu}$). ESI-MS m/z 641.3 ($M\text{-}PF_6^-$)$^+$, 663.3 (M+Na)$^+$.

General procedure for compounds 49a-e to 56 and 58-67. Compound 54

PNA-Cysteine (1.7 mg, 0.35 μmol) and TBDPS-tetraguanidinium mesylate **18** (2.5 mg, 1.5 μmol, See Experimental Section Chapter 1) were dissolved in a mixture of buffer phosphate (pH 10, 0.1M), acetonitrile and water (1 mL, 1:1:0.5). This solution was sealed in an Eppendorf tube under N_2 atmosphere and heated at 60 ºC overnight. The mixture was purified by semipreparative HPLC and afterwards lyophilized to obtain **54** as a white powder.

Experimental Procedure for TEM imaging

A drop of a concentrated aqueous solution of compound **54** was deposited with a micropipette on top of a 200 mesh copper grid with a thin film of Formvar polymer. To improve the sharpness of the images, a 5% ammonium phosphomolybdate solution was added and mixed with the sample acting as a contrast agent. After evaporation of the sample at room temperature, a film was obtained. TEM experiments were performed using a JEOL 1011 transmission electron microscope operating at 80 KeV with an ultra-high-resolution pole piece providing a point resolution of 2 Å. Micrographs were acquired using a Megaview III multiscan-CCD camera.

Dynamic light scattering studies

Different aliquots from an aqueous concentrated solution of sample **54** were prepared in order to study the particle diameter and the size distribution by means of dynamic light scattering. The measurements were done using Zeta Sizer 3000H [He-Ne laser (633 nm), detector angle of 90º] equipment from Malvern Instruments, Inc., which measures the rate of fluctuation of the light scattered from the particles using photon correlation spectroscopy.

UNIVERSITAT ROVIRA I VIRGILI
BICYCLIC GUANIDINIUM OLIGOMERS FOR RECOGNITION, CELL DELIVERY, AND MOLECULAR MATERIALS
Julián Valero Moreno
DL:T. 276-2012

UNIVERSITAT ROVIRA I VIRGILI
BICYCLIC GUANIDINIUM OLIGOMERS FOR RECOGNITION, CELL DELIVERY, AND MOLECULAR MATERIALS
Julián Valero Moreno
DL:T. 276-2012

Chapter 3

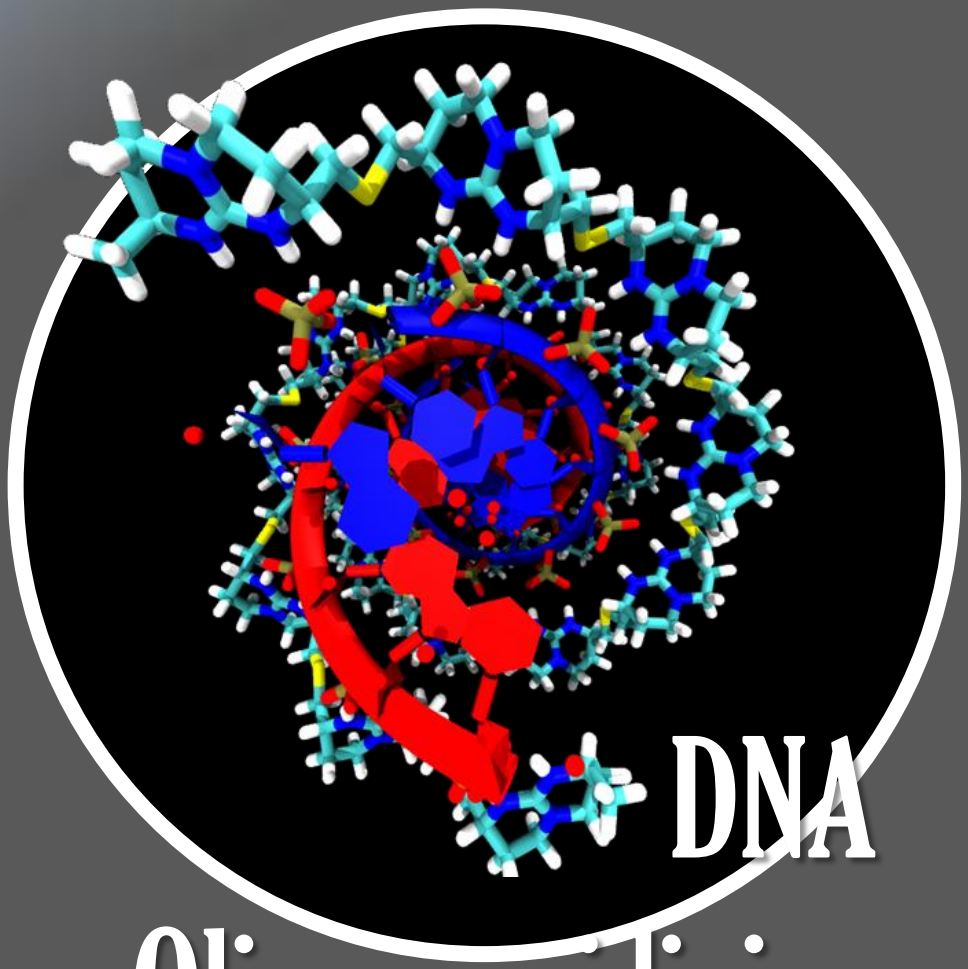

DNA Oligoguanidinium Interactions

UNIVERSITAT ROVIRA I VIRGILI
BICYCLIC GUANIDINIUM OLIGOMERS FOR RECOGNITION, CELL DELIVERY, AND MOLECULAR MATERIALS
Julián Valero Moreno
DL:T. 276-2012

Chapter 3

Design and Synthesis of Peptide-Oligoguanidinium Conjugates for Specific DNA Sequence Recognition and Binding Enhancement

3.1 Introduction and Objectives

Gene transcription and regulation is mainly controlled by several proteins called transcription factors which are responsible for tightly binding to specific sequences of DNA and promoting the subsequent initiation of transcription machinery.[1] This process is essential for the expression of proteins and, depending on the requirements of the organism, any anomaly in the mechanism can result in a cellular malfunction.[2] One of the major interests in the study of these transcription factors is the assessment of their specificity towards certain DNA sequences, which is key to discriminate between a vast number of genes.

[1] Orphanides, G.; Reinberg, D. *Cell* **2002**, *108*, 439-451.

[2] (a) Pandolfi, P. P. *Oncogene* **2001**, *20*, 3116-3127. (b) Darnell, J. E. *Nat. Rev. Cancer* **2002**, *2*, 740-749. (c) Hurley, L. H. *Nat. Rev. Cancer* **2002**, *2*, 188-200.

Some common structural elements in these transcription factors are essential for achieving efficient DNA-protein interactions.[3] Basically there are four types of interactions that drive protein-DNA assembly.[4] Firstly, the DNA phosphodiester backbone is prone to interact *via* salt bridges and hydrogen bonding with the basic amino acids (Lys, Arg and His). Usually, this assembly does not confer binding selectivity but increases the affinity of the association and anchors the protein complex to the DNA skeleton, favoring its optimal orientation for a proper recognition. Secondly, specific hydrogen bond contacts between several amino acid residues and DNA nucleobases are responsible for the specificity of the protein-DNA binding. Proteins preferentially interact with DNA through the major groove, allowing hydrogen bonding of amino acids such as Arg, Lys, Asp or Gln with the exposed functional groups of the nucleobases (Figure 1). Protein binding usually does not disturb base pairing, and thus functional groups involved in regular Watson-Crick interactions are not affected. Finally, to a lesser extent, hydrophobic interactions, van der Waals forces and secondary water-mediated hydrogen bonding also influence and contribute to the overall protein-DNA binding. However, these interactions are considered secondary, and owing to the inherent lack of directionality or geometrical constraints, they are usually not responsible for the sequence selectivity displayed by the transcription factors.

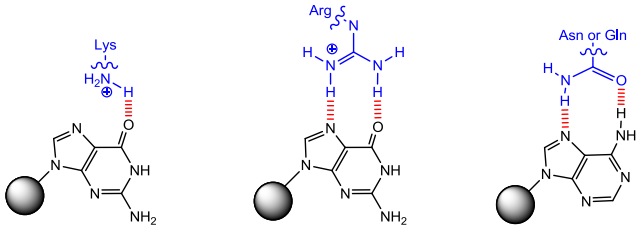

Figure 1. *Specific interactions between nucleobases and hydrogen bond donor residues in protein-DNA assemblies.*

[3] Choo, Y.; Klug, A. *Curr. Opin. Struct. Biol.* **1997**, *7*, 117-125.

[4] (a) Larson, C. L.; Verdine, G. L. *Bioorganic Chemistry: Nucleic acids* **1999**, Ed. S. M. Hetch, Oxford University Press, NY. (b) Luscombe, N. M.; Laskowski, R. A. *Nucleic Acids Res.* **2001**, *29*, 2860-2874.

There are several families of transcription factors classified by their structural domains.[5] As previously mentioned, DNA recognition essentially occurs *via* major groove insertion of specific recognition motifs. These motifs are analogous in all the transcription factors, but not their geometrical disposition and quaternary folding, which mainly depends on the so-called structural domains. These domains are not responsible to only hold the protein structure together, but also to afford the correct orientation of the recognition domains towards the DNA.[6]

Some of the most representative families of transcription factors are HTH (helix-turn-helix) and the homeodomain families, the zinc finger proteins (ZFP) or bZIP (basic region-leucine zipper) and bHLH (basic region-helix-loop-helix) families (Figure 2).

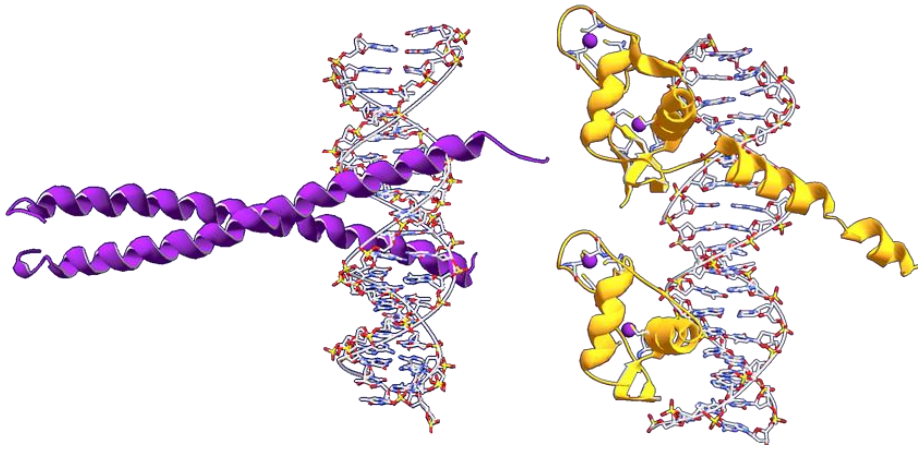

Figure 2. *Structures of the two most representative transcription factors bound to their respective DNA sequences. (Left) bZIP structure in purple (PDB entry: 1YSA).*[7] *(Right) Zinc finger protein in yellow (PDB entry: 2NLL).*[8]

[5] (a) Tan, S.; Richmond, T. J. *Curr. Opin. Struct. Biol.* **1998**, *8*, 41-48. (b) Latchman, D. S. *Transcriptional Factors: Structural Families and Principles of DNA Recognition*, **1998**, Academic Press, San Diego.

[6] Pabo, C. O. *Annu. Rev. Biochem.* **1992**, *61*, 1053-1095.

[7] Ellenberger, T. E.; Brandl, C. J.; Struhl, K.; Harrison, S. C. *Cell* **1992**, *71*, 1223-1237.

[8] Rastinejad, F.; Perlman, T.; Evans, R. M.; Sigler, P. B. *Nature* **1995**, *375*, 203-211.

Two of the most widespread transcription factors for eukaryotic gene regulation are the zinc finger and bZIP families. Zinc finger proteins[9,10] are based on regular peptide sequences containing His and Cys residues in certain positions to favor chelation with Zn. These residues, upon tetrahedral coordination with a Zn^{2+} ion, promote the correct structural folding to enable DNA-protein complex formation.[11] On the other hand, bZIP[12] family consists of α-helix dimeric structures containing two subdomains: the basic region, which is located in the *N*-terminus and is responsible for interaction with the DNA sequence; and the *C*-terminal leucine-rich area, which promotes helix dimerization through a parallel coiled-coil.[13] A special feature of these transcription factors is that the basic region of bZIP only adopts the helical secondary structure in the presence of the complementary DNA sequence.[14] Moreover, dimerization is required in order to afford a stable complex by cooperativity of both α-helices of the domain, and thus compensating the unfavourable entropic term derived from DNA-protein complexation. Indeed, it has been reported that monomers or minimized basic regions of bZIP proteins are unable to effectively recognize DNA consensus sequences.[15]

---

[9] Brown, S. R.; Sander, C.; Argos, P. *FEBS Lett.* **1985**, *186*, 271-274.

[10] For reviews see: (a) Berg, J. M. *Science* **1986**, 232, 485-487. (b) Kaptein, R. *Curr. Opin. Struct. Biol.* **1991**, *1*, 63-70. (c) Berg, J. M. *Curr. Opin. Struct. Biol.* **1993***, 3,* 11-16. (d) Hurst, H. C. *Protein Profile*, **1995**, *2*, 101-164. (e) Wolfe, S. A.; Nekludova, L. Pabo, C. O. *Annu. Rev. Biophys. Biomol. Struct.* **2000**, *29*, 183-212. (f) Laity, J. H.; Lee, B. M.; Wright, P. E. *Curr. Opin. Struct. Biol.* **2001**, *11*, 39-46.

[11] Elrod-Erikson, M.; Benson, T. E.; Pabo, C. O. *Structure* **1998**, *6*, 451-464.

[12] Landschulz, W. H.; Johnson, P. F.; McKnight, S. L. *Science* **1998**, *240*, 1759-1764.

[13] For reviews see: (a) Pathak, D.; Sigler, P. B. *Curr. Opin. Struct. Biol.* **1991**, *2*, 116-123. (b) Kerppola, T. K.; Curran, T. *Curr. Opin. Struct. Biol.* **1991***, 1,* 71-79. (c) Ellenberger, T. *Curr. Opin. Struct. Biol.* **1994**, 4, 12-21.

[14] (a) Weiss, M. A.; Ellenberger, T.; Wobbe, C. R.; Lee, P. J. ; Harrison, S. C.; Struhl, K. *Science* **1990**, *347*, 575-578. (b) O'Neil, K. T.; Shuman, J. D.; Ampe, C.; DeGrado, W. F. *Biochemistry* **1991**, *30*, 9030-9034. (c) Zhang, M.; Wu, B.; Zhao, H.; Taylor, J. W. *J. Peptide Sci.* **2002***, 8*, 125-136.

[15] (a) Turner, R.; Tjian, R. *Science* **1989**, *243*, 1689-1694. (b) Neuberg, M.; Adamkiewicz, J.

In recent years, the design and synthesis of miniaturized transcription factors have raised special interest.[16] These modified constructs are capable of interacting strongly with specific DNA sequences owing to the recognition properties of the original transcription factors. These chimera proteins would act as "synthetic transcription factors" able to promote or inhibit the transcription of genes, hence regulating the expression of certain proteins. Indeed, protein engineering of these artificial DNA binders have become a promising tool for gene targeting and gene therapy.

Most of the strategies reported on miniaturized transcription factors have been based on the recognition motif of the bZIP family. Early work by Kim *et al.*, described an artificial bZIP protein in which, upon removal of the leucine rich region, the basic recognition motifs were tied together through a disulfide bond in order to form the active dimeric species (Figure 3).[17] This artificial dimerization approach has been explored by other groups using covalent and non-covalent linkers such adamantane@cyclodextrin dyads[18] or Fe(II) terpyridine metal complexes.[19] Mascareñas *et al.* reported the first light triggered DNA-binding peptide.[20] By covalent attachment of two basic regions of GCN4 (a well-known transcription factor from bZIP family) to an azobenzene central moiety, they were able to control the conformation of the azo group by light irradiation, and therefore the affinity towards the target DNA sequence (Figure 3). Indeed, while the *cis* conformer binds at low nanomolar affinity, the corresponding *trans* isomer showed about 60-fold decrease.

Hunter, J. P.; Muller, R. *Nature* **1989**, *341*, 243-245.

[16] For reviews see: (a) Vázquez, M. E.; Caamaño, A. M.; Mascareñas, J. L. *Chem. Soc. Rev.* **2003**, *32*, 338-349. (b) Jantz, D.; Amann, B. T.; Gatto, G. J. Jr.; Berg, J. M. *Chem. Rev.* **2004,** *104,* 789-799. (c) Majmudar, C. Y.; Mapp, A. K. *Curr. Opin. Chem. Biol.* **2005**, *9*, 467-474.

[17] Talanian, R. V.; McKnight, C. J.; Kim, P. S. *Science* **1990**, *249*, 769-771.

[18] (a) Ueno, M.; Murakami, A.; Makino, K.; Morii, T. *J. Am. Chem. Soc.* **1993**, *115*, 12575-12576. (b) Ueno, M.; Sawada, M.; Makino, K.; Morii, T. *J. Am. Chem. Soc.* **1994**, *116*, 11137-11138.

[19] Cuenoud, B.; Schepartz, A. *Science* **1993**, *259*, 510-513.

[20] Caamaño, A. M.; Vázquez, M. E.; Martínez-Costas, J.; Castedo, L.; Mascareñas, J. L. *Angew. Chem. Int. Ed.*, **2000**, *39*, 3104-3107.

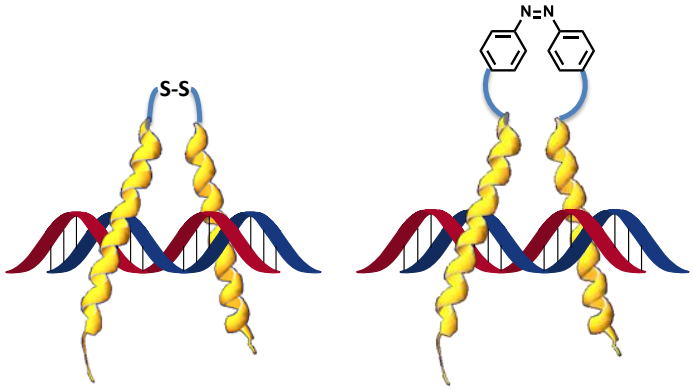

Figure 3. *Schematic representation of the artificial dimerization strategies explored by Kim et al.*[17] *(left) and Mascareñas et al.*[20] *(right).*

Another strategy used for the design of these DNA molecular binders consists of the combination of the monomeric binding motifs to small synthetic molecules which can interact with DNA. These molecules are based on DNA intercalating agents or minor groove binders and generally show low affinity and specificity to DNA, as compared with natural transcription factors and its derived constructs. However, their combination has been successful in acting cooperatively and enhancing the binding properties of these artificial DNA receptors. Woodbury *et al.* reported the attachment of an intercalating cyanide dye to different DNA-binding proteins which improved the affinity with selected DNA sequences up to 100 times, compared with the unmodified peptide.[21] This dye not only increased the interaction with DNA and showed interesting fluorescence properties for detection purposes but also can act as a photo-cleaving agent. This would open the possibility for the construction of synthetic nucleases able to recognize and cleave specific DNA sequences. Mascareñas *et al.* reported the synthesis of a hybrid conjugate based on a bZIP monomeric analogue linked to a minor-groove binder such as Distamycin.[22] This concave shape molecule is

[21] Thompson, M.; Woodbury, N. W. *Biophys. J.* **2001**, *81*, 1793-1804.

[22] Vázquez, M. E.; Caamaño, A. M.; Martínez-Costas, J.; Castedo, L.; Mascareñas, J. L. *Angew. Chem. Int. Ed.*, **2001**, *40*, 4723-4725.

known to effectively intercalate with the narrow minor groove of A/T-rich DNA sequences. Special attention was required to choose the appropriate linker between Distamycin and the peptide. This geometrical requirement is essential to afford the simultaneous binding of both moieties, thus docking selectively with the target oligonucleotide.

As previously described in Chapter 1, oligoguanidinium molecules are able to recognize polyanionic peptide sequences. By means of hydrogen bonding and electrostatic interactions, each bicyclic guanidine unit faces a carboxylate from the side chain of an aspartate or glutamate residue. However, some spatial requirements are essential to allow binding. For peptides, the optimal distance between the anionic amino acids for an optimal interaction with a tetraguanidinium framework is *i, i+3* or *i, i+4*.[23] This distance permits the correct orientation, and thus interaction of the guanidinium moieties with each acid residue.

To further extend this study to the recognition of other biologically relevant systems, we propose that oligoguanidinium molecules would also be able to efficiently interact with oligonucleotide strands. Indeed, preliminary molecular modeling studies[24] revealed that bicyclic guanidinium moieties tethered by thioether linkages can interact with DNA structures by means of hydrogen bonding and salt bridge contacts with its phosphodiester backbone (Figure 4). This assembly is unspecific since it takes place mostly *via* electrostatic contacts with the phosphodiester chain. However, this has become controversial since different studies reported the specific sequence recognition of DNA by several naturally occurring polyamines.[25] The distance between phosphate

[23] (a) Peczuh, M. W.; Hamilton, A. D.; Sánchez-Quesada, J.; de Mendoza, J.; Haack, T.; Giralt, E. *J. Am. Chem. Soc.* **1997**, *119,* 9327-9328. (b) Haack, T.; M. W.; Peczuh, M. W.; Salvatella, X.; Sánchez-Quesada, J.; de Mendoza, J.; Hamilton, A. D.; Giralt, E. *J. Am. Chem. Soc.* **1999**, *121,* 11813-11820. (c) Salvatella, X.; Martinell, M.; Gairí, M.; Mateu, M.; Feliz, M.; Hamilton, A. D.; de Mendoza, J.; Giralt, E. *Angew. Chem. Int. Ed.* **2004**, *43*, 196-198.

[24] Molecular modeling studies performed by Dr. Eva Santos (group of Prof. C. Bo).

[25] (a) Lindemose, S.; Nielsen, P. E.; Møllegaard, N. E. *Nucleic Acids Res.* **2005**, *33*, 1790-1803. (b) Patel, M. M.; Anchordoquy, T. J. *Biophys. Chem.* **2006**, *122*, 5-15. (c) Venkiteswaran, S.; Thomas,

groups is not regular along a DNA strand and their spatial disposition mainly depends on the sequence. Hence, even flexible molecules such polyamines which interact mainly through electrostatic contacts with DNA backbone, can discriminate between diverse DNA sequences due to these spatial constraints. Therefore, our bicyclic guanidinium oligomers may eventually show specific binding with DNA sequences.

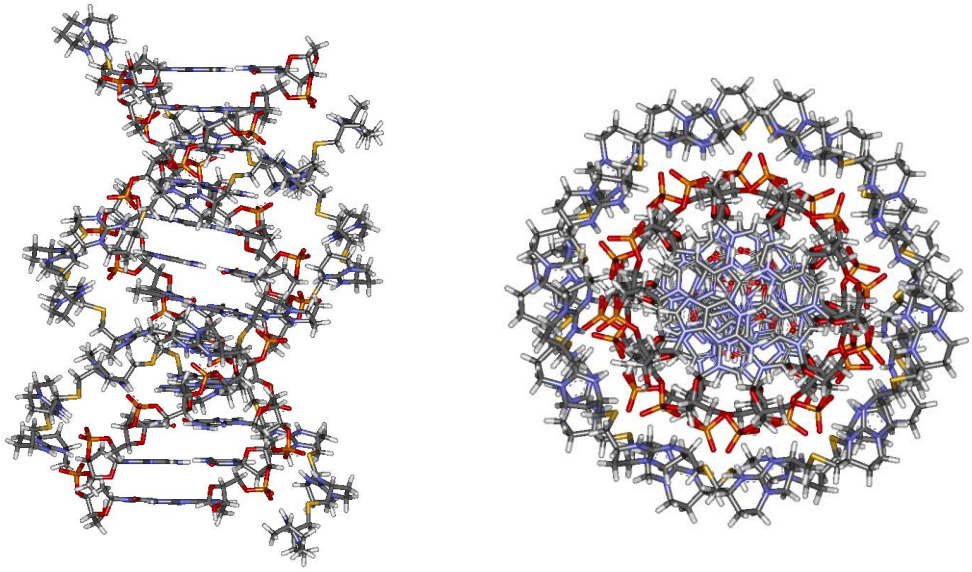

Figure 4. *Top and side view of the molecular model between two undecaguanidinium strands interacting together with a double stranded DNA.*[24]

Our initial approach will combine oligoguanidinium strands with peptide sequences, which bind certain DNA tracks, to enhance this interaction. These peptide sequences derived from natural transcription factors (TFs), bind to specific DNA sequences with high affinity to control the flow (or transcription) of genetic information from DNA to mRNA.

In particular, we will use the widespread basic region of the GNC4 protein, which

T.; Thomas, T. J. *Polyamine Cell Signaling: Physiology, Pharmacology, and Cancer Research* **2006**, Ed. Wang, J.-Y.; Casero, R. A.; Jr. Humana Press *Inc.*, Totowa, NJ.

belongs to the bZIP family. As previously mentioned, most of the isolated monomeric DNA-binding motifs are unable to associate with their complementary DNA sequences. Indeed, the GNC4 protein only adopts the active helical structure upon binding with its specific DNA sequence. By conjugation with different oligoguanidinium strands we will study the binding properties of these hybrid constructs, which should increase the affinity and selectivity towards target DNA sequences. Furthermore, owing to the membrane-permeable character of these bicyclic guanidinium oligomers, this approach could offer some advantages in future therapeutic applications.

3.2 Design and Molecular Modeling Studies

Kim *et al.* described the synthesis of different derivatives of GNC4 in order to identify the essential residues for specific DNA-binding by a disulfide dimerization strategy.[26] Based on this pioneering work, we selected a minimalist structure of the basic region of GNC4 protein to be covalently attached to our synthetic oligoguanidinium strand. Previous accounts from Mascareñas' group pointed out the importance of the linker between both molecules, which is crucial to fit the supramolecular ligand on the DNA structure. However, due to the high flexibility of the bicyclic guanidinium oligomers, we first decided to directly connect this molecule through a *C*-terminal cysteine present in the peptide motif. Likely, the oligoguanidinium strand would unspecifically interact with the phosphodiester backbone, thus considerably reducing any geometrical constraint or sequence requirements to maximize contacts with the DNA sequence.

Modeling studies were performed from the X-ray crystal structure of the leucine zipper GNC4 interacting with the AP-1 site (a DNA specific sequence) reported by Harrison *et al.* (PDB entry: 1YSA) as a reference.[7] We selected one of the monomers, in particular the peptide fragment responsible for the specific binding to the major groove. Subsequently, we replaced the Arg249 residue for a cysteine and attached a bicyclic guanidinium pentamer from the previous minimized structure with the Dickerson-Drew dodecamer. Rearrangement of the oligoguanidinium strand along the new DNA sequence and geometry optimization of the new linkage finally gave rise to the structure depicted in Figure 5.

[26] Talanian, R. V.; McKnight, C. J.; Rutkowski, R.; Kim, P. S. *Biochemistry* **1992**, *31*, 6871-6875.

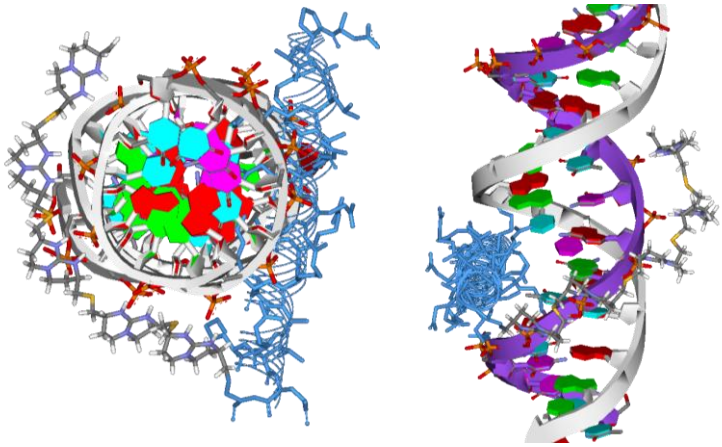

Figure 5. *(Left) Top view of the complex between the oligoguanidinium-peptide conjugate and the DNA structure. (Right) Side view evidencing the major groove binding of the peptidic sequence. DNA (in ribbon), GNC4-based peptide (in blue) and pentaguanidinium oligomer (stick representation in CPK colors).*

Each guanidinium moiety nicely fits in front of a phosphodiester unit from the DNA sequence, forming a ladder-shape structure. The first guanidinium linked to the peptide is partially distorted with respect to the others due to the geometrical constraints imposed by the peptide. However, the bicyclic guanidine establishes salt bridges and hydrogen bond contacts with the closest non-bound phosphate in the sequence. This seems to be the most feasible binding mode, as the next phosphate is not at a suitable distance to interact properly with this first guanidinium molecule. As shown in Figure 5, this leads to the formation of a pincer like structure where the specific recognition is driven by the peptide binding, which is interacting with AP-1 site (ATGACTCAT), with the oligoguanidinium strand bound to the DNA skeleton through unspecific ionic contacts. Hence, it is expected that the oligoguanidium-peptide hybrids enhance the binding to the corresponding DNA sequences by the cooperative contribution of both molecules.

The synthesis and the determination of the binding properties of these constructs have been performed by Jesús Mosquera under the supervision of Prof. Mascareñas (University of Santiago).

3.3 Synthesis of Oligoguanidinium-Peptide Conjugates

The synthesis of the oligoguanidinium-peptide conjugates was achieved following a similar strategy as previously described for oligoguanidinium-PNA conjugates. Therefore, the *C*-terminal cysteine from the peptide sequence was used to covalently attach the corresponding mesyl derivative of the oligoguanidinium. Milder conditions compared to those reported in Chapter 2 were employed to avoid racemization of the α-peptide. Thus, the reaction was performed in a (1:1) acetonitrile:phosphate buffer solution (0.1 N, pH 10) at 40 ºC overnight. Three different conjugates were synthesized: pentaguanidinium **69** and tetraguanidinium analogues **68** and **70** (Scheme 1) starting from the previously described tetra- and pentaguanidinium precursors (**18** and **48**). With these compounds it would be possible to determine the influence of the guanidinium oligomer length and the spacer between the peptide and the polycationic strands on the binding.

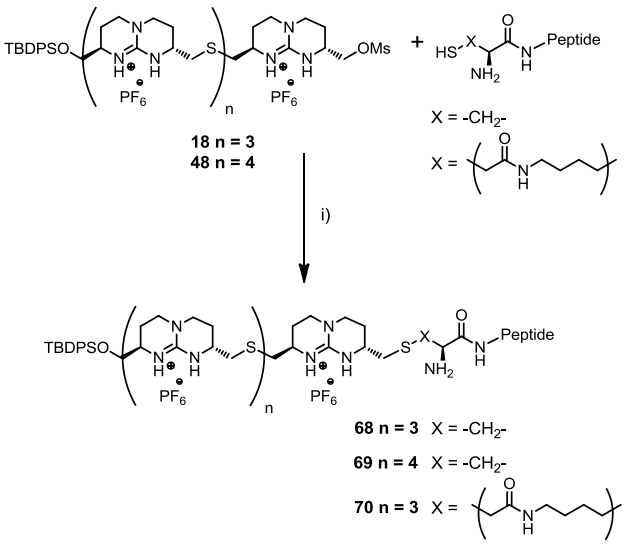

Scheme 1. *Synthesis of oligoguanidinium-peptide conjugates. Conditions: i) ACN/phosphate buffer (pH 10) mixture at 40ºC. Peptide sequence: DPAALKRARNTEAARRSRARKLQ-C(or K). The N-terminus was modified as p-acetamidobenzoate to facilitate quantification by UV spectroscopy.*

For the conjugates directly attached to the terminal cysteine, conversion was completed after 14 h. With the lysine derivative (**70**), bearing an extended linker, longer reaction times were required (up to 3 days) and lower conversions (20%) were obtained.

3.4 Preliminary Binding Assays and Specific Sequence Affinity

Circular dichroism (CD) was employed to study the binding of oligoguanidinium-GNC4 conjugates with DNA sequences. The monomeric basic regions derived from the GNC4 protein are unable to bind to their complementary DNA sequence. In solution the peptide shows a random structure in the absence of the target DNA, only forming the active α-helical conformation upon specific DNA binding. Consequently, binding to DNA can be monitored by measuring the α-helical content in solution. This can be achieved by monitoring the variation of the negative band intensity at 222 nm in the CD spectrum. The experiments were performed with the tetraguanidinium-GNC4 conjugate **68** in the presence of two different DNA sequences (ADN04 and ADN139). ADN139 contains the binding site for the GCN4 peptide, whilst ADN04 is a random sequence employed as a control to evaluate the sequence specificity of the hybrid. As shown in Figure 6, the presence of the DNA target sequence (ADN139) induced an increase in the helicity of compound **68** (red line), whereas the non-complementary DNA sequence did not produce any effect, as expected (green line).

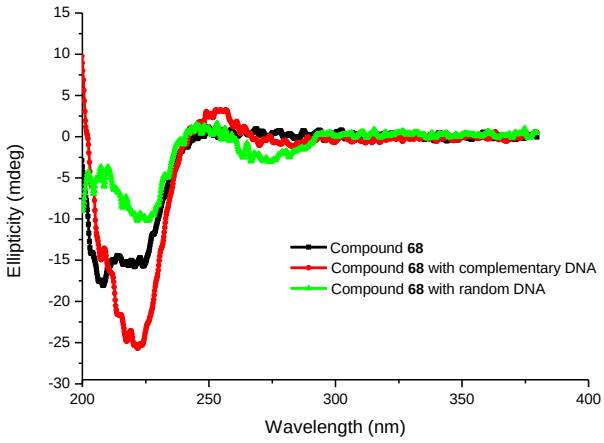

Figure 6. *Circular dichroism spectra of compound* ***68*** *in absence (black line) and in the presence of a complementary (red line) and a random (green line) DNA sequence.*

To further assess the association ability of these artificial constructs towards different DNA sequences, fluorescence electrophoretic mobility shift assays (EMSA) were performed. This is a common technique used for the affinity determination of DNA or RNA with proteins and other complexes. The oligonucleotides are shifted under the influence of an electric field in agarose or acrilamide gels and its mobility depends on the size and the charge of the overall complex. Protein complexation should slow down the mobility of these molecules due to steric hindrance. Moreover, protein-DNA binders usually interact through electrostatic contacts, compensating the negative charge of the oligonucleotides and thus affecting its mobility in the assays. Thus, the affinity of oligoguandinium-GNC4 compounds (**68**-**70**) towards the two different oligonucleotide sequences previously tested in the CD assays (ADN04 and ADN139) was evaluated. As shown in Figure 7, tetraguanidinium compound **68** displays moderate affinity towards ADN139, and no binding with control ADN04, even at micromolar concentrations. A similar effect was also observed with pentaguanidinium **69**. Indeed, this new conjugate exhibited higher affinity to the target DNA sequence than tetraguanidinium **68**.

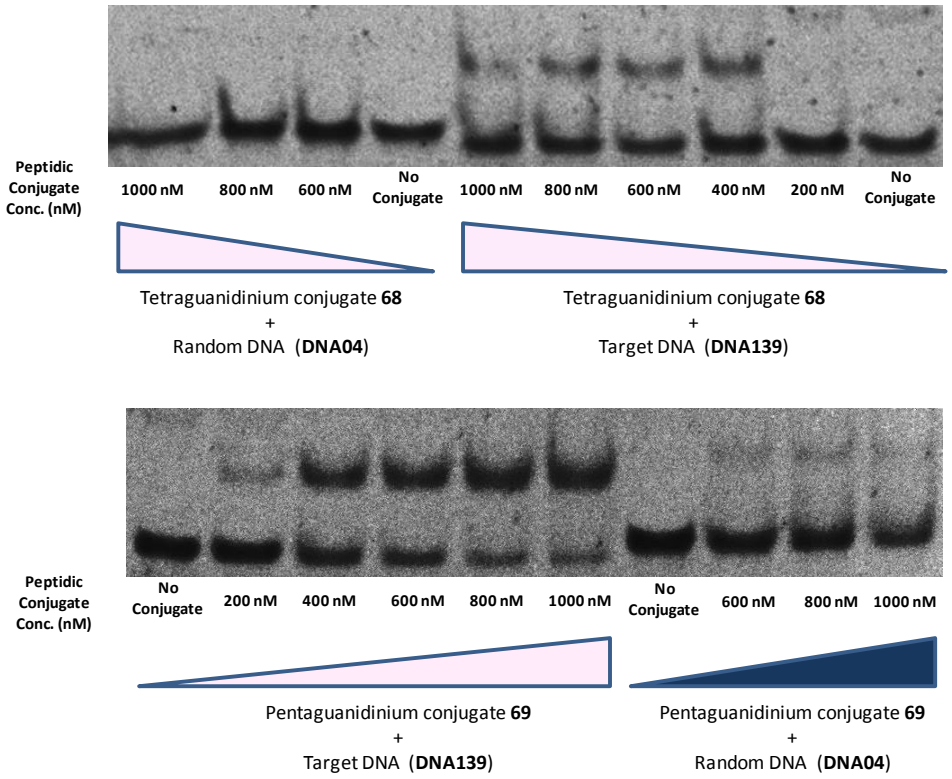

Figure 7. *Fluorescence EMSA analysis of oligoguanidinium conjugates* ***68*** *and* ***69*** *at different concentrations (0.2 to 1 μM) in the presence of target ADN139 and random sequence ADN04 (at constant 50 nM concentration).*

Introduction of a longer linker between the peptide and the guanidinium oligomer (compound **70**) resulted in the loss of binding affinity with respect to the analogous tetraguanidinium compound **68**, as depicted in Figure 8.

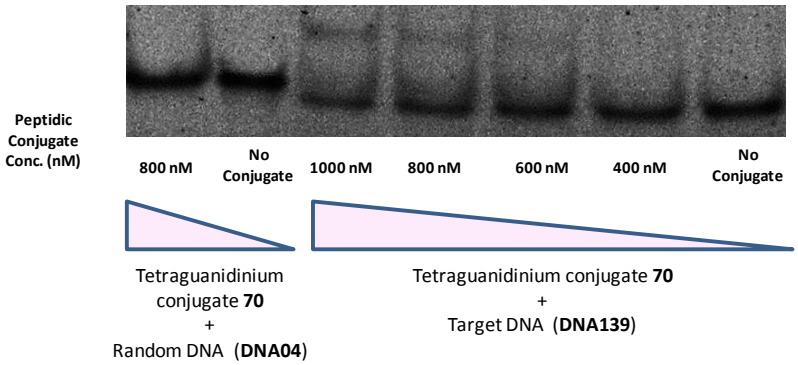

Figure 8. *Fluorescence EMSA assay of compound* ***70*** *in the presence of both the target and the control sequences.*

This suggests that although longer linkers favor the enthalpic term of the association, the entropic penalty paid for such flexible and highly adaptable systems contributes negatively to the overall binding and finally results in formation of a thermodynamically less stable complex.

The specificity shown by these conjugates confirmed the predicted mode of binding with the selected DNA sequences in which the peptide is bound to the major groove through sequence specific interactions, and in which the oligoguanidium moiety should be mainly bound to the phosphodiester backbone. In addition, as predicted by molecular modeling, direct thioether linkage of the peptide fragment to the polycationic oligoguanidine afforded the correct spatial disposition of the ligand to efficiently assemble with DNA.

3.5 Preliminary Thermal Stability Study of Bicyclic Guanidinium Oligomer-DNA Complexation

To further assess the association mode and consequences of the interaction between oligoguanidinium molecules and DNA, thermal stability UV studies were performed. This work was done under the supervision of Prof. Peter E. Nielsen.

As previously discussed, naturally occurring polyamines are able to interact with the phosphodiester chains of DNA and RNA *via* electrostatic interactions, although it has also been reported that polyamines can bind within the minor and the major grooves. In fact, specific DNA binding in the major groove of G/C rich sequences,[27] TATA elements and bent adenine tracks have been described.[25,28] Despite the molecular mechanisms of action are not well understood, implications in functions ranging from gene expression to cell growth regulation have been reported.[29] Interestingly, these molecules are able to bind and stabilize double stranded DNA forms, favoring duplex formation even under non-optimal conditions. Owing to the similarities between oligoguanidinium molecules and cationic polyamines, as both are positively charged and flexible, we decided to study DNA duplex stabilization upon oligoguanidinium complexation. Melting temperatures (Tm) were therefore measured (by UV) for the different oligonucleotides, in the presence of spermine and tetraguanidinium compound **13** (Figure 9). These cationic molecules provide the ionic strength necessary to shield and stabilize the anionic phosphodiester DNA skeleton, thus favoring base pairing and double helix formation. Kan *et al.* reported the effect of several cationic

[27] (a) Feuerstein, B. G.; Pattabiraman, N.; Marton, L. J. *Nucleic Acids Res.* **1990**, *18*, 1271-1282. (b) Haworth, I. S.; Rodger, A.; Richards, W. G. *Proc. R. Soc. Lond. B Biol. Sci.* **1991**, *244*, 107-116.
[28] Zakrzewska, K.; Pullman, B. *Biopolymers* **1986**, *25*, 375-392.
[29] (a) Cohen, S. S. *A Guide to the Polyamines* **1998**, Oxford University Press, NY. (b) Igarashi, K.; Kashiwagi, K. *Biochem. Biophys. Res. Commun.* **2000**, *271*, 559-564.

molecules, especially polyamines, on duplex formation.[30] Indeed, at pH 7.3, the effectiveness of helix stabilization by different cations followed the order of: spermine > spermidine > Mg^{+2} > Na^{+} > Tris buffer alone, suggesting that polyamines, and particularly spermine, allow stabilization of abnormal DNA structures such as loops, hairpins and mismatch sequences.

Initially, we decided to evaluate the thermal stabilities of short oligonucleotides rich in A/T bases at different concentrations of spermine and tetraguanidinium compound **13** (See experimental details in Chapter 1). As a control, Tm curves were also recorded in a buffer solution with a high ionic strength (100 mM NaCl and 20 mM $MgCl_2$). Despite the obvious structural differences between both molecules, we selected spermine as control since it is one of the most effective polyamines for double helix DNA stabilization and because both compounds have the same number of positive charges.

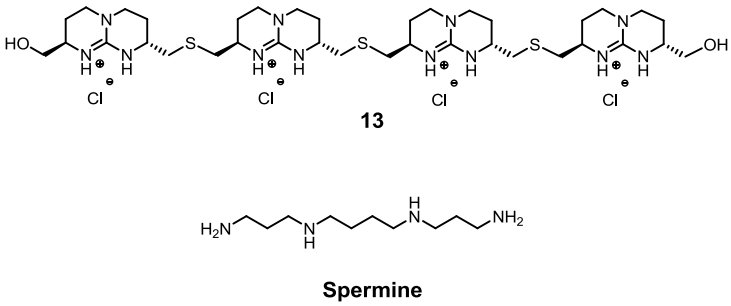

Figure 9. *Chemical structures of compound* ***13*** *and spermine.*

As depicted in Figure 10, the three oligonucleotides selected showed low melting temperatures (*ca.* 10-15 ºC) in Tris buffer (20 mM, pH 7.3), as a consequence of their short lengths, combined with their high A/T base content, which is related with less stable DNA duplex structures. As expected, addition of NaCl and $MgCl_2$ salts at high

[30] Hou, M.-H.; Lin, S.-B.; Yuann, J.-M. P.; Lin, W.-C.; Wang, A. H.-J.; Kan, L.-S. *Nucleic Acids Res.* **2001**, *29*, 5121-5128.

concentrations provoked a considerable increase in Tm due to the inherent rise in ionic strength. This effect was improved in the presence of spermine (above 0.1 mM), and the enhancement became even more evident with compound **13**.

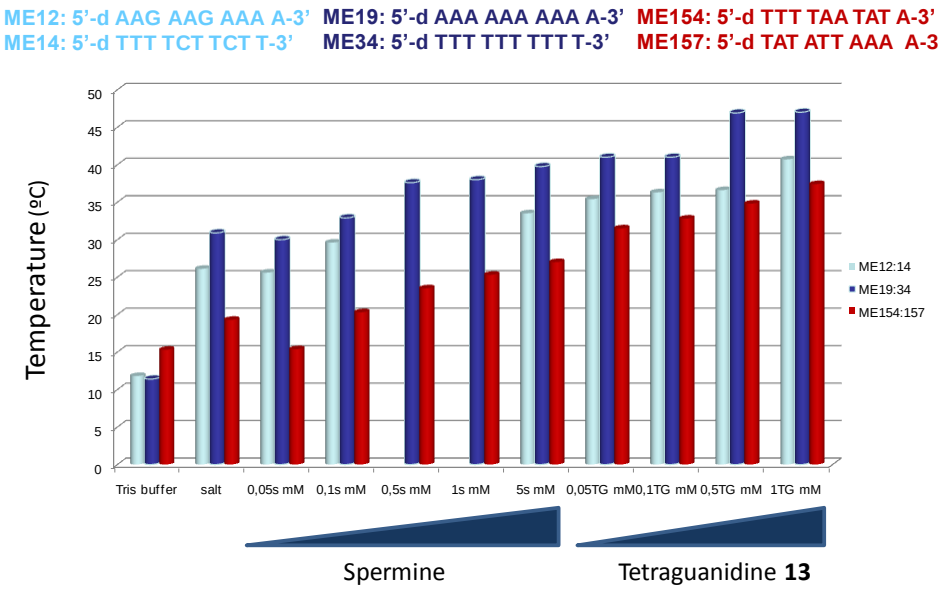

Figure 10. *Melting temperatures Tm (ºC) of A/T rich oligonucleotide sequences in the presence of different concentrations of spermine and tetraguanidine* ***13****. Oligonucleotide concentration 0.6 O. D. units (ca. 10-5 μM depending on the oligonucleotide).*

This result implies that at low concentrations (0.5-1.0 mM), tetraguanidinium **13** is able to stabilize the double stranded form of DNA oligonucleotides even at physiological temperature (*ca.* 37 ºC).

We also evaluated the stabilization effect in a mismatch oligonucleotide sequence (Figure 11). The mismatch oligonucleotide has a Tm value below 5 ºC (our lower experimental limit) and thus behaves as a single strand in solution. Addition of 50 μM of the tetraguanidinium compound **13** provoked an effect comparable with the stabilization produced by a highly concentrated solution of Na^{+} and Mg^{+2} salts. Interestingly, a noticeable increase in thermal stability (*ca.* 25%) was also reached upon

raising the concentration of **13** to 0.5 mM with respect to an experiment in the absence of this compound.

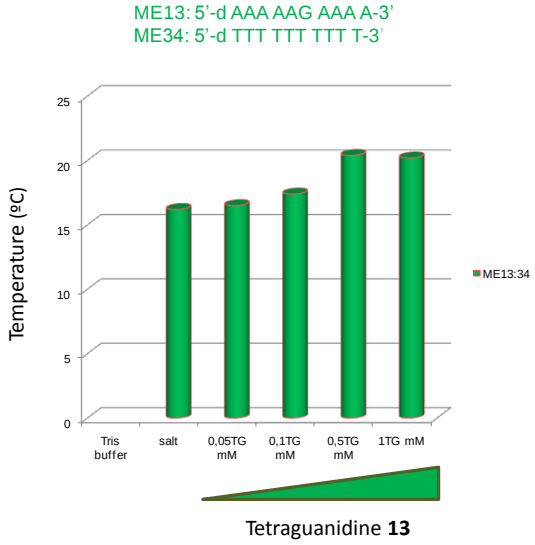

Figure 11. *Melting temperatures of a mismatch oligonucleotide sequence at different concentrations of* ***13****.*

High concentrations of spermine (5 mM) did not produce a significant increase in Tm for the mismatch oligonucleotide compared with the melting temperature found in highly ionic strength medium.

Finally, we tested the thermal stability of G/C rich oligonucleotide sequences upon addition of compound **13**. Unfortunately, precipitation occurred even at low concentrations of the tetraguanidine and consequently it was not possible to accurately assess Tm values in this case. Considering a mode of binding similar to that suggested by molecular modeling (see section 3.1), DNA-oligoguanidinium complexation should cause a change in the solubility character of the overall complex. Bicyclic guanidinium moieties interact with the phosphodiester skeleton of the double stranded DNA, thus decreasing its hydrophilicity and eventually leading to the collapse of the complex in aqueous solution. This could imply different binding modes for sequences depending

on the GC/AT base pair content, suggesting a preferential sequence binding behavior. Nonetheless, more experiments would be required to corroborate this hypothesis.

3.6 Experimental Section

Compounds **18** and **48** were synthesized as previously described in Chapters 1 and 2 (Experimental Section), respectively. Conjugation with the corresponding GNC4 peptide giving rise to the corresponding compounds **68**-**70** was performed by Jesús Mosquera (group of Prof. Mascareñas) in University of Santiago de Compostela.

Tm measurements were performed on a Cary 300 Bio UV-visible spectrophotometer (Varian, Cary, NC, USA) connected to a temperature controller.

Thermal denaturation (Tm)

800 μL of aqueous Tris-buffered solutions of oligonucleotide at 0.6 O.D. concentration were placed in 1 ml cuvettes (1 cm path length). Subsequently, a temperature ramp program (using heating-cooling cycles) was performed, first from 90 to 5 ºC (to ensure no hybridization artifacts at the earlier steps), and then from 5 to 90º (which gives the final Tm value, $\Delta T = 0.5$ºC), acquiring at 260 nm wavelength. The melting temperature (Tm) was determined from the maximum of the first derivative of the heating curve.

All the solutions measured contained a fixed oligonucleotide concentration of 0.6 O.D. which corresponds with a 10-5 μM concentration depending on the extinction coefficient (ε_{260}) of the oligomer. The solutions were prepared from 10-60 O.D. concentrated solutions of each single stranded oligonucleotide. Spermine and tetraguanidinium compound **13** were added from CH_3CN/H_2O (1:1) stock solutions.

UNIVERSITAT ROVIRA I VIRGILI
BICYCLIC GUANIDINIUM OLIGOMERS FOR RECOGNITION, CELL DELIVERY, AND MOLECULAR MATERIALS
Julián Valero Moreno
DL:T. 276-2012

UNIVERSITAT ROVIRA I VIRGILI
BICYCLIC GUANIDINIUM OLIGOMERS FOR RECOGNITION, CELL DELIVERY, AND MOLECULAR MATERIALS
Julián Valero Moreno
DL:T. 276-2012

Chapter 4

Supramolecular Containers

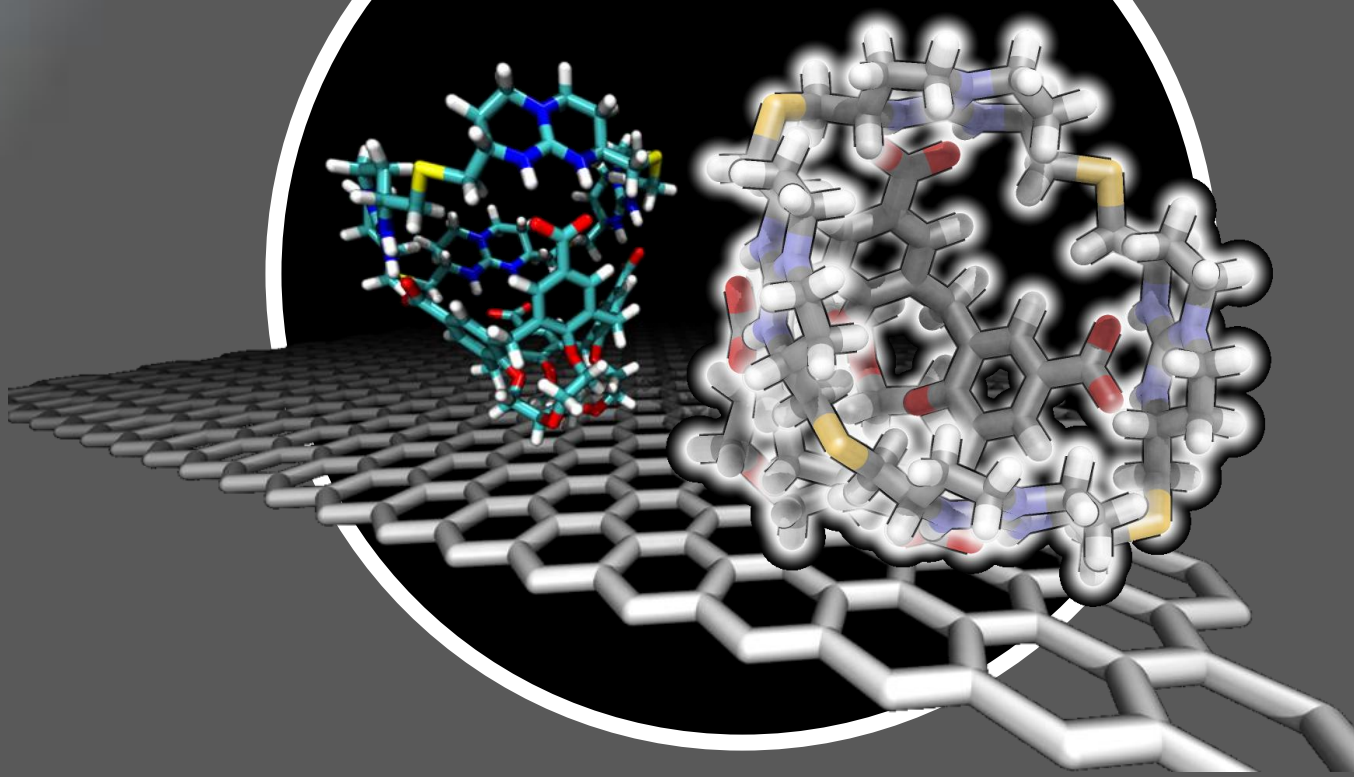

UNIVERSITAT ROVIRA I VIRGILI
BICYCLIC GUANIDINIUM OLIGOMERS FOR RECOGNITION, CELL DELIVERY, AND MOLECULAR MATERIALS
Julián Valero Moreno
DL:T. 276-2012

Chapter 4

A Tetraguanidinium Macrocycle for the Recognition and Cavity Expansion of Calix[4]arene Tetraoxoanions

4.1 Introduction and Objectives

Nature uses clefts, well-defined pockets and solvent-hindered structures to allow direct and efficient molecular recognition. By means of size and shape discrimination, in addition to other essential interactions, biological systems are able to selectively bind target molecules. This enables their transport, delivery to a different organelle, or diverse synthetic transformations. This is mainly possible due to the existence of robust architectures capable of reversibly accommodating guest molecules inside, such as in the case of enzymatic active sites, allosteric pockets or transmembrane pore channel proteins. Increasing one step further in complexity, nature utilizes a variety of tools, from virus capsids and cellular membrane systems to tissue compartmentalization, to ensure segregation of different biological events, thus providing diverse chemical environments (Figure 1).

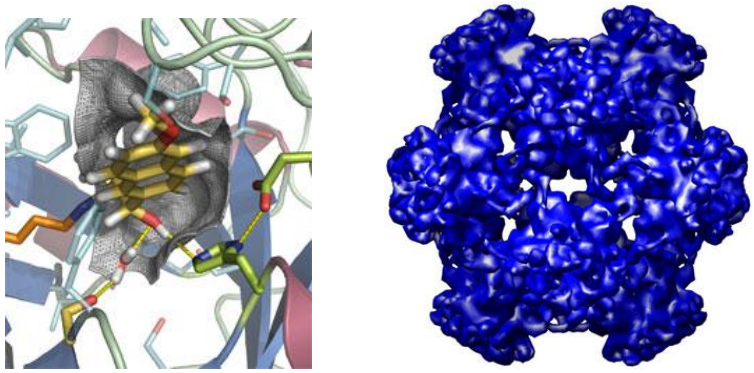

Figure 1. *(Left) Retro-aldolase enzymatic pocket. (Right) Papillomavirus capsid.*

Inspired by these complex systems, synthetic molecular containers are based on the same fundamental principles that govern host-guest recognition at biological level. Different pre-organized concave scaffolds such as resorcinarenes, calixarenes or cyclotriveratrylenes have been used as supramolecular baskets and capsules for binding, isolation and sensing of small molecules and ions,[1] catalysis,[2] or trapping of unstable intermediates.[3]

Two main strategies have been explored for the construction of molecular containers. Early work by Cram,[4] Sherman,[5] Collet,[6] and others, described the

---

[1] (a) Rebek, J. Jr. *Chem. Commun.* **2000**, 637-643. (b) Biros, S. M.; Rebek, J. Jr. *Chem. Soc. Rev.* **2007**, *36*, 93-104. (c) Schmuck, C. *Angew. Chem. Int. Ed.* **2007**, *46*, 5830-5833. (d) Ballester, P. *Chem. Soc. Rev.* **2010**, *39*, 3810-3830.

[2] Vriezema, D. M.; Comellas Aragonès, M.; Elemans, J. A. A. W.; Cornelissen, J. J. L. M.; Rowan, A. E.; Nolte, R. J. M. *Chem. Rev.* **2005**, *105*, 1445-1489. (b) Lützen, A. *Angew. Chem. Int. Ed.* **2005**, *44*, 1000-1002. (c) Koblenz, T. S.; Wassenaar, J.; Reek, J. N. H. *Chem. Soc. Rev.* **2008**, *37*, 247-262. (d) Lützen, A. *ChemCatChem* **2010**, *2*, 1212-1214.

[3] Mal, P.; Breiner, B.; Rissanen, K.; Nitschke, J. R. *Science* **2009**, *324*, 1697-1699.

[4] (a) Cram, D. J. *Science* **1983**, *219,* 1177-1183. (b) Sherman, J. C.; Cram, D. J. *J. Am. Chem. Soc.* **1989**, *111,* 4527-4528. (c) Sherman, J. C.; Knobler, C. B.; Cram, D. J. *J. Am. Chem. Soc.* **1991**, *113,* 2194-2204.

formation of covalently linked capsules able to accommodate guest molecules inside (Figure 2). Carceplexes and carcerands (with and without the guest inside, respectively) do not allow the reversible binding of the target molecule which is permanently imprisoned inside the cavity unless some covalent bonds are broken. On the other hand, although covalently bonded, hemicarcerands and hemicarceplexes contain "windows" large enough to allow the entrance and exit of small molecules in their cavities upon heating.

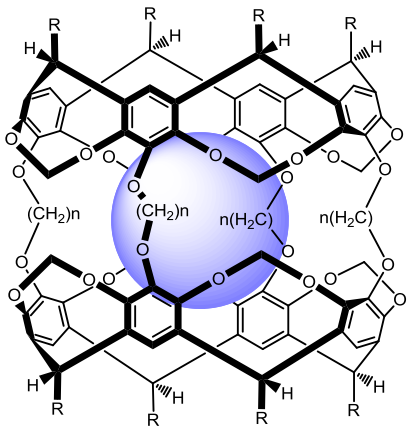

Figure 2. *Cram's carceplexes (n = 1) and hemicarceplexes (n = 4).*

A second approach towards molecular cages is based on the self-assembly of different building blocks by means of non-covalent interactions. This strategy is similar to the processes encountered in nature, as it provides more flexibility, binding reversibility and a wide variety of stimuli to trigger host-guest complexation. A number

---

[5] (a) Chapman, R. G.; Chopra, N.; Cochien, E. D.; Sherman, J. C. *J. Am. Chem. Soc.* **1994**, *116,* 369-370. (b) Chapman, R. G.; Sherman, J. C. *J. Org. Chem.* **1998**, *63,* 4103-4110.

[6] (a) Canceill, J.; Lacombe, L.; Collet, A. *J. Am. Chem. Soc.* **1985**, *107,* 6993-6996. (b) Collet, A. *Tetrahedron* **1987**, *43*, 5725-5759. (c) Collet, A.; Dutasta, J.-P.; Lozach, B.; Canceill, J. *Top. Curr. Chem.* **1993**, *165*, 103-129.

of examples can be found in the literature depending on the driving force of the assembly.

Rebek and de Mendoza reported the first example of the so-called "tennis ball" structure based on the hydrogen bonding self-assembly of two glycoluril-derived moieties (Figure 3). This association not only affords a robust architecture capable of binding different guests,[7] but also a system that can function as a molecular reactor. As an example, the Diels-Alder reaction in this confined space inside a larger glycoluril-based capsule was reported.[8]

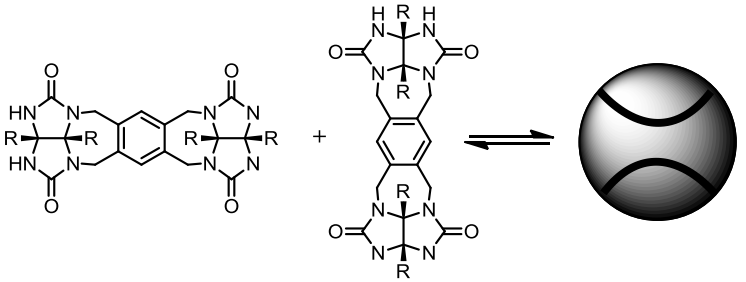

Figure 3. *Self-assembly of two glycoluryl moieties into the "tennis ball" structure.*

Hydrogen-bonded dimeric capsules based on cavitands such as calixarenes and resorcinarenes have been extensively described by Rebek, Böhmer, de Mendoza and Shinkai.[9] In the solid state, larger hexameric cages have been reported by Atwood *et al.* (Figure 4) taking advantage of the hydrogen bonding properties of resorcinarenes and

---

[7] (a) Wyler, R.; de Mendoza, J.; Rebek, J. Jr. *Angew. Chem. Int. Ed. Engl.* **1993**, *32*, 1699-1701. (b) Meissner, R. S.; Rebek, J. Jr.; de Mendoza, J. *Science* **1995**, *270*, 1485-1488.

[8] (a) Kang, J.; Rebek, J. Jr. *Nature* **1997**, *385*, 50-52. (b) Kang, J.; Hilmersson, G.; Santamaria, J.; Rebek, J. Jr. *J. Am. Chem. Soc.* **1998**, *120*, 3650-3656.

[9] (a) Koh, K.; Araki, K.; Shinkai, S. *Tetrahedron Lett.* **1994**, *35*, 8255-8258. (b) Conn, M. M.; Rebek, J. Jr., *Chem. Rev.* **1997**, *97*, 1647-1668. (c) Ebbing, M. H. K.; Villa, M.-J.; Valpuesta, J.-M.; Prados, P.; de Mendoza, J. *Proc. Natl. Acad. Sci. USA* **2002**, *99*, 4962-4966. (d) Rudzevich, Y.; Rudzevich, V.; Böhmer, V. *Supramol. Chem.* **2010**, *22*, 717-725.

pyrogallol[4]arenes.[10] These large spherical complexes are able to encapsulate solvent molecules and a range of different ions such as tetraalkylammonium salts.[11]

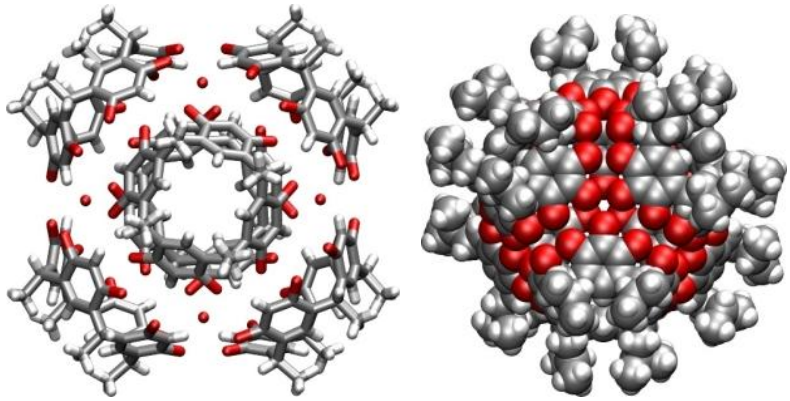

Figure 4. *X-ray structures of two different hexameric capsules in stick and space filling representation, respectively, described by Atwood et al.*[10]

To ensure assembly in aqueous solvents, Reinhoudt *et al.* described the design of water-soluble calix[4]arene capsules formed by means of electrostatic interactions between positively charged amidinium groups and negatively charged carboxylate or sulfonate groups (Figure 5).[12] This type of interaction is widely present in biological systems and displays a robust bonding even in competitive polar solvents.[13] Hence, the reported oppositely charged cavitands self-assemble with association constants ranging from 10^5 to 10^6 M^{-1} to afford stable closed-shell molecular containers. These systems

---

[10] Atwood, J. L.; Barbour, L. J.; Jerga, A. *Proc. Natl. Acad. Sci. USA* **2002**, *99*, 4837-4841.

[11] Avram, L.; Cohen, Y.; Rebek, J. Jr. *Chem. Commun.* **2011**, *47*, 5368-5375.

[12] (a) Corbellini, F.; Di Costanzo, L.; Crego-Calama, M.; Geremia, S.; Reinhoudt, D. N. *J. Am. Chem. Soc.* **2003**, *125*, 9946-9947. (b) Corbellini, F.; Knegtel, R. M. A.; Grootenhuis, P. D.; Crego-Calama, M.; Reinhoudt, D. N. *Chem. Eur. J.* **2005**, *11*, 298-307. (c) Corbellini, F.; van Leeuwen, F. W. B.; Beijleveld, H.; Kooijman, H.; Spek, A. L.; Verboom, W.; Crego-Calama, M.; Reinhoudt, D. N. *New J. Chem.* **2005**, *29*, 243-248.

[13] Goshe, A. J.; Steele, I. M; Ceccarelli, C.; Rheingold, A. L.; Bosnich, B. *Proc. Natl. Acad. Sci. USA* **2002**, *99*, 4823-4829.

showed efficient guest inclusion of small molecules such as acetylcholine, tetramethylammonium salts, and *N*-methylquinuclidinium cations.[14]

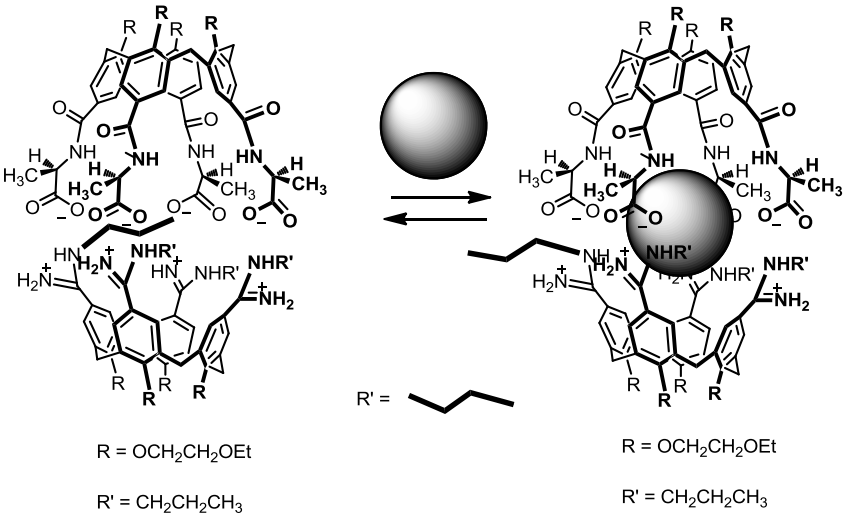

Figure 5. *Water-soluble molecular capsules described by Reinhoudt.*

By means of metal coordination, a range of cavitands have been employed to self-assemble and form dimeric cages with diverse affinity properties in their inner void.[15] Special attention should be paid to the work described by Stang and Fujita on metallocages,[16] which illustrate the construction of macromolecular and robust

[14] Corbellini, F.; Fiammengo, R.; Timmerman, P.; Crego-Calama, M.; Versluis, K.; Heck, A. J. R.; Luyten, I.; Reinhoudt, D. N. *J. Am. Chem. Soc.* **2002**, *124*, 6569-6575.

[15] (a) Fox, O. D.; Dalley, N. K.; Harrison, R. G. *J. Am. Chem. Soc.* **1998**, *120*, 7111-7114. (b) Ikeda, A.; Yoshimura, M.; Udzu, H.; Fukuhara, C.; Shinkai, S. *J. Am. Chem. Soc.* **1999**, *121*, 4296-4297. (c) Zhong, Z.; Ikeda, A.; Ayabe, M.; Shinkai, S.; Sakamoto, S.;Yamaguchi, K. *J. Org. Chem.* **2001**, *66,* 1002-1008. (d) Fochi, F.; Jacopozzi, P.; Wegelius, E.; Rissanen, K.; Cozzini, P.; Marastoni, E.; Fisicaro, E.; Manini, P.; Fokkens, R.; Dalcanale E. *J. Am. Chem. Soc.* **2001**, *123*, 7539-7552.

[16] (a) Fujita, M.; Umemoto, K.; Yoshizawa, M.; Fujita, N.; Kusukawa, T.; Biradha, K. *Chem. Commun.* **2001**, 509-518. (b) Seidel, S. R.; Stang, P. J. *Acc. Chem. Res.* **2002**, *35*, 972-983. (c)

complex host 3D architectures from well-established simple 2D ligands and metals with different geometries. Small modifications in the ligand (e.g. size, flexibility, shape) or the nature of the metal resulted in formation of a wide variety of nanoscale molecular cavities. Moreover, Fujita *et al.* reported the crystal structure of some of these metallocages and explored their behavior in the solid state. These new and stable "crystalline molecular flasks" (Figure 6) showed inherent crystal porosity and were able to incorporate guest molecules with reactivities dissimilar from those observed in solution.[17]

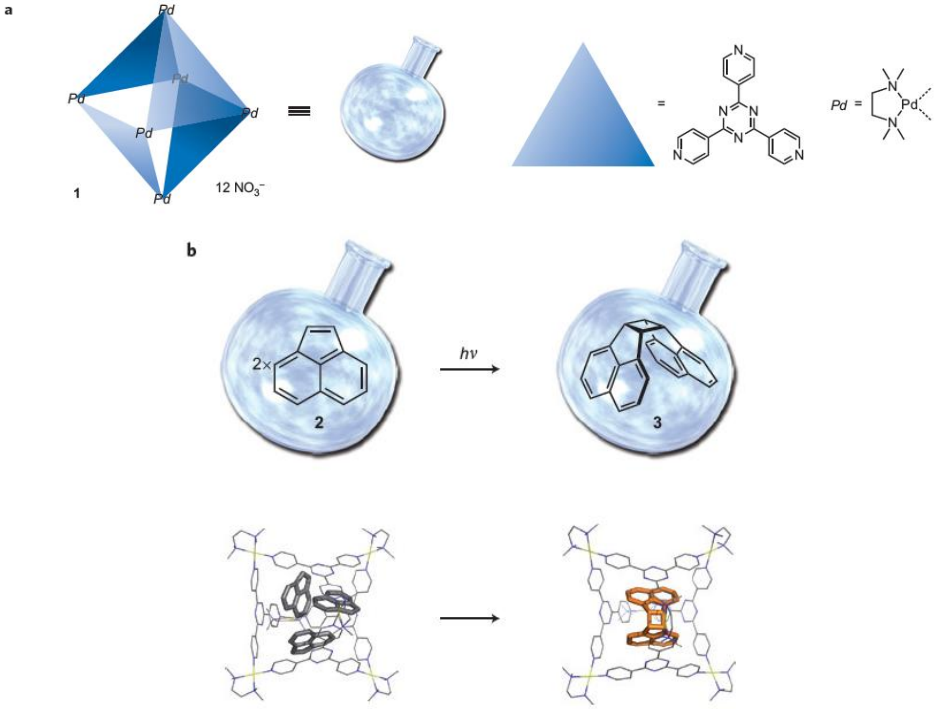

Figure 6. *Illustrative example of Fujita's crystalline "molecular flasks" (reproduced from reference 17).*

Northrop, B. H.; Yang, H.; Stang, P. J. *Chem. Commun.* **2008**, 5896-5908.

[17] Inokuma, Y.; Kawano, M.; Fujita, M. *Nat. Chem.* **2011**, *3*, 349-358.

Another significant group of molecular containers is based upon the expansion of hollow cavitands to afford open void-like molecular architectures. Rebek and others explored this approach by deepening resorcinarenes-based self-assembled cavities.[18] Recently, our group detailed different examples of calix[4]arene deep cavitands, in which the confined space was locked by either hydrogen bonding[19] or metallobridges[20] between their aromatic extended walls (Figure 7). These interactions prevented the molecules from adopting partially collapsed pinched conformations. These molecular vessels offer a solvent accessible space to effectively encapsulate different guests inside without the dependence on the dynamic assembly of diverse components, due to the fact that encapsulation occurs with closed capsular-like structures. Indeed, guest inclusion of smaller calix[4]arenes and resorcinarenes inside these large extended cavities through size, shape and electronic complementarity was reported.

---

[18] (a) Tucci, F. C.; Renslo, A. R.; Rudkevich, D. M.; Rebek, J. Jr. *Angew. Chem. Int. Ed.* **2000**, *39*, 1076-1079. (b) Menozzi, E.; Onagi, H.; Rheingold, A. L.; Rebek, J. Jr. *Eur. J. Org. Chem.* **2005**, 3633-3636. (c) Ajami, D.; Rebek, J. Jr. *Proc. Natl. Acad. Sci. USA* **2007**, *104*, 16000-16003. (d) Lledó, A.; Rebek, J. Jr. *Chem. Commun.* **2010**, *46*, 8630-8632.

[19] Botana, E.; Nättinen, K.; Prados, P.; Rissanen, K.; de Mendoza, J. *Org. Lett.* **2004**, *6*, 1091-1094.

[20] (a) Botana, E.; Da Silva, E.; Benet-Buchholz, J.; Ballester, P.; de Mendoza, J. *Angew. Chem. Int. Ed.* **2007**, *46*, 198-201. (b) Botana, E.; Lubinu, M. C.; Da Silva, E.; Espinet, P.; de Mendoza, J. *Chem. Commun.* **2010**, *46*, 4752-4754.

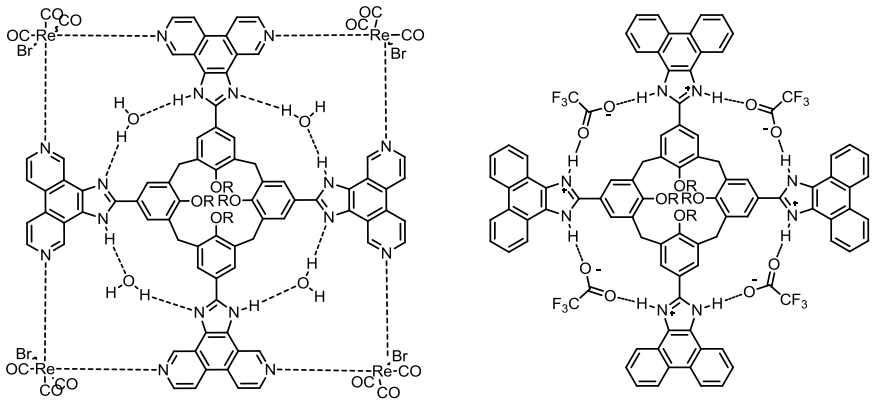

Figure 7. *Expanded calix[4]arenes reported by de Mendoza and co-workers.*

Herein, we describe the construction of stable and robust open molecular containers based on the binding between different oxoanionic calix[4]arenes and the cationic macrocyclic tetraguanidinium ligand **71** (Figure 8). Namely, ligand **71** should stabilize the cone conformation of these calix[4]arenes by means of electrostatic interactions and expand the inner volume of the cavity allowing association with a guest that would otherwise not fit inside. To the best of our knowledge, this is the first example of a cavity expansion promoted by non-covalent reversible bonds to generate an open-shell construct.

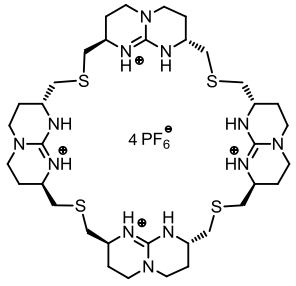

71

Figure 8. *Tetraguanidinium macrocyclic ligand **71**.*

4.2 Design and Synthesis of the Tetraguanidinium Macrocycle 71

Macrocyclic tetraguanidinium hexafluorophosphate salt **71** was prepared after five synthetic steps starting from functionalized monoguanidines **2** and **3** (Scheme 1). *R,R*-Thioacetylated monoguanidine **3** was coupled by nucleophilic attack of its thiolate to *S,S*-guanidine mesylate **2**, giving rise to *R,R*-*S,S*-diguanidinium **4**. Cleavage of the silyl groups and activation of the diol with methanesulfonic anhydride afforded dimesylate diguanidinium **6** in good yields. Thioacetylation of **6** resulted in dithiolate precursor **7**. Finally, coupling of diguanidinium dimesylate **6** with dithioacetylated diguanidinium salt **7** afforded tetraguanidine **71** in a 21% overall yield.

The macrocyclization step deserves several considerations. First, high dilution conditions are required to avoid formation of undesirable linear oligomeric or polymeric products. In that sense, it is worth mentioning that the configuration of each stereogenic center in the molecule is not trivial. Indeed, *R,R*-*S,S*-diguanidines ("*meso*"), despite their inherent flexibility, should provide the correct orientation of their reactive side-arms pointing towards the same face of the molecule to allow formation of the macrocycle.

On the other hand, a polymer bound phosphine is used to prevent oxidation of the dithiolate precursor and thus formation of disulfide by-products.

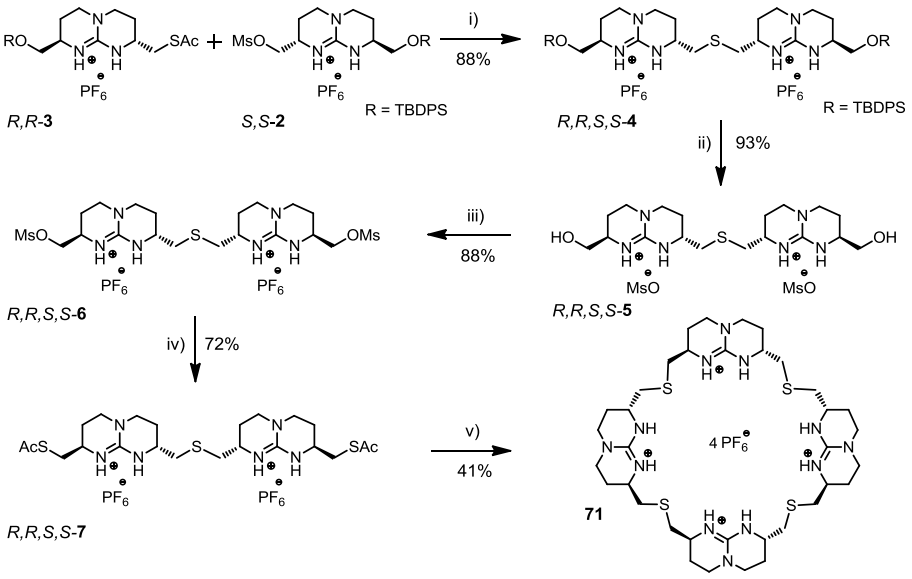

Scheme 1. *Synthesis of tetraguanidinium macrocycle* ***71****. Conditions: i) 2.7 eq.* Cs_2CO_3*, MeOH/ACN,* N_2*; ii) MsOH, THF/*H_2O*; iii)* Ms_2O*, NMM in* CH_2Cl_2*; iv)* $KSCOCH_3$*, ACN, reflux; v) 1 eq.* ***6****, 2.7 eq.* Cs_2CO_3*, (*^{t}*Bu)*$_2$*PhP polystyrene, in MeOH/ACN (high dilution conditions), 2 days,* N_2*.*

In collaboration with Dr. Vera Martos and Dr. Aritz Durana from our research group, calix[4]arenes (**a**, **c**-**e**) were synthesized whereas compound **b** was commercially available (see further details in experimental section) (Figure 9). Formylation of the corresponding *O*-alkyl calix[4]erenes, followed by oxidation with sulfamic acid and sodium chlorite afforded tetracarboxylic compounds **a**, **c** and **d** in moderate to good yields. Subsequent *O*-debenzylation of compound **a** gave rise to calix[4]arene **e**.

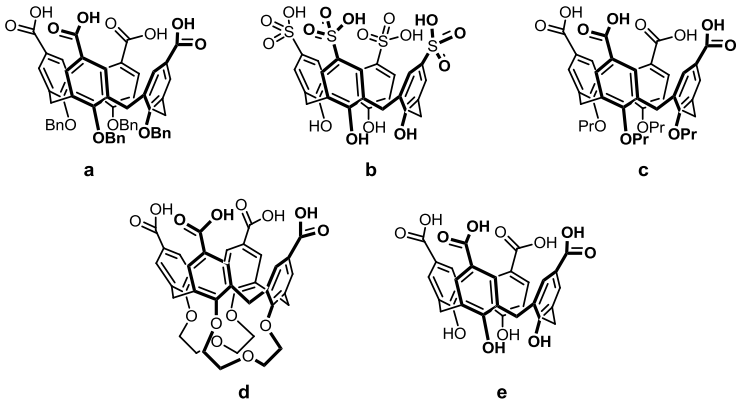

Figure 9. *Calix[4]arene tetracarboxylic and sulfonic acids* ***a-e****.*

4.3 Preliminary Characterization of the Complexes

The ^{1}H-NMR spectra of 1:1 mixtures of macrocyclic tetraguanidine **71** and the sodium salts of calix[4]arenes **a**, **b** and **c** revealed no significant chemical shifts with respect to the original calix[4]arene signals in a CD_3CN/D_2O (2:1) mixture. However, the broadening of the original proton signals of the independent species indicated that molecular assembly was likely taking place.

Molecular models of macrocyclic tetraguanidinium calix[4]arenate complexes pointed out that molecule **71** should sit on the anionic edge of the calix[4]arenes, compensating the four positive charges of **71**. Hence, it was expected to find nOe contacts between the upper rim proton signals of the calix[4]arene and tetraguanidinium molecule **71**. To corroborate this hypothesis, NMR ROESY experiments were performed. Indeed, after selective irradiation of the aromatic signals of calix[4]arene **c**, 1D ROESY showed nOe contacts with almost all signals of macrocyclic tetraguanidinium **71** (Figure 10).

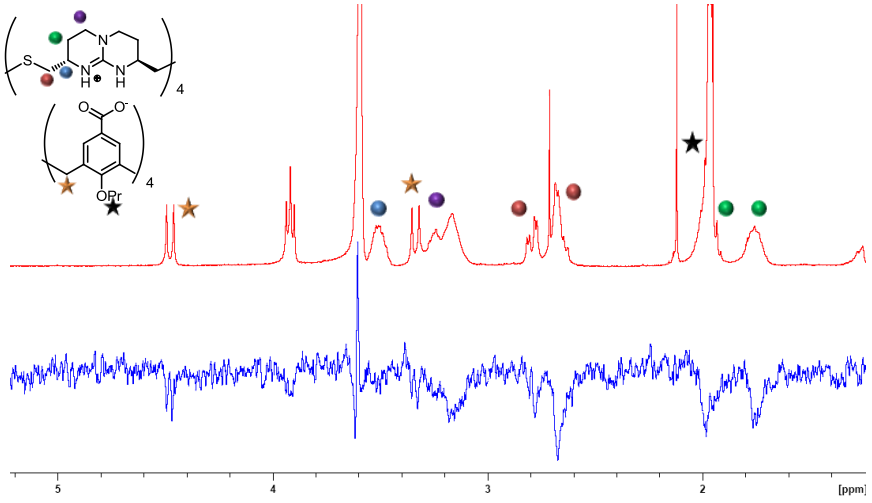

Figure 10. *1D ROESY experiment showing contacts between the aromatic part of calixarene* ***c*** *and* ***71****.*

From the molecular model it can be assumed that only the CH_2S and CHα protons of macrocycle **71** should be within the optimal distance to display nOe contacts with the aromatic protons of the calix[4]arene. However, the β and γ methylene protons also showed nOe contacts, indicating that the inherent flexibility of macrocycle **71** could allow for the dynamic bending and twisting of some of the bicyclic guanidines of the ring, resulting in a closer proximity of these protons to the aromatic protons of the calixarene in the NMR time scale.

In addition, **71@a** and **71@b** were also characterized by means of mass spectrometry analysis[21] ($[M-H]^-$ = 1555.8 and 1531.5 m/z, respectively), revealing the interaction between the anionic calix[4]arenates with tetraguanidinium **71**. The masses of the individual species were also found in the gas phase, as a result of complex fragmentation.

Further structural studies were carried out by NMR DOSY experiments. This technique affords information about the number of species in solution and their diffusion coefficients.[22] Experimental hydrodynamic radii for each species can be calculated by utilizing the Stokes-Einstein equation ($R_h = K_bT/6\eta\pi D$) where D is the diffusion coefficient of the species as determined by DOSY. The experimental radii can then be compared with the calculated hydrodynamic radii for the different species.[23]

DOSY spectra of complexes **71@a** and **71@c** were measured in a D_2O:CD_3CN (1:3) solvent mixture. For each sample, one sharp DOSY peak was observed, accounting for

---

[21] Zadmard, R.; Kraft, A.; Schrader, T.; Linne, U. *Chem. Eur. J.* **2004**, *10*, 4233-4239.

[22] Cohen, Y.; Avram, L.; Frish, L. *Angew. Chem. Int. Ed.* **2005**, *44*, 520-554.

[23] (a) Timmerman, P.; Weidmann, J.-L.; Jollife, K. A.; Prins, L. J.; Reinhoudt, D. N.; Shinkai, S.; Frish L.; Cohen, Y. *Perkin Trans. 2* **2000**, *2*, 2077-2089. (b) Giuseppone, N.; Schmitt, J.-L.; Allouche, L.; Lehn, J.-M. *Angew. Chem. Int. Ed.* **2008**, *120*, 2267-2271. (c) Oliva, A. I.; Gómez, K.; González, G.; Ballester, P. *New J. Chem.* **2008**, *32*, 2159-2163. (d) Metselaar, G. A.; Sanders, J. K. M.; de Mendoza, J. *Dalton Trans.* **2008**, 588-590.

a single complexed species in solution and thus no scrambling between the free species in the NMR time scale was detected (Figure 11).

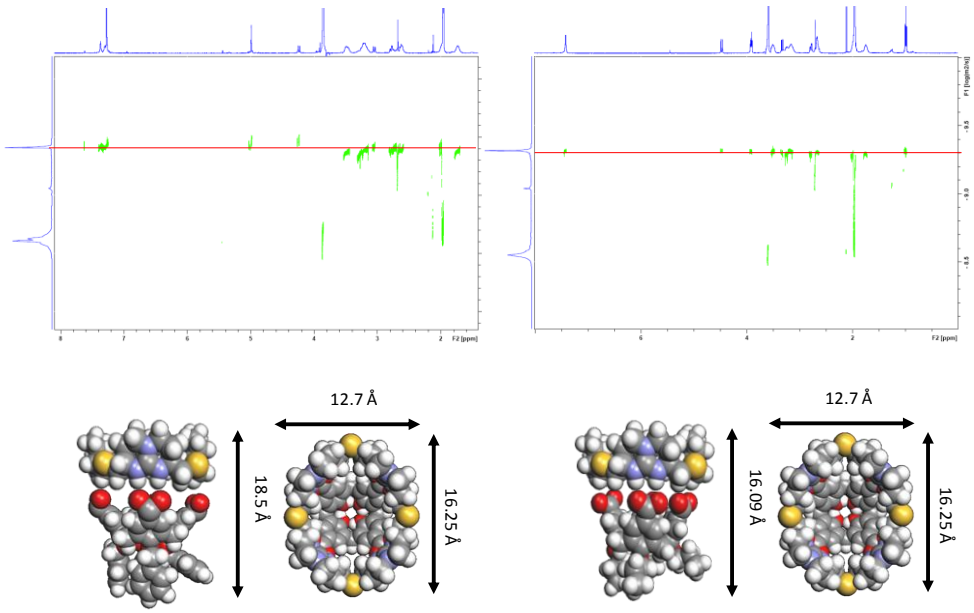

Figure 11. *DOSY spectra of* ***71@a*** *(left) and* ***71@c*** *measured in D_2O:CD_3CN (1:3) (right) with the corresponding molecular models used to calculate their theoretical R_h.*

Hydrodynamic radii of a range of free and complexed species were determined both experimentally and theoretically. As illustrated in Table 1, theoretical hydrodynamic radii of the calix[4]arene carboxylate salts and macrocycle **71** are similar, and therefore it was expected to observe similar values of the hydrodynamic radii as well as for the complexes. Indeed, the experimental hydrodynamic radii obtained for the complexes are in good fit with the calculated ones. Two theoretical radii were considered depending on the conformation of the calix[4]arene **a**: 5.9Å for the *cone* conformation and 6.5Å for the *pinched cone*, which is the preferred conformation for this compound. Indeed, the experimental hydrodynamic radius (6.7Å) is in good agreement with the one extracted from the model. Moreover, the X-ray crystal structure of the molecule

finally confirmed this pinched disposition and the resulting hydrodynamic radius (Figure 12).

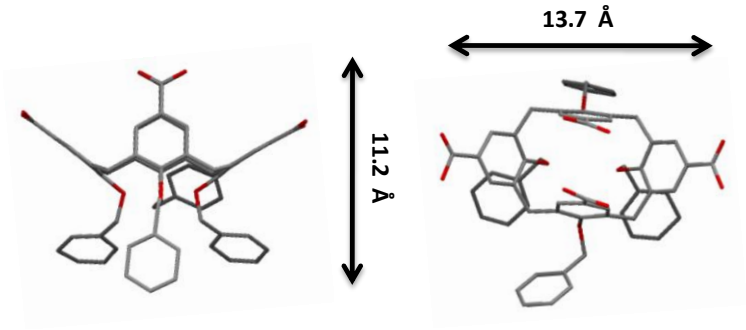

Figure 12. *X-ray structure of Calix (OBn)* ***a****.*

Table 1. *Theoretical and experimental hydrodynamic radius extracted from the molecular models and DOSY experiments, respectively.*

	Rcalc (Å)	**Rexp (Å)**
Tetraguanidinium **71**	5.6	5.1
Calix (OBn) **a**	5.9/6.5	6.7
Calix (OPr) **c**	5.6	--
Complex **71@a**	8.1	8.9
Complex **71@c**	7.5	7.8

In conclusion, the data provides qualitative information about the complexation that validates the postulated model for the association.

4.4 Conformational Study of the Tetraguanidinium Calix[4]arenate Complexes in Solution

Calixarenes can adopt different conformations due to the inherent flexibility of the phenol rings around the methylene bridges. Several factors can drastically influence the most stable conformation of the calixarene, and therefore its geometrical and spatial disposition.[24]

Calix[4]arenes with bulky substituents such as **a** and **c** (i.e. benzyl or propyl chains at the lower rim) show a restricted conformation due to obvious sterical reasons, whereas the aryl moieties of calix[4]arenes **b** and **e**, with hydroxyl groups at the lower rim, can unrestrictedly rotate. These hydroxyl groups provide an intramolecular hydrogen bonding array which predominantly stabilizes the *cone* conformation. However, in the presence of polar solvents, hydrogen bonding is disrupted and consequently the ^{1}H-NMR signal of the methylene protons appears as a broad singlet indicating a statistical distribution of the different conformations due to a rapid exchange between conformers.

The macrocyclic tetraguanidinium compound **71** should stabilize the cone conformation of otherwise flexible calix[4]arenes, providing a strong and robust complex which should prevent or slow down the conformational exchange. Each bicyclic guanidinium may face a negatively charged group of the calix[4]arene, hereby influencing its orientation by means of electrostatic and hydrogen bonding interactions. Therefore, the association should increase the inversion energy barriers which can be measured by the determination of coalescence temperatures using variable temperature ^{1}H-NMR experiments.

---

[24] (a) Jaime, C.; de Mendoza, J.; Prados, P.; Nieto, P. M.; Sánchez, C. *J. Org. Chem.* **1991**, *56*, 3372-3376. (b) Iwamoto, K.; Araki, K.; Shinkai, S. *J. Org. Chem.* **1991**, *56*, 4955-4962.

In order to perform these experiments, the solvent should provide good solubility for both the complex and the calix[4]arenes and should afford a wide range of temperatures in which the conformational interconversion occurs. Sodium calix[4]arenate salts of **b** and **e** required solvent mixtures containing D_2O, which restricts the lower limit of the ramp temperature. Thus, tetrabutylammonium salts of the anionic calix[4]arenes were formed to enhance their solubility in organic solvents. Hence, mixtures of CD_3CN:CD_3OD (6:4) which tolerate a wide range of temperatures (from -45 to 55º C) were used in the variable temperature NMR experiments.

As shown in Figure 13, the methylene protons of calix[4]arene **b** appeared as a broad signal at room temperature, accounting for a rapid interconversion between different conformers in solution. Upon cooling, the *cone* conformation was stabilized and thus, the proton signal became a doublet at 278 K. Conversely, at room temperature in the presence of tetraguanidinium ligand **71**, the calix[4]arene **b** adopted a more stable *cone* conformation which should facilitate the complexation with this polycationic molecule. Consequently, the doublet signal was observed up to 318 K (the upper temperature limit for this solvent system). A similar trend was observed for calix[4]arene **e**.

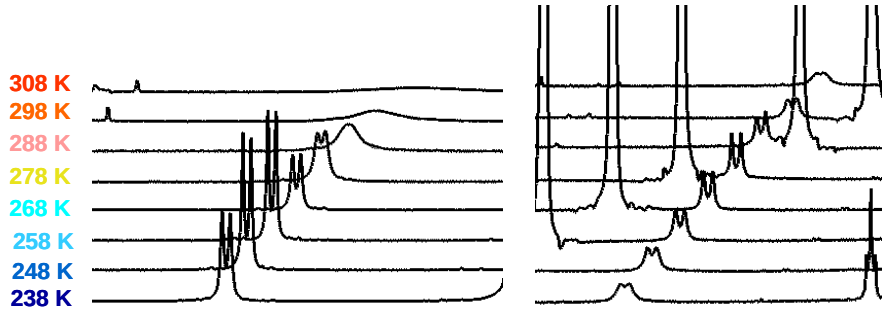

Figure 13. *Example of a variable temperature ^{1}H-NMR experiment monitoring the protons in the methylene bridge of calix[4]arene* ***b*** *with* ***71*** *(right) and without* ***71*** *(left).*

Gutsche *et al.* described a method to assess conformational mobilities in calix[n]arenes by means of dynamic ^{1}H-NMR spectroscopy (Figure 14).[25,26] Applying this methodology, conformational barriers of calix[4]arene inversions with and without ligand **71** were deduced from the coalescence temperatures extracted from the variable temperature ^{1}H-NMR data.

$$kc = 2.22(\Delta\upsilon + 6J_{AB}^2)^{1/2}$$

$$\Delta G^{\neq} = 4.58T_c(10.32 + log\frac{T_c}{k_c})/1000$$

Figure 14. *Formula used for determining conformational barriers of calixarenes and calixarene-guanidinium complexes.*

Table 2 summarizes the data obtained from these experiments. In general, tetrabutylammonium calix[4]arene salts display lower coalescence temperatures (Tc) than the corresponding tetraguanidinum calix[4]arenate complexes. The numbers were calculated assuming an accuracy of ±5º C for the value of Tc; ± 15 Hz for the value of Δν and ± 1 Hz for the value of J_{AB}. It is also estimated that $\Delta G^{\neq}$ values are accurate to ± 0.4 kcal/mol.

[25] (a) Gutsche, C. D.; Bauer, L. J. *J. Am. Chem. Soc.* **1985**, *107*, 6052-6059. (b) Kanamathareddy, S.; Gutsche, C. D. *J. Org. Chem.* **1994**, *59*, 3871-3879. (c) Stewart, D. R.; Gutsche, C. D. *J. Am. Chem. Soc.* **1999**, *121*, 4136-4146.

[26] van Hoorn, W. P.; Briels, W. J.; van Duynhoven, J. P. M.; van Veggel, F. C. J. M.; Reinhoudt, D. N. *J. Org. Chem.* **1998**, *63*, 1299-1308.

Table 2. *Calculated values for the coalescent constant (K_c) and $\Delta G^{\neq}$ in the system depicted.*

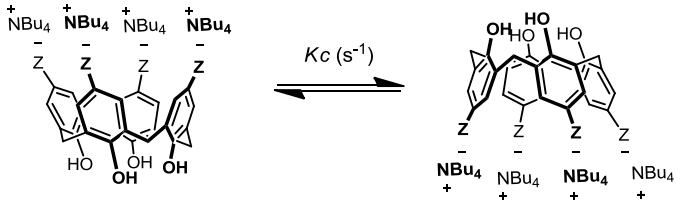

In CD_3CN/CD_3OD	**Tc (K)**	**Δν**	J_{AB}	***Kc*** **(s^{-1})**	$\Delta G^{\neq}$ (±0.4 kcal/mol)
Calix **b** (Z = SO_3^-)	308-318	280	12.5	626.4	14.36
Calix **e** (Z = CO_2^-)	308-318	255	12.9	570.5	14.42
Complex **71@b**	>328	271	12.9	609.0	---
Complex **71@e**	>328	273	12.5	608.7	---

However, Tc values are higher than 328 K for the tetraguanidinium calix[4]arenate complexes and therefore free energy interconversion barriers cannot be accurately determined since the solvent mixture employed (CD_3CN/CD_3OD) does not allow to reach this temperature.

In DMSO, the upper limit of the temperature range increases, but extrapolation from previous experiments made in CD_3CN/CD_3OD mixture was necessary for parameters such as J_{AB} and Δν, since the lower temperature limit of DMSO does not allow their direct measurement.

Control tests with mono- and diguanidinium calix[4]arene salts were performed to evaluate their effect in the conformational stability of the complexes. Addition of stoichiometric amounts (4 equivalents) of a bicyclic guanidinium monomer **72** (see formula in Figure 16, Section 4.5) did not influence the interconversion rate (Table 3), the calix[4]arene carboxylate salts showing similar coalescence temperatures as the tetrabutylammonium salts. Interestingly, diguanidine **4** had an effect on the

conformational barrier of calix[4]arene tetracarboxylate **e** but not on tetrasulfonate **b**. This accounts for the stronger interaction of guanidinium cations with carboxylates than with sulfates.[27] This trend is also observed with macrocyclic tetraguanidinium ligand **71** (the complex **71@e** showed higher coalescence temperatures (up to 408 K) than the **71@b** adduct (*ca.* 393 K)).

Table 3. *Calculated values for the coalescent constant (K_c) and $\Delta G^{\neq}$ in DMSO.*

In DMSO	**Tc (K)**	**Δν (Hz)**	J_{AB} **(Hz)**	***Kc*** **(s^{-1})**	$\Delta G^{\neq}$ (±0.4 kcal/mol)
Calix **b** (Z = SO_3^-)	298-308	280	12.5*	626.4	13.9
Calix **b** + 4 eq. **72**	298-308	280	12.5*	626.4	13.9
Calix **b** + 2 eq. **4**	298-308	280	12.5*	626.4	13.9
Complex **71@e**	388-398	210	12.8	471.4	18.4
Calix **e** (Z = CO_2^-)	318-328	200	12.95*	438.6	15.3
Calix **e** + 4 eq. **72**	318-328	200	12.95*	438.6	15.3
Calix **e** + 2 eq. **4**	368-378	200	12.95*	438.6	17.4
Complex **71@b**	>408	232.5**	12.45**	520.6	>19.1

**Extrapolated from the experiment performed in CD_3CN/MeOD (6/4). **These numbers correspond to the last complex observed.*

In conclusion, binding of tetraguanidinium multivalent ligand **71**, and to a lesser extent diguanidine **4**, stabilizes the conformation of oxoanionic calix[4]arenes by hindering the mobility of their aryl moieties. This effect is not attributable to the intrinsic interaction of four "monovalent" guanidine ligands with anionic calix[4]arenes

[27] Jadhav, V. D.; Herdtweck, E.; Schmidtchen, F. P. *Chem. Eur. J.* **2008**, *14*, 6098-6107.

as demonstrated by control experiments. The higher conformational stabilization of the calix[4]arene carboxylates over the corresponding sulfonates indicates that a stronger interaction results in a structurally more stable complex. Indeed, as the number of guanidinium moieties increases, the strength of the interaction should also increase, both by effective molarity (EM) and by the cooperativity effect.

This structural behavior in solution is essential to allow molecular recognition at these interfaces, because stabilization of the *cone* conformations allows for the formation of robust and well-defined void-like structures which are able to bind other guest molecules even at high temperatures.

4.5 Isothermal Titration Calorimetry (ITC) Studies

Isothermal titration calorimetry (ITC) was used to assess quantitatively and qualitatively the thermodynamic factors of the binding between macrocyclic tetraguanidinium ligand **71** and tetraoxoanionic calix[4]arenes. The experiments were carried out in a THF/H_2O (3:1) mixture to allow solubilization of the more hydrophilic sodium calix[4]arenate salts **a**-**d** (Figure 15).

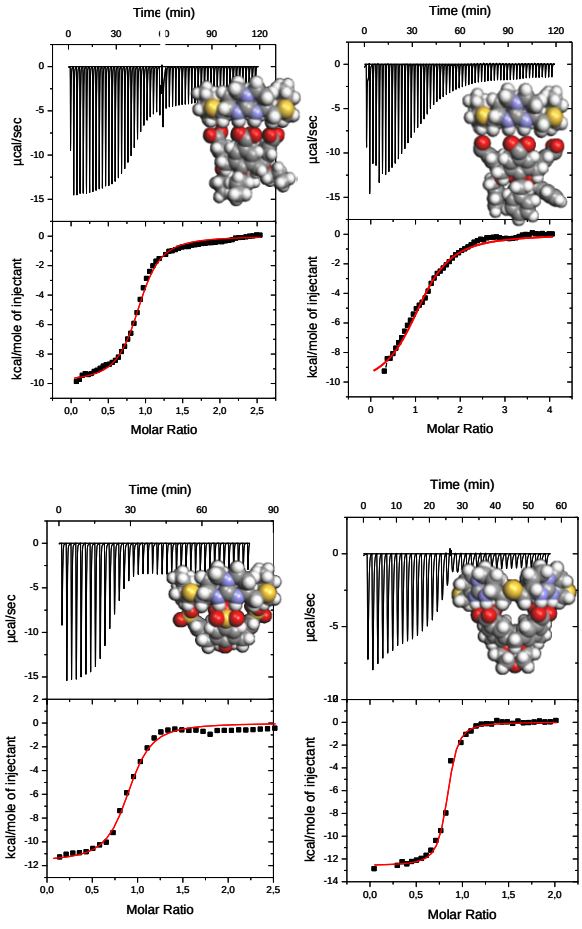

Figure 15. *ITC curves for the titrations with calix[4]arene anions.*

Binding constants were high (within the range of 10^4-10^6 M^{-1}, see Table 4) even in the presence of polar solvents such as water, accounting for a robust and cooperative enthalpically driven interaction. Hence, the binding is dominated by hydrogen bonding and ion-pair formation. Conversely, the entropic factor, which mainly depends on disorder in the molecular assembly process, solvation effects and solvent-shell reorganization upon complexation, has only a minor contribution in these systems.

Table 4. *Thermodynamic data obtained by ITC measurements.*

	Complex **71@a**	Complex **71@b**	Complex **71@c**	Complex **71@d**
K_a (M^{-1})	2.46 x 10^4	2.03 x 10^5	8.25 x 10^5	2.45 x 10^6
ΔH (Kcal·mol^{-1})	-10.4	-11.7	-9.9	-12.6
ΔS (cal·mol^{-1}·K^1)	-14.7	-14.8	-10.8	-12.9
ΔG (Kcal·mol^{-1})	-6.0	-7.3	-6.7	-8.8

As previously discussed, molecular modeling and VT ^{1}H-NMR experiments suggested that the preferred calix[4]arene conformation to maximize the interaction with macrocyclic tetraguanidinium ligand **71** is the *cone* conformation.

In fact, the highly preorganized calix[4]arene **d** showed an association constant with ligand **71** up to two orders of magnitude higher than the more flexible calix[4]arenes **a** and **c**. This molecule, bearing bridges between vicinal phenols at the lower rim, displays a restricted *cone* conformation[28] which promotes and facilitates the interaction with **71**. Tetrasulfonato calix[4]arene **b** should also show a preferred cone conformation due to the intramolecular hydrogen bonding array between the phenolic groups of the lower rim. However, in polar media this array is less stable. Indeed, the binding constant drops by one order of magnitude due to the weaker sulfonate-

[28] Arduini, A.; Fabbi, M.; Mantovani, M.; Mirone, L.; Pochini, A.; Secchi, A.; Ungaro, R. *J. Org. Chem.* **1995**, *60*, 1454-1457.

guanidinium interaction, and also the fact that this molecule is conformationally less robust than calix[4]arene **d**. Indeed, compounds **a** and **c** preferentially display a *pinched* conformation which results in weaker binding to the tetraguanidinium ligand **71** (K_a = 2.5 x 10^4 and 8.3 x 10^4 M^{-1}, respectively). This *pinched* disposition of the aryl moieties prevents interaction with the macrocyclic tetraguanidine and thus lack of a correct preorganization in a conical shape translates into a lower association constant.

Finally, titrations with bicyclic guanidinium monomer **72** and diguanidinium **5** did not produce any significant heat exchange in the presence of tetracarboxylic calix[4]arene **a**, as illustrated in Figure 16. This highlights the requirement of having multivalent systems such as ligand **71** to allow complexation even in highly competitive polar solvents.

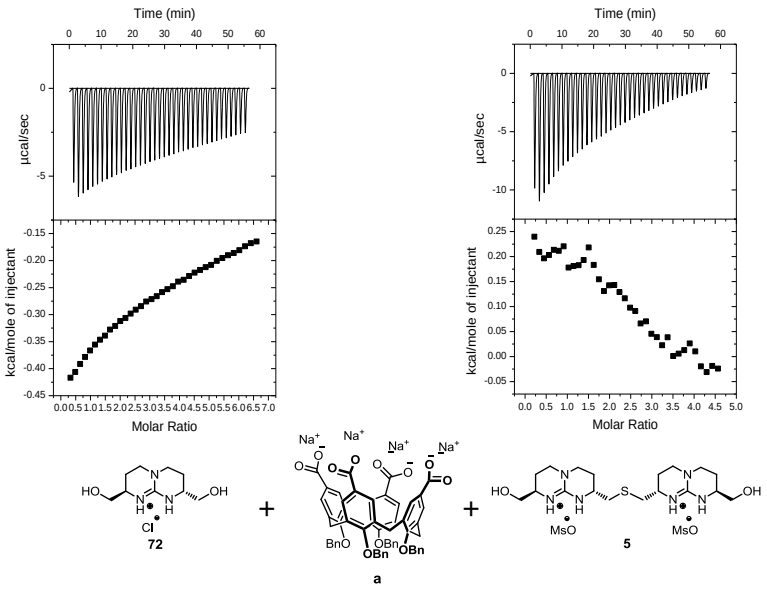

Figure. 16*. ITC curves for the blank experiments with monoguanidinium* ***72*** *and diguanidinium* ***5*** *molecules, respectively, showing no relevant heat exchange.*

From these calorimetric measurements it can be concluded that binding of the oxoanionic calix[4]arene anions with tetraguanidinium ligand **71** is an enthalpically driven process involving ion-pairing and hydrogen bonding interactions. Moreover, the sum of these interactions in a cooperative and multivalent fashion is essential for the successful complexation.

4.6 Guest Complexation in Calix[4]arene-Tetraguanidinium Expanded Cavities

As shown in previous molecular models, complexation of the tetraguanidinium ligand **71** with oxoanionic calix[4]arenes by means of ionic interactions may result in the increase of the inner volume of these molecular containers. Herein, to the best of our knowledge we present the first example of non-covalently expanded calix[4]arene with an open cavity structure.

To demonstrate the ability of calixarene-guanidinium expanded cavities to effectively include and bind guest molecules, titration experiments of **71@d** with two different quinolinium iodide salts (**73** and **74**) (Figure 17) were carried out. For this purpose, we selected the most robust tetraguanidinium calix[4]arenate complex (**71@d**) in terms of binding and structural stability.

Figure 17. *2-Methylisoquinolinium and 1-ethyl-2methylquinolinium iodide salts* ***73*** *and* ***74****, respectively.*

Host-guest interactions between calixarenes and ammonium salts have been extensively reported.[29] Their inclusion is mainly driven by cation-π, CH-π and π-π contacts, although hydrophobic effects should be also taken into account in polar solvents (Figure 18).

[29] For reviews see: (a) Abraham, W. *J. Incl. Phen. Macrocyc. Chem.* **2002**, *43*, 159-174. (b) Mutihac, L.; Lee, J. H.; Kim, J. S.; Vicens, J. *Chem. Soc. Rev.* **2011**, *40*, 2777-2796.

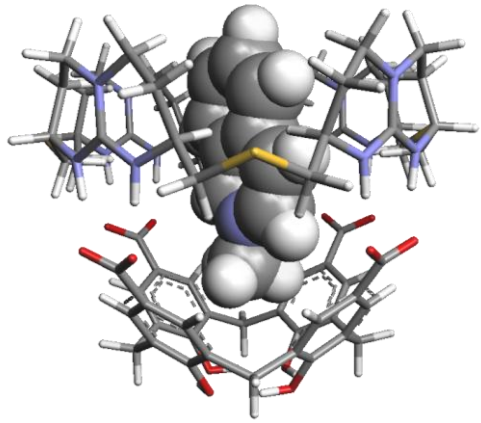

***Figure 18**. Molecular model (MM3) of guest encapsulation complex **73**@[**71**@**e**].*

In terms of size it is likely that the 2-methylisoquinolinium guest **73** should not allow an effective complexation with a simple calix[4]arene. Indeed, no binding was observed by ^{1}H-NMR titration experiments between calix[4]arenate **d** and quinolinium **73** (Figure 19) in the absence of tetraguanidinium. Also, no appreciable changes in the spectra were observed upon adding guest **73** to a solution containing macrocyclic tetraguanidine **71**.

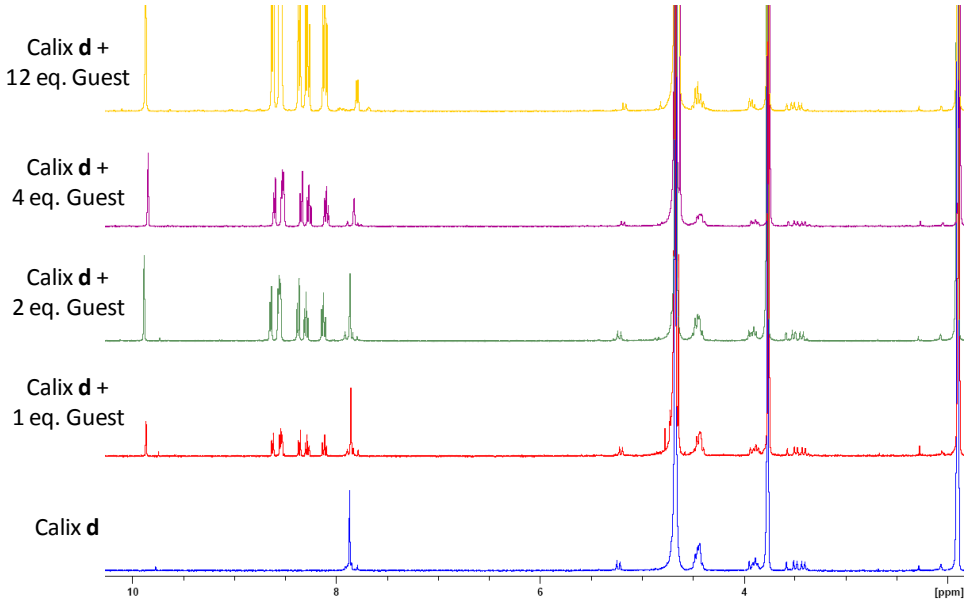

Figure 19. *^{1}H-NMR titration (in 3:1 THF-d_6/D_2O mixture) of the selected guest* ***73*** *with oxoanionic calix[4]arene* ***d****.*

^{1}H-NMR titration experiments with guest **73** in the presence of the supramolecular tetraguanidinium calix[4]arenate host **71@d** (Figure 20) in a (3:1) THF-d_6/D_2O mixture revealed upfield shifting of the guest proton signals, accounting for a molecular encapsulation process. As illustrated in Figure 20, the addition of an excess of ammonium guest resulted in the appearance of new broad signals which corresponds in chemical shift with the free 2-methylisoquinolinium guest in solution. The data strongly support slow exchange equilibrium between the free and the bound guest.[30] The broadness of the signals did not allow an accurate integration for the association constant determination.

[30] (a) Saito, S.; Nuckolls, C.; Rebek, J. Jr. *J. Am. Chem. Soc.* **2000**, *122,* 9628-9630. (b) Trembleau, L.; Rebek, J. Jr. *Science* **2003**, *301*, 1219-1220.

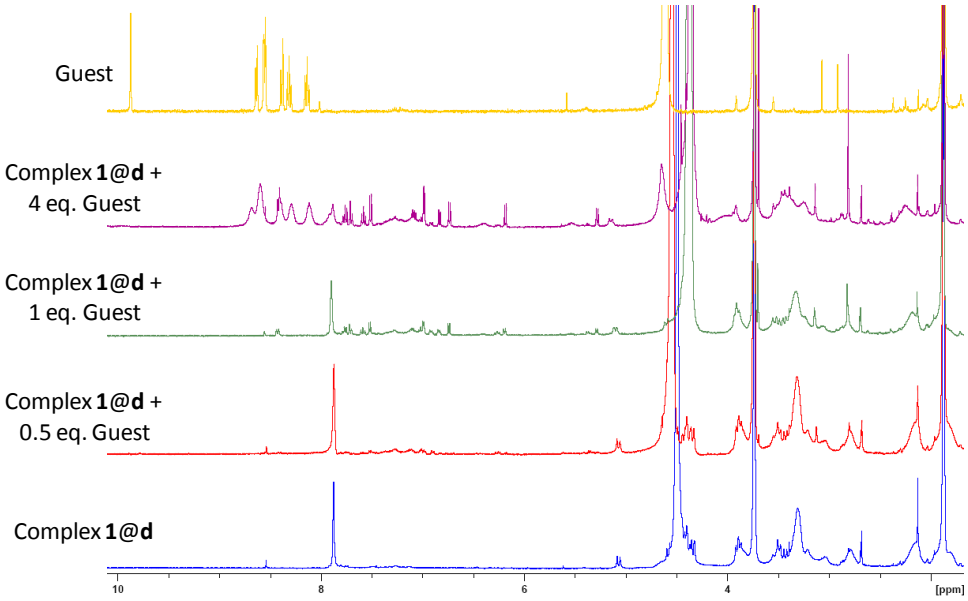

Figure 20. *^{1}H-NMR titration (in 3:1 THF-d_8/D_2O mixture) of guest* ***73*** *with the complex* ***71@d****.*

As shown in Figure 21, nOe crosspeaks between these two bound and free species confirmed the existence of a chemical exchange due to guest inclusion.

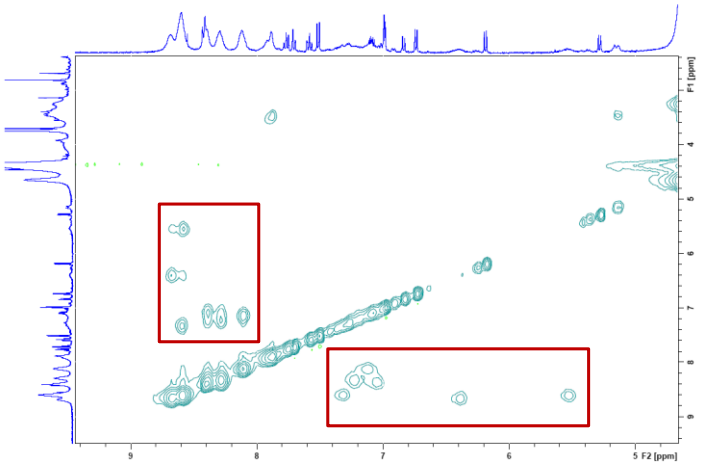

Figure 21. *NOESY spectrum showing exchange crosspeaks between free and bound guest (****73****) signals.*

^{1}H-NMR titrations in a (3:1) THF-d_6/D_2O mixture with 1-ethyl-2-methylquinolinium iodide guest **74** were also performed to explore the possibility of this bulkier molecule to be included into **71@d** complex. Indeed, the spectra showed well defined upfield shifted signals accounting for the complexation of **74** (Figure 22). When an excess guest was added, a new set of signals corresponding to the free species appeared, clearly indicating a slow exchange process on the NMR time scale.

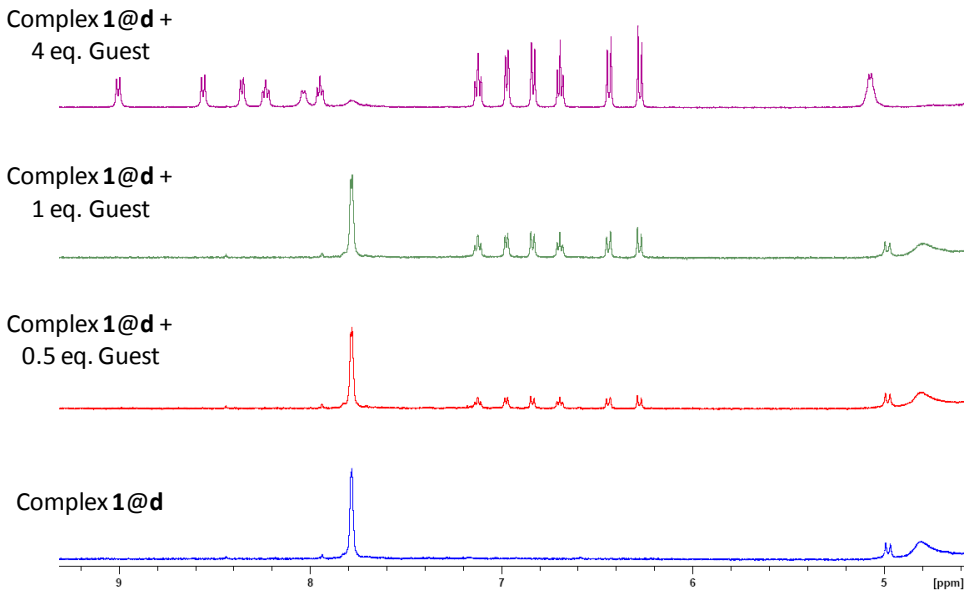

Figure 22. *^{1}H-NMR titration (in 3:1 THF-d_6/D_2O mixture) of guest **74** with the complex **71@d**.*

The chemical exchange observed in the NOESY spectrum (Figure 23) confirmed this two-state (free and bound) behavior for guest **74**.

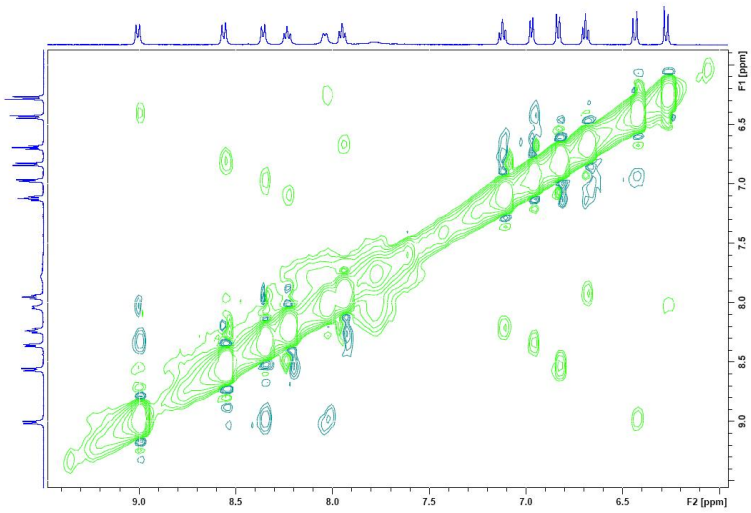

Figure 23. *NOESY spectrum showing exchange crosspeaks between free and bound guest (**74**) signals.*

4.7 Experimental Section

4.7.1 Materials and Methods

Calorimetric measurements were preformed in an isothermal titration microcalorimeter Microcal VP-ITC. The operating temperature range varies from 2 ºC up to 80 ºC with a noise level of 1 nanocal/sec (4 nanowatts).

4.7.2 Synthesis

Calix[4]arenes **a**, **c**, **d** and **e** were synthesized according to described procedures.[31] Calix[4]arene tetrasulfonic acid **b** was commercially available.

(2*S*,8*S*)-2-(*tert*-Butyldiphenylsilanyloxymethyl)-8-methanesulfonyloxymethyl-3,4, 6,7,8,9,-hexahydro-2*H*-pyrimido[1,2-*a*]pyrimidin-1-ium hexafluorophosphate (2).

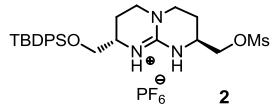

2

To a solution of mono-deprotected guanidine (PF_6^-) (1.23 g, 2.11 mmol) in dry CH_2Cl_2 (25 mL) was added Ms_2O (1.84 g, 10.55 mmol) and NMM (1.87 ml, 16.87 mmol) and the mixture was stirred for 4 h at room temperature. After evaporation of the solvent, the resulting solid was dissolved in CH_2Cl_2 (100 mL) and washed with a

[31] (a) Sansone, F.; Barboso, S.; Casnati, A.; Fabbi, M.; Pochini, A.; Ugozzoli, F.; Ungaro, R. *Eur. J. Org. Chem.* **1998**, 897-905. (b) Sansone, F.; Barboso, S.; Casnati, A.; Sciotto, D.; Ungaro, R. *Tetrahedron Lett* **1999**, *40*, 4741-4744. (c) Zhou, H.; Wang, D.; Baldini, L.; Ennis, E.; Jain, R.; Carie, A.; Sebti, S. M.; Hamilton, A. D. *Org. Biomol. Chem.* **2006**, *4*, 2376-2386. (d) Martos, V.; Bell, S. C.; Santos, E.; Isacoff, E. Y.; Trauner, D.; de Mendoza, J. *Proc. Natl. Acad. Sci. USA* **2009**, *106*, 10482-10486.

0.1N NH_4PF_6 solution (2 × 50 mL). The organic layer was filtered over cotton and concentrated at reduced pressure. Purification by silica gel column chromatography (CH_2Cl_2/MeOH, 98:2) afforded the corresponding mesylate **2** (1.23 g, 88%) as a white solid. M.p. 60-61 °C. $[\alpha]^{25}_D$ +78 (c = 0.8, $CHCl_3$). ^{1}H-NMR (400 MHz, $CDCl_3$) δ 7.68-7.63 (m, 4H, CH_{Ar}), 7.50-741 (m, 6H, CH_{Ar}), 6.28 (s, 1H, NH), 6.12 (s, 1H, NH), 4.33 (dd, J = 4.5, 10.3 Hz, 1H, CH_2OMs), 4.19 (dd, J = 6.5, 10.3 Hz, 1H, CH_2OMs), 3.86-3.79 (m, 1H, CH_α), 3.72-366 (m, 2H, CH_2OSi), 3.63-3.56 (m, 1H, CH_α), 3.43-3.27 (m, 4H, $CH_{2\gamma}$), 3.11 (s, 3H, CH_{3MsO}), 2.15-1.87 (m, 4H, $CH_{2\beta}$), 1.08 (s, 9H, $CH_{3t\text{-}Bu}$). ^{13}C-NMR (100 MHz, $CDCl_3$) δ 150.7 (C_{guan}), 135.6, 135.5, 132.6, 132.5, 130.1, 130.1, 128.0 (CH_{Ar}, C_{Ar}), 69.5 (CH_2OMs), 65.4 (CH_2OSi), 50.2, 47.8 (CH_α), 45.4, 45.0 ($CH_{2\gamma}$), 37.2 (CH_{3MsO}), 26.8 ($CH_{3t\text{-}Bu}$), 22.5, 22.0 ($CH_{2\beta}$), 19.2 ($C_{t\text{-}Bu}$). HRMS calcd. for $[C_{26}H_{38}N_3O_4SSi]^+$ 516.2352; found 516.2354.

(2*S*,8*S*)-2-(*tert*-Butyldiphenylsilanyloxymethyl)-8-[(2*R*,8*R*)-8-(*tert*-butyldiphenylsilanyloxymethyl)-3,4,6,7,8,9-hexahydro-2*H*-pyrimido[1,2-*a*]pyrimidin-2-ylmethylsulfanylmethyl-1-ium hexafluorophosphate]-3,4,6,7,8,9-hexahydro-2*H*-pyrimido[1,2-*a*]pyrimidin-1-ium hexafluorophosphate (4).

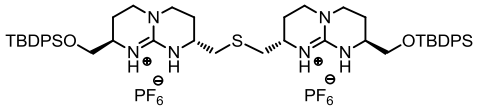

4

A mixture of compound *R,R*-**3** (751 mg, 1.17 mmol), mesylate *S,S*-**2** (774 mg, 1.17 mmol) and Cs_2CO_3 (761 mg, 2.34 mmol) was dissolved in 20 mL of degassed (3:1) CH_3CN/MeOH at 0 ºC under N_2 and the solution was stirred for 4 h. The solvent was evaporated under vacuum at room temperature. The crude was dissolved in CH_2Cl_2 (20 mL) and washed with aqueous 1N NH_4PF_6 (2 × 15 mL). The organic phase was filtered over cotton and concentrated to dryness to give a crude residue which was purified by silica gel (with KPF_6) column chromatography (CH_2Cl_2/MeOH, 96:4), affording symmetric diguanidinium **4** (1.20 g, 88%) as a white solid. M.p. 84-86 °C. $[\alpha]^{25}_D$ +3 (c = 1.0, $CHCl_3$). ^{1}H-NMR (400 MHz, $CDCl_3$) δ 8.24 (s, 2H, NH), 8.05

(s, 2H, NH), 7.71-7.55 (m, 8H, CH_{Ar}), 7.50-7.33 (m, 12H, CH_{Ar}), 3.73 (dd, J = 4.7, 9.8 Hz, 2H, CH_2O), 3.67-3.50 (m, 5H, CH_2O, CH_α), 3.48-3.10 (m, 9H, CH_α,$CH_{2\gamma}$), 3.00 (dd, J = 2.7, 13.5 Hz, 2H, CH_2S), 2.59 (dd, J = 10.8, 13.5 Hz, 2H, CH_2S), 2.18-1.69 (m, 8H, $CH_{2\beta}$), 1.06 (s, 18H, $CH_{3t\text{-}Bu}$). ^{13}C-NMR (100 MHz, $CDCl_3$) δ 151.2 (C_{guan}), 135.6, 135.6, 132.8, 132.7, 129.9, 127.9, 127.9 (CH_{Ar}, C_{Ar}), 65.2 (CH_2O), 49.7, 48.3 (CH_α), 45.1, 44.7 ($CH_{2\gamma}$), 38.5 (CH_2S), 26.9 ($CH_{3t\text{-}Bu}$), 26.2, 22.6 ($CH_{2\beta}$), 19.2 ($C_{t\text{-}Bu}$). HRMS calcd. for $[C_{50}H_{69}N_6O_2SSi_2]^+$ 873.4741; found 873.4754.

(2*S*,8*S*)-2-Hydroxymethyl-8-[(2*R*,8*R*)-8-hydroxymethyl-3,4,6,7,8,9-hexahydro-2*H*-pyrimido[1,2-*a*]pyrimidin-2-ylmethylsulfanylmethyl-1-ium hexafluorophosphate]-3,4,6,7,8,9-hexahydro-2*H*-pyrimido[1,2-*a*]pyrimidin-1-ium mesylate (5).

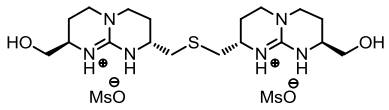

5

A solution of **4** (1.20 g, 1.03 mmol) and MsOH (1.46 mL, 22.53 mmol) in a mixture of THF/H_2O (3:1, 40 mL) was heated overnight at 76 ºC. The solvent was evaporated, the acid mixture diluted in water and washed with CH_2Cl_2 (2 × 50 mL). The aqueous phase was partially evaporated under reduced pressure. Afterwards $KHCO_3$ was added until a neutral pH was reached. The water was evaporated, and the crude was dissolved in a mixture of CH_2Cl_2/MeOH (1:20, 50 mL). The resulting precipitate was filtered off. The polarity of the solvent mixture was gradually reduced until pure CH_2Cl_2. The solvent was then evaporated to afford compound **5** (573 mg, 93%) as a pale-yellow powder. ^{1}H-NMR (400 MHz, MeOD) δ 3.78 (dd, J = 4.0, 11.7 Hz, 2H, CH_2O), 3.68-3.48 (m, 6H, CH_2O, CH_α, $CH_{2\gamma}$), 3.60-3.40 (m, 10H, CH_α, $CH_{2\gamma}$), 3.01 (dd, J = 3.9, 13.8 Hz, 2H, CH_2S), 2.75 (dd, J = 8.0, 13.8 Hz, 2H, CH_2S), 2.19-2.08 (m, 2H, $CH_{2\beta}$), 2.07-1.84 (m, 6H, $CH_{2\beta}$).^{13}C-NMR (100 MHz, MeOD) δ 152.1 (C_{guan}), 65.0 (CH_2O), 51.7 (CH_α), 46.4 ($CH_{2\gamma}$), 36.6 (CH_2S), 26.7, 23.5 ($CH_{2\beta}$). ESI-MS m/z 397.3 $(M - HCl - Cl^-)^+$, 199.1 $(M - 2Cl^-)^{2+}$. HRMS calcd. for $[C_{18}H_{33}N_6O_2S]^+$ 397.2386; found 397.2381.

(2*S*,8*S*)-2-Methanesulfonyloxymethyl-8-[(2*R*,8*R*)-8-methanesulfonyloxymethyl-3,4,6,7,8,9-hexahydro-2*H*-pyrimido[1,2-*a*]pyrimidin-2-ylmethylsulfanylmethyl-1-ium hexafluorophosphate]-3,4,6,7,8,9- hexahydro-2*H*-pyrimido[1,2-*a*]pyrimidin-1-ium hexafluorophosphate (6).

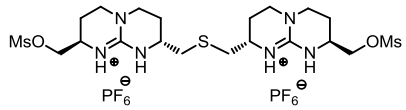

6

Compound **5** (610 mg, 1.04 mmol) and NMM (1.84 mL, 16.59 mmol) were mixed in dry CH_2Cl_2 (25 mL) under N_2 at 0 ºC and the mixture was stirred for 5-10 minutes. Then, Ms_2O (1.81 g, 10.37 mmol) was added and the stirring was continued for 24 h. The solution was directly washed with a 0.1N NH_4PF_6 solution (2 × 15 mL). The organic layer was filtered over cotton and left slowly to evaporate. A white precipitate was filtered off affording **6** (771 mg, 88%) as a yellowish oil. ^{1}H-NMR (400 MHz, CD_3CN) δ 6.60 (s, 2H, NH), 6.50 (s, 2H, NH), 4.32 (dd, J = 4.1, 10.5 Hz, 2H, CH_2O), 4.15 (dd, J = 7.1, 10.5 Hz, 2H, CH_2O), 3.87-3.77 (m, 2H, CH_α), 3.61-3.51 (m, 2H, CH_α), 3.44-3.29 (m, 8H, $CH_{2\gamma}$), 3.12 (s, 6H, CH_{3MsO}), 2.83 (dd, J = 5.4, 14.0 Hz, 2H, CH_2S), 2.64 (dd, J = 8.4, 13.9 Hz, 2H, CH_2S), 2.17-2.05 (m, 4H, $CH_{2\beta}$), 1.94-1.80 (m, 4H, $CH_{2\beta}$).^{13}C-NMR (100 MHz, CD_3CN) δ 150.4 (C_{guan}), 70.4 (CH_2O), 47.5, 47.4 (CH_α), 44.8, 44.4 ($CH_{2\gamma}$), 36.4 (CH_{3MsO}) 35.3 (CH_2S), 24.6, 21.3 ($CH_{2\beta}$). HRMS calcd. for $[C_{20}H_{38}N_6O_6S_3PF_6]^+$ 699.1657; found 699.1630.

(2*S*,8*S*)-2-(Acetylthiomethyl)-8-[(2*R*,8*R*)-8-(acetylthiomethyl)-2,3,4,6,7,8-hexahydro-1*H*-pyrimido[1,2-*a*]pyrimidin-9-ium-2-yl)methylthio)methyl)-2,3,4,6,7,8-hexahydro-1*H*-pyrimido[1,2-*a*]pyrimidin-9-ium hexafluorophosphate (7).

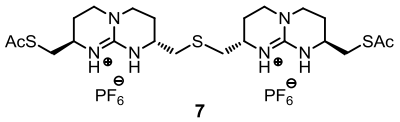

7

A mixture of **6** (250 mg, 0.296 mmol) and potassium thioacetate (203 mg, 1.776 mmol) in CH_3CN (20 mL) was stirred and refluxed overnight. Then, the solution was evaporated under vacuum, dissolved in CH_2Cl_2 and washed with a 0.1N NH_4PF_6 solution (2 × 20 mL). The organic layer was filtered over cotton and evaporated giving a crude residue which was purified by silica gel (with KPF_6) column chromatography (CH_2Cl_2/MeOH, 98:2 → 96:4), affording **7** (171 mg, 72%) as a brownish oil. ^{1}H-NMR (400 MHz, CD_3CN δ 6.15 (bs, 4H, NH), 3.63-3.49 (m, 4H, CH_α), 3.44-3.28 (m, 8H, $CH_{2\gamma}$), 3.14-3.03 (m, 4H, CH_2SCO), 2.78 (dd, J = 5.8, 13.7 Hz, 2H, CH_2S), 2.62 (dd, J = 7.9, 13.7 Hz, 2H, CH_2S), 2.40 (s, 6H, CH_3COS), 2.15-2.03 (m, 4H, $CH_{2\beta}$), 1.90-1.78 (m, 4H, $CH_{2\beta}$). ^{13}C-NMR (100 MHz, CD_3CN) δ 195.1 (SCO), 150.2 (C_{guan}), 47.6, 47.4 (CH_α), 44.8, 44.5 ($CH_{2\gamma}$), 37.5 (CH_2SCO), 35.3 (CH_2S), 30.8 (CH_3COS), 24.6, 21.5 ($CH_{2\beta}$). ESI m/z 659.4 $(M - PF_6^-)^+$, 513.6 $(M - PF_6^- - HPF_6^-)^+$.

Compound 71

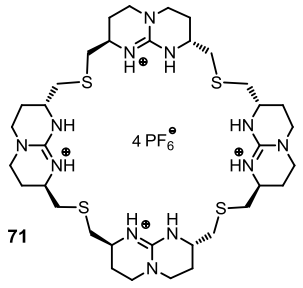

71

A solution of compound **7** (95 mg, 0.118 mmol), cesium carbonate (173 mg, 0.531 mmol) and $(^nBu)_2$PhP polystyrene resin (323 mg, 0.260 mmol) in dry MeOH (40 mL)

was stirred under inert atmosphere for 20 minutes. Then, a solution of compound **6** in MeCN (100 mL) was added dropwise and the final mixture was stirred for 2 days. The phosphine resin was filtered off and the solvent was evaporated under vacuum, dissolved in CH_2Cl_2 and washed with a 0.1N NH_4PF_6 solution (3 × 30 mL). The organic phase was filtered over cotton and concentrated to dryness to give a crude residue which was purified by silica gel (with KPF_6) column chromatography (CH_2Cl_2/MeOH, 100:0 → 94:6), affording cyclic tetraguanidinium **71** (60 mg, 41%) as a pale yellow solid. ^{1}H-NMR (400 MHz, CD_3CN:D_2O (3:1)) δ 3.58-3.45 (m, 8H, CH_α), 3.41-3.25 (m, 16H, $CH_{2\gamma}$), 2.91-2.77 (m, 8H, CH_2S), 2.68-2.52 (m, 8H, CH_2S), 2.15-2.02 (m, 8H, $CH_{2\beta}$), 1.87-1.67 (m, 8H, $CH_{2\beta}$). ^{13}C-NMR (100 MHz, CD_3CN) δ 151.2, 151.1 (C_{guan}), 48.4, 48.2, 47.5 (CH_α), 45.0, 44.9, 44.8 ($CH_{2\gamma}$), 37.8, 37.5, 36.3 (CH_2S), 25.7, 25.4, 25.3, 22.5 ($CH_{2\beta}$). MALDI *m/z* 789.6 (M - PF_6^- -3HPF_6^-)$^+$. HRMS calcd. for $[C_{36}H_{61}N_{12}S_4]^+$ 789.4019; found 789.4458.

(2*S*,8*S*)-2,8-Bis-(hydroxymethyl)-3,4,6,7,8,9-hexahydro-2*H*-pyrimido-[1,2-*a*]-pyrimidin-1-ium chloride (72)

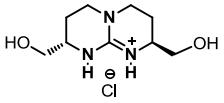

A solution of **1** (3 g, 5.1 mmol) in 3N HCl/CH_3CN (1:2, 75 mL) was stirred at room temperature for 2 days. The solvent was removed and the resulting crude was dissolved in H_2O (50 mL) and washed with CH_2Cl_2 (4 × 50 mL). The aqueous phase was evaporated under reduced pressure affording **72** (1.16 mg, 97%) as a white solid. Mp 178-180°C. $[\alpha]^{25}_D$ -64 (c = 0.5, H_2O). ^{1}H-NMR (400 MHz, D_2O) δ 3.46 (m, 2H, CH_2O), 3.35 (m, 2H, CH_2O), 3.32 (m, 2H, CH_α), 3.26-3.13 (m, 4H, $CH_{2\gamma}$), 1.86-1.66 (m, 4H, $CH_{2\beta}$). ^{13}C-NMR (100 MHz, D_2O) δ 151.2 (C_{guan}), 64.3 (CH_2OSi), 48.8 (CH_α), 45.0 ($CH_{2\gamma}$), 22.7 ($CH_{2\beta}$). ESI *m/z* 200.13 [(M - Cl^-)$^+$, 100%].

4.7.3 ^{1}H-NMR complexation host-guest studies

These experiments were done mixing 1:1 equivalents of the host and the guest, in

the solvents specified before. All trials were made at the millimolar range concentration.

4.7.4 Variable temperature ^{1}H-NMR experiments

These experiments required the formation of the tetrabutylammonium salt of the corresponding calix[4]arene for solubility. After adding 4 equivalents of 1M tetrabutylammonium hydroxide solution to 1 equivalent of tetraacid calix[4]arene, the mixture was evaporated until dryness. Then, another equivalent of tetraguanidinium salt was added and the resulting powder was dissolved in the methanol:acetonitrile mixture as previously described.

4.7.5 ITC studies

The general conditions for the performance of these experiments consist of previously dissolving all the species in THF/H_2O (8:2), and adding a 4 mM solution of oxoanionic calix[4]arene (syringe) over a 0.5 mM solution of the cyclic tetraguanidine at 25 ºC.

4.7.6 Host-Guest encapsulation experiments

These experiments were done in (3:1) THF/D_2O in the millimolar range (between 2 and 10 mM), successively adding different amounts of isoquinolinium guests (**73** and **74**) to tetraguanidinium calixarenate (**71@d**) complex.

UNIVERSITAT ROVIRA I VIRGILI
BICYCLIC GUANIDINIUM OLIGOMERS FOR RECOGNITION, CELL DELIVERY, AND MOLECULAR MATERIALS
Julián Valero Moreno
DL:T. 276-2012

UNIVERSITAT ROVIRA I VIRGILI
BICYCLIC GUANIDINIUM OLIGOMERS FOR RECOGNITION, CELL DELIVERY, AND MOLECULAR MATERIALS
Julián Valero Moreno
DL:T. 276-2012

Chapter 5

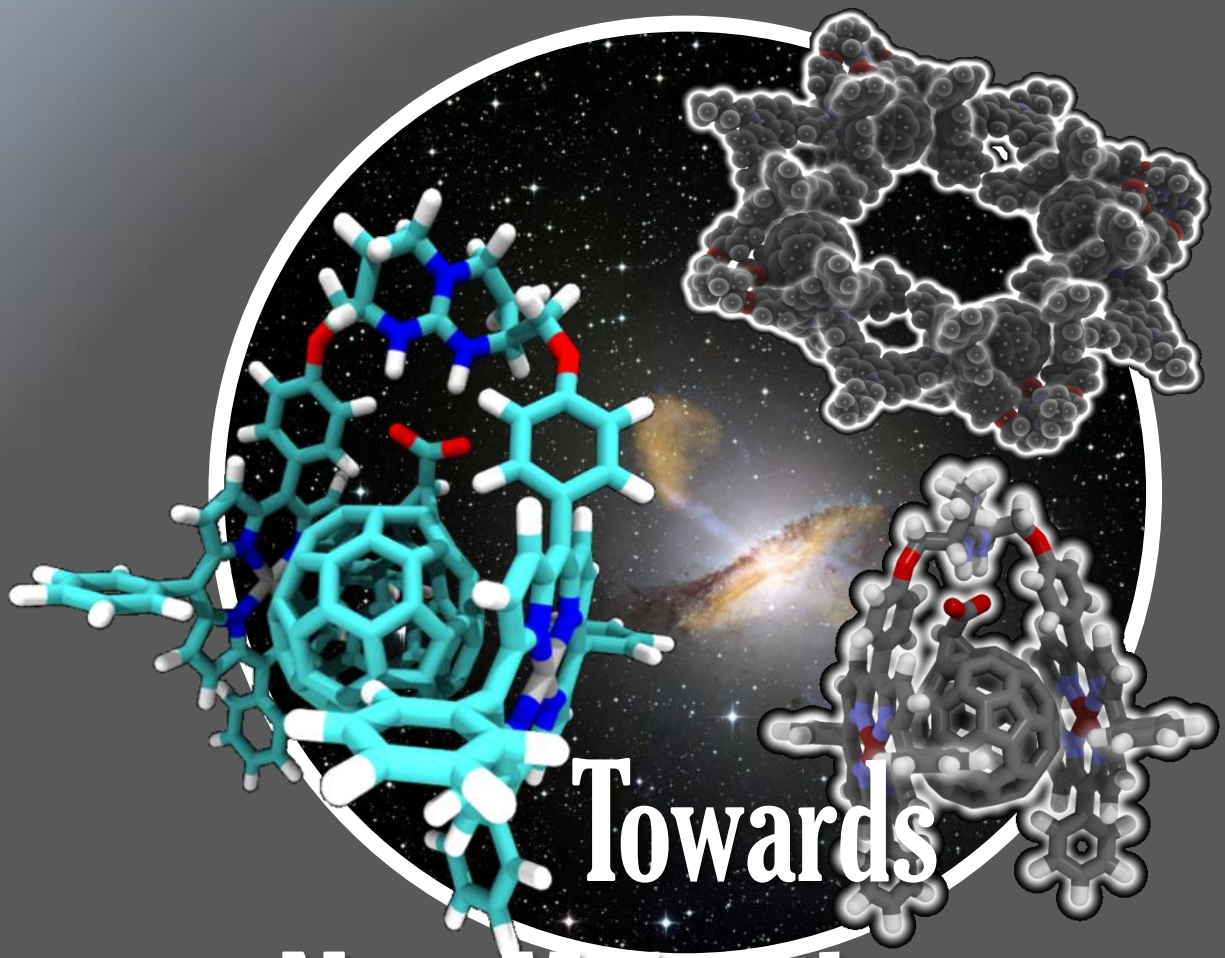

Towards New Molecular Materials

UNIVERSITAT ROVIRA I VIRGILI
BICYCLIC GUANIDINIUM OLIGOMERS FOR RECOGNITION, CELL DELIVERY, AND MOLECULAR MATERIALS
Julián Valero Moreno
DL:T. 276-2012

Chapter 5

Guanidinium Bis-porphyrin Tweezers for the Complexation of Fullerene Carboxylate Derivatives

5.1 Introduction

Fullerene-porphyrin dyads have been widely studied over the last decade, not only for their inherent strong affinity but also for the attractive electronic and photophysical properties they display.[1] Charge transfer processes have been described between the electron-rich porphyrin and the electron-acceptor fullerene, similar to those observed in natural photosynthetic systems.[2] Most strategies for the construction of these supramolecular complexes consist of a careful design of porphyrin-based receptors which bind strongly to the fullerene guest, resulting in the assembly of stable and

[1] (a) Guldi, D. M. *Chem. Commun.* **2000**, 321-327. (b) Sun, D.; Tham, F. S.; Reed, C. A.; Boyd, P. D. W. *Proc. Natl. Acad. Sci. USA* **2002**, *99*, 5088-5092. (c) Guldi, D. M. *Chem. Soc. Rev.* **2002**, *31*, 22-36. (d) Boyd, P. D. W.; Reed, C. A. *Acc. Chem. Res.* **2005**, *38*, 235-242. (e) Tashiro, K.; Aida, T. *Chem. Soc. Rev.* **2007**, *36*, 189-197.

[2] (a) Gust, D.; Moore, T. A.; Moore, A. L. *Acc. Chem. Res.* **2001**, *34*, 40-48. (b) Imahori, H.; Fukuzumi, S. *Adv. Func. Mater.* **2004**, *14*, 525-536.

robust architectures. In particular, major efforts have been focused in the design of dimeric porphyrin systems. Aida and co-workers reported the first cyclic bis-porphyrin host **I** for fullerene recognition in 1999 (Figure 1).[3] This macrocyclic receptor contained two Zn-porphyrins tied together *via* hexyl bridges and exhibited efficient C_{60} inclusion through π-electron donor-acceptor interactions, with high binding affinities (6.7×10^5 M^{-1}). By exchanging the Zn metal for Rh or Ir, the association constants further experienced a 10^3-fold increase.[4] Other modifications of this original scaffold have been recently reported to allow the enantiomeric spectroscopic resolution of chiral (±)-C_{76}.[5]

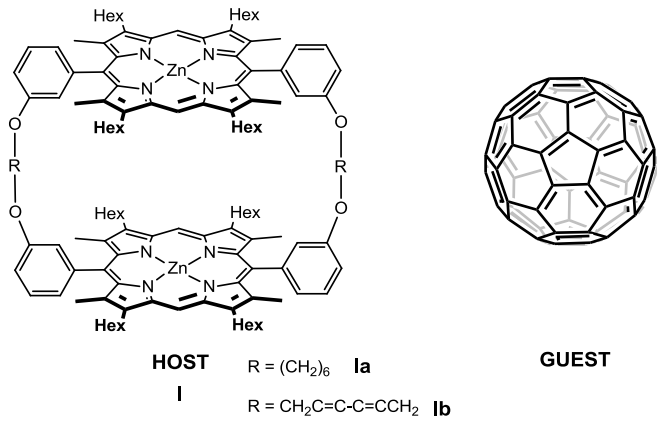

Figure 1*. Macrocyclic bis-porphyrin host* ***I*** *reported by Aida et al.*[3]

[3] Tashiro, K.; Aida, T.; Zheng, J.-Y.; Kinbara, K.; Saigo, K.; Sakamoto,. S.; Yamaguchi, K. *J. Am. Chem. Soc.* **1999**, *121*, 9477-9478.

[4] (a) Zheng, J. Y.; Tashiro, K.; Hirabayashi, Y.; Kinbara, K.; Saigo, K.; Aida, T.; Sakamoto, S.; Yamaguchi, K. *Angew. Chem. Int. Ed.* **2001**, *40*, 1857-1861. (b) Tashiro, K.; Hirabayashi, Y.; Aida, T.; Saigo, K.; Fujiwara, K.; Komatsu, K.; Sakamoto, S.; Yamaguchi, K. *J. Am. Chem. Soc.* **2002**, *124*, 12086-12087. (c) Yanagisawa, M.; Tashiro, K.; Yamasaki, M.; Aida, T. *J. Am. Chem. Soc.* **2007**, *129*, 11912-11913.

[5] Shoji, Y.; Tashiro, K.; Aida, T. *J. Am. Chem. Soc.* **2010**, *132*, 5928-5929.

The first acyclic bis-porphyrin receptor was described by Boyd *et al.*[6] This "jaws porphyrin" host **II** was formed through a $PdCl_2$ linkage between two *meso*-pyridyl functionalized porphyrins (Figure 2). An association constant of 5.2 x 10^3 M^{-1} was determined for C_{60} by ^{13}C-NMR titrations. The study was extended by introduction of novel covalently-attached jaws porphyrin structures.[7] The effect of the porphyrin metal on the binding of C_{60} and C_{70} guests was also assessed. Unexpectedly, the free-base bis-porphyrins showed higher binding affinities as compared to the metallated ones. Another example based on a metallo-bridge acyclic bis-porphyrin receptor was reported by Shinkai and co-workers.[8] They reported a covalently linked tweezer structure which was capable of switching from the *anti* to the *syn* conformation by coordination with a Pd(II) complex. Indeed, the *syn* conformer was able to bind C_{60} (5.1 x 10^3 M^{-1}) due to the cleft formed between the porphyrins.

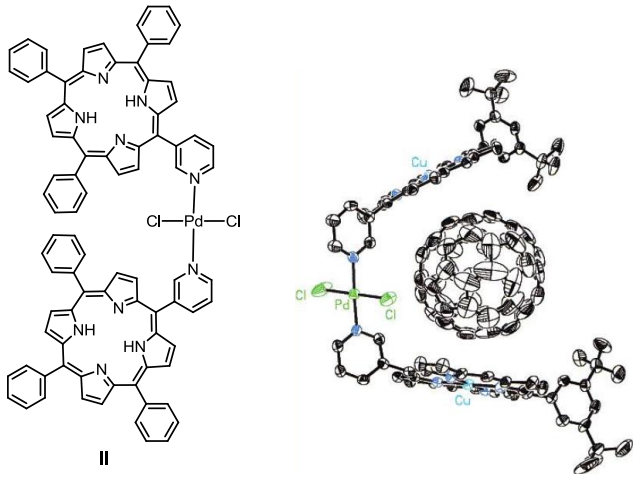

***Figure 2**. "Jaws" porphyrin receptor **II** reported by Boyd et al.*[6]

[6] Sun, D.; Tham, F. S.; Reed, C. A.; Chaker, L.; Burgess, M.; Boyd, P. D. W. *J. Am. Chem. Soc.* **2000**, *122*, 10704-10705.

[7] Sun, D. Y.; Tham, F. S.; Reed, C. A.; Chaker, L.; Boyd, P. D. W. *J. Am. Chem. Soc.* **2002**, *124*, 6604-6612.

[8] Ayabe, M.; Ikeda, A.; Shinkai, S.; Sakamoto, S.; Yamaguchi, K. *Chem. Commun.* **2002**, 1032-1033.

Li and co-workers reported an elegant example of tweezer-like structures based on hydrogen-bonded preorganized architectures (Figure 3).[9] Different aryl amide frameworks were employed in the design. However, only receptor **III** with a suitable porphyrin separation to encapsulate fullerenes showed high binding affinities (from 10^5 to 10^6 M^{-1}, depending on the fullerene guest). Addition of a competitive solvent such as methanol to the system resulted in a drop of affinity constants by about two orders of magnitude. This suggests that disruption of the hydrogen-bonded network caused by the polar solvent hampers its preorganization. A similar water-soluble receptor **IV** was designed to effectively encapsulate fullerene dicarboxylate derivatives in polar solvents (K_a = 1.1 x 10^5 M^{-1}).[10] In this particular system, the binding is mainly driven by electrostatic interactions, which compensates the loss of the preorganized hydrogen-bonded structure.

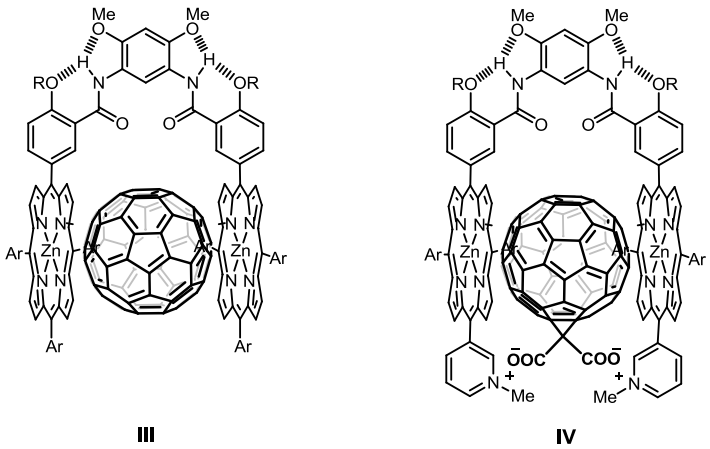

***Figure 3**. Amide-based bis-porphyrin receptors described by Li et al.*[9,10]

[9] Wu, Z.-Q.; Shao, X.-B.; Li, C.; Hou, J.-L.; Wang, K.; Jiang, X.-K.; Li, Z. T. *J. Am. Chem. Soc.* **2005**, *127*, 17460-17468.

[10] Liu, H.; Wu, J.; Jiang, X.-K.; Li, Z.-T. *Tetrahedron Lett.* **2007**, *48*, 7327-7331.

There are several reports on tweezer bis-porphyrin receptors using calix[4]arenes as central supramolecular scaffolds.[11] The calixarene scaffold provides the necessary cofacial arrangement of the alternated substituents for the design of porphyrin-based fullerene receptors. Indeed, lower and upper rim bis-porphyrin 1,3-substituted calix[4]arenes, as well as more sophisticated ones such as thiocalix[4]arene-based receptors,[12] have been reported to efficiently bind fullerene guest molecules.

Supramolecular fullerene@bis-porphyrin interactions have been further explored in the stabilization and isolation of potential bullvalene bis-porphyrin receptors from a population of hundreds of interconverting structural isomers. Indeed, binding studies of a bullvalene-based receptor with C_{60} demonstrated the shifting of the dynamic isomeric equilibrium towards the most favourable isomers for the encapsulation of a fullerene guest (Figure 4).[13]

[11] (a) Dudič, M.; Lhoták, P.; Král, V.; Lang, K.; Stibor, I. *Tetrahedron Lett.* **1999**, *40*, 5949-5952. (b) Dudič, M.; Lhoták, P.; Stibor, I.; Dvořáková, H.; Lang, K. *Tetrahedron* **2002**, *58*, 5475-5482. (c) Dudič, M.; Lhoták, P.; Stibor, I.; Lang, K.; Prošková, P. *Org. Lett.* **2003**, *5*, 149-152. (d) Dudič, M.; Lhoták, P.; Petříčková, H.; Stibor, I.; Lang, K.; Sýkora, J. *Tetrahedron* **2003**, *59*, 2409-2415. (e) Hosseini, A.; Taylor, S.; Accorsi, G.; Armaroli, N.; Reed, C. A.; Boyd, P. D. W. *J. Am. Chem. Soc.* **2006**, *128*, 15903-15913.

[12] (a) Dudič, M.; Lhoták, P.; Stibor, I.; Petříčková, H.; Lang, K. *New J. Chem.* **2004**, *28*, 85-90. (b) Kundrát, O.; Tkadlecová, M.; Lang, K.; Cvacka, J.; Stibor, I.; Lhoták, P. *Tetrahedron. Lett.* **2007**, *48*, 6620-6623.

[13] (a) Lippert, A. R.; Keleshian, V. L.; Bode, J. W. *Org. Biomol. Chem.* **2009**, *7*, 1529-1532. (b) Lippert, A. R.; Naganawa, A.; Keleshian, V. L.; Bode, J. W. *J. Am. Chem. Soc.* **2010**, *132*, 15790-15799.

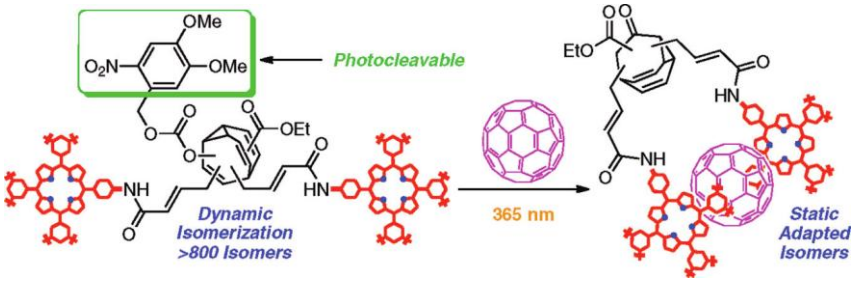

Figure 4. *Bullvalene-based acyclic bis-porphyrin receptor (reproduced from ref. 13b).*

A novel example of a cyclic bis-porphyrin fullerene receptor was reported using dynamic combinatorial chemistry with disulfide bridges as linkage between the porphyrin molecules.[14] These flexible connections afforded the complexation with fullerene guests among with other ditopic amines such DABCO or 4,4'-bipyridine. Conversely, a rigid porphyrin dimer was described by Tani and co-workers.[15] This cyclic bis-porphyrin was attached by butadiyne moieties and contained up to four *p*-pyridyl groups that formed stable hydrogen bonds with the pyrrole-β CH protons of a contiguous cyclic porphyrin. Hence, the bis-porphyrin molecules self-assembled into tubular arrays capable of entrapping C_{60} guests.

Although most of the reported fullerene receptors based on the porphyrin moiety are dimers, there are also relevant examples on extended porphyrin as trimeric, tetrameric or even hexameric assemblies (Figure 5). In this context, Anderson and co-workers reported a cyclic porphyrin trimer (**V**) able to strongly bind C_{60} and C_{70} (K_a = 2 x 10^6 and 2 x 10^8 M^{-1} in toluene, respectively). Indeed, this receptor showed increased affinity for higher fullerenes and endohedral fullerenes such as C_{86} or La@C_{82}.[16] As an example of a tetramer-based receptor, the Ni-porphyrin nano-barrel

[14] Kieran, A. L.; Pascu, S. I.; Jarrosson, T.; Sanders, J. K. M. *Chem. Commun.* **2005**, 1276-1278.
[15] (a) Nobukuni, H.; Shimazaki, Y.; Tani, F.; Naruta, Y. *Angew. Chem. Int. Ed.* **2007**, *46*, 8975-8978. (b) Nobukuni, H.; Shimazaki, Y.; Uno, H.; Naruta, Y.; Ohkubo, K.; Kojima, T.; Fukuzumi, S.; Seki, S.; Sakai, H.; Hasobe, T.; Tani, F. *Chem. Eur. J.* **2010**, *16*, 11611-11623.
[16] Gil-Ramírez, G.; Karlen, S. D.; Shundo, A.; Porfyrakis, K.; Ito Y.; Briggs, G. A. D.; Morton, J. J. L.; Anderson H. L. *Org. Lett.* **2010**, *12*, 3544-3547.

VI was reported to effectively encapsulate C_{60}.[17] This barrel-like structure was synthesized by a convenient 2+2 Suzuki cross-coupling between a tetraboronylporphyrin and a tetra(-6-bromopyridyl)porphyrin, giving rise to a structure composed of four covalently attached porphyrin walls on a concave shape. The X-ray crystal structure confirmed the inclusion of a C_{60} molecule in the void of this porphyrin nano-wheel. Recently, a cubic porphyrin self-assembled array (**VII**) was described by Nitschke *et al.*[18] This hexameric architecture is bridged through six C_3 symmetric iron (II) tris(bipyridylimine) centers. Moreover, large π-electron rich guests (i.e. coronene, C_{60} and C_{70}) were accommodated inside this cubic receptor.

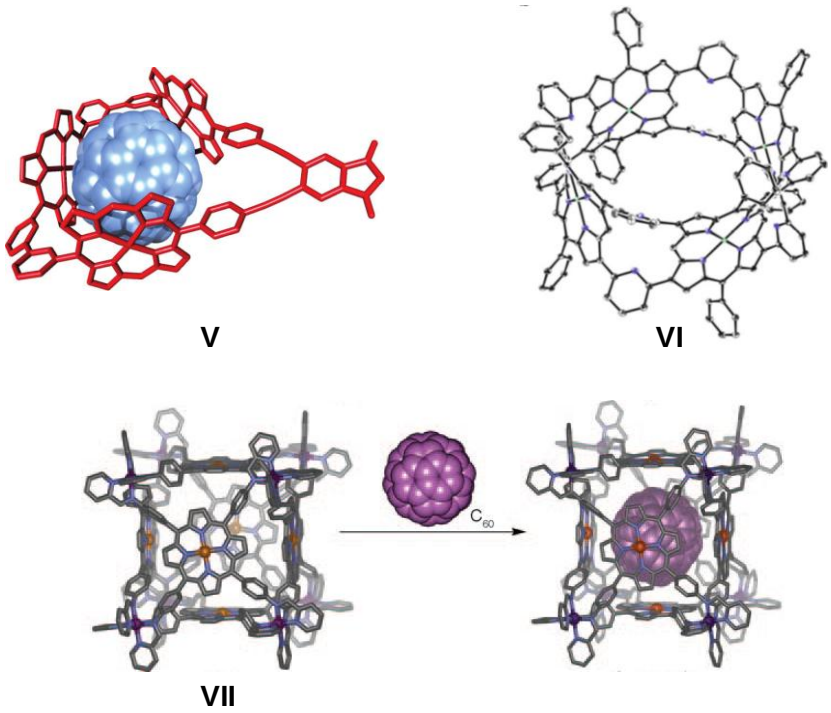

Figure 5. *Porphyrin receptors based on trimeric,*[16] *tetrameric,*[17] *and hexameric*[18] *assemblies (reproduced from the corresponding references).*

[17] Song, J.; Aratani, N.; Shinokubo, H.; Osuka, A. *J. Am. Chem. Soc.* **2010**, *132*, 16356-16357.

[18] Meng, W.; Breiner, B.; Rissanen, K.; Thoburn, J. D.; Clegg, J. K.; Nitschke, J. R. *Angew. Chem. Int. Ed.* **2011**, *50*, 3479-3483.

Our research group has extensively worked in the design of new supramolecular fullerene receptors. In particular, the CTV-based dimeric capsule **VIII** was found to bind different fullerene derivatives upon ureidopyrimidinone hydrogen bonding self-assembly (Figure 6).[19] Indeed, these concave capsules showed high selectivity towards C_{84}, allowing its enrichment from fullerene mixtures.[20] Tripodal exTTF-CTV host **IX** was also reported to bind fullerenes by a combination of shape and charge complementarity with high affinity ($K_a > 10^5$ M^{-1}).[21]

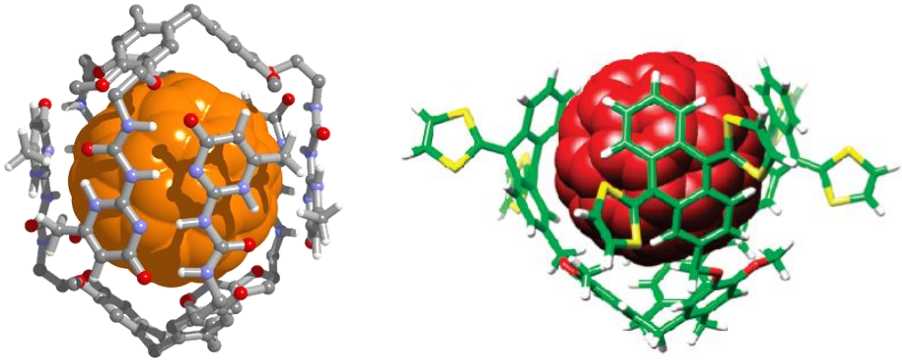

Figure 6. *Model of the CTV-ureidopyrimidinone capsule* ***VIII*** *and CTV-exTTF host* ***IX*** *with* C_{60} *guests.*

On the other hand, the synthesis and the study of stable supramolecular donor-acceptor dyads (**Xa-b** and **XIa-b**) were reported in our laboratories.[22] The approach consisted of the assembly of the electron rich C_{60} derivative with a donor tetrathiafulvalene (TTF) moiety through complementary guanidinium-carboxylate

[19] Huerta, E.; Metselaar, G. A.; Fragoso, A.; Santos E.; Bo, C.; de Mendoza, J. *Angew. Chem. Int. Ed.* **2007**, *46*, 202-205.

[20] Huerta, E.; Cequier, E.; de Mendoza, J. *Chem. Commun.* **2007**, 5016-5018.

[21] Huerta, E.; Isla, H.; Pérez, E. M.; Bo, C.; Martín, N.; de Mendoza, J. *J. Am. Chem. Soc.* **2010**, *132*, 5351-5353.

[22] Segura, M.; Sanchez, L.; de Mendoza, J.; Martin, N.; Guldi, D. M. *J. Am. Chem. Soc.* **2003**, *125*, 15093-15100.

interactions (Figure 7). From the spectroscopic characterization, formation of charge-separated radical pairs $C_{60}^{\bullet-}$-$TTF^{\bullet+}$, exhibiting lifetimes in the range of hundreds of nanoseconds, was demonstrated. Indeed, the flexibility of the system and the spatial proximity of the two moieties *via* non-covalent interactions facilitate through-space electron-transfer processes.

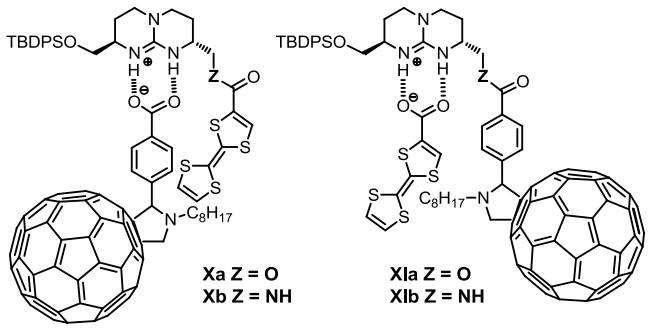

Figure 7. *TTF-C_{60} assemblies based on carboxylate-guanidinium dyads reported by de Mendoza et al.*[22]

5.2 Objectives

To further expand the robustness and possibilities of these systems we describe herein the synthesis and properties of guanidinium bis-porphyrin **75** which has been specifically designed to interact with fullerene carboxylate **76** (Figure 8). It is expected that this novel dyad will increase the stability and the strength of the complex with respect to the previously reported dyads, and would likely display interesting photoelectronic properties.

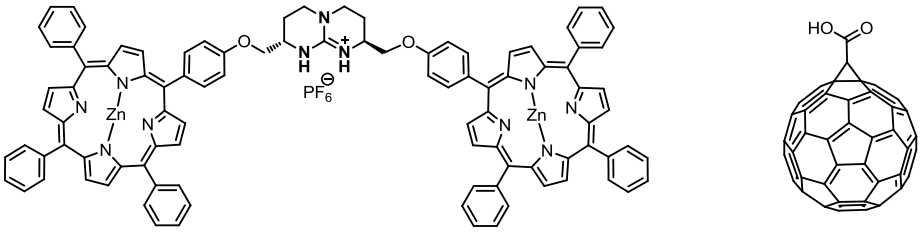

75 **76**

Figure 8. *Guanidinium bis-porphyrin host* ***75*** *and fullerene carboxylate guest* ***76****.*

With this aim, we decided to replace the TTF moiety by two Zn-porphyrins attached to the guanidinium scaffold. This porphyrin-based tweezer should show effective interaction with fullerene molecules, as the porphyrin molecules are facing each other with the right spacer to accommodate these large aromatic guests. In terms of complementarity, fullerenes act as electron-withdrawing molecules and thus are known to bind strongly to electron-rich aromatic surfaces, such as porphyrins. Depending on their association and proximity, electron transfer effects can occur between both systems. Bicyclic guanidines bind a wide variety of anions, in particular oxoanions due to the possibility of establishing well oriented hydrogen-bonded ion pairs.[23] Thus, the

[23] Blondeau, P.; Segura, M.; Pérez-Fernández, R.; de Mendoza, J. *Chem. Soc. Rev.* **2007**, *36*, 198-210.

guanidinium scaffold not only acts as a structural linker between the two porphyrins but it has an active role to complement anionic guests. In fact, (1,2-methanofullerene C_{60})-61-carboxylic acid **76** seems to fit nicely with the geometrical and electronic requirements of supramolecular host **75**. We will evaluate the binding affinity of receptor **75** for both C_{60} and carboxylate C_{61} molecules. Furthermore, the contribution of each binding motif will be evaluated by comparison with suitable models, to allow an estimation of cooperative effects.

Photophysical measurements will afford information about possible electron/energy-transfer processes. Finally, inspired by biological photosynthetic systems, we will try to self-assemble several fullerene@bis-porphyrin complexes by using a bipyiridine carbazole linker which would eventually coordinate with the Zn centres of these constructs, in a wheel-like supramolecular assembly (Figure 9).

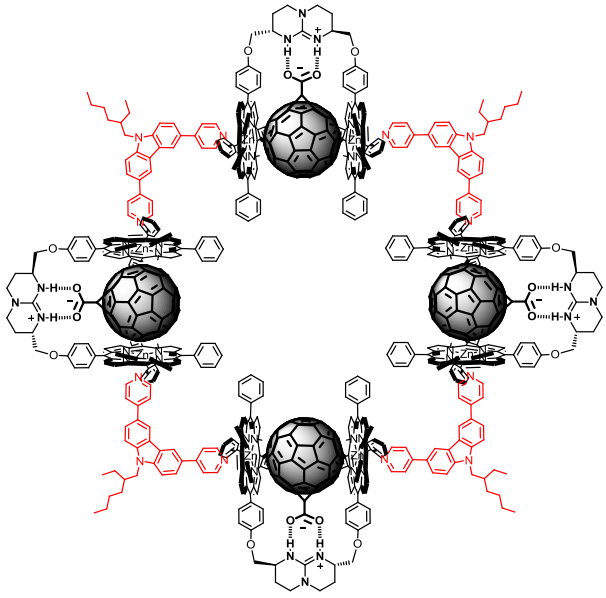

Figure 9. *Expected tetrameric assembly by the coordination of four bipyridines to the Zn centers of* ***76@75*** *complex.*

5.3 Design and Synthesis of Guanidinium Bis-porphyrin Tweezer

The choice of the spacer and bonding between the guanidinium scaffold and the porphyrin moieties was evaluated by molecular modeling. The ether linkage fits nicely with the geometrical and spatial requirements of the complex. Longer spacers would increase the distance between the porphyrin planes and also with the bicyclic guanidinium scaffold, disfavouring binding of the fullerene carboxylate guest. Indeed, subtle structural considerations are essential for the design of this receptor. For instance, *p*-phenoxy-porphyrins are required to afford the correct geometry for guest complexation. As shown in Figure 10, the molecular model of complex **76@75** indicates that the porphyrin planes are at a 12.2 Å distance in a parallel orientation, thus inducing a proper fitting with the C_{60} scaffold. A search through the Cambridge Structural database[16] indicates that average distance between the centroids of the Zn-porphyrin plane and C_{60} was 6.28±0.08 Å (mean value for 21 C_{60}@Zn-porphyrin co-crystal structures). This value is consistent with the calculated for our **76@75** complex. With *meso*-substitution, the distance between porphyrins in parallel disposition would be above 14 Å, and therefore the porphyrins would be forced to bend to provide a proper complexation with fullerene guests. Moreover, *meso* substituted porphyrins would remain too close to the guanidinium scaffold, and thus would not allow the suitable orientation and distance to form simultaneously the salt bridge with the carboxylate and the corresponding π-electron interactions with the fullerene.

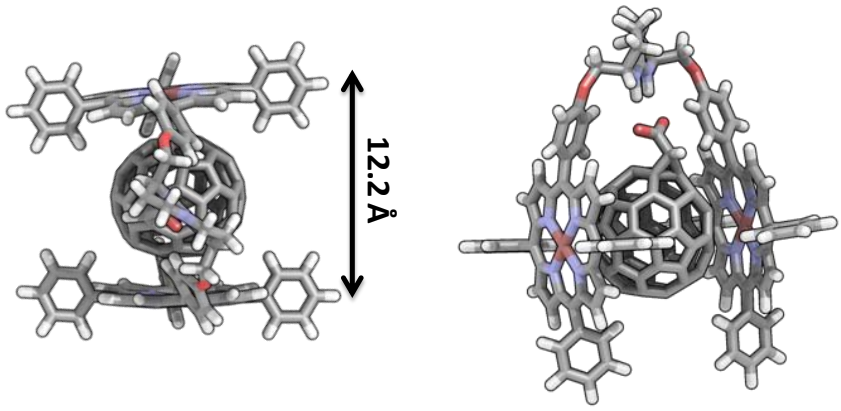

Figure 10. *Optimized structure (SCIGRESS, standard conditions, no solvent) of the* ***76@75****complex in top view (left) and front view (right). Zn-fullerene distance is ca. 3.2 Å.*

Nevertheless, the acyclic receptor **75** is highly adaptable since the porphyrins are only tethered from one side. However, the binding of fullerene guest **76** should restrict the conformation of the molecule, thus favouring the parallel conformation of the two porphyrins as shown in molecular models.

The *Zn-meso*-5-(4'-hydroxyphenyl)-10,15,20-triphenylporphyrin (**77**) was synthesized as reported,[24] by mixing statistical proportions of the corresponding benzaldehydes with freshly distilled pyrrole and refluxing in propionic acid. On the other hand, guanidinium bis-porphyrin tweezer receptor was prepared by *O*-alkylation of **77** with guanidinium compound **78** in 42% yield. Previous zinc metallation of the porphyrin is necessary in order to avoid the undesired *N*-alkylation of the pophyrin nitrogens (Scheme 1).

[24] Slagt, V. F.; van Leeuwen, P. W. N. M.; Reek, J. N. H. *Chem. Commun.* **2003**, 2474-2475.

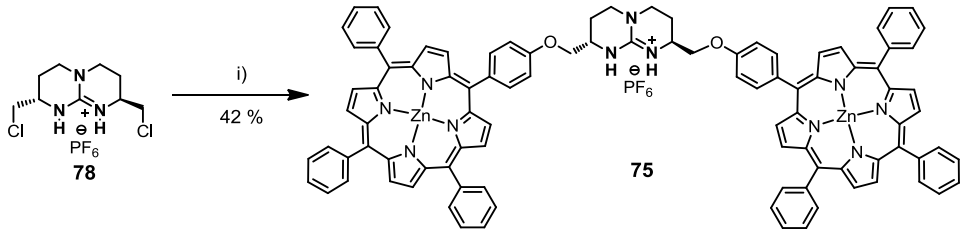

Scheme 1. *Synthesis of guanidinium bis-porphyrin tweezer* ***75****. Conditions: i) 2.2 eq. of* ***77****, 4.5 eq.* K_2CO_3*, acetone, reflux.*

The (1,2-methanofullerene C_{60})-61-carboxylic acid guest **76** is commercially available. The corresponding carboxylate tetrabutylammonium salt was prepared by addition of equimolar amounts of tetrabutylammonium hydroxide to a solution of **76** in *o*-dichlorobenzene to improve the solubility of this aromatic guest.

Guanidinium hexafluorophosphate salt **79** was prepared as a control receptor for the individual assessment of the guanidinium-carboxylate contribution to the overall binding with guest **76**. Synthesis of **79** was achieved as previously described by *O*-alkylation of phenol with guanidinium **78** (Scheme 2, see details in the experimental section).

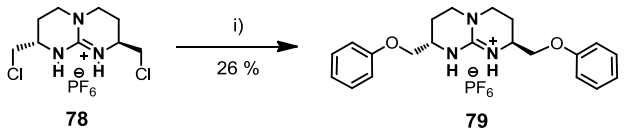

Scheme 2. *Synthesis of bis-aryl guanidinium control* ***79****. Conditions: i) 2.9 eq. of phenol, 5 eq.* K_2CO_3*, acetone, reflux.*

Finally, guanidinium mono-porphyrin compound **80** was synthetized as a reference molecule to gain a better insight into the thermodynamics of the association process, including the determination of the effective molarity (EM) and the assessment of the cooperative factor. Following the methodology depicted above, *O*-alkylation of Zn-

phenolporphyrin **77** with mono-protected guanidine **81**[25] afforded compound **80** in good yields (Scheme 3).

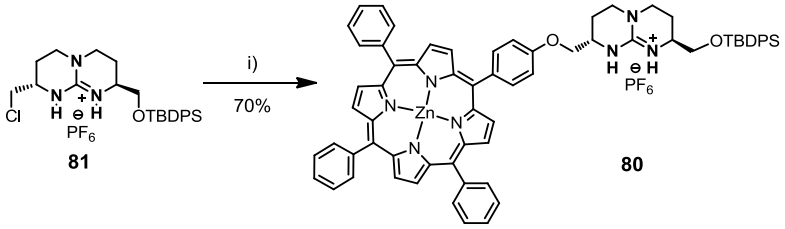

Scheme 3. *Synthesis of guanidinium mono-porphyrin compound **80**. Conditions i) 1.5 eq of **81**, 1 eq. of **77**, 1.5 eq. K_2CO_3, acetone, reflux.*

[25] Sánchez-Quesada, J. *PhD Thesis*, Universidad Autónoma de Madrid, **1996**.

5.4 Preliminary Complexation Studies with C_{60} and C_{61}-Carboxylate

In order to evaluate the binding mode and association constants of receptor **75** with C_{60} and fullerene-carboxylate **76**, preliminary ^{1}H-NMR experiments were performed. As shown in Figure 11, only small changes were observed upon addition of C_{60} to the guanidinium bis-porphyrin receptor in deuterated toluene.

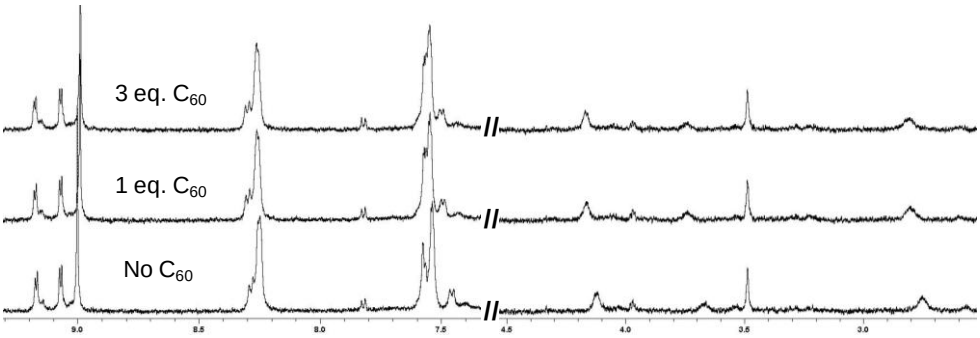

Figure 11. *^{1}H-NMR spectra (in toluene-d_8) of bis-pophyrin receptor* ***75*** *with and without C_{60} in toluene.*

In contrast, ^{13}C-NMR spectrum of the complex in tetrachloroethane showed an upfield shift of the C_{60} signal accounting for an effective guest complexation as previously reported by Boyd *et al.*[7] C_{60} has a unique ^{13}C signal due to the equivalence of all its carbons. Complexation results in a chemical shift (average signal corresponding to free and complexed fullerene) (Figure 12). Upon heating, the stability of the complex decreases, and the signal shifts towards the resonance for free C_{60}. On the contrary, the association process becomes more favorable at lower temperatures. However, we were unable to reach the coalescence temperature where the equilibrium is slow enough to detect both signals accounting for the bound and free species.

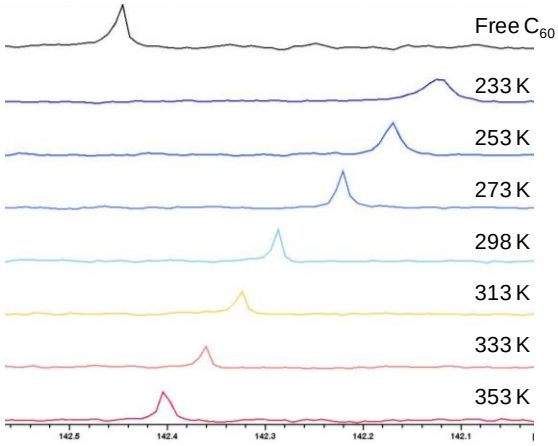

Figure 12. *^{13}C-NMR spectra (in TCE-d_2) of free and bound C_{60} guest.*

The **C_{60}@75** complex was further characterized by mass spectrometry analysis (ESI M^+ = 2269.5 *m/z* for the complex and M^+ = 1548.5 *m/z* for receptor **75** alone). As shown in Figure 13, the experimental and the calculated isotopic pattern fit nicely.

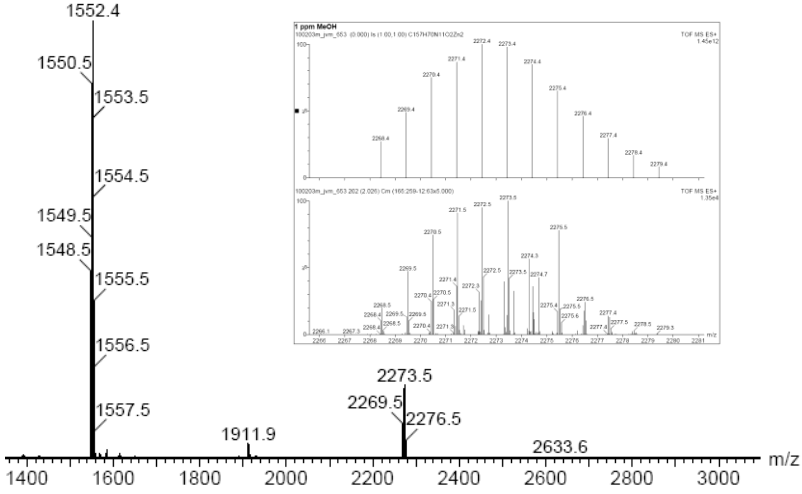

Figure 13. *Mass profile of the C_{60}@**75** complex.*

Therefore, it can be concluded that guanidinium bis-porphyrin receptor **75** binds C_{60}

and this interaction has been unambiguously assessed by means of ^{13}C-NMR spectroscopy and mass spectrometry. Quantification of the binding affinity for this supramolecular dyad was further assessed by UV-vis titration experiments (see section 5.5).

Preliminary ^{1}H-NMR titrations were also performed with fullerene carboxylate guest **76**. As with C_{60}, the spectra showed minor chemical shifts in *o*-dichlorobenzene (Figure 14). Upfield shifts of the guanidinium protons suggested a structural rearrangement of the flexible scaffold in order to maximize and enhance the interaction with the fullerene-carboxylate guest. Aromatic protons in the *ortho* positions of the phenoxy moieties also showed both upfield shifts and broadening. Moreover, complex **76@75** was also detected by mass spectrometry analysis (MALDI m/z 2328 (M^+)).

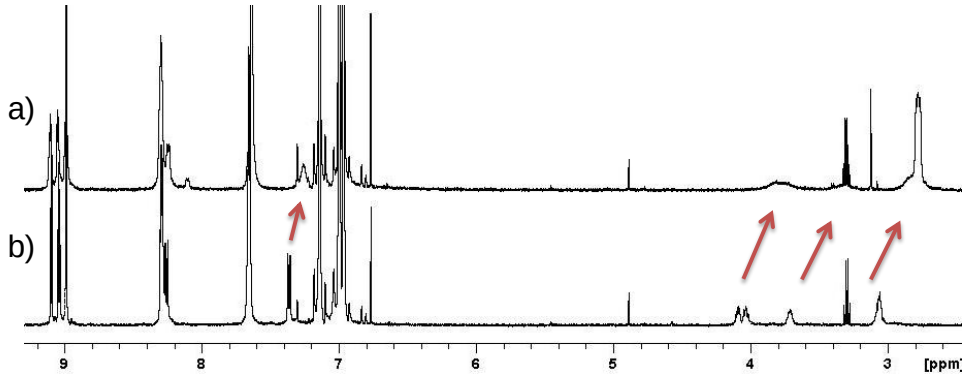

Figure 14. *^{1}H-NMR spectra (in ODB-d_4) of guanidinium bis-porphyrin host* ***75*** *in presence (a) and absence (b) of tetrabutylammonium fullerene-carboxylate guest* ***76****.*

Finally, ^{1}H-NMR titration in chlorobenzene-d_5 of model receptor **79** with fullerene-carboxylate **76** was performed in order to assess the binding contribution of the guanidinium-carboxylate salt bridge. As depicted in Figure 15, the downfield shift of the guanidinium protons upon complexation was used to estimate an association constant of 3.3 x 10^3 M^{-1} for this system. This value is consistent with the association constants previously determined for other guanidinium carboxylate systems in non-

polar media.[23,26]

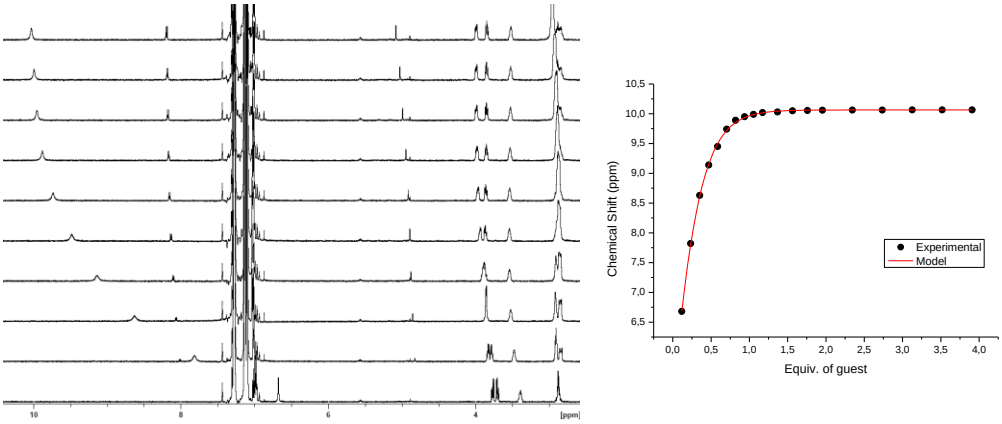

Figure 15. *^{1}H-NMR titration in chlorobenzene-d_5 of model guanidinium* ***79*** *with fullerene-carboxylate* ***76****.*

Thus, preliminary ^{1}H-NMR studies and mass spectrometry analysis of the complexes demonstrated the interaction of C_{60} and fullerene carboxylate guest **76** with receptor **75**. By means of variable temperature ^{13}C-NMR studies the encapsulation of C_{60} with the bis-porphyrin tweezer receptor **75** was demonstrated. The nature of this complexation relies on the electronic complementarity between the electron rich porphyrin tweezer and the electron poor fullerene. With the fullerene-carboxylate guest, the higher chemical shifts corresponded to the guanidinium scaffold protons, as expected. This pointed to a structural rearrangement of the flexible moiety to properly adapt and dock with guest **76**.

[26] Blondeau, P. *PhD Thesis*, Universidad Autónoma de Madrid, **2007**.

5.5 UV-Visible Spectroscopy Titration Studies

To further assess the strength of the interaction between this bisporphyrin host tweezer and the different fullerene guests, UV–visible titrations were performed. Complexation of similar porphyrin receptors with fullerene guests has been widely described to provoke changes in the Soret band of the bis-porphyrin host. The spectrophotometric titrations were performed using micromolar solutions of receptor and adding fullerene guest solution in tetrachloroethane (TCE). UV titration of receptor **75** with C_{60} showed the expected quenching of the Soret absorption band, suggesting that the binding takes place through π-electron interactions. As depicted in Figure 16, an association constant of 7.8 x 10^3 M^{-1} was determined for this system.

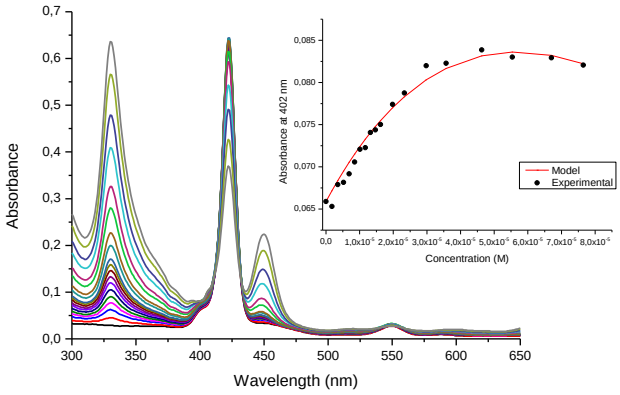

Figure 16. *UV titration spectra in TCE of the complex between receptor* ***75*** *and C_{60} guest (inside: isotherm curve at 402 nm).*

The association constant is in agreement with previous values reported in the literature for acyclic fullerene@porphyrin assemblies. For macrocyclic Zn-porphyrin dimers such as those described by Aida *et al.*[3], the association constant of the corresponding complexes with C_{60} increases to 6.7 x 10^5 M^{-1}, due to the highly

preorganized nature of the system. Tweezer-like structures such as our guanidinium bis-porphyrin receptor are more flexible and thus the association constant should drop.

UV titrations of host **75** with tetrabutylammonium fullerene-carboxylate guest **76** showed the same spectroscopic behavior as for regular C_{60}. This suggests that the type of host-guest interactions relies on the same π-electronic contacts as before. However, higher association constant was observed for this supramolecular complex. Thus, a preliminary titration at the same concentration range as for regular C_{60} afforded an estimated value of 10^8 M^{-1}. We decide to work more diluted in view of the high association constant value determined. Hence, at 0.3 μM a value of K_a = 1.4 x 10^8 M^{-1} in TCE was obtained (Figure 17), which indeed is still too high to be unambiguously assigned by UV titrations.

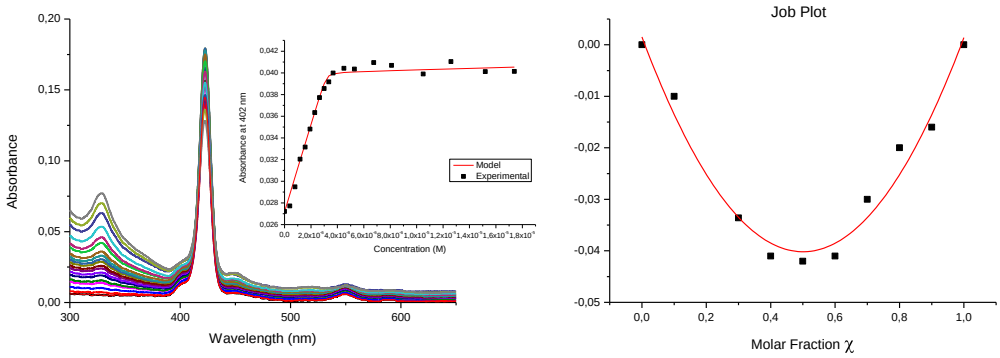

Figure 17. *(Left) UV-vis titration spectra (in TCE) of complex* ***76@75*** *(inside: isotherm curve at 402 nm). (Right) Job plot indicating a 1:1 complex.*

A 1:1 binding stoichiometry was unambiguously assessed by Job´s titration curves. Indeed, this binding mode fitted nicely with the previous UV data.

Finally, UV titration of reference guanidinium mono-porphyrin compound **80** with **76** gave rise to a similar spectroscopic behavior, yielding a stability constant of 1.8 x 10^5 M^{-1} in TCE (Figure 18). This value is consistent with the combination of the carboxylate-guanidinium pairing and the π-π contacts between the

fullerene@porphyrin dyad, which contributes simultaneously in the enhancement of the interaction strength.

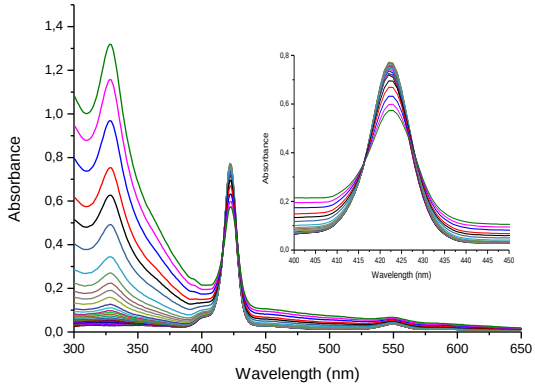

Figure 18. *UV titration spectra (in TCE) of complex* ***76@80*** *(inside: detail of the Soret region).*

With this data in hand, the contribution of each individual interaction and the possible cooperativity effects arising from these multivalent systems were discussed. Indeed, for the binding of **76** with **75**, we should take into account different stepwise equilibrium processes, as depicted in Scheme 4. The order of events should not alter the overall process. Hence, initially guanidinium-carboxylate pairing takes place (K_1) followed by the intramolecular (EM_1) binding of one of the porphyrin arms (K_2). Successive intramolecular (EM_2) binding of the second porphyrin (K_2) leads to the formation of the final complex.

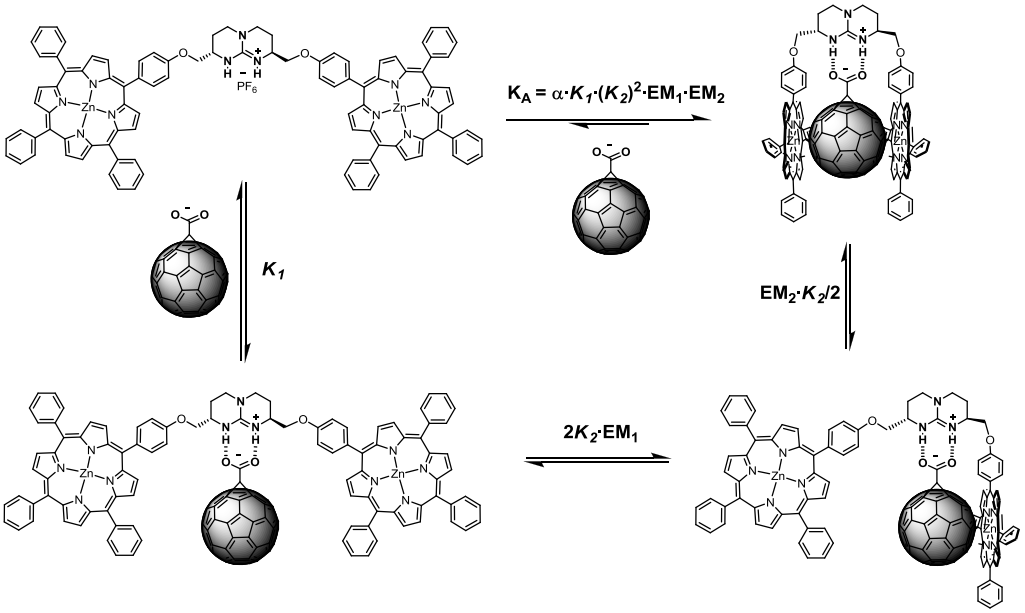

Scheme 4. *Possible equilibria involved in the binding of fullerene-carboxylate* ***76*** *with receptor* ***75****.*

By definition, cooperativity factor (α) is the ratio between the experimental association constant, affected by cooperative interactions (K_A), and the statistical or the reference constant (K_{ref}).[27] A consistent cooperativity factor should tend to 1 in absence of cooperativity and consequently differ from this value in the case of positive (α>1) or negative (α<1) cooperativity. In our system, chelate cooperativity should be considered as there are two or more intramolecular binding interactions interplaying collectively. However, chelate cooperativity depends on ligand concentration and for clarity, in this case we will assume the simplified definition described in Equation 1.

[27] (a) Hunter, C. A.; Anderson, H. L. *Angew. Chem. Int. Ed.* **2009**, *48*, 7488-7499. (b) Ercolani, G.; Schiaffino, L. *Angew. Chem. Int. Ed.* **2011**, *50*, 1762-1768.

$$\alpha = \frac{K_A}{K_{ref}}$$

Equation 1. *Cooperativity factor (α) formula considered for our supramolecular system.*

Assuming a microscopic constant for the fullerene@Zn-porphyrin interaction (K_2) of 1 x 10^3 M^{-1}, we will be able to calculate the effective molarities (EM_1 and EM_2) from the stability constant values of the **76@80** and **C_{60}@75** complexes, respectively. This data will allow us to estimate a reference constant for this system that will be the constant in the denominator for the determination of the cooperativity factor. In the numerator we will use the experimental stability constant found for the **76@75** complex.

As shown in Scheme 5, the complexation between guanidinium mono-porphyrin **80** and the fullerene carboxylate **76** (K_B = 1.8 x 10^5 M^{-1}), can be used to determine the first effective molarity (EM_1) that we defined in our system.

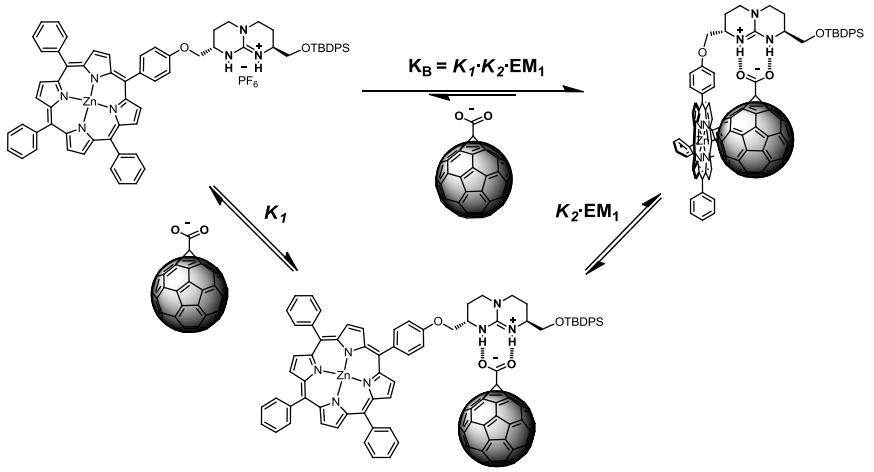

Scheme 5. *Thermodynamic equilibrium processes involving the complexation of ditopic guanidinium mono-porphyirin compound **80** with **76**.*

The guanidinium-carboxylate stability constant can be extrapolated from the titration of bis-aryl guanidinium compound **79** with **76** (K_1 = 3.3 x 10^3 M^{-1}). Using the estimated

value previously described for the microscopic constant (K_2), we calculated an EM_1 value of 5.4 x 10^{-2} M.

Likewise, by using the experimental association constant (K_C = 7.8 x 10^3 M^{-1}) from the complexation between compound **75** and C_{60} (Scheme 6), we were able to determine an EM_2 value of 7.8 x 10^{-3} M.

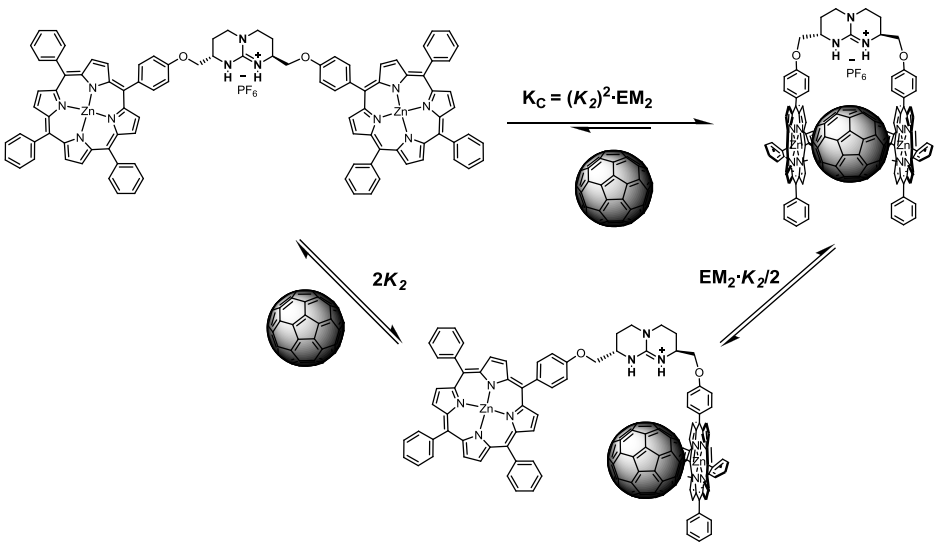

Scheme 6. *Thermodynamic equilibrium processes involving the complexation of guanidinium bis-porphyrin* ***75*** *with* C_{60}.

With this data in hand, we were able to estimate a K_{ref} of 1.4 x 10^6 M^{-1}, which divided by the experimental stability constant previously found for **76@75** complex (K_A = 1.4 x 10^8 M^{-1}), afforded a cooperative factor of $\alpha \approx 100$. This suggests that positive cooperativity is influencing the interaction and thus enhancing the thermodynamic stability of **76@75** complex. However, as previously pointed out, experimental error derived from the determination of this high association constant by UV-visible spectroscopy should be considered. Besides, to facilitate the interpretation of this system, we have dismissed side-processes (such as self-aggregation or higher stoichiometries) which can possibly occur during the equilibrium between the species depicted above. Therefore, those values should be analyzed qualitatively rather than

quantitatively and their significance should be placed within this context.

To conclude, we have demonstrated the formation of a stable and robust fullerene@bis-porphyrin dyad which interacts not only by electronic complementarity but also by means of hydrogen bonding and electrostatic interactions between the bicyclic guanidinium scaffold and the carboxylate moiety of the fullerene.

Moreover, Zn metallic centers of the porphyrin can be used to self-assemble this robust dyad by means of axial coordination with mono- and bidentate ligands. The geometry of the ligand should determine the spatial disposition of the resulting porphyrin array (see section 5.7).

5.6 Preliminary Photophysical Characterization of Complex 76@75

Femtosecond transient absorption experiments were performed to study the excited-state interactions between bis-porphyrin **75** and fullerenes C_{60} and **76**. This work was carried out by Dr. Bruno Grimm and Rafael Krick Calderon under the supervision of Prof. Dirk Guldi (University of Erlangen).

Laser pulse irradiation at 420 nm yielded the formation of the bis-porphyrin singlet excited state. In the case of 1:1 mixtures with fullerene **76**, this is followed by charge-transfer to the electron-deficient fullerene. This provokes a charge separated **76**$^{\bullet-}$**@75**$^{\bullet+}$ radical-ion-pair state which decays *via* charge recombination to the ground state (Figure 19). Generation of the fullerene **76** anion is unequivocally proven by the appearance of the absorption peak between 1000 and 1100 nm. Moreover, excitation at 420 nm gives rise to transient absorption changes when parts of the bound and free fullerene species are excited to its singlet excited state (singlet-singlet absorption in the near-infrared, around 900-950 nm) which rapidly decays through intersystem crossing to the energetically lower triplet excited state (that absorbs around 750 nm). As a result of the weaker binding of **75** with C_{60}, charge transfer spectral features are barely observed in 1:1 mixtures and presumably higher proportions of this fullerene are required in order to unequivocally form the complex at the concentration range of the experiment, thus yielding efficient electron-transfer processes.

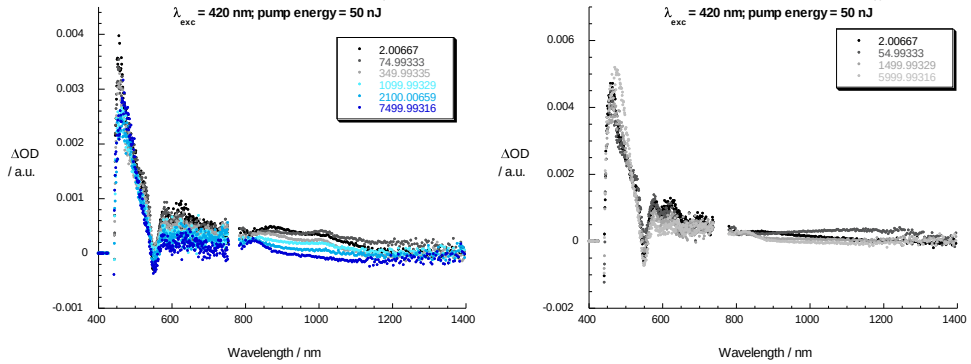

Figure 19. *Differential absorption spectra (visible and near-infrared) obtained upon femtosecond laser photolysis (420 nm) in Ar saturated toluene with time delays between 2 and 7500 ps of 1:1 mixtures of bis-porphyrin* ***75*** *with* ***76*** *(left) and C_{60} (right).*

Finally, kinetic analysis of this data provided a lifetime of the charge separated state for the **76@75** complex in oDCB around 1.3 ns (fitted by the decay of the fullerene anion at different wavelengths: 970, 1000 and 1030 nm). Longer lifetimes are expected for this complex in toluene. However, it seems that more than one process is involved in the decay of the fullerene anion in this solvent and thus, a careful analysis of the data is required in order to provide reliable lifetimes for this system.

5.7 Cyclic Poly-Porphyrin Arrays Derived from the Guanidinium Bis-porphyrin-Fullerene Scaffold

5.7.1 Introduction and Objectives

Nature uses photosynthetic systems to obtain energy from light, transforming and storing this energy into chemical energy.[28] In particular, light harvesting antenna complexes absorb one photon from sunlight and this follows with an efficient energy migration until reaching the enzymatic reaction center. These large protein complexes contain several chromophores or pigments (mainly porphyrins and porphyrinoids) with an optimal orientation and distance to allow electron coupling, photon caption and electron/energy transfer processes.[29] Thus, the peptide scaffold acts as a structural template to hold this supramolecular chromophore array in a ring-shaped disposition (Figure 20).[30]

[28] (a) Moser, C. C.; Keske, J. M.; Warncke, K.; Farid, R. S.; Dutton, P. L. *Nature* **1992**, *355*, 796-802. (b) Wasielewski, M. R. *Chem. Rev*. **1992**, *92*, 435-461. (c) Regan, J. J.; Onuchic, J. N. In *The Reaction Centers of Photosynthetic Bacteria*; Michel-Beyerle, M. E., Ed.; Springer: Berlin, **1996**.

[29] Pullerits, T.; Sundström, V. *Acc. Chem. Res.* **1996**, *29*, 381-389.

[30] McDermott, G.; Prince, S. M.; Freer, A. A.; Hawthornthwaite-Lawless, A. M.; Papiz, M. Z.; Cogdell, R. J.; Isaacs, N. W. *Nature* **1995**, *374*, 517-521.

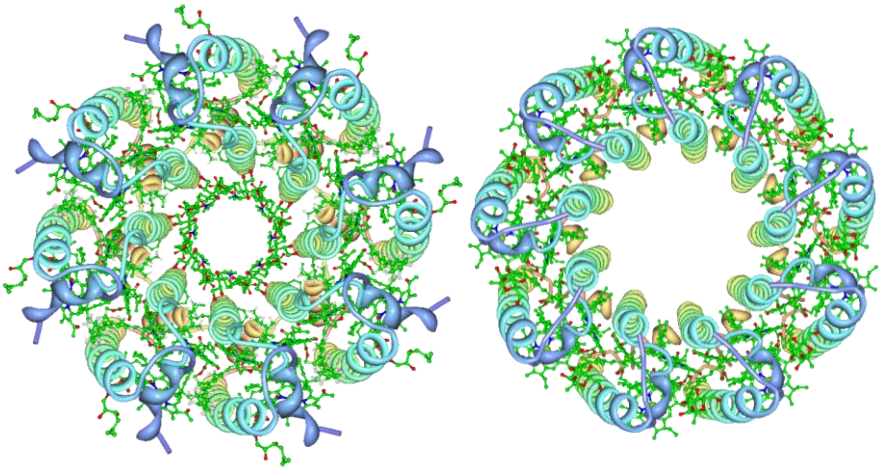

Figure 20. *Light-harvesting complexes II from Rhodospirillum molischianum (left, PDB entry: 1LGH)*[31] *and Rhodopseudomonas acidophila (right, PDB entry: 1KZU).*[32]

The energetic efficiency in light-harvesting bacteriochlorophyll systems relies in the interaction between the chlorin (chromophoric) moieties by means of π-π interactions and metal-coordination through the central magnesium ion of the macrocycle, among other non-covalent contacts involving different domains of the protein. Inspired by these biological assemblies, many efforts have been dedicated to pursue such energy efficient synthetic chromophoric arrays.[33] In particular, due to their similarities with chlorophyll-based light-harvesting complexes, porphyrin cyclic arrays have raised an enormous interest in the field. Indeed, they have been extensively studied for assessing the basis of the energy transfer (ET) mechanism and to improve the efficiency of the process.

Different strategies have been designed to afford these cyclic structures by means of

[31] Koepke, J.; Hu, X.; Muenke, C.; Schulten, K.; Michel, H. *Structure* **1996**, *4*, 581-597.

[32] Prince, S. M.; Papiz, M. Z.; Freer, A. A.; McDermott, G.; Hawthornthwaite-Lawless, A. M.; Cogdell, R. J.; Isaacs, N. W. *J. Mol. Biol.* **1997**, *268*, 412-423.

[33] (a) Ward, M. D. *Chem. Soc. Rev.* **1997**, *26*, 365-375. (b) Balaban, T. S. *Acc. Chem. Res.* **2005**, *38*, 612-623. (c) Gust, D.; Moore, T. A.; Moore, A. L. *Acc. Chem. Res.* **2009**, *42*, 1890-1898.

covalent bonds,[34] non-covalent bonds and metal coordination.[35] In theory, the non-covalent and metal coordinating strategies are synthetically more accessible than the covalent one, but the resulting complexes are obviously less stable. In fact, the presence of competitive solvents or coordinating ligands could result in the disruption of these assemblies.

Our approach consists of the generation of a light-haversting photosystem mimic using the robust fullerene@guanidinium bis-porphyrin (**76@75**) complex. As we have described, the fullerene-carboxylate guest would afford the contact between two bridged porphyrins by means of π-electron interactions and would template their orientation in a parallel disposition to maximize the binding strength as shown in the molecular model (Figure 9). On the other hand, we will use a bidentate ligand to connect two of these fullerene@bis-porphyrin complexes, taking advantage of the coordinating properties of Zn porphyrins. Both the geometry of the ligand and the coordination sphere of the metal dictate the shape of the supramolecular assembly. In some way, the fullerene scaffold and the bidentate ligand should play the role of the peptidic matrix which templates the spatial orientation of the pigments in the natural photosynthetic systems. However, owing to their donor-acceptor electronic characteristics they are not "innocent" structural factors and presumably will influence the electronic properties of the assembly.

[34] (a) Burrell, A. K.; Officer, D. L.; Plieger, P. G.; Reid, D. C. W. *Chem. Rev.* **2001**, *101*, 2751-2796.

[35] For reviews see: (a) Wojaczynski, J.; Latos-Grazynski, L. *Coord. Chem. Rev.* **2000**, *204*, 113-171. (b) Sugiura, K. *Top. Curr. Chem.* **2003**, *228*, 65-85. (c) Elemans, J. A. A. W.; van Hameren, R.; Nolte, R. J. M.; Rowan, A. E. *Adv. Mater.* **2006**, *18*, 1251-1266. (d) Nakamura, Y.; Aratani, N.; Osuka, A. *Chem. Soc. Rev.* **2007**, *36*, 831-845. (e) Aratani, N.; Kim, D.; Osuka, A. *Acc. Chem. Res.* **2009**, *42*, 1922-1934.

5.7.2 Design and Molecular Modeling

As previously described, the geometry of the bidentate ligand plays a pivotal role in the resulting geometry of the assembly. In order to mimic the circular shape of the biological photosystems, we selected a bidentate ligand with a bend angle of 90º between the coordinative positions. This would allow the formation of square-like structures, assuming that the porphyrin moieties remain planar and parallel with respect to each other by sandwiching the fullerene guest. The bis-pyridine-carbazole ligand **82** fulfills both the coordination and geometrical prerequisites to give rise to the desired assembly. On one hand, pyridine ligands have been widely reported to axially bind to Zn porphyrins with stability constants about 10^3-10^4 M^{-1}. On the other hand, the carbazole scaffold affords a 90º angle between its substituents at the 3 and 6 positions, respectively. Moreover, solubility issues will be avoided by *N*-alkylation of the carbazole with 2-ethylhexyl bromide (Figure 21).

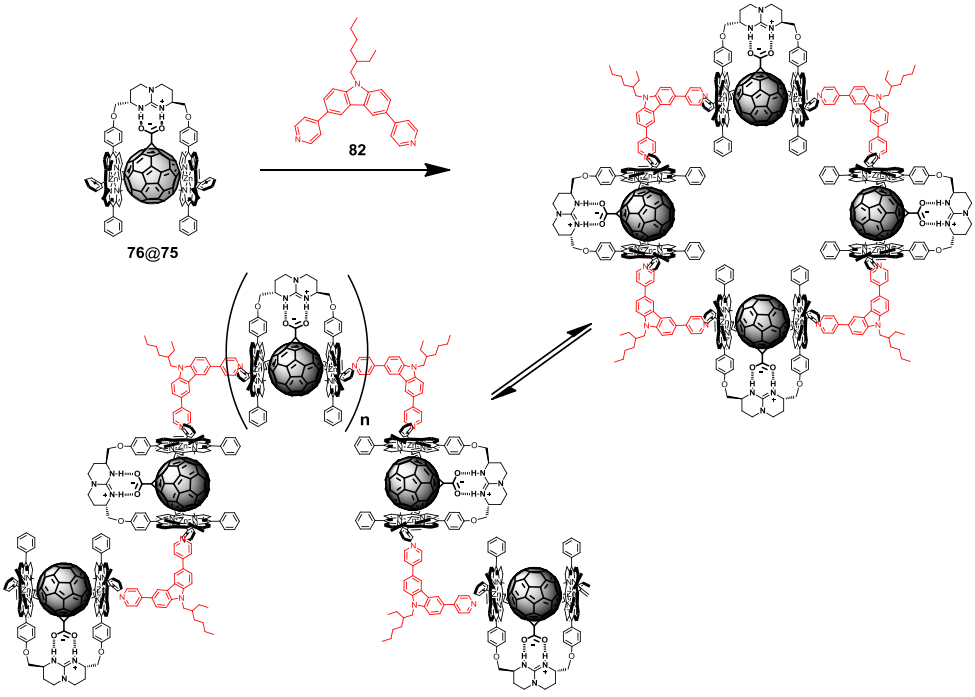

Figure 21. *Schematic representation of the cyclic assembly proposed between* ***82*** *and complex* ***76@75****.*

Higher aggregates or polymers could also be formed despite these options are entropically unfavorable. As shown in the molecular model (Figure 22), four bipyridine carbazole ligands are bridging up to eight porphyrins which simultaneously form stable donor-acceptor dyads with four fullerene carboxylate guests. The strength of the fullerene@bis-porphyrin complex is essential for the formation of the cyclic porphyrin array. Indeed, the binding of the fullerene-carboxylate guest restricts the conformational movement of the flexible guanidinium receptor, forcing the parallel orientation of its pendant porphyrins. Previously reported bis-porphyrin tweezer receptors showed association constant values of approximately 10^3 M^{-1} with C_{60}. For our guanidinium-based receptor this experimental assessment on the association constant was confirmed (7.8 x 10^3 M^{-1}). However, bipyridine ditopic ligands are known to bind bis-porphyrin receptors 10 to 100 fold stronger than C_{60}.[36] This would result in the displacement of C_{60} guest by the bipyridine ligand. To avoid this situation, we decided to use the fullerene-carboxylate derivative which binds strongly (*ca.* 10^8 M^{-1}) to the guanidinium bis-porphyrin host, thus preventing complex disruption upon addition of the bipyridine cabazole ligand and consequently favoring intermolecular coordination.

[36] Camara-Campos, A.; Hunter, C. A.; Tomas, S. *Proc. Natl. Acad. Sci. USA* **2006**, *103*, 3034-3038.

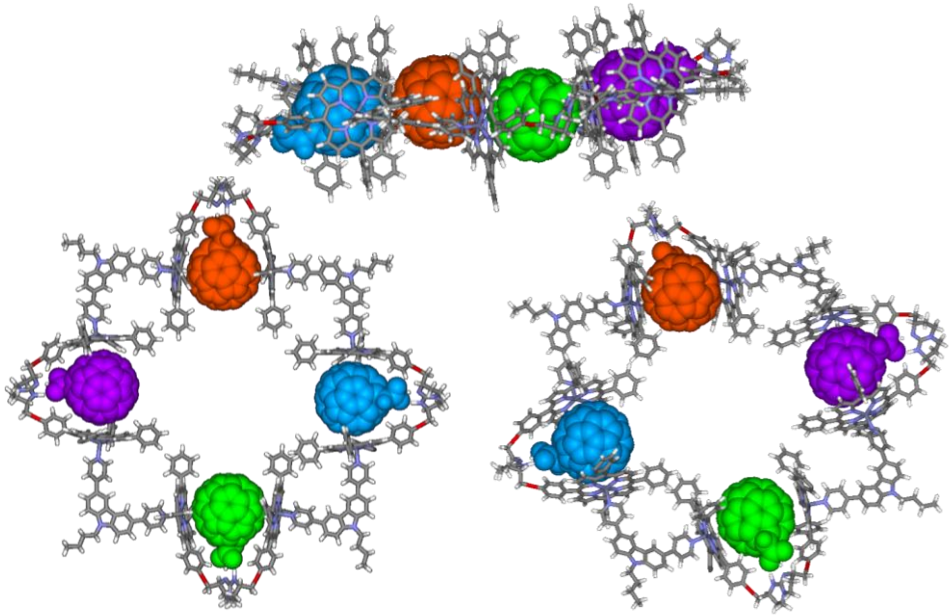

Figure 22. *Minimized structures (SCIGRESS, standard conditions, no solvent) of the tetrameric assembly containing up to eight porphyrins and four fullerene moieties.*

5.7.3 Synthesis of the 3,6-Bis(4-pyridyl)carbazole Ligand 82

As depicted in Scheme 7, bipyridine carbazole ligand **82** was achieved in 3 steps starting from carbazole. Bromination and subsequent *N*-alkylation with 2-ethylhexyl bromide gave rise to compound **83**.[37] Finally, Suzuki coupling of 3,6-dibromo-9-ethylhexyl-carbazole with 4-pyridyl boronic acid[38] yielded the desired carbazole ligand **82**.

[37] Huang, J.; Niu, Y.; Yang, W.; Mo, Y.; Yuan, M.; Cao, Y. *Macromolecules* **2002**, *35*, 6080-6082.
[38] Kim, H.-J.; Lee, E.; Park, H.-S.; Lee, M. *J. Am. Chem. Soc.* **2007**, *129*, 10994-10995.

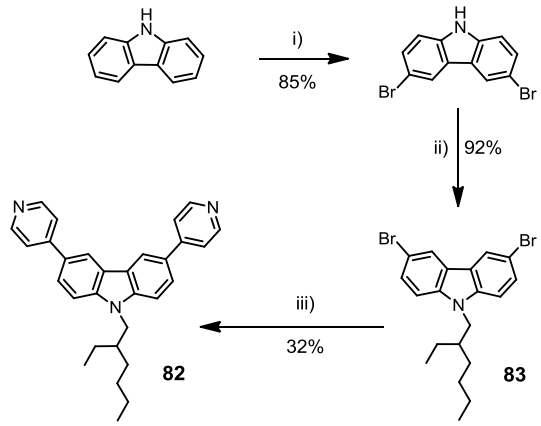

Scheme 7. *Synthesis of bipyridine carbazole* ***82****. Conditions: i) Br_2, pyr; ii) 2-ethylhexyl bromide, NaH in THF; iii) 4-pyridine boronic acid, Na_2CO_3, 15% mol $Pd(PPh_3)_4$.*

This ditopic ligand **82** displays the correct angle to fulfill the geometrical requirements for the formation of fullerene@bis-porphyrin arrays.

5.7.4 Complexation Studies with 82 and Complex 76@75

Preliminary ^{1}H-NMR titrations of complex **76@75** with bis-pyridyl carbazole derivative **82** showed evident chemical shifts from both the complex and the protons of **82** (Figure 23). Upon addition of almost 20 equivalents of **82**, no free ligand was observed. Broadness of the proton signals prevented to assign them and thus to extract further information about the complex structure.

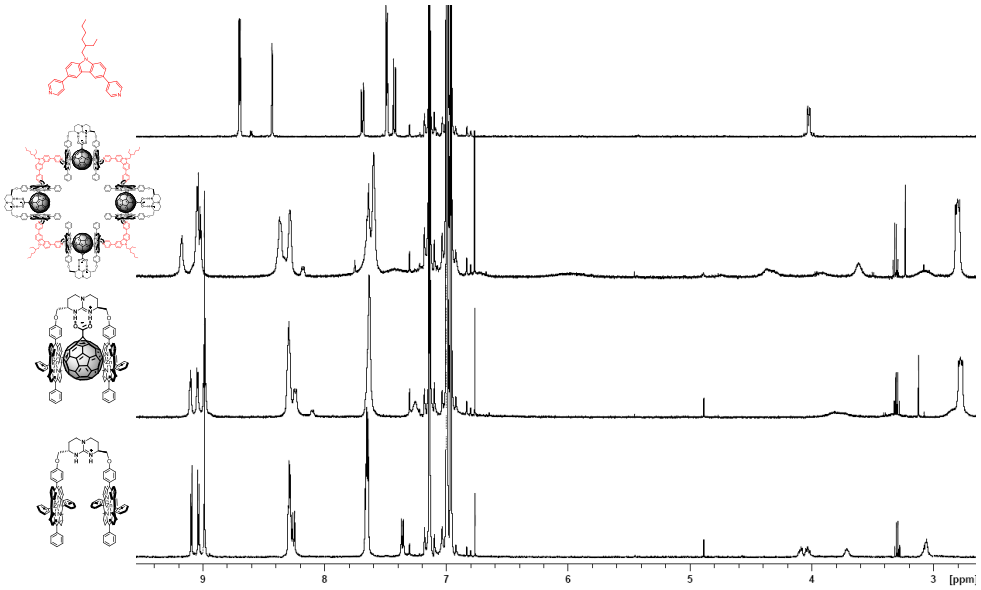

Figure 23. *^{1}H-NMR spectra (in chlorobenzene) of the different supramolecular complexes and ligand* ***82*** *(top).*

In addition, it was difficult to assign a diffusion coefficient value from the DOSY spectrum of the 1:1 mixture of **82** and **76@75** complex. However, a unique species seemed to be present in solution. Size exclusion chromatography (SEC/GPC) was also explored in order to observe the formation of higher aggregates upon addition of the carbazole ligand **82** to the bisporphyrin-fullerene complex. Different GPC columns, eluents (THF, toluene and dichloromethane) and chromatographic conditions were tested to assess variations in size between the different species. However, guanidinium bisporphyrin compound **75** tends to self-aggregate under these analytic conditions and it was not possible to obtain reliable information from these experiments.

UV titrations were set up in order to assess the binding affinity of this carbazole ligand towards the bis-porphyrin fullerene complex. As shown in Figure 24, the Soret band of **76@75** complex is quenched upon addition of ligand **82** and a new red-shifted band emerges, as expected for Zn-porphyrins upon coordination of an axial nitrogen

containing ligand.[39] In Zn bis-porphyrin systems, the shift of this band is indicative of the exiton coupling between the Zn-porphyrin transitions when they are cofacially oriented upon amine axial coordination. The association constant measured for the assembly was 1.3 x 10^5 M^{-1} in TCE (Figure 24).

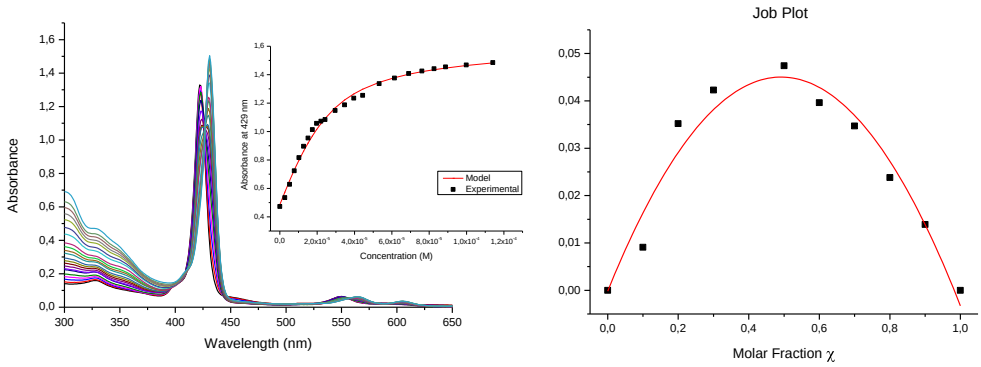

Figure 24. *UV-vis titration (in TCE) and Job´s plot measurements of complex* ***76@75*** *with bispyridyl carbazole ligand* ***82****.*

This value is higher than expected as we had anticipated an affinity constant close to the simple pyridine:Zn-porphyrin coordination (10^3-10^4 M^{-1}). Instead, we found a value close to the intramolecular binding of a bipyridine ligand with a bis-porphyrin receptor. This has two possible interpretations; on one hand, the bis-pyridyl carbazole ligand could compete with the fullerene-carboxylate guest, displacing it. This would result in the intramolecular binding of the ditopic ligand. It is reported in the literature that this intramolecular bis-pyridyl binding is approximately two orders of magnitude higher than that of the monotopic pyridine:Zn-porphyrin complex. However, this binding mode is unlikely since the fullerene guest blocks the inner face of the bis-porphyrin tweezer and this complex is quite stable. Indeed, it has been described that higher stoichiometries could result from binding of a ditopic DABCO ligand with an acyclic

[39] Anderson, H. L. *Inorg. Chem.* **1994**, *33*, 972-981.

bis-porphyrin which is conformationally unable to form intramolecular 1:1 complexes. Instead, intermolecular 2:2 stoichiometries were found for these assemblies.[40] In our particular system we expected the formation of 4:4 complexes due to the geometrical restrictions imposed. On the other hand, the last ditopic interaction should be considered as intramolecular and hence would be energetically more favourable, due to the ring closing effect of the cyclic aggregate. This would result in a higher value of the association constant, in agreement with our experimental data. Both the titration and Job´s plot experiments pointed to 1:1 stoichiometry for the complexation. Nevertheless, this model fits with all kinds of cyclic aggregates, linear polymers or even intramolecular complexes.

Further experiments should be performed to precisely determine the stoichiometry and the association mode of this supramolecular assembly. However, due to the relative weakness of the interactions involved in the formation of this porphyrin array, it can be anticipated that a mixture of different species exists in solution under thermodynamic equilibrium. Regarding this, we are currently working in collaboration with Prof. Hans Elemans (Univ. of Nijmegen) in order to detect by scanning probe microscopy (STM) those aggregates in surface.

[40] Ballester, P.; Costa, A.; Castilla, A. M.; Deya, P. M.; Frontera, A.; Gomila, R. M.; Hunter, C. A. *Chem. Eur. J.* **2005**, *11*, 2196-2206.

5.8 Experimental Section

5.8.1 Materials and Methods

UV-visible spectra were measured on a UV-Vis spectrophotometer Shimadzu UV-2401PC. The experimental data was fitted using SPECFIT software, version 3.0; Spectra Software Associates, Marlborough, MA (USA), 2007.

5.8.2 Synthesis

Compound 75

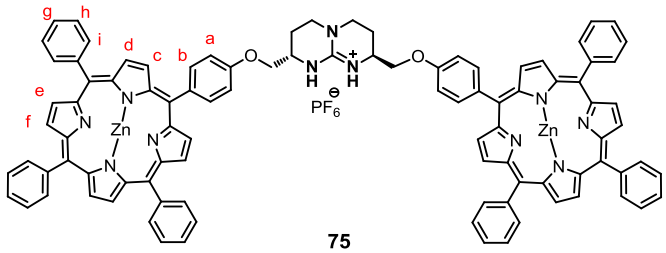

75

A mixture of phenol porphyrin **77** (200 mg, 0.290 mmol), guanidinium salt **78** (50 mg, 0.132 mmol) and potassium carbonate (72 mg, 0.521 mmol) in acetone (15 mL) was placed in a sealed tube and refluxed for two days. After removing the solvent, the resulting solid was dissolved in CH_2Cl_2 and washed with a 0.1N NH_4PF_6 aqueous solution (2 x 20 mL). Subsequently, the organic phase was filtered over cotton and concentrated *in vacuo*. Purification by silica gel column chromatography (slow gradient of CH_2Cl_2/MeOH, 100:0 to 96:4) afforded **75** as a purple solid (93 mg, 42%). ^{1}H-NMR (400 MHz, *d6*-acetone) δ 8.93-8.85 (m, 16H, CH_{pyrrol}), 8.27-8.20 (m, 12H, $CH_{Ar(g,j)}$), 8.19 (d, J = 8.6 Hz, 4H, $CH_{Ar(b)}$), 7.89-7.74 (m, 16H, $CH_{Ar(h,i)}$), 7.45 (d, J = 8.6 Hz, 4H, $CH_{Ar(a)}$), 4.67 (dd, J = 3.8, 9.7 Hz, 1H, CH_2O), 4.47 (t, J = 9.0 Hz, 2H, CH_2O), 4.38-4.30 (m, 2H, CH_α), 3.92-3.83 (m, 4H, $CH_{2\gamma}$), 2.60-2.49 (m, 2H, $CH_{2\beta}$), 2.41-2.28 (m, 2H, $CH_{2\beta}$). ^{13}C-NMR (100 MHz, *d6*-acetone).δ 158.0 ($C_{Ar\text{-}phenol}$), 150.2 150.0, 149.9, 143.3, 143.2, 136.4 (C_{guan}, C_{Ar}), 135.4 ($CH_{Ar\text{-}phenol}$), 134.3 (CH_{Ar}), 131.5, 131.4 (CH_{pyrrol}),

127.4, 126.5 (CH_{Ar}), 120.6, 120.2 (C_{Ar}), 112.7 ($CH_{Ar\text{-}phenol}$), 70.1 (CH_2O), 48.6 (CH_α), 45.5 ($CH_{2\gamma}$), 22.7, 22.5 ($CH_{2\beta}$). ESI-MS *m/z* 1548.5 $(M - PF_6^-)^+$. HRMS calcd. for $[C_{97}H_{70}N_{11}O_2Zn_2]^+$ 1548.4291; found 1548.4194.

***Zn-meso*-5-(4'-Hydroxyphenyl)-10,15,20-triphenylporphyrin (77)**

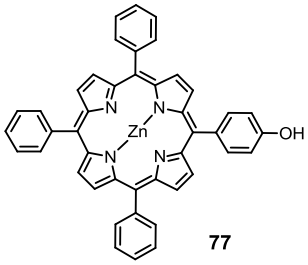

77

A mixture of benzaldehyde (4.14 mL, 40.9 mmol) and 4-hydroxybenzaldehyde (2 g, 16.4 mmol) was dissolved in propionic acid (250 mL) and heated until reflux. Then, fresly distilled pyrrole (4.26 mL, 61.4 mmol) was added and the mixture was heated for an additional hour. The solvent was evaporated and the residue was eluted through a Florisil column (CH_3Cl). The organic phase was concentrated *in vacuo* and purified by silica gel column chromatography (Hexane/CH_3Cl, 50:50 → 0:100) affording the non-metallated porphyrin (730 mg, 7%) as a purple solid. Subsequently, the free porphyrin (730 mg, 1.16 mmol) and $Zn(OAc)_2$ (2.12 g, 11.57 mmol) were dissolved in a (7:3) CH_3Cl/MeOH mixture (15 mL) and stirred overnight. Afterwards, this solution was washed with water (3 x 15 mL) and the organic phase was evaporated, yielding **77** as a dark purple solid (800 mg, quantitative from the free porphyrin precursor). ^{1}H-NMR (400 MHz, CD_3Cl) δ 9.00 (d, *J* = 4.6 Hz, 2H, CH_{pyrrol}), 8.97 (d, *J* = 4.6 Hz, 2H, CH_{pyrrol}), 8.96 (s, 4H, CH_{pyrrol}), 8.24 (dd, *J* = 1.9, 7.8 Hz, 6H, CH_{Ar}), 8.10 (d, *J* = 8.5 Hz, 2H, CH_{Ar}), 7.84-7.73 (m, 8H, CH_{Ar}), 7.24 (d, *J* = 8.5 Hz, 2H, CH_{Ar}), 5.13 (s, 1H, OH). ^{13}C-NMR (100 MHz, $CDCl_3$) δ 150.5, 150.3, 150.2, 142.8 (C_{Ar}), 135.5 ($CH_{Ar\text{-}phenol}$), 135.4 (C_{Ar}), 134.5 (CH_{Ar}), 132.0 (CH_{pyrrol}), 127.5, 126.6 (CH_{Ar}), 113.6 ($CH_{Ar\text{-}phenol}$). HRMS calcd. for $[C_{44}H_{28}N_4OZn]^+$ 692.1549; found 692.1596.

(2*S*,8*S*)-2,8-Bis-(chloromethyl)-3,4,6,7,8,9-hexahydro-2*H*-pyrimido-[1,2-*a*]-pyrimidin-1-ium hexafluorophosphate (78)

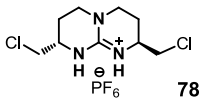

78

A solution of compound **72** (350 mg, 1.48 mmol) in $SOCl_2$ (12 mL) was stirred under reflux for 4 h. The solvent was removed, re-dissolved in CH_2Cl_2 and washed with 0.1N NH_4PF_6 aqueous solution. The organic phase was filtered over cotton, concentrated *in vacuo* and purified by silica gel column chromatography eluting with a solvent mixture (CH_2Cl_2/MeOH, 98:2 →96:4) to afford **78** (379 mg, 95%) as a light yellowish solid. Mp 76-79°C. ^{1}H-NMR (500 MHz, $CDCl_3$) δ 6.30 (s, 2H, NH), 3.57-3.53 (m, 2H, CH_2Cl), 3.50-3.40 (m, 4H, CH_2Cl, CH_α), 3.28-3.25 (m, 4H, $CH_{2\gamma}$), 2.02-1.96 (m, 2H, $CH_{2\beta}$), 1.86-1.80 (m, 2H, $CH_{2\beta}$). ^{13}C-NMR (100 MHz, $CDCl_3$) δ 151.3 (C_{guan}), 49.4 (CH_2Cl), 48.2 (CH_α), 45.6 ($CH_{2\gamma}$), 23.5 ($CH_{2\beta}$). ESI-MS m/z 236.1 $(M - Cl^-)^+$. HRMS calcd. for $[C_9H_{16}Cl_2N_3]^+$ 236.0721; found 236.0722.

(2*S*,8*S*)-2,8-Bis-(phenoxymethyl)-3,4,6,7,8,9-hexahydro-2*H*-pyrimido-[1,2-*a*]-pyrimidin-1-ium hexafluorophosphate (79)

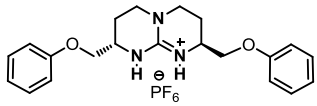

79

A mixture of phenol (66 mg, 0.713 mmol), guanidinium salt **78** (90 mg, 0.242 mmol) and potassium carbonate (130 mg, 0.945 mmol) in acetone (10 mL) was placed in a sealed tube and refluxed overnight. After removing the solvent, the resulting solid was dissolved in CH_2Cl_2 and washed with a 0.1N NH_4PF_6 aqueous solution (2 x 15 mL). The organic phase was filtered over cotton and concentrated *in vacuo*. Purification by silica gel column chromatography (CH_2Cl_2/MeOH, 100:0 → 95:5) afforded **79** as a white solid (30 mg, 26%). ^{1}H-NMR (400 MHz, CD_3CN) δ 7.33 (t, J = 8.0 Hz, 4H, CH_{Ar}), 7.03-6.94 (m, 6H, CH_{Ar}), 6.40 (s, 2H, NH), 4.15 (dd, J = 3.7, 9.3 Hz, 2H, CH_2O), 3.88 (dd, J = 8.7, 9.3 Hz, 2H, CH_2O), 3.86-3.78 (m, 2H, CH_α), 3.48-3.34 (m,

4H, $CH_{2\gamma}$), 2.16-2.08 (m, 2H, $CH_{2\beta}$), 1.92-1.83 (m, 2H, $CH_{2\beta}$). ^{13}C-NMR (100 MHz, CD_3CN) δ 158.2 (C_{Ar}), 150.9 (C_{guan}), 129.7, 121.4, 117.3, 114.5 (CH_{Ar}, C_{Ar}), 69.6 (CH_2O), 48.2 (CH_α), 45.2 ($CH_{2\gamma}$), 22.2 ($CH_{2\beta}$). HRMS calcd. for $[C_{21}H_{26}N_3O_2]^+$ 352.2025; found 352.2020.

Compound 80

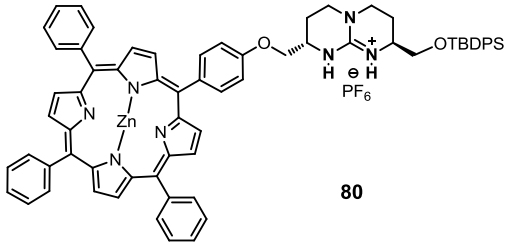

80

A mixture of phenol porphyrin **77** (55 mg, 0.079 mmol), guanidinium salt **81** (71 mg, 0.119 mmol) and potassium carbonate (16 mg, 0.119 mmol) in acetone (25 mL) was placed in a sealed tube and refluxed overnight. After removing the solvent, the resulting solid was dissolved in CH_2Cl_2 and washed with a 0.1N NH_4PF_6 aqueous solution (2 x 20 mL). Subsequently, the organic phase was filtered over cotton and concentrated *in vacuo*. Purification by silica gel column chromatography (slow gradient of CH_2Cl_2/MeOH 100:0 to 95:5) afforded **80** as a purple solid (70 mg, 70%). ^{1}H-NMR (400 MHz, CD_3Cl) δ 8.99-8.93 (m, 8H, CH_{pyrrol}), 8.27-8.20 (m, 6H, $CH_{Ar\ (g,j)}$), 8.12 (d, J = 8.6 Hz, 2H, $CH_{Ar(b)}$), 7.82-7.71 (m, 10H, $CH_{Ar(h,i)}$), 7.70-7.65 (m, 4H, CH_{Ar}), 7.51-7.39 (m, 6H, CH_{Ar}), 7.28 (d, J = 8.5 Hz, 2H, $CH_{Ar(a)}$), 6.75 (s, 1H, NH), 6.46 (s, 1H, NH), 4.31 (d, J = 5.7 Hz, 2H, CH_2O), 4.10-4.00 (m, 1H, CH_α), 3.81-3.70 (m, 2H, CH_2O), 3.69-3.61 (m, 1H, CH_α), 3.60-3.35 (m, 4H, $CH_{2\gamma}$), 2.37-2.20 (m, 2H, $CH_{2\beta}$), 2.12-1.93 (m, 2H, $CH_{2\beta}$), 1.10 (s, 9H, $CH_{3t\text{-}Bu}$). ^{13}C-NMR (100 MHz, $CDCl_3$).δ 157.5 ($C_{Ar}O$), 150.9, 150.4, 150.2, 142.8, 136, 2 (C_{Ar}, C_{guan}), 135.6, 135.5, 135.5, 134.4 (CH_{Ar}), 132.6, 132.5, 132.0, 130.1, 130.0, 128.0, 127.5, 126.5 (C_{Ar}), 121.1, 121.0, 120.6 (CH_{Ar}), 112.8 ($CH_{Ar\text{-}phenol}$),. 69.2 (CH_2O), 65.5 (CH_2O), 50.2, 48.2 (CH_α), 45.5 ($CH_{2\gamma}$), 26.8 ($CH_{3t\text{-}Bu}$), 23.0, 22.7 ($CH_{2\beta}$), 19.2 ($C_{t\text{-}Bu}$). HRMS calcd. for $[C_{69}H_{62}N_7O_2SiZn]^+$ 1112.4020; found 1112.4123.

Compound 81

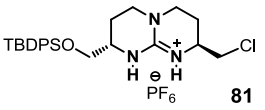

81

A solution of monodeprotected guanidine (See Experimental Section, Chapter 1) derived from compound **1** (500 mg, 1.05 mmol) in $SOCl_2$ (5 mL) was stirred refluxing it for 2 h. The solvent was removed and the resulting crude dissolved in CH_2Cl_2 (50 mL) and washed with a saturated solution of $NaHCO_3$ (50 mL) and NH_4PF_6 1N (50 mL). Purification by silica gel column chromatography (CH_2Cl_2/MeOH, 95:5) afforded **81** (498 mg, 97%) as a brownish solid. ^{1}H-NMR (400 MHz, $CDCl_3$) δ 7.69-7.61 (m, 4H, CH_{Ar}), 7.49-7.39 (m, 6H, CH_{Ar}), 6.15 (s, 1H, NH), 6.02 (s, 1H, NH), 3.74-3.52 (m, 6H, CH_2O, CH_α, CH_2Cl), 3.76-3.75 (m, 1H, CH_2O), 3.44-3.26 (m, 4H, $CH_{2\gamma}$), 2.18-1.97 (m, 3H, $CH_{2\beta}$), 1.95-1.84 (m, 1H, $CH_{2\beta}$), 1.08 (s, 9H, $CH_{3t\text{-}Bu}$). ^{13}C-NMR (100 MHz, $CDCl_3$) δ 150.5 (C_{guan}), 135.6, 135.5, 132.6, 132.5, 130.1, 128.0 (CH_{Ar}, C_{Ar}), 65.5 (CH_2O), 50.3, 49.8 (CH_α), 45.5 45.2, 44.9 (CH_2Cl, $CH_{2\gamma}$), 26.8 ($CH_{3t\text{-}Bu}$), 23.3, 22.5 ($CH_{2\beta}$), 19.1 ($C_{t\text{-}Bu}$). ESI-MS m/z 456.2 $(M - PF_6^-)^+$.

3,6-Bis(4-pyridyl)carbazole bipyridine (82)

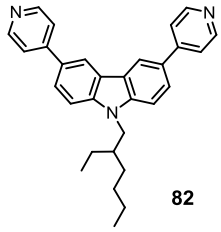

82

3,6-Dibromo-9-(2-ethylhexyl)carbazole (**83**) (220 mg, 0.503 mmol), 4-pyridyl boronic acid (309 mg, 2.52 mmol), and $Pd(PPh_3)_4$ (233 mg, 0.201 mmol) were added to a mixture of 1,4-dioxane (5 mL) and 2M Na_2CO_3 aqueous solution (5 mL). The mixture was degassed and then heated at 60ºC for 24 hours. Subsequently, the solvent was evaporated and the resulting crude was poured into water and extracted with CH_2Cl_2. The organic solution was washed with distilled water, filtered over cotton, and

evaporated again. Finally, the crude was purified by silica gel column chromatography (MeOH/EtOAC, 0:100 →10:90) to yield compound **82** (70 mg, 32 %) as a yellowish oil. ^{1}H-NMR (400 MHz, CD_3Cl) δ 8.71 (d, J = 6.1 Hz, 4 H, CH_{Ar}), 8.48 (d, J = 1.7 Hz, 2H, CH_{Ar}), 7.83 (dd, J = 1.7, 8.5 Hz, 2H, CH_{Ar}), 7.68 (d, J = 6.1 Hz, 4H, CH_{Ar}), 7.54 (d, J = 8.5 Hz, 2H, CH_{Ar}), 4.27 (dd, J = 2.7, 7.5 Hz, 2H, CH_2N), 2.18-2.08 (m, 1H, CH), 1.53-1.30 (m, 8H, CH_2), 0.97 (t, J = 7.3 Hz, 3H, CH_3), 0.89 (t, J = 7.3 Hz, 3H, CH_3). ^{13}C-NMR (100 MHz, $CDCl_3$) δ 149.8, 125.3, 121.7, 119.1, 110.0 (CH_{Ar}), 47.8 (CH_2N), 39.6 (CH), 31.0, 28.8, 24.4, 23.0 (CH_2), 14.0, 10.9 (CH_3). ESI-MS m/z 434.2 $(M+H)^+$.

3,6-Dibromo-9-(2-ethylhexyl)carbazole (83)[37]

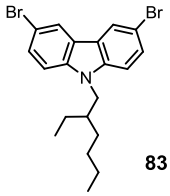

83

To a solution of 3,6-dibromocarbazole[37] (1.00 g, 3.10 mmol) in THF (15 mL) was added NaH (111 mg, 60% in mineral oil, 4.65 mmol) gradually to the mixture. The reaction was stirred at room temperature for 30 min. and 2-ethyl-hexyl bromide (0.692 mg, 3.61 mmol) was added and the mixture was refluxed overnight under argon. Water was added to destroy the excess of NaH, and the organic phase was evaporated under reduced pressure, the crude dissolved in CH_2Cl_2 and washed with 2N HCl (2 x 15 mL) and water (15 mL). The organic phase was concentrated *in vacuo* and the crude was purified by silica gel column chromatography (Et_2O/EtOAc, 5:1) to yield compound **83** (1.23 g, 92%) as a colorless oil. ^{1}H-NMR (400 MHz, CD_3Cl) δ 8.16 (d, J = 2.0 Hz, 2H, CH_{Ar}), 7.65 (dd, J = 2.0, 7.6 Hz, 2H, CH_{Ar}), 7.27 (d, J = 8.0 Hz, 2H, CH_{Ar}), 4.13 (dd, J = 2.0, 7.5 Hz, 2H, CH_2N), 2.08-1.96 (m, 1H, CH), 1.45-1.20 (m, 8H, CH_2), 0.97-0.82 (m, 6H, CH_3).

5.8.3 UV-Vis Titrations

UV-visible titrations were carried out by running a spectrum of the host solution of host (usually guanidinium bis-porphyrin compound) in tetrachloroethane, at low μM concentration range in a 1 cm path length quartz cuvette, and adding incremental amounts of host solution (fullerene or bispyridine). To avoid dilution effects, the guest solution was prepared using the host starting solution.

5.8.4 ^{1}H-NMR Titration

To a 1 mM solution of compound **79** it was added aliquots of a 10 mM solution of guest **76** in deuterated chlorobenzene, until approximately 7.5 eq. of guest. Chemical shift of guanidinium NHs signals was taken to fit the data into a theoretical model using Origin software.

UNIVERSITAT ROVIRA I VIRGILI
BICYCLIC GUANIDINIUM OLIGOMERS FOR RECOGNITION, CELL DELIVERY, AND MOLECULAR MATERIALS
Julián Valero Moreno
DL:T. 276-2012

UNIVERSITAT ROVIRA I VIRGILI
BICYCLIC GUANIDINIUM OLIGOMERS FOR RECOGNITION, CELL DELIVERY, AND MOLECULAR MATERIALS
Julián Valero Moreno
DL:T. 276-2012

Chapter 6

Diguanidinum-based Organogels

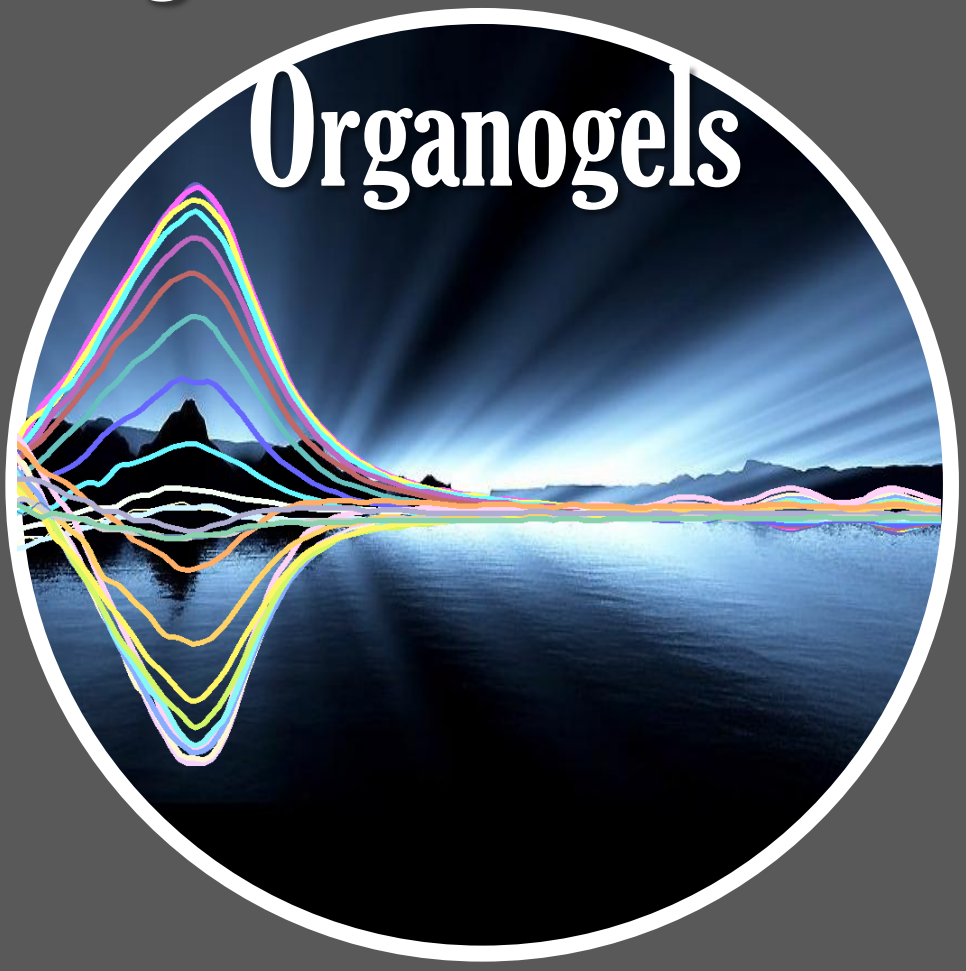

UNIVERSITAT ROVIRA I VIRGILI
BICYCLIC GUANIDINIUM OLIGOMERS FOR RECOGNITION, CELL DELIVERY, AND MOLECULAR MATERIALS
Julián Valero Moreno
DL:T. 276-2012

Chapter 6

Anion-Responsive Diguanidinium-Based Organogelators

6.1 Introduction

Gels are materials commonly found in our everyday life (shampoos, toothpastes, gelatins, contact lenses, etc.) that are used for a wide variety of applications such as cosmetics, medicine, food or materials science, among others. Although gels are usually composed of polymeric gelators which have been known for centuries, a new class of low molecular weight gelators (LMWGs) has raised an enormous interest over the last few decades.[1] These are gel-phase materials composed of small molecules able to self-assemble and to aggregate (supramolecular gelators), thus creating reticular colloidal networks in which the solvent molecules are trapped. Depending on the nature of the solvent, these LMWGs can be classified as organogelators (organic solvents) or hydrogelators (aqueous solvents). Supramolecular gelators self-assemble mainly *via* non-covalent interactions, such metal coordination, hydrogen bonding, ion-pairing, and van der Waals or hydrophobic contacts, among others. However, it is

[1] For reviews see: (a) Terech, P.; Weiss, R. G. *Chem. Rev.* **1997**, *97*, 3133-3159. (b) Abdallah, D. J.; Weiss, R. G. *Adv. Mater.* **2000**, *12*, 1237-1247. (c) George, M.; Weiss, R. G. *Acc. Chem. Res.* **2006**, *39*, 489-497. (d) Dastidar, P. *Chem. Soc. Rev.* **2008**, *37*, 2699-2715.

difficult to predict gelation phenomena and the relationship between the molecular structure and the final reticular gel structure and properties.[2]

A large variety of chemical motifs and structures, such as steroids,[3] alkyl chains, amino acids,[4] nucleobases,[5] amides and ureas,[6] peptides, saccharides, metal-coordinating ligands[7] or dendrimers,[8] are commonly found in molecular gelators. These components are essential for the molecular arrangement allowing formation of an ordered fibrillar network. Indeed, gelation can be considered as a midway process between crystallization (highly ordered self-assembled molecular architectures) and precipitation (random aggregation resulting in amorphous structures).[9] Supramolecular gels are usually formed by means of a heating-and-cooling method. However, recent developments on gels obtained upon sonication have also been reported.[10]

Over the last years, molecular gelators capable of tuning by means of an external chemical or physical stimulus have gained increasing occurrence. Changes in temperature, pH, light wavelength, oxidation state, ion binding or guest inclusion phenomena[11] can reversibly trigger the gel-to-sol phase and/or modify its physical properties. These stimuli-response gelators have found innovative applications in a

---

[2] van Esch, J. H. *Langmuir* **2009**, *25*, 8392-8394.

[3] (a) Mallia, V. A.; Tamaoki, N. *Chem. Soc. Rev.* **2004**, *33*, 76-84. (b) Žiníc, M.; Vögtle, F.; Fages F. *Top. Curr. Chem.* **2005**, *256*, 39-76.

[4] Suzuki, M.; Hanabusa, K. *Chem. Soc. Rev.* **2009**, *38*, 967-975.

[5] Araki, K.; Yoshikawa, I. *Top. Curr. Chem.* **2005**, *256*, 133-165.

[6] Fages F.; Vögtle, F.; Žiníc, M. *Top. Curr. Chem.* **2005**, *256*, 77-131.

[7] (a) Fages, F. *Angew. Chem. Int. Ed.* **2006**, *45*, 1680-1682. (b) Piepenbrock, M-O. M.; Lloyd, G. O.; Clarke, N.; Steed, J. W. *Chem. Rev.* **2010**, *110,* 1960-2004.

[8] (a) Hirst, A. R.; Smith, D. K. *Top. Curr. Chem.* **2005**, *256*, 237-273. (b) Smith, D. K. *Chem. Commun.* **2006**, 34-44.

[9] Liu, X. Y. *Top. Curr. Chem.* **2005**, *256*, 1-37.

[10] (a) Cravotto, G.; Cintas, P. *Chem. Soc. Rev.* **2009**, *38*, 2684-2697. (b) Bardelang, D. *Soft Matter* **2009**, *5*, 1969-1971.

[11] Foster, J. A.; Steed, J. W. *Angew. Chem. Int. Ed.* **2010**, *49*, 6718-6724.

range of currently relevant areas such as biomedicine,[12] catalysis,[13] nanotemplated synthesis,[14] light harvesting,[15] photonics or electro-optics,[16] taking advantage of their on-off (switchable) behavior.

Shinkai *et al.* have extensively studied cholesterol-based organogels with photoisomerizable groups which respond to UV-light changes.[17] An interesting example of photo-switchable gelators was reported by Feringa and coworkers, in which control of the gelation process of dithyenylethene **I**, both thermally and photochemically, caused the chirality of the gel to switch due to high stereoselective aggregation (Figure 1).[18]

[12] (a) Zhao, F.; Ma, M. L.; Xu, B. *Chem. Soc. Rev.* **2009**, *38*, 883-891. (b) Shah, R. N.; Shah, N. A.; Del Rosario Lim, M. M.; Hsieh, C.; Nuber, G.; Stupp, S. I. *Proc. Natl. Acad. Sci. USA* **2009**, *107*, 3293-3298. (c) Zelzer, M. M; Ulijn, R. V. *Chem. Soc. Rev.* **2010**, *39*, 3351-3357.

[13] (a) Escuder, B.; Rodríguez-Llansona, F.; Miravet, J. F. *New J. Chem.* **2010**, *34*, 1044-1054. (b) Rodríguez-Llansona, F.; Miravet, J. F.; Escuder, B. *Chem. Eur. J.* **2010**, *16*, 8480-8486.

[14] (a) Jung, J. H.; Shinkai, S. *Top. Curr. Chem.* **2004**, *248*, 223-260. (b) Kimura, M.; Kobayashi, S.; Kuroda, T.; Hanabusa, K.; Shirai, H. *Adv. Mater.* **2004**, *16*, 335-338. (c) Moffat, J. R.; Coates, I. A.; Leng, F. J.; Smith, D. K. *Langmuir* **2009**, *25*, 8786-8793.

[15] Ajayaghosh, A.; Praveen, V. K.; Vijayakumar C. *Chem. Soc. Rev.* **2008**, *37*, 109-122.

[16] (a) Kato, T. *Science*, **2002**, *295*, 2414-2418. (b) Kato, T.; Mizoshita, N.; Moriyama, M.; Kitamura T. *Top. Curr. Chem.* **2005**, *256*, 219-236.

[17] (a) Murata, K.; Aoki, M.; Nishi, T.; Ikeda, A.; Shinkai, S. *Chem. Comm.* **1991**, 1715-1718. (b) Murata, K.; Aoki, Suzuki, T.; Harada, T.; Kawabata, H.; Komori, T.; Ohseto, F.; Ueda, K.; Shinkai *J. Am. Chem. Soc.* **1994**, *116*, 6664-6676. (c) Sugiyasu, K.; Fujita, N.; Shinkai, S. *Angew. Chem. Int. Ed.* **2004**, *43*, 1229-1233. (d) Kawano, S.; Fujita, N.; Shinkai, S. *J. Am. Chem. Soc.* **2004**, *126*, 8592-8593. (e) Kawano, S.; Fujita, N.; Shinkai, S. *Chem. Eur. J.* **2005**, *11*, 4735-4742.

[18] de Jong, J. J. D.; Lucas, L. N.; Kellogg, R. M.; van Esch, J. H.; Feringa, B. L. *Science* **2004**, *304*, 278-281.

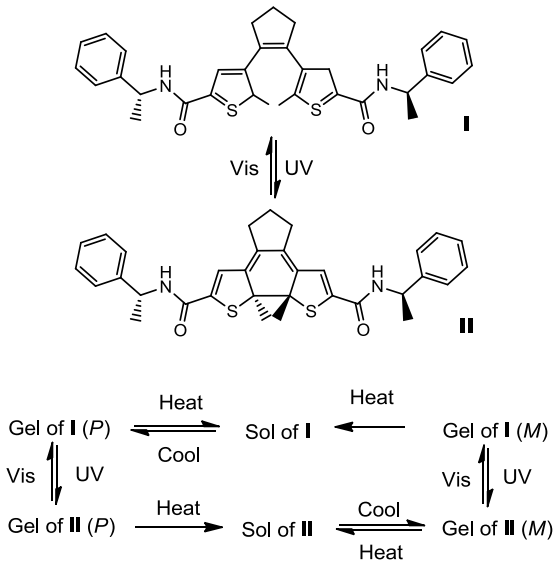

Figure 1. *Example of a photoswitchable chiral gelator reported by Feringa et al.*

pH sensitive gelators based on scaffolds such as calix[4]arenes[19] and resorcin[4]arenes[20] have been described by several authors. Ballester *et al.* recently reported a calix[4]pyrrole gelator capable of triggering its gel flow behavior through subtle changes in pH or in the presence of sodium cations.[21]

Another elegant application of cavities not used as scaffolds, but as active elements which confer structural features to the gelators has been reported by Harada *et al.*[22] Thus, acrilamide-based gelators functionalized with either cyclodextrin hosts (**III**) and different hydrocarbon guests (**IV**) were synthesized in order to study molecular recognition at the macroscopic level (Figure 2). By modulating the size and shape of

[19] Becker, T.; Goh, C. Y.; Jones, F.; McIldowie, M. J.; Mocerino, M.; Ogden M. I. *Chem. Commun.* **2008**, 3900-3902.

[20] Haines, S. R.; Harrison, R. G. *Chem. Commun.* **2002**, 2846-2847.

[21] Verdejo, B.; Rodríguez-Llansola, F.; Escuder, B.; Miravet, J. F.; Ballester P. *Chem. Commun.* **2011**, *47*, 2017-2019.

[22] Harada, A.; Kobayashi, R.; Takashima, Y.; Hashidzume, A.; Yamaguchi, H. *Nat. Chem.* **2011**, *3*, 34-37.

the host and guest moieties, different gels can assemble selectively, taking advantage of the cavity insertion phenomenon at the molecular scale. Hence, this leads to the construction of programmable "smart" materials capable of binding exclusively its complementary guest molecule, even in the presence of other building blocks.

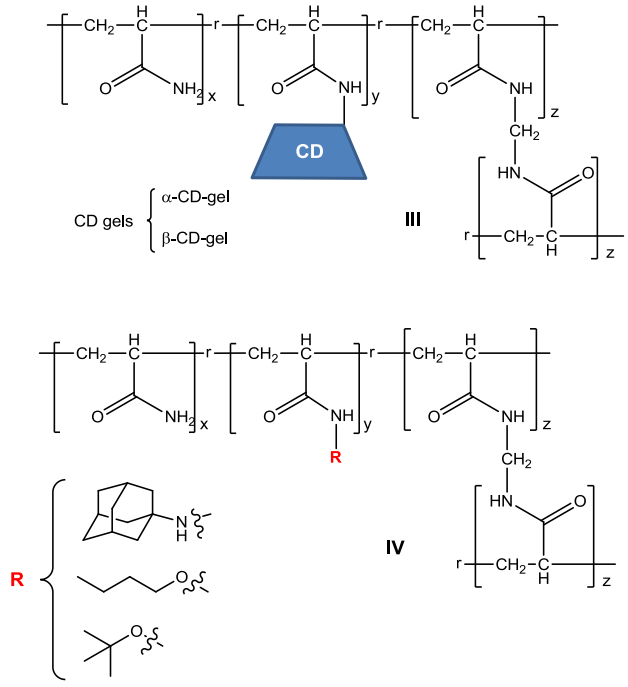

Figure 2. *Acrilamide-based gelators with macroscopic self-assembly properties.*

Ion binding can be used to tune molecular self-assembly and thus gelation. Cation-dependent gels (also known as metallogels)[6] have been designed by introducing coordinating subunits as structural components in the gelator. Work by Lehn *et al.* has shown that use of naturally occurring cation-templated structures such as G-quartets (**V**), can afford gelation under certain pH and cation concentration conditions (Figure 3).[23] This association can be reversibly triggered with cryptands capable of arresting K^+

[23] Ghoussoub, A.; Lehn, J-M. *Chem. Commun.* **2005**, 5763-5765.

cations from the supramolecular assembly. Complex dynamic hydrogels were also reported using hydrazine derived G-quartet architectures in the presence of aldehydes to allow reversible formation of gels with diverse structures and physical features.[24]

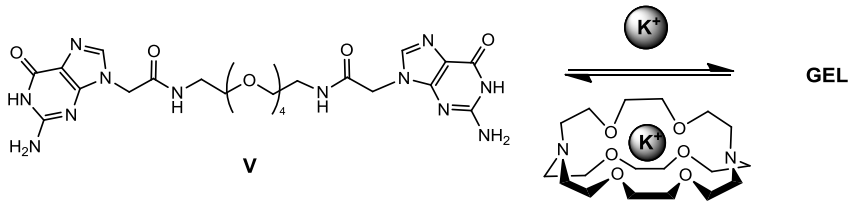

Figure 3. *Bis-guanine gelator repored by Lehn and coworkers.*

Over the last few years, anion-responsive supramolecular gels have raised a growing interest due to their tunability and unique reversible characteristics.[7b,25] The structural information contained in these architectures is highly dependent on the choice of both the ligand and the anion. The design of these anion-switchable gelators and the study of macroscopic changes induced by subtle variations at the molecular level is one of the major goals in this field.

Amide and urea based organogelators capable of tuning their properties in the presence of certain anions have been recently described. For example, the tris-urea compound **VI** (Figure 4) forms opaque gels in acetone after sonication.[26] In the presence of anions such as Cl^- or F^-, the gel is transformed into a solution, although this behavior is not observed with BF_4^-. Sol-to-gel transitions occur with $BF_3{\cdot}OEt_2$ even in the presence of Cl^- anions. $ZnBr_2$ was used as a non-specific chemical stimulus for the recovery of the gel phase previously disrupted by the addition of other anions.

[24] Sreenivasachary, N.; Lehn, J-M. *Proc. Natl. Acad. Sci. USA* **2005**, *106*, 5938-5943.

[25] For reviews see: (a) Maeda, H. *Chem. Eur. J.* **2008**, *14*, 11274-11282. (b) Lloyd, G. O.; Steed, J. W. *Nat. Chem.* **2009**, *1*, 437-442.

[26] Yamanaka, M.; Nakamura, T.; Nakagawa, T.; Itagaki, H. *Tetrahedron Lett.* **2007***, 48*, 8990-8993.

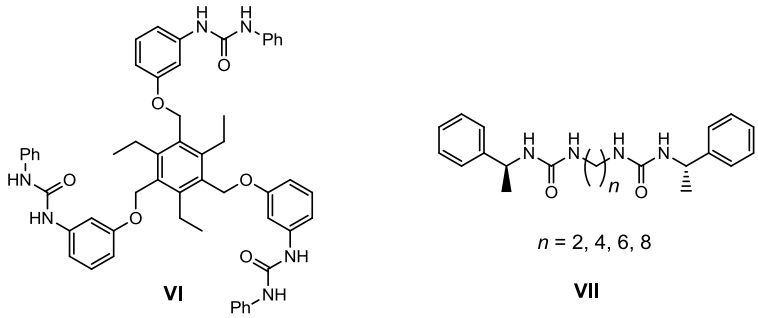

Figure 4. *Examples of urea-based anion-responsive gelators.*

Steed *et al.* reported a bis-urea-based series of compounds (**VII**) in which the number of methylene groups in the bridge between the urea moieties was found to be essential for gelation control (Figure 4).[27] With an even number of methylene units (n = 2, 4, 6, 8) gels were successfully formed. Conversely, only solutions were obtained when an odd number of carbon atoms were present (n = 3, 5, 7, 9). This behavior can be explained by the relative orientation of the urea moieties, which is critical for the molecular self-assembly. Moreover, the rheological properties of these gels change dramatically upon addition of specific anions, affecting the hydrogen bonding network between the ureas. In this case, not only sol-to-gel transitions were detected, but also the strength of the gel decreased in the presence of small amounts (0.1 equiv. of TBA salts) of AcO^-, Cl^- or BF_4^-.

Proline functionalized calix[4]arene **VIII** forms gels only in the presence of nitrate or halide anions (Figure 5).[19] Therefore, anion binding can be seen as a structural factor in this system, in order to induce molecular aggregation, thus enhancing gelation.

[27] Piepenbrock, M.-O. M.; Lloyd, G. O.; Clarke, N.; Steed, J. W. *Chem.Commun.* **2008**, 2644-2646.

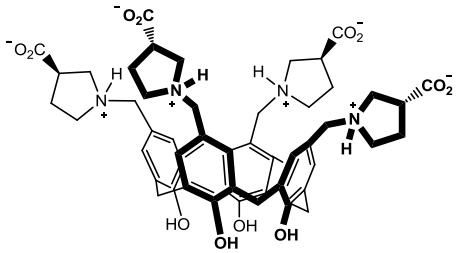

Figure 5. *Calix[4]arene* ***VIII*** *forms stable anion-tunable gels.*

A further step in the rational design of anion-tunable gelators was made by Chiu *et al.*[28] They introduced the urea-based rotaxane **IX** (Figure 6) to switch reversibly from gel to sol phase by means of anion exchange and pH variation. Selective anion coordination was responsive to provoke molecular motion over the rotaxane framework thus inhibiting or enhancing the correct geometry to induce gelation.

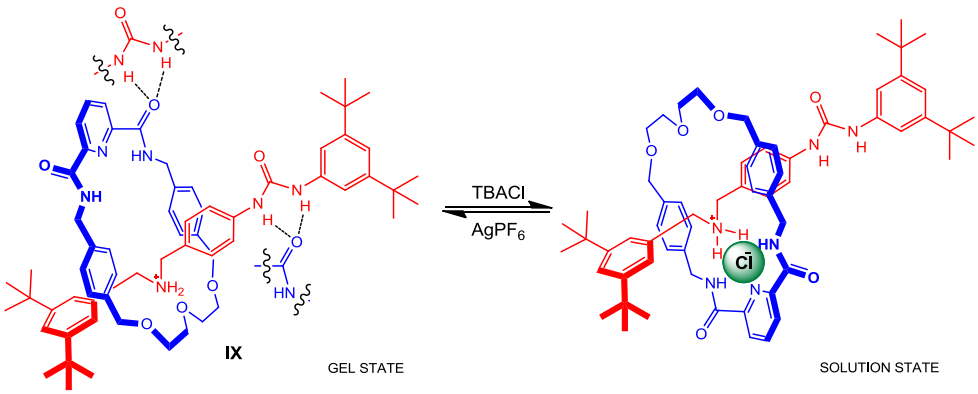

Figure 6. *Anion switchable rotaxane gelator* ***IX*** *reported by Chiu et al.*

[28] Hsueh, S-Y.; Kuo, C-T.; Lu, T-W.; Lai, C-C.; Liu, Y-H.; Hsu, H-F.; Peng, S-M.; Chen, C.; Chiu, S-H. *Angew. Chem. Int. Ed.* **2010**, *49*, 9170-9173.

These new types of innovative materials with switchable properties have raised a big interest over the last decade,[29,30] mainly due to their adaptability to different stimulus and stresses, which is a major issue in areas such as medicine or electronics.

Within this context, we introduce herein a new family of anion responsive chiral gels, which are able to shift from the gel to the sol phase in the presence of specific chemical stress.

Enantiomerically pure oligomers of chiral bicyclic guanidinium salts have been successfully employed for the molecular recognition of oxoanions, such as sulfates, carboxylates, phosphates (nucleotides), and other anions.[31] These molecules have been widely studied in solution, but since only a few crystallographic data were thus far available, the structural packing and the tridimensional network that these compounds adopt in the solid state was largely unknown. We now describe how diguanidinium molecule **4** (Scheme 1) can form gels under certain conditions and solvents (See Table 1). These gels are formed in the concentration range between 0.5-1.5% wt. depending on the solvent used. The study of the properties and the structural features of these colloidal systems could be extremely interesting for achieving molecular recognition at those interfaces. Part of this work (microscopy and NMR characterization) has been done in collaboration with Prof. Beatriu Escuder in Universitat Jaume I.

[29] Hirst, A. R.; Escuder, B.; Miravet, J. F.; Smith, D. K. *Angew. Chem. Int. Ed.* **2008**, *47*, 8002-8018.

[30] de Loos, M.; Feringa, B. L.; van Esch, J. H. *Eur. J. Org. Chem.* **2005**, 3615-3631.

[31] Blondeau, P.; Segura, M.; Pérez-Fernández, R.; de Mendoza, J. *Chem. Soc. Rev.* **2007**, *36*, 198-210.

6.2 Synthesis, Characterization and Gelation Behavior of Bicyclic Diguanidinium Organogelators

As previously reported, synthesis of diguanidinium chloride **4** was achieved by nucleophilic attack of the monoguanidinium thiolate precursor **3** on mesylate **2**, yielding diguanidine **4** as a white solid (Scheme 1).

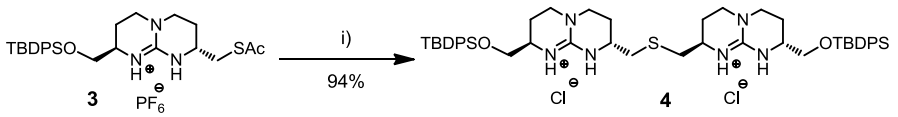

Scheme. 1*. Synthetic scheme for diguanidinium salt* ***4****. Conditions: i) 1 eq.* ***2****, 2.7 eq.* Cs_2CO_3, N_2.

To have an insight on the conformation of this molecule in the solid state, preliminary crystallization experiments were performed in a variety of solvents and solvent mixtures. Unfortunately, no single crystals were obtained under any of these conditions. Instead, gelation was observed in some cases. Table 1 summarizes the solvents employed.

Table 1. *Representative solvent conditions for gelation of* ***4*** *(chloride).*

Solvent	Result	Solvent	Result	Solvent	Result
Toluene	G	Acetonitrile	S	Toluene/Hexane	G
Hexane	I	Acetone	S	THF/Hexane	G
Chloroform	S	Chloroform/Ether	G	AcOEt/Hexane	G
DCM	S	Acetonitrile/Ether	I	Chloroform/Hexane	PG
THF	S	THF/Ether	PG	THF/Water	I
iPrOH	S	iPrOH/Ether	I	MeOH/Water	I
EtOH	S	Toluene/Ether	I	Ether	I
MeOH	S	Hexane/EtOH	I	p-Xylene	G
AcOEt	S	Acetone/Ether	I	Mesitylene	G

[gelator]=10.5 mM at room temp., I= Insoluble, S= Solution, G= Gel, PG = Partial Gel

In general, **4** (chloride) formed gel phases in solvents such as chloroform, THF, toluene, or ethyl acetate when mixed with diethyl ether or hexane, in the concentration range 0.5-1.5 % w/w. This behavior was also observed with pure aromatic solvents such as toluene, *p*-xylene and mesitylene.

Gelation experiments with unprotected diguanidinium diol **5** (Figure 7), showed no gel under similar conditions and solvents as for gelation of **4**, revealing the important role of the bulky hydrophobic TBDPS groups in the gelation process.

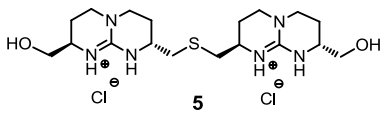

5

Figure 7. *Diguanidinium diol* ***5.***

As expected, when the configuration of the chiral centers was switched from *R,R-R,R* to *S,S-S,S* (named as **(*R*)-4** and **(*S*)-4**, respectively), the gelation properties remained the same. On the contrary, no gel was observed for the *R,R-S,S* diastereoisomer (**(*R,S*)-4**). Moreover, mixtures of the enantiomerically pure **(*R*)-4** and **(*S*)-4** enantiomers gave rise to weaker gels or even to total disruption of the aggregates. This highlights the relevance of stereochemistry in the gelation process.

Exchange of the counterion from chloride to hexafluorophosphate resulted in the collapse of the gel. This points out the pivotal role of the anion in the self-assembly and gelation of diguanidinium salt **4**. Chiral effects and anion stimulus over gelator **4** will be discussed in more detail later on.

The thermal stability of gelator **4**, was assessed by simple tube inversion experiments.[32] Aromatic solvents afforded robust and transparent gels, suggesting good solubility behavior. Hence, gels formed in toluene, *p*-xylene and mesitylene were

[32] Raghavan, S. R.; Cipriano, B. H. Gel Formation: Phase Diagrams using Tables of Rheology and Calorimetry. In *Molecular Gels: Materials with Self-Assembled Fibrillar Networks*; Weiss, R. G., Terech, P., Eds.; Springer: Dordrecht, The Netherlands, **2006**; Chapt. 8.

selected to construct their corresponding thermal profiles. In addition, both enantiomers (**(*R*)-4** and **(*S*)-4**) were tested independently at different concentrations to evaluate their stability upon heating. Typically, as the concentration of gelator increases, the sol-gel transition temperature (T_{gel}) also raises until reaching a plateau, as depicted in Figure 8.

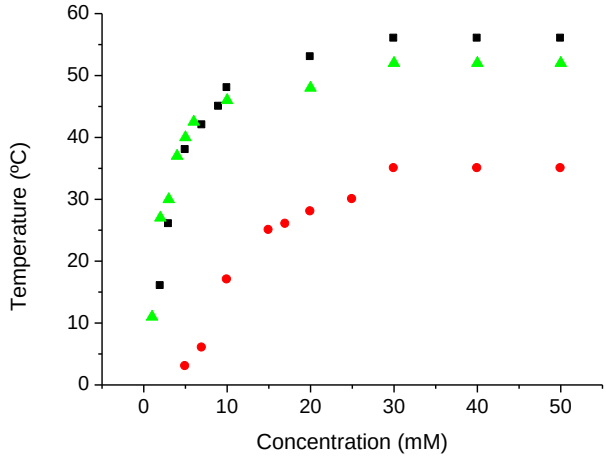

Figure 8. *Thermal profiles showing sol-gel transition processes depending on the aromatic solvent used (● toluene, ■ xylene, ▲ mesitylene).*

Gels in toluene showed a maximum T_{gel} at 32 ºC, whereas those formed in xylene and mesitylene (56 and 52 ºC, respectively) were thermally more stable.

To better understand these differences, thermodynamic parameters (ΔH, ΔS) for the sol-gel process were deduced from the slopes of T_{gel} curves, using a derivation of the van't Hoff equation (Equation 1).

$$\log[conc.] = -\frac{\Delta H}{R\,T_{gel}} + \frac{\Delta S}{R}$$

Equation 1. *Van't Hoff derived equation for the thermodynamics involving sol-gel processes.*

Linear plots of the fitting curves resulting from this formula are shown in Figure 9.

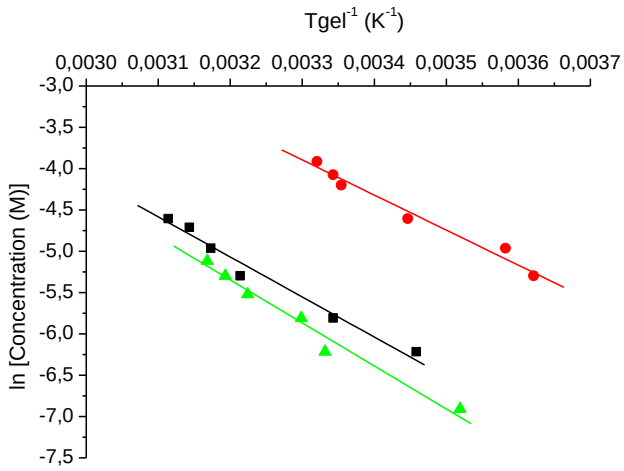

Figure 9. *T_{gel}^{-1} vs. ln[conc.] slopes for the estimation of the thermodynamic parameters involving gelation process (● toluene, ■ xylene, ▲ mesitylene).*

The enthalpic contribution increases as the number of methyl substituents of the solvent increase (Table 2). A feasible explanation for this solvent-dependent gelation tendency relies in considering the solution of the gel as a two independent step processes. The first one would be the gel-to-sol phase transition followed by a second one which implies the discrete dispersion of the organogelator into the solvent.[17b]

Obviously, the solvent will affect this second process, except when differences in solubility of organogelator **4** are negligible. The gel-to-sol phase transition step could be also influenced by the solvent if it forms an active part of the reticular structure.

Table 2. *Thermodynamic values extracted from the van't Hoff derived equation.*

Solvent	**(*R*)-4** Toluene	**(*R*)-4** *p*-Xylene	**(*R*)-4** Mesitylene	**(*R*)-4** / **(*S*)-4** (1:1) *p*-Xylene
ΔH (KJ mol^{-1})	34.4 (2.7)	39.3 (3.1)	42.3 (3.3)	56.2 (4.0)
$T\Delta S$ (KJ mol^{-1})*	24.2 (2.8)	25.0 (3.0)	27.1 (3.2)	45.4 (4.0)
ΔG (KJ mol^{-1})*	10.3	14.4	15.2	10.8

**⊥G and T⊥S values calculated at T=298.15 K. Numbers in parenthesis represent the associated error.*

In addition, 1:1 enantiomeric mixtures (**(*R*)-4**/**(*S*)-4**) of the bicyclic guanidinium dimer in *p*-xylene were studied in order to establish their sol-gel transition temperatures and thus the thermodynamic parameters involving gelation process. As previously observed, these gels are less stable that the enantiomerically pure ones and therefore higher concentrations of gelator are required (Figure 10). Indeed, for the heterochiral gel in *p*-xylene the entropic penalty is higher than for the homochiral one but this is compensated by a more favorable enthalpic term. This results in a lower free energy (10.8 KJ·mol^{-1} for **(*R*)-4**/**(*S*)-4** and 14.4 KJ·mol^{-1} for **(*R*)-4** in *p*-xylene), which is in good agreement with the differences in thermal stability (T_{gel}), and minimum gelation concentration (MGC) found for both gels.

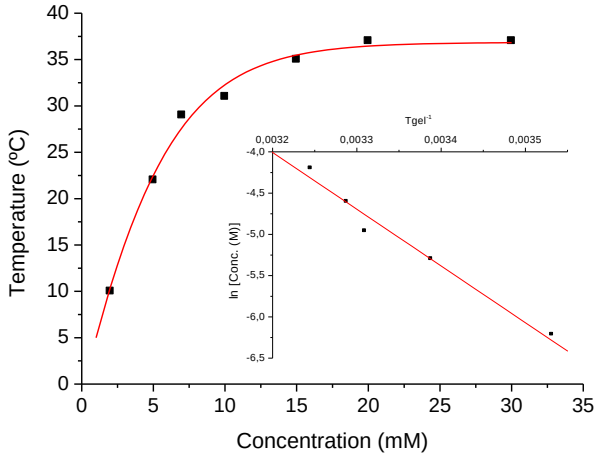

Figure 10. *Thermal profiles of the racemic diguanidinium mixture in p-xylene.*

6.3 Microscopy Imaging

To determine the morphology of these gels, diverse microscopic techniques were employed. Optical micrographs were taken from toluene gels as shown in Figure 11. These gels were composed by bundles of macroscopic crystalline-like fibers able to disperse polarized light.

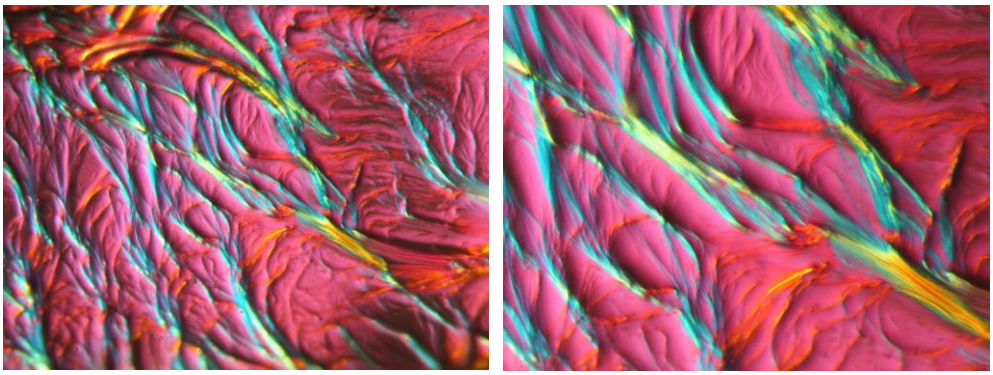

Figure 11. *Optical micrographs of* ***(R)-4*** *gels formed in toluene.*

Transmission electron microscopy (TEM) confirmed the existence of well-defined fibrillar structures of approximately 20-30 nm width and several micrometers length (Figure 12).

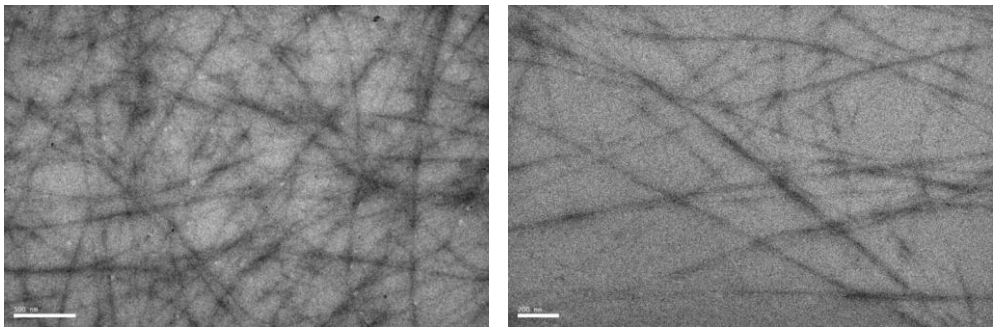

Figure 12. *TEM images of* ***(R)-4*** *gels formed in toluene.*

Besides, Field Emission Scanning Electron Microscopy (FESEM) imaging clearly showed how the matrix microstructure was altered from fibrillar to vesicular nanostructures upon changing the solvent (Figure 13). This emphasizes again the role of the solvent in the colloidal network formation.

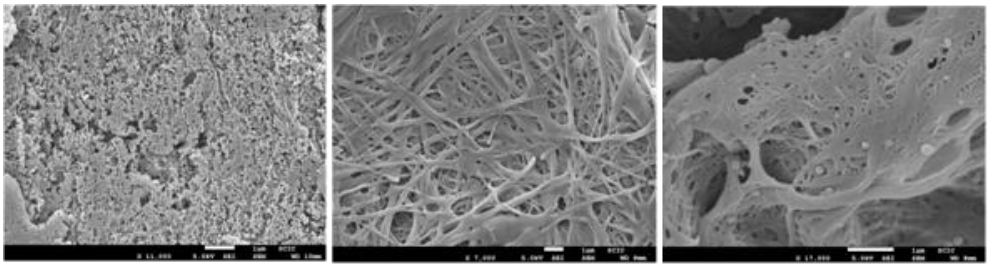

Figure 13. *FESEM images of* ***(R)-4*** *gels formed in toluene/hexane, chloroform/hexane and ethyl acetate/hexane mixtures (from left to right, respectively).*

Finally, TEM images of both enantiomeric gels in *p*-xylene evidenced unambiguously the existence of supramolecular chiral induction. As shown in Figure 14, gels composed by the diguanidinium salt **(*R*)-4** provided left handed coils whereas the **(*S*)-4** enantiomer produced the inverse right handed helices. This observation fully supports the experimental data from the circular dichroism (see section 6.5), pointing

out to the effective expression of the molecular chirality into helical fibers.

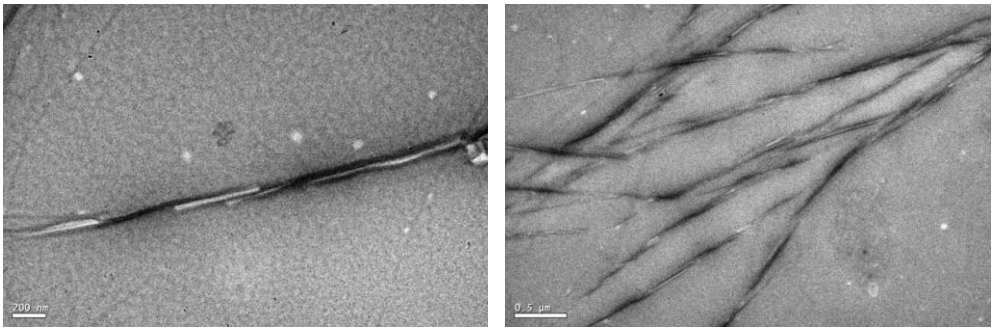

Figure 14. *TEM images of* ***(R)-4*** *(left) and* ***(S)-4*** *(right) which form chiral gels in p-xylene.*

6.4 NMR Studies

To further examine the sol-to-gel transition of organogelator **4**, concentration-dependent ^{1}H-NMR experiments were performed.

Different concentrations (from 2.5 to 30 mM) of **(*R*)-4** in deuterated toluene were measured in order to obtain additional information about the self-assembly process which controls gelation.

As the concentration increases the signals became broader suggesting molecular aggregation, and a restricted molecular motion resulting in larger relaxation times relative to the free species in solution.

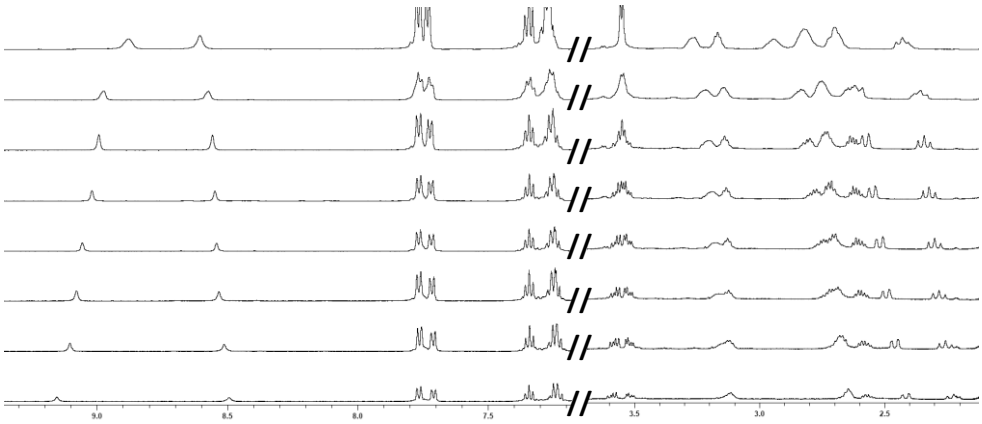

Figure 15. *^{1}H-NMR spectra (in toluene-d_8) of organogelator* ***(R)-4*** *at different concentrations (from 2.4 to 30 mM).*

The NH guanidinium protons were shifted up- and downfield, respectively, as the amount of organogelator raised (Figure 15). Split signals corresponding to CH_2O protons also merged into a unique doublet indicating a similar chemical environment for both protons caused by inherent molecular interactions upon self-assembly.

The guanidine skeleton and the CH_2S protons also showed downfield shifts, supporting the aggregation. With these NMR data in hand, several aggregation models

were considered but any of them fitted with the experimental values obtained and thus, the stability constant of the aggregation could not be unequivocally determined. To overcome this, different experimental conditions (temperature, solvent) are currently investigated.

NOESY experiments were performed at different concentrations to get a better insight on the aggregation of compound **(*R*)-4** in deuterated toluene. Unexpected intermolecular nOe contacts were found between different protons in the concentrated gel sample which supports a new spatial disposition of diguanidinium chloride **4** upon aggregation (Figure 16). Control experiments with the diluted sample showed the predicted nOe contacs for these molecules, corroborating this aggregation process.

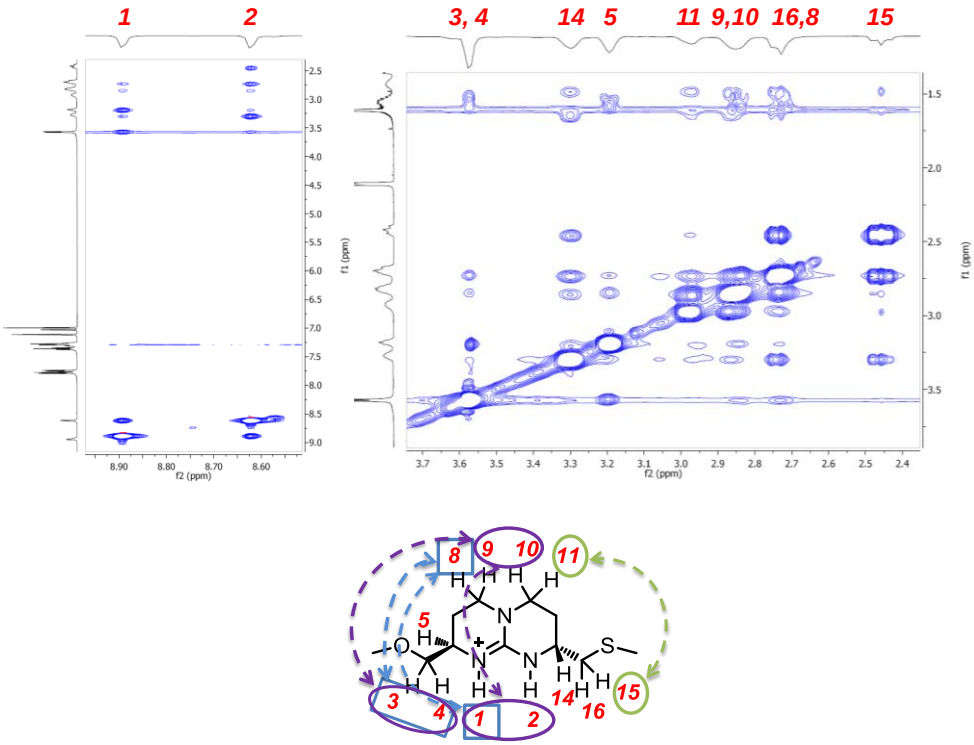

Figure 16. *(Top) Sections of the NOESY spectrum of organogelator* ***(R)-4*** *in toluene-d_8 at 21.4 mM. (Below) Scheme of the most representative nOe contacts.*

6.5 Role of Chirality on Gelation

Circular dichroism (CD) studies were performed to assess the supramolecular helicity observed by microscopy and to study in detail the chiral induction process from diguanidinium chloride **4** to the corresponding gel-phase material.[33]

Previous studies and molecular modeling demonstrated that guanidinium oligomers fold into helical systems in the presence of suitable tetrahedral counterions. Indeed, tetraguanidinium strands were able to wrap around sulfate anions forming double helicates (Figure 17).[34] It is likely that the aggregates resulting from **4** are also organized into helical fibers.

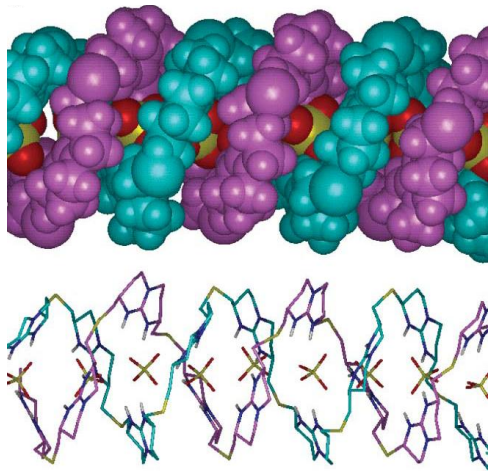

Figure 17*. Optimized model of a sulfate helicate from (S,S)-guanidines.*

Aromatic solvents were avoided because their λ cutoff directly interferes with the CD signal of the gel. Hence, CD experiments were carried out in a (1:3) THF:hexane

[33] For reviews see: (a) Brizard, A.; Oda, R.; Huc, I. *Top. Curr. Chem.* **2005**, *256*, 167-218. (b) Gottarelli, G.; Lena, S.; Masiero, S.; Pieraccini, S.; Spada, G. P. *Chirality* **2008**, *20*, 471-485. (c) Smith, D. K. *Chem. Soc. Rev.* **2009**, *38*, 684-694.

[34] Sánchez-Quesada, J.; Seel, C.; Prados, P.; de Mendoza, J. *J. Am. Chem. Soc.* **1996**, *118,* 277-278.

mixture at 0.3 mM concentration. Transparent gels were in situ formed in a 0.1 cm path length cuvette. Gels of **(*R*)-4** enantiomer produced a strong positive band at 225 nm, while the **(*S*)-4** ones gave the inverse negative Cotton effect, as expected. Interestingly, ellipticity of **(*R*)-4** in solution using pure THF at the same concentration significantly decreased and showed opposite sign compared to the corresponding gel. This indicates that the formation of a gel-phase material alters the intrinsic chirality of the system and therefore a strong cooperative effect in the molecular stacking is responsible for inducing supramolecular helicity. Indeed, this is a well-known phenomenon extensively occurring in nature, where for instance L-amino acids fold into α-helix as a secondary structure with opposite ellipticity.[35]

To demonstrate that gel integrity is directly related to its chiral behavior, temperature-dependent CD experiments were performed (Figure 18). As the sample was slowly heated up, ellipticity gradually decreased until showing almost a silent CD at 65 ºC. At this temperature the gel disassembled and the CD spectrum was similar to the one of the molecule in solution. Signal was recovered upon cooling down and increased considerably at lower temperatures (5 ºC). Hence, the stability of the gel-phase is essential for the maintenance of its helicity.

[35] (a) Pauling, L.; Corey, R. B.; Bramson, H. R. *Prod. Natl. Acad. Sci. USA* **1951**, *37*, 205-211. (b) Dunitz, J. D. *Angew. Chem. Int. Ed.* **2001**, *40*, 4167-4173.

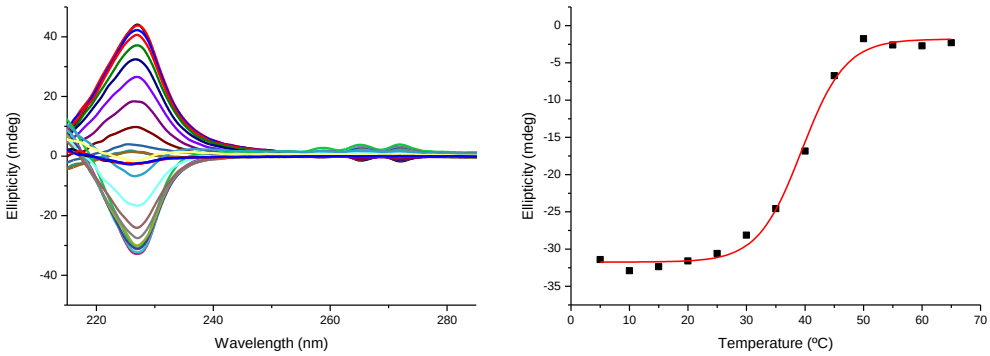

Figure 18. *(Left) Temperature-dependent (from 65 to 5 ºC) circular dichroism spectra of enantiomers* ***(R)-4*** and ***(S)-4*** *performed in THF:hexane (1:3). (Right) Helicity values at 227 nm for* ***(S)-4*** *at different temperatures.*

As previously reported, the gelation was dramatically affected by the chiral nature of diguanidinium gelator. Indeed, the "meso" diguanidinium diastereoisomer **(*R,S*)-4** was not capable of forming gels under the standard gelation conditions. Besides, 1:1 mixtures of the **(*R*)-4** and **(*S*)-4** enantiomers required higher amounts of organogelator to form the colloid. Moreover, these "racemic" gels in xylene showed lower sol-gel temperatures (37 ºC) than the enantiomerically pure ones (56 ºC).

Chiral amplification CD measurements with mixtures of enantiomers of **4** were performed to further discuss the effect on the stability and the intrinsic ellipticity of the gel.[36]

On one hand, gels of enantiomerically pure diguanidinium choride salts were doped with different amounts of the mirror enantiomer. For systems driven by the so-called

[36] (a) van Gorp, J. J.; Vekemans, J. A. J. M.; Meijer, E. W. *J. Am. Chem. Soc.* **2002**, *124*, 14759-14769. (b) Cai, W.; Wang, G-T.; Du, P.; Wang, R-X.; Jiang, X-K.; Li, Z-T. *J. Am. Chem. Soc.* **2008**, *130*, 13450-13459. (c) Das, R. K.; Kandanelli, R.; Linnanto, J.; Bose, K.; Maitra, U. *Langmuir* **2010**, *26*, 16141-16149.

"majority rule" effect,[37,38] the major enantiomer dictates the helicity of the aggregate, even in the presence of the opposite enantiomer. In our system, supramolecular chirality is governed by the formation of stable aggregates able to gel. However, these enantiomeric mixtures provide weaker gels. Thus, when the gel-phase is not well defined, it is expected that the overall ellipticity decreases upon decreasing the optical purity of the mixture.

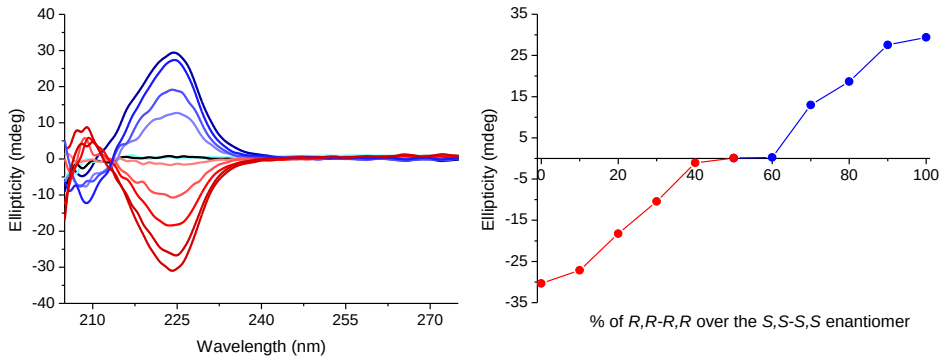

Figure 19. *(Left) Circular dichroism spectra (in THF:hexane (1:3)) of different enantiomeric mixtures (R,R-R,R and S,S-S,S) of diguanidinium organogelator* ***4****. (Right) Ellipticity values at 225 nm at different enantiomeric ratios of organogelator.*

As shown in Figure 19, this is the general tendency at room temperature. Nevertheless, the trend is not completely linear accounting for chiral amplification due to an appreciable "majority rule" effect. Ellipticity is maintained upon addition of small

[37] (a) Green, M. M.; Peterson, N. C.; Sato, T.; Teramoto, A.; Cook, R.; Lifson, S. *Science* **1995**, *268*, 1860-1866. (b) Green, M. M.; Park, J.-W.; Sato, T.; Teramoto, A.; Lifson, S.; Selinger, R. L. B.; Selinger, J. V. *Angew. Chem. Int. Ed.* **1999**, *38*, 3138-3154. (c) Green, M. M.; Cheon, K.-S.; Yang, S.-Y.; Park, J.-W.; Swansburg, S.; Liu, W. *Acc. Chem. Res.* **2001**, *34*, 672-680. (d) van Gestel, J. *Macromolecules* **2004,** *37,* 3894-3898. (e) Smulders, M. M. J.; Stals, P. J. M.; Mes, T.; Paffen, T. F. E.; Schenning, A. P. H. J.; Palmans, A. R. A.; Meijer, E. W. *J. Am. Chem. Soc.* **2010**, *132*, 620-626.

[38] Langeveld-Voss, B. M. W.; Waterval, R. J. M.; Janssen, R. A. J.; Meijer, E. W. *Macromolecules* **1999**, *32,* 227-230.

amounts of the opposite enantiomer (80% ee) and subsequently, the intensity of CD signal decreases linearly until 20% ee, where it becomes almost negligible. Within this enantiomeric excess range (0-20 % ee), gel samples collapse and supramolecular chiral contribution is lost.

On the other hand, gels containing **(*R*)-4** enantiomer were doped with different amounts of "meso" diguanidinium salt **(*R,S*)-4** in order to evaluate its chiral and structural contribution. The "meso" diguanidinium diastereoisomer has an almost silent CD signal and is not able to form gels. As observed in Figure 20, helicity decreases as the amount of the "meso" diastereoisomer increases. At 40% diasteroisomer content, the gel-phase is disrupted with a consequent loss of ellipticity.

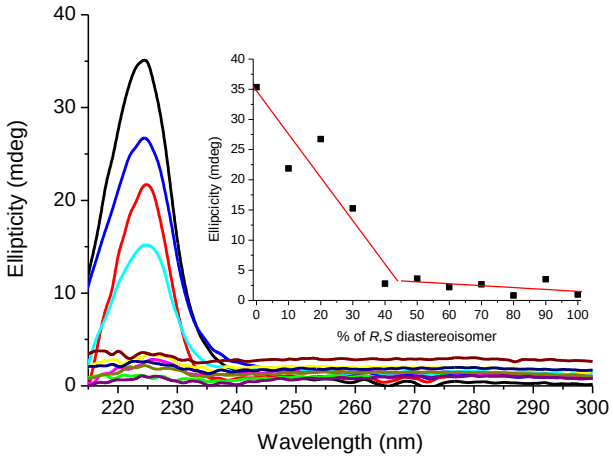

Figure 20. *Circular dichroism spectra of different enantiomeric mixtures of diguanidinium organogelator* ***(R)-4*** *and* ***(R,S)-4*** *at 25 ºC in THF:hexane (1:3). (inside: ellipticity values at different ratios of diguanidines* ***(R)-4*** *and* ***(R,S)-4****).*

When cooling down at 5 ºC the trend was similar although the ellipticity was maintained unambiguously up to 20% diastereoisomer content, as depicted in Figure 21.

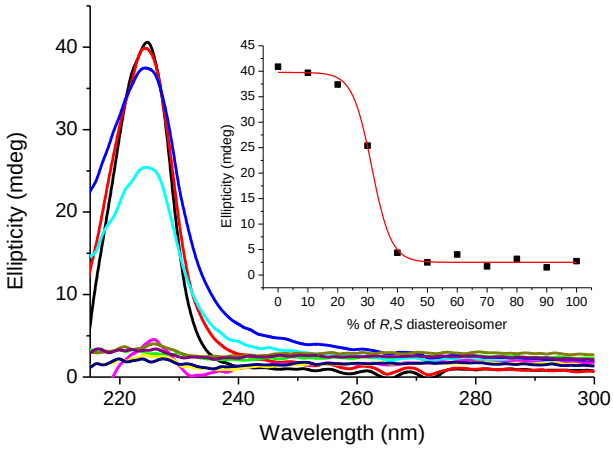

Figure 21. *Circular dichroism spectra of different enantiomeric mixtures of diguanidinium organogelator* ***(R)-4*** *and* ***(R,S)-4*** *at 5 ºC in THF:hexane (1:3). (inside: ellipticity values at different ratios of diguanidines* ***(R)-4*** *and* ***(R,S)-4****).*

In conclusion, the "meso" diguanidinium molecule provokes a destabilization on the aggregate architecture, which affects the overall ellipticity. However, at lower temperatures the chiral and structural features of the gel are preserved, even in the presence of small amounts of diastereoisomer **(*R,S*)-4**. As demonstrated, at 5 ºC gel stability is higher and small changes in composition do not drastically influence its helicity. Those experiments rely on the "sergeants-and-soldiers" fundaments, where some chiral "sergeant" molecules dictate the overall ellipticity of a system mainly composed by achiral "soldier" molecules.[39] In our case, the chiral "sergeant", namely diguanidinium enantiomer **(*R*)-4**, is able to retain the initial ellipticity only in the presence of a small amount of "meso" diguandinium "soldiers", thus maintaining the gel chiral information. These soldiers are not purely achiral but at those concentrations they show no significant CD signal and are able to induce gel disruption. Thus, it can be pointed out that chiral amplification subtly occurs.

[39] Nam, S. R.; Lee, H. Y.; Hong, J-I. *Chem. Eur. J.* **2008**, *14*, 6040-6043.

6.6 Anion Responsive Properties

Previous experiments with diguanidininum hexafluorophosphate salts showed no gel formation, pointing out once again to the influence of the anion on the gelation process. Some literature examples report this anion tunability and its potential applications.[25] For instance, Steed *et al* described a bis-urea type organogelators for the crystal growth of pharmacological active molecules and their subsequent release using anion switchable conditions.[40]

Anion exchange experiments were designed in order to examine this effect in more detail. Diguanidinium chloride gels of **(*R*)-4** formed in toluene and *p*-xylene and were tested in concentration ranges from 10 to 20 mM. Approximately the same volume (150 μL) of different aqueous ammonium salt solutions (0.1M) was added to each of the samples. Upon heating, a liquid-liquid biphase was formed and efficient anion exchange was promoted by mixing it vigorously. Finally, the biphasic system was cooled down to room temperature, allowing the sol-gel transition to occur.

Interestingly, aqueous ammonium and tetrabutylammonium solutions of chloride or bromide anions led to the formation of stable gels whereas solutions containing AcO^-, BzO^-, NO_3^-, PF_6^-, HSO_4^- resulted in disruption of the colloid.

This process was completely reversible (up to 5 cycles) upon removal of the aqueous phase and subsequent replacement by another one able to cause a change in the sol-gel transition (Figure 22).

[40] Foster, J. A.; Piepenbrock, M-O. M.; Lloyd, G. O.; Clarke, N.; Howard, J. A. K.; Steed, J. W. *Nat. Chem.* **2010**, *2*, 1037-1043.

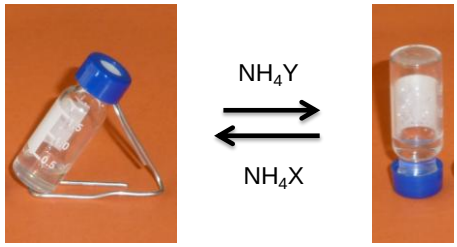

Figure 22. *Schematic representation of the anion dependent sol-gel transition.*

This suggests that the anion dependence on gel formation mainly responds to geometrical and spatial factors. Likely, spherical halides such as chloride or bromide allow for a correct arrangement of aggregates while oxoanions with different geometries such as acetates, sulfates and nitrates do not permit a suitable interaction between diguanidinium molecules, preventing gel formation. This explanation is extensive for less coordinative anions such as hexafluorophosphate. Probably, the p*Ka* variation between diverse diguanidinium salts also influences the NH-anion distance, the aggregation behavior and therefore the gelation process. However, it has been widely discussed that the protonation state of the bicyclic guanidinium moiety in organic solvents is not affected within the p*Ka* range used in our experiments,[41] meaning that the sol-gel transition is not governed by a simple protonation/deprotonation step.

In addition, solubility is dramatically affected by the counterion of these cationic compounds, and this property has been recently described as a determinant factor for the gelation ability of a molecule.[42] Indeed, this study pointed out the use of Hansen solubility parameters to predict the range of solvents that are likely to be gelled by a given gelator.

[41] Ratel, F. *PhD Thesis*, Universidad Autónoma de Madrid, **2009**.

[42] Raynal, M.; Bouteiller, L. *Chem. Commun.* **2011**, *47*, 8271-8273.

6.7 X-ray Diffraction Studies

Serendipitously, single crystals suitable for X-ray diffraction analysis from an abandoned solution of **(*S*)-4** enantiomer in a toluene/diethyl ether mixture were observed upon evaporation of the solvent over several months. The solid-state structure (Figure 23) revealed the unexpected formation of diguanidinium sulfone **84**. The crystals were re-dissolved and by means of mass spectrometry analysis it was corroborated the presence of the three possible oxidation states of the sulfur-containing products (thioether, sulfoxide and sulfone). Likely some ether peroxides were formed during the long crystallization period in the presence of oxygen and light, which could oxidize the thioether bond to the corresponding sulfoxide and sulfone derivatives, respectively. In view of the negative attempts to obtain a crystal structure of **4**, X-ray diffraction data of the corresponding sulfone was analyzed to search for structural and conformational similarities between both molecules.

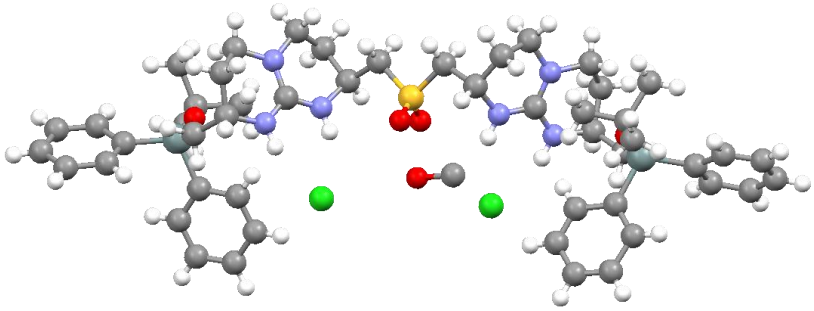

Figure 23. *Crystal structure of diguanidinium sulfone* ***84****.*

In the crystal structure the chloride anions are located in front of each guanidinium subunit and interact with the NHs by hydrogen bonding (Figure 23). A closer look into the molecular packing indicates a head-to-head disposition of the diguanidines, where the silyl groups are interacting through π-π and CH-π contacts. The solvophobic effect

governs the crystal packing in which the polar parts of the molecule are buried inside the "bilayer-like" structure formed by the bulky and solvent-exposed TBDPS groups (Figure 24).

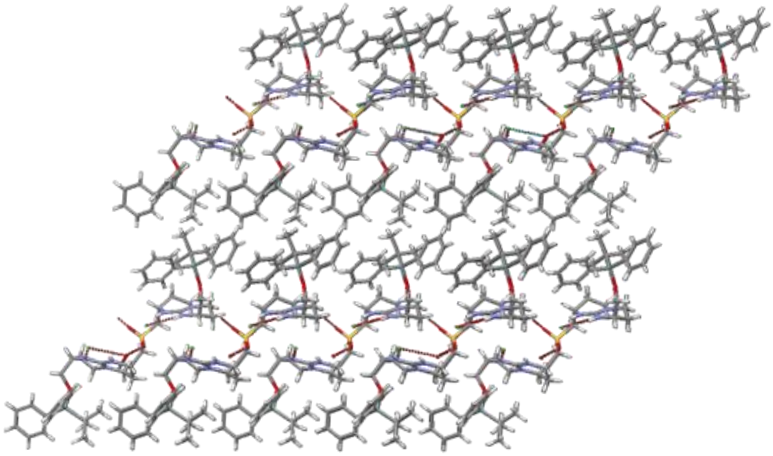

Figure 24. *Molecular packing of diguanidinium sulfone* ***84****.*

Diguanidinium sulfone **(*R*)-84** was independently synthesized from **(*R*)-4** using m-CPBA as oxidizing agent. Unfortunately, after an extensive screening for gelation conditions, only weak and unstable gels were found in toluene at high concentrations (up to 30 mM) and low temperatures (5-8ºC). Therefore, **(*R*)-4** and its sulfone adduct **(*R*)-84** exhibit different gelation abilities and their structural features and molecular packing likely differ. Indeed, the sulfone group has a pivotal role in the crystal structure. Its tetrahedral geometry forces the conformation and the orientation of the diguanidinium molecule. Moreover, one of the sulfone oxygens is hydrogen-bonded to a methanol molecule, which is filling an empty space in the crystal packing and thus preventing collapse of the structure.

Further information about the molecular arrangement of the diguanidinium gelator **4** was obtained from powder X-ray diffraction experiments.[43] As depicted in Figure 25, the diffractogram of the dried xerogel in *p*-xylene showed wide but regular peaks indicating some degree of periodicity. The most intense peak corresponds to a distance of *ca.* 21 Å which is close to the distance between the layers previously found in the crystal packing of the analogous sulfone **84**, suggesting a similar layered pattern. Hence, electrostatic interactions would influence the directionality of the fibrils, whereas different layers of this structure would be joined by means of weaker contacts.

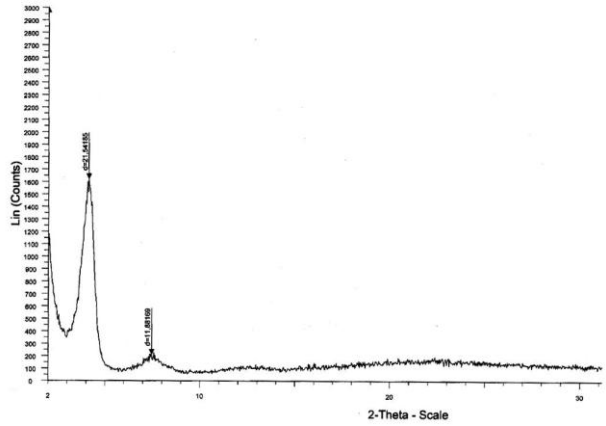

Figure 25. *X-ray diffractogram of the xerogel formed in p-xylene.*

Thus, a model can be considered where columnar arrays of diguanidinium molecules are organized in layers, as illustrated in Figure 26. The spacing between the subunits is compatible with the experimentally found in the low-angle diffraction peaks.

[43] Ostuni, E.; Kamaras, P.; Weiss. R. G. *Angew. Chem. Int. Ed.* **1996**, *35*, 1324-1326.

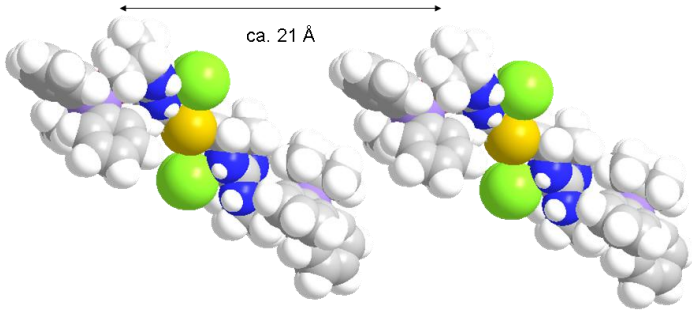

Figure 26. *Proposed model for the arrangement of organogelator* ***4****.*

6.8 Drug Release Experiments

One of the potential applications of low molecular gelators is the controlled release of a pharmacologically active drug through the gel fibrillar matrix. Despite the relatively high number of literature precedents on hydrogels about this topic, only a few examples relate to biologically active organogels for drug release. Their use is still limited due to scarce toxicological information about these drug delivery systems. However, applications of organogels for the administration of pharmaceutical active compounds (mainly hydrophobic) *via* diverse routes such as oral, parenteral or transdermal are known.

Herein, we describe initial attempts to use our diguanidinium organogelator as a potential platform for the controlled delivery of bioactive drugs. A key factor is the choice of a biocompatible solvent system for gelation. After an extensive screening, formation of robust gel phase materials was observed with mixtures of ethyl esters (ethyl acetate or ethyl benzoate, commonly used in food industry as artificial fruit flavors) with isopropyl palmitate (with applications in cosmetics and drug formulations) in the presence of gelator **4**.

Owing to the chirality of these organogelators, it would be feasible to find differences in the kinetic release of two enantiomeric drugs. Assuming that there is a certain degree of interaction between the organogel and the drug, the diffusion of the enantiomers through this chiral supramolecular matrix should be highly dependent on the helical packing of the gel. This hypothesis has been widely proven in other closely related systems such as in chiral chromatography or stereoselective catalysis using supramolecular gelators as active media,[13] but not further developed for drug delivery

applications.[44]

S- and *R*-naproxen enantiomers were tested as a model drug for these proof-of-concept experiments. Naproxen is hydrophobic enough to be delivered by organogels and contains a good chromophore which would facilitate its eventual quantification by HPLC. Gels containing 2.5 mg of diguanidinium gelator **(*R*)-4** and 0.75 mg of *S*- or *R*-naproxen were formed in an ethyl acetate/isopropyl palmitate mixture (1:3, 165 μL) and placed in a 5 mL vial with a 1 mL aqueous buffer solution. The presence of chloride (or bromide) anions in the buffer is critical for the integrity of the organogel, as previously indicated. PBS (with a high concentration of NaCl) at pH 7.4, and NH_4Cl buffers at pH 5.4 and 7.4, respectively, were tested to assess the effect of the pH and the anion content in the naproxen release. As shown in Figure 27, small but significant differences in the release of naproxen enantiomers was found in all cases. As a general trend, *R*-naproxen showed enhanced release with respect to the *S* enantiomer (up to 6% ee at pH 5.4). However, these differences were almost negligible if compared within the standard deviation range. The almost similar release behavior could be also explained due to the overloading of the gel matrix with naproxen molecules. Indeed, the gels contain an excess naproxen relative to diguanidinium chloride **4** (1.2:1, naproxen:diguanidine). Hence, as it occurs in chiral chromatography when there is overloading of the column, both enantiomers would elute together with no substantial kinetic differences in release.

[44] (a) Suedee, R.; Bodhibukkana, C.; Tangthong, N.; Amnuaikit, C.; Kaewnopparat, S.; Srichana, T. *J. Cont. Rel.* **2008**, *129*, 170-178. (b) Solinís, M. A.; de la Cruz, Y.; Hernández, R. M.; Gascón, A. R.; Calvo, B.; Pedraz, J. L. *Int. J. Pharm.* **2002**, *239*, 61-68.

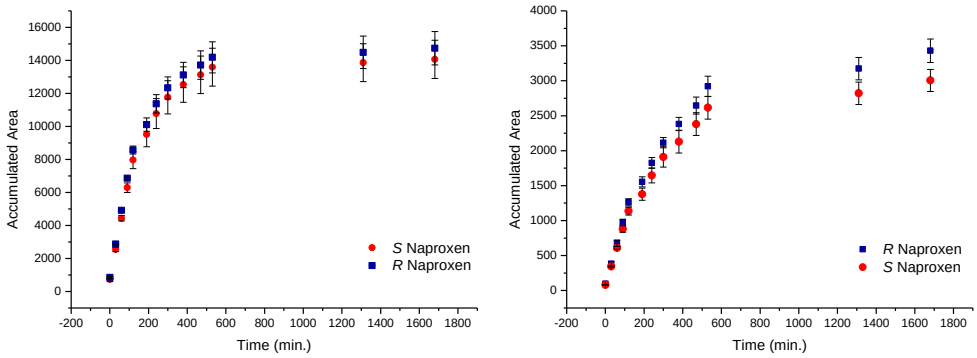

Figure 27. *Drug release kinetics of diguanidinium organogels loaded with R- and S-naproxen, respectively, in PBS buffer at pH 7.4 (left) and NH_4Cl buffer at pH 5.4 (right).*

On the other hand, evidences for a differential release behavior were found when these experiments were performed at different pH, as depicted below (Figure 28).

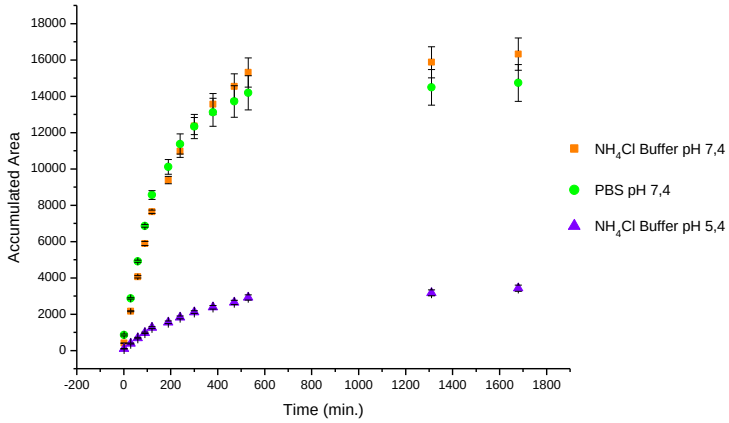

Figure 28. *Drug release kinetics of diguanidinium organogels loaded with R-naproxen, with the three different buffers tested as receiving phase.*

Two factors are indeed responsible for the different release kinetics: the limited solubility of protonated naproxen in water,[45] and the erosion of the matrix system, as the structural integrity of organogels depends on the buffer composition of the receiving phase. As previously demonstrated, these gels can transit from gel to sol phase by means of anion switching and thus the presence of OH^- anions should affect the stability of the gel. In fact, gels remained almost intact when buffer at pH 5.4 was used for release, but degradation was noticeable after 1 day in contact with buffers at physiological pH.

The release behaviour of a drug is determined by its hydrosolubility, the more hydrosoluble it is the more relevant would be the diffusion contribution. Conversely, the erosion factor would predominate in less water soluble drugs.[46] Hence, in naproxen delivery, the integrity of the matrix is essential to determine and control the release rate.

To further study the release kinetics, the data were adjusted to different drug release kinetic models, which afford relevant information about the release mechanism.[47] Higuchi model fits nicely with the data obtained at acidic pH, whereas kinetic rate curves obtained at physiological pH were more consistent with the Korsmeyer-Peppas model.[48] From the diffusion exponent obtained applying Korsmeyer-Peppas model the drug release mechanism can be assessed. For $n > 0.5$ a non-Fickian diffusion model is described for these systems, where a combination of both erosion and diffusion through the matrix is acting together in the release.

As concluding remarks, kinetic release experiments demonstrate a slow controlled

[45] Yazdanian, M.; Briggs, K.; Jankovsky, C.; Hawi, A. *Pharm. Res.* **2004**, *21*, 293-299.

[46] Vázquez, M. J.; Pérez-Marcos, B.; Gómez-Amoza, J. L.; Martínez-Pacheco, R.; Souto, C.; Concheiro, A. *Drug Dev. Ind. Pharm.* **1992**, *18*, 1355-1375.

[47] (a) Shoaib, M. H.; Tazeen, J.; Merchant, H. A.; Yousuf, R. I. *Pak. J. Pharm. Sci.* **2006**, *19*, 119-124. (b) Dash, S.; Murthy, P. N.; Nath, L.; Chowdhury, P. *Acta Pol. Pharm.* **2010**, *67*, 217-223.

[48] (a) Korsmeyer, R. W.; Gurny, R.; Doelker, E.; Buri, P.; Peppas, N. A. *Int. J. Pharm.* **1983**, *15*, 25-35. (b) Peppas, N. A. *Pharm. Acta Helv.* **1985**, *60*, 110-111.

release of naproxen through a diguanidinium-based gel matrix and the tunability of the drug delivery rate by anion triggering. Further studies accounting for the enantioselective release of chiral drugs should be performed to account on the scope and limitations of this method.

6.9 Experimental Section

6.9.1 Materials and Methods

Crystal data set were collected on a Bruker-Nonius diffractometer equipped wth APPEX 24K CCD area detector, a FR597 rotating anode with $Mo_{K\alpha}$ radiation, Montel mirrors as monochromator and a Kryoflex low temperature device (T=-173 ºC). CD measurements were carried out in a Chirascan circular dichroism spectrometer from Applied Photophysics, with simultaneous measurement of UV-vis and CD spectra in the range 165 to 900 nm. The device is equipped with a Peltier thermal control unit (-40/+100 ºC) with possibility of temperature ramp control.

6.9.2 General Procedure for Gelation of Diguanidine 4

Compound **(*R*)-4** (chloride) (1 mg) was dissolved in a minimum amount (between 50 and 100 μL aprox.) of chloroform (or other solubilizing solvent such as THF, toluene, AcOEt, etc.) and then hexane or ether were slowly added dropwise until turbidity was observed (0.2-0.5 mL) or the gel was spontaneously formed at room temperature. Gelation with pure aromatic solvents such as toluene, *p*-xylene or mesitylene also occurs.

6.9.3 General Procedure for Anion Exchange Experiments

Gels formed in toluene or *p*-xylene (10-20 mM) were placed in a vial and subsequently the same approximate volume of an aqueous ammonium solution (0.1N) containing the anion to exchange was added. The mixture was heated until a liquid biphase was formed and then the phases were mixed vigorously. Once the two phases separated defined again, the system was cooled at the fridge or slowly cooled down to room temperature.

6.9.4 General Procedure for VT-Circular Dichroism Experiments

To a solution of diguanidinium **(*R*)-4 (Cl^-)** in THF (50 μL) was added hexane (150 μL) in a 0.1 cm path length quartz cuvette, and subsequently the corresponding gel was formed. To obtain a homogeneous mixture sometimes heating was required. The sample was subjected to dirverse cooling-heating cycles (from -5ºC to 65ºC) and the corresponding curves were collected each 5ºC step at the specified wavelength range.

6.9.5 Synthesis

General procedure for 2. See Experimental Section in Chapter 1 for the synthesis and further characterization (MS, ^{1}H- and ^{13}C-NMR) of compound **2**.

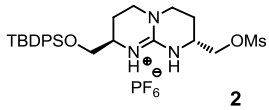

2

(*R*)-2 $[\alpha]^{25}_D$ -45 (c = 0.5, $CHCl_3$).

(*S*)-2 $[\alpha]^{25}_D$ +78 (c = 0.8, $CHCl_3$).

General procedure for 3. See Experimental Section in Chapter 1 for the synthesis and further characterization (MS, ^{1}H- and ^{13}C-NMR) of compound **3**.

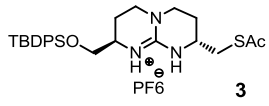

3

(*R*)-3 $[\alpha]^{25}_D$ -42 (c = 0.3, $CHCl_3$).

(*S*)-3 $[\alpha]^{25}_D$ +54 (c = 0.4, $CHCl_3$).

General procedure for 4 (Cl-). See Experimental Section in Chapter 1 for the synthesis of compound **4**. For Compound **(*R,S*)-4** See Experimental Section in Chapter 4.

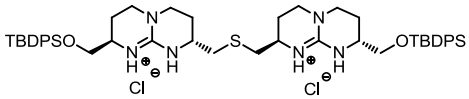

4

(*R*)-4 (Cl-) $[\alpha]^{25}_{D}$ -64 (*c* = 0.9, $CHCl_3$). ^{1}H-NMR (400 MHz, $CDCl_3$) δ 8.36 (s, 2H, NH), 8.14 (s, 2H, NH), 7.67-7.58 (m, 8H, CH_{Ar}), 7.50-7.34 (m, 12H, CH_{Ar}), 3.68 (dd, *J* = 4.8, 10.5 Hz, 2H, CH_2O), 3.62-3.53 (m, 4H, CH_2O, CH_α), 3.49-3.41 (m, 2H, CH_α), 3.39-3.14 (m, 8H, $CH_{2\gamma}$), 2.91 (dd, *J* = 2.5, 13.3 Hz, 2H, CH_2S), 2.55 (dd, *J* = 11.5, 13.3 Hz, 2H, CH_2S), 2.12-1.99 (m, 4H, $CH_{2\beta}$), 1.97-1.81 (m, 4H, $CH_{2\beta}$), 1.06 (s, 18H, $CH_{3t\text{-}Bu}$). ^{13}C-NMR (100 MHz, $CDCl_3$) δ 151.2 (C_{guan}), 135.6, 135.5, 132.8, 132.7, 129.9, 127.9, 127.8 (CH_{Ar}, C_{Ar}), 65.1 (CH_2O), 49.2, 46.4 (CH_α), 45.1, 44.4 ($CH_{2\gamma}$), 36.0 (CH_2S), 26.9 ($CH_{3t\text{-}Bu}$), 26.3, 22.2 ($CH_{2\beta}$), 19.2 ($C_{t\text{-}Bu}$). ESI-MS *m/z* 873.5 $(M - HCl - Cl^-)^+$, 437.3 $(M - 2Cl^-)^{2+}$. HRMS calcd. for $[C_{50}H_{69}N_6O_2SSi_2]^{2+}$ 873.4741; found 873.4754.

(*S*)-4 (Cl-) $[\alpha]^{25}_{D}$ +84 (*c* = 1.2, $CHCl_3$).

(*R,S*)-4 (Cl-) $[\alpha]^{25}_{D}$ +3 (*c* = 1.0, $CHCl_3$). ^{1}H-NMR (400 MHz, $CDCl_3$) δ 8.24 (s, 2H, NH), 8.05 (s, 2H, NH), 7.71-7.55 (m, 8H, CH_{Ar}), 7.50-7.33 (m, 12H, CH_{Ar}), 3.73 (dd, *J* = 4.7, 9.8 Hz, 2H, CH_2O), 3.67-3.50 (m, 5H, CH_2O, CH_α), 3.48-3.10 (m, 9H, CH_α ,$CH_{2\gamma}$), 3.00 (dd, *J* = 2.7, 13.5 Hz, 2H, CH_2S), 2.59 (dd, *J* = 10.8, 13.5 Hz, 2H, CH_2S), 2.18-1.69 (m, 8H, $CH_{2\beta}$), 1.06 (s, 18H, $CH_{3t\text{-}Bu}$). ^{13}C-NMR (100 MHz, $CDCl_3$) δ 151.2 (C_{guan}), 135.6, 135.6, 132.8, 132.7, 129.9, 127.9, 127.9 (CH_{Ar}, C_{Ar}), 65.2 (CH_2O), 49.7, 48.3 (CH_α), 45.1, 44.7 ($CH_{2\gamma}$), 38.5 (CH_2S), 26.9 ($CH_{3t\text{-}Bu}$), 26.2, 22.6 ($CH_{2\beta}$), 19.2 ($C_{t\text{-}Bu}$).

Procedure for Compound 5. See Experimental Section in Chapter 1 for the synthesis of compound **5**.

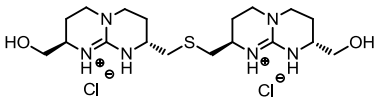

5

$[\alpha]^{25}_{D}$ -95 (c = 0.5, $CHCl_3$).

(2*R*,8*R*)-2-(*tert*-Butyldiphenylsilyloxymethyl)-8-[(2*R*,8*R*)-8-(*tert*-butyldiphenylsilyloxymethyl)-2,3,4,6,7,8-hexahydro-*1H*-pyrimido[1,2-*a*]pyrimidin-9-ium-2-ylmethylsulfonylmethyl chloride]-2,3,4,6,7,8-hexahydro-1H-pyrimido[1,2-*a*]pyrimidin-9-ium chloride (84)

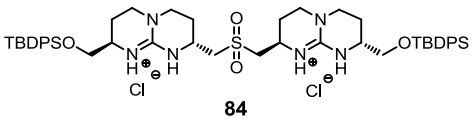

84

A mixture of compound **(*R*)-4** (PF_6^-) (30 mg, 0.026 mmol) and *m*-chloroperbenzoic acid (9.4 mg, 0.054 mmol) was dissolved in CH_2Cl_2 (5 mL) and stirred at room temperature for 4 h. Then, more solvent was added (10 mL) and the mixture was washed with aqueous 1N NH_4PF_6 (2 × 10 mL). The organic phase was filtered over cotton and concentrated to dryness to give a crude residue which was purified by silica gel column chromatography (CH_2Cl_2/MeOH, 97:3), affording symmetric diguanidinium **(*R*)-84** (PF_6^-) as a white solid (28 mg, 91%). The solid was redissolved in CH_2Cl_2 and washed again with aqueous 1N NH_4Cl (2 × 10 mL) giving rise to the corresponding diguanidinium chloride salt. ^{1}H-NMR (400 MHz, $CDCl_3$) δ 8.90 (s, 2H, NH), 8.46 (s, 2H, NH), 7.69-7.60 (m, 8H, CH_{Ar}), 7.50-7.35 (m, 12H, CH_{Ar}), 4.36-4.14 (m, 4H, CH_2O, CH_α), 3.81-3.46 (m, 10H, CH_2O, CH_α, $CH_{2\gamma}$), 3.31-3.07 (m, 6H, $CH_{2\gamma}$, CH_2S), 2.29-1.83 (m, 8H, $CH_{2\beta}$), 1.07 (s, 18H, $CH_{3t\text{-}Bu}$). ^{13}C-NMR (100 MHz, $CDCl_3$) δ 150.9 (C_{guan}), 135.6, 135.5, 132.7, 132.7, 130.0, 127.9, 127.9 (CH_{Ar}, C_{Ar}), 65.3 (CH_2O), 59.5, 49.4 (CH_α), 44.9, 43.8 ($CH_{2\gamma}$), 29.7 (CH_2S), 26.9 ($CH_{3t\text{-}Bu}$), 26.0, 22.5 ($CH_{2\beta}$), 19.2 ($C_{t\text{-}Bu}$). ESI-MS m/z 905.2 (M - HCl - Cl^-)$^+$, 453.1 (M – 2 Cl^-)$^{2+}$.

Conclusions

This thesis overviews the synthesis and design of different bicyclic guanidinium oligomers, exploring their principal features and potential applications in biomolecular recognition, cell delivery and material science.

In Chapter 1, we describe the synthesis of a family of oligoguanidinium ligands for the tetramerization domain of p53. These polycationic compounds are designed to effectively interact with a conserved region of acidic residues by means of hydrogen bonding and salt bridges. Moreover, we introduce aromatic moieties to enhance the hydrophobic contacts with the domain. A deeper analysis of these ligand-protein interactions would be crucial for designing attractive drug candidates to target and stabilize this key protein.

Chapter 2 explores the use of these oligomers as internalization vectors for drug delivery inside the cell. Indeed, their attachment to different peptide nucleic acids (PNAs) provokes an increase in the antisense effect of those molecules. Cell uptake was found to be concentration dependant for some of these conjugates and several studies supported an aggregation mechanism for enhancing cell penetration. Antibacterial oligoguanidinium-PNA compounds targeting *E. coli* showed high bactericide activity compared to other related PNA structures.

We report in Chapter 3 the design and synthesis of miniaturized transcription factors (TF) based on a peptide fragment of GNC4 protein which provides specificity towards consensus DNA sequences, conjugated with tetra- or pentaguanidinium compounds which should strongly bind to the anionic phosphodiester skeleton of DNA, thus increasing the association constant of the ligand. Stabilization effect of bicyclic guanidinium tetramer **13** on double stranded DNA structure is compared with natural polyamines and briefly discussed.

The design and synthesis of tetraguanidinium macrocycle **71** are described in Chapter 4. This compound is capable of strongly interact with oxoanionic calix[4]arenes with

Ka ≥ 10^4-10^6 M^{-1}even in competitive polar media. As a result of this complexation, the cone conformation of the calixarenes is stabilized and their concave cavity expanded, thus allowing the inclusion of bulky isoquinolinium salt guests.

In Chapter 5, we study fullerene@bis-porphyrin dyads bearing guanidinium-carboxylate functionalities in order to enhance the robustness of the association. Herein, stable complexes are formed and used as molecular scaffolds for constructing macrocyclic porphyrin:fullerene arrays inspired in biological photosystems. Even though, only some preliminary experiments and molecular modelling studies have been performed to-date.

Finally, Chapter 6 explores the use of diguanidine **4** as organogelator. This chiral compound is able to form gels and self-assemble into nanoscopic helical fibers. Indeed, circular dichroism (CD) and thermal analysis experiments stressed out the role of chirality in the gelation process. Besides, these colloidal materials are capable of reversibly switching from gel-to-sol via anion exchange. Finally, the use of this new diguanidinium-based gelator as matrix for drug delivery is explored.

Resumen

El presente trabajo tiene por objetivo el diseño y la síntesis de diferentes oligómeros de guanidina bicíclica, así como el estudio de sus propiedades. El grupo guanidinio es conocido por su capacidad para interaccionar con aniones (especialmente oxonaniones) mediante puentes de hidrógeno e interacciones de tipo electrostático. En nuestro grupo de investigación se ha descrito cómo oligómeros lineales de guanidina bicíclica (concretamente tetrámeros) son capaces de interaccionar con secuencias peptídicas específicas, ricas en aminoácidos cargados negativamente (ácidos aspártico y glutámico) e incluso mostrar gran afinidad por determinadas secuencias del dominio de tetramerización de p53 (proteína cuya actividad resulta esencial en el mecanismo de reparación génica celular).

Los tres primeros capítulos de esta tesis están dedicados al estudio de la interacción de derivados oligoméricos de guanidina bicíclica con sistemas biológicos de gran relevancia.

Concretamente, en el Capítulo 1 se asientan las bases metodológicas para la síntesis de estos compuestos policationicos. Asimismo, se estudia la interacción de dichos compuestos con el dominio de tetramerización de p53 (p53TD). El ligando hexaguanidinio cumple con todos los requisitos geométricos para el reconocimiento específico de la superficie proteica de dicho dominio, puesto que cada monómero de p53TD contiene una secuencia altamente conservada de 6 aminoácidos ácidos a una distancia óptima (*i*, *i+3*; *i*, *i+4*) para la unión con estos compuestos oligoguanidínicos. Otros ligandos fueron sintetizados con el objetivo de evaluar mediante RMN (trabajo realizado por la Dra. Susana Gordo, bajo la supervisión del profesor Giralt en el IRB) la influencia de factores como la longitud del oligómero o la presencia de grupos aromáticos en la interacción con la proteína.

En el capítulo 2 se explora la utilización de estos compuestos oligoguanidínicos como vectores no-proteicos de internalización celular. Dado su carácter catiónico y

amfifílico estas moléculas son capaces de interaccionar y traspasar la membrana celular, siendo potencialmente activas en el trasporte de fármacos u otras moléculas con actividad terapéutica dentro de la célula. En colaboración con el grupo del Prof. Peter E. Nielsen se prepararon diversos conjugados oligoguanidínicos unidos a ácidos peptidonucleicos (PNAs) para evaluar su actividad antisentido (corrigiendo el pre-ARNm aberrante que codifica para la proteína luciferasa), íntimamente relacionada con su capacidad como agente internalizante. Se determinó también que la elevada actividad mostrada por ciertos conjugados era consecuencia directa de su mecanismo de internalización, basado en la formación de agregados de tipo liposomal. Por último, la unión de tetra- y pentaguanidinios a un PNA con actividad bactericida contra *E. coli*, resultó en el aumento drástico de su efecto antisentido al permitir su transporte a través de la pared celular bacteriana.

En colaboración con el grupo del Prof. J. L. Mascareñas, en la universidad de Santiago, se estudió la interacción de híbridos oligoguanidina-péptido con determinadas secuencias consenso de ADN (capítulo 3), siendo la secuencia peptídica una versión miniaturizada del factor de transcipción (GNC4) perteneciente a la familia de las cremalleras de leucina. Estudios preliminares demuestran cómo estos compuestos policatiónicos aumentan la afinidad de dichos péptidos por el ADN sin perder especificidad de unión. Mediante estudios de desnaturalización térmica de diversas secuencias de ADN se determinó el efecto de estabilización que tienen estos compuestos oligoguanidínicos sobre la estructura de doble hélice del ADN, mayor incluso que el efecto de poliaminas naturales como espermina o espermidina.

Los tres últimos capítulos de este trabajo doctoral versan sobre la capacidad que tienen las guanidinas bicíclicas para auto-ensamblarse formando complejos supramoleculares con diferentes compuestos oxoaniónicos y las propiedades físico-químicas derivadas de esa unión.

Así, en el Capítulo 4 se describe la síntesis del macrociclo tetraguanidínico y su interacción con diversos calixarenos tetraoxoaniónicos. Dicha unión restringe conformacionalmente la movilidad de los arilos y produce un considerable aumento

del tamaño de la cavidad del calix[4]areno, permitiendo la inclusión de diversas moléculas en su interior.

El Capítulo 5 abarca la formación de díadas bis-porfirina:fullereno mediante la utilización del par iónico guanidina-carboxilato. La contribución de cada uno de los elementos partícipes de la interacción es medida individualmente para evaluar su aportación en la formación de la díada. Se explorará la auto-asociación de dicho compuesto mediante interaciones no-covalentes Zinc-piridina, creando complejos supramoleculares macrocíclicos similares a los fotosistemas porfirínicos artificiales descritos por otros grupos. Actualmente se están realizando diversos estudios para elucidar el estado de agregación de estos compuestos tanto en solución como en estado sólido.

Por último, el Capítulo 6 trata sobre la capacidad de determinados compuestos quirales diguanidínicos para formar geles (proyecto en el cuál ha participado activamente la Dra. Beatriu Escuder de la universidad de Castellón). Estas moléculas auto-agregan para dar lugar a fibras quirales y cuyo entramado tridimensonal alberga las moléculas de disolvente que componen estos organogeles. Además, se estudió como el intercambio aniónico en estos compuestos catiónicos afecta a su transición líquido-gel y como ésta puede modularse fácilmente mediante extracciones líquido-líquido. Por último, se explora la posible utilidad de estos geles para albergar fármacos en su interior y facilitar así su liberación gradual y controlada a través de estas fases coloidales.

UNIVERSITAT ROVIRA I VIRGILI
BICYCLIC GUANIDINIUM OLIGOMERS FOR RECOGNITION, CELL DELIVERY, AND MOLECULAR MATERIALS
Julián Valero Moreno
DL:T. 276-2012

UNIVERSITAT ROVIRA I VIRGILI
BICYCLIC GUANIDINIUM OLIGOMERS FOR RECOGNITION, CELL DELIVERY, AND MOLECULAR MATERIALS
Julián Valero Moreno
DL:T. 276-2012

UNIVERSITAT ROVIRA I VIRGILI
BICYCLIC GUANIDINIUM OLIGOMERS FOR RECOGNITION, CELL DELIVERY, AND MOLECULAR MATERIALS
Julián Valero Moreno
DL:T. 276-2012